

**Investigating human Schwann cell phenotypes and
outcome measures of muscle reinnervation**

MATTHEW BENJAMIN WILCOX

Thesis submitted in partial fulfilment of the requirements for the degree of
Doctor of Philosophy

Eastman Dental Institute

University College London

August 2020

Declaration

I, Matthew Benjamin Wilcox confirm that the work presented in this thesis is my own. Where information has been derived from other sources, I confirm that this has been indicated in the thesis.

Signed: Matthew Benjamin Wilcox

Date: 04/08/2020

Acknowledgements

I owe this PhD thesis to Mr. Tom Quick and Prof. James Phillips. Their mentorship over many years allowed me to overcome numerous academic and non-academic obstacles encountered during my research. I am indebted to them for the time, effort and expertise they have invested in me during my first steps as a clinician and researcher.

I extend my thanks to the entire team at the Peripheral Nerve Injury Unit, Royal National Orthopaedic Hospital for supporting and facilitating the research presented in this thesis. In particular, Neena Kerai for help with co-ordinating the studies presented in **Chapter 4**, **Chapter 5** and **Chapter 7** as well as Hazel Brown for sharing her knowledge on the clinical assessment of nerve injury. I am also grateful to Dr. Bill Andrews from the UCL Division of Biosciences for his advice on the optimisation of the RT-qPCR assays presented in **Chapter 4** and to Dr. Naomi Guppy for performing the immunohistochemistry staining presented in **Chapter 4**. Professor Kristjan Jessen and Professor Rhona Mirsky provided invaluable expertise which assisted with the interpretation of the findings presented in **Chapter 4**. Dr. Simão Laranjeira also provided invaluable statistical expertise which informed the analysis of the data presented in **Chapter 4** and **Chapter 5**.

I am also grateful to Dr. Tom Tidswell from the Royal Free Hospital for performing the Motor Unit Number Estimation protocol used to acquire the data presented in **Chapter 5** as well as Professor Martin Koltzenburg for sharing his neurophysiological expertise, Dr. Victoria Robertson for performing the surgery described in **Section 2.3.1** and her supervision, Dr. Rikin Hargunani and Rodney Santiago from the Royal National Orthopaedic Hospital for acquiring the MRI scans analysed in **Chapter 7**, Dr. Liane Dos Santos Canas and Dr. Marc Modat from Kings College London for their assistance with processing of the MRI scans presented and analysed in **Chapter 7**. I

also acknowledge my friends and Dr. Kununya Pimolbutr for their invaluable and sustained support throughout this project.

Lastly but most importantly, I thank my family for their unconditional support despite my irritating stubbornness in the pursuit of my ambitions. I dedicate this thesis to them and all those who were instrumental in making this body of work possible.

Publications

Papers

Wilcox, M., H. Gregory, R. Powell, T. J. Quick and J. B. Phillips (2020). "Strategies for Peripheral Nerve Repair." *Current Tissue Microenvironment Reports* 1(2): 49-59.

Wilcox, M. B., S. G. Laranjeira, T. M. Eriksson, K. R. Jessen, R. Mirsky, T. J. Quick and J. B. Phillips (2020). "Characterising cellular and molecular features of human peripheral nerve degeneration." *Acta Neuropathologica Communications* 8(1): 51.

Wilcox, M., I. Stephen and T. Quick (2020). "100 years of BOA nerve repair." *Journal of Trauma and Orthopaedics* (*in press*).

Wilcox, M. and T. Quick (2020). "How to assess recovery of muscular function following nerve injury; a view from surgeons and patients." *Journal of Plastic, Reconstructive & Aesthetic Surgery* (*under review*).

Wilcox, M., H. Brown, K. Johnson, M. Sinisi and T. Quick (2020). "An assessment of co-contraction in reinnervated elbow flexor muscles." *Journal of Plastic, Reconstructive & Aesthetic Surgery* (*under review*).

Wilcox, M., T. Tidswell, S. Gomes, J. B. Phillips (2020). "Motor Unit Number Estimation following nerve transfer to reanimate elbow flexion". (*Paper under preparation*).

Wilcox, M., L. D. S. Canas, R. Hargunani, T. Tidswell, H. Brown, J. B. Phillips, M. Modat, S. Ourselin, T. Quick (2020). "Quantitative MRI; a potential outcome measure of muscle reinnervation". (*Paper under preparation*).

Rayner, M. L. D., H. L. Brown, **M. Wilcox**, J. B. Phillips and T. J. Quick (2019). "Quantifying regeneration in patients following peripheral nerve injury." *Journal of Plastic, Reconstructive & Aesthetic Surgery*.

Wilcox, M., H. Brown, K. Johnson, M. Sinisi and T. Quick (2019). "An assessment of fatigability following nerve transfer to reinnervate elbow flexor muscles." *The Bone & Joint Journal* 101-B: 867-871.

Wilcox, M., T. J. Quick and J. B. Phillips (2019). "The Effects of Surgical Antiseptics and Time Delays on RNA Isolated From Human and Rodent Peripheral Nerves." *Frontiers in Cellular Neuroscience* 13: 189-189.

Book chapters

Wilcox, M., H. L. Brown, T. Quick (2020). Clinical outcome measures following peripheral nerve repair. *Tissue Engineering and Regeneration. Peripheral Nerve Tissue Engineering and Regeneration.* J. B. Phillips, D. Hercher, T. Hausner. London, Springer Nature Switzerland.

Wilcox, M., A. Fisgun, A. Hoke (2020). Regenerative therapies for acquired axonal neuropathies. *Tissue Engineering and Regeneration. Peripheral Nerve Tissue Engineering and Regeneration.* J. B. Phillips, D. Hercher, T. Hausner. London, Springer Nature Switzerland (*in production*).

Conference proceedings

Wilcox, M., L. Canos, R. Hargunani, T. Tidswell, H. Brown, M. Modat, J. B. Phillips, T. Quick (2020). MRI biomarker assessment following nerve transfer to reinnervate elbow flexor muscles; a potential outcome measure of muscle reinnervation. *European Society of Musculoskeletal Radiology, Annual Meeting, virtual meeting due to the COVID-19 pandemic.*

Johnson, A., J. Joseph, J. Scheib, R. Mi, F. Millesi, N. Guionneau, **M. Wilcox**, F. Zhang, G. Ming, S. Tuffaha, A. Hoke (2020). M6A methylation defect in Schwann cells impairs myelination and peripheral nerve regeneration. *American Neurological Association, Annual Meeting, virtual meeting due to the COVID-19 pandemic.*

Wilcox, M., T. Tidswell, J. B. Phillips, T. Quick (2019). MUNE following nerve transfer to reinnervate elbow flexor muscles. *Adrian Prize Candidate at the British Society of Clinical Neurophysiology Autumn Scientific Meeting, London (United Kingdom)*.

Wilcox, M., S. Gomes, T. Eriksson, K. Jessen, R. Mirsky, T. Quick, J. B. Phillips (2019). Characterising cellular and molecular features of human peripheral nerve degeneration. *International Symposium on Peripheral Nerve Regeneration, Porto (Portugal)*.

Wilcox, M., H. Brown, K. Johnson, M. Sinisi and T. Quick (2019). An assessment of fatigability and co-contraction following nerve transfer to reinnervate elbow flexor muscles. *Narakas, Leiden (Netherlands)*.

Wilcox, M., H. Brown, K. Johnson, M. Sinisi and T. Quick (2018). An assessment of fatigability and co-contraction following nerve transfer to reinnervate elbow flexor muscles. *American Society for Peripheral Nerve Meeting, California (USA)*.

Wilcox, M., T. Quick and J. B. Phillips (2019). The Effects of Surgical Antiseptics and Time Delays on RNA Isolated From Human and Rodent Peripheral Nerves. *American Society for Peripheral Nerve Meeting, California (USA)*.

Wilcox, M., T. Quick (2018). 100 years of peripheral nerve repair. *British Orthopaedic Association meeting, Birmingham (United Kingdom)*.

Wilcox, M., H. Brown, K. Johnson, M. Sinisi and T. Quick (2018). An assessment of fatigability and co-contraction following nerve transfer to reinnervate elbow flexor muscles. *Peripheral Nerve Society Annual Meeting, Baltimore (USA)*.

Wilcox, M., T. Quick and J. B. Phillips (2018). Advancing the available therapeutic options for nerve injury. *UCL Faculty of Medical Sciences Dean's Research Day, London (United Kingdom)*.

Wilcox, M., T. Quick and J. B. Phillips (2017). Advancing the available therapeutic options for nerve injury. *UCL Eastman Dental Institute Research Away Day 3 minute Thesis (Runner Up), London (United Kingdom).*

Abstract

Peripheral Nerve Injury (PNI) often causes partial or complete paralysis and/or loss of sensation of the segment of the body involved. Traumatic PNI is a global problem and can result in significant disability and socio-economic impacts.

Clinical translation of new therapeutics for the treatment of PNI is challenged by the little information that is known about the cellular and molecular features that underpin human nerve regeneration. Moreover, clinical models and measurements that can quantify the efficacy of new treatments for PNI are not well established. Therefore, this PhD explored injured and healthy human nerve samples liberated from reconstructive nerve procedures to characterise the cellular and molecular features of human peripheral nerve degeneration. Associated with this theme of characterisation of human nerve injury, the recovery of motor units in reinnervated elbow flexor muscles following nerve transfer was quantified using Motor Unit Number Estimation (MUNE). In order to better understand the relationship of MUNE with the biological process of nerve regeneration, an animal model of nerve injury was used to investigate the association between MUNE and histological markers of regeneration. MUNE was found to be a sensitive marker of muscle reinnervation in human and animal models of nerve regeneration. Moreover, MUNE demonstrated a correlation with histological markers of muscle reinnervation.

It is known that these changes in the number of motor units are accompanied by changes in muscle volume. Therefore, using the same surgical scenario of nerve transfer to reanimate elbow flexor muscles, this PhD measured the recovery of muscle volume following nerve transfer to reanimate elbow flexor muscles using quantitative Magnetic Resonance Imaging (MRI) techniques. It was found that MRI assessment of muscle volume is a measure that is sensitive to the biological process of nerve regeneration. With further data, this has the capacity to determine the

efficacy of new therapeutics for the treatment of PNI and predict the likely functional recovery following PNI.

In summary, the findings represent an important step towards understanding the in vivo cellular and molecular events in human nerve degeneration. In addition, MUNE and quantitative MRI techniques were found to represent sensitive and responsive measures of nerve regeneration. With further data, the findings presented here will help new therapeutic options for human nerve injury advance.

Impact statement

This thesis contributes to translational research in peripheral nerve injury (PNI). A number of therapeutics for the treatment of PNI have been developed in animal models such as engineered neural tissues and drugs that promote nerve regeneration. However, there are many challenges associated with the clinical translation of these and other therapies with the potential to improve nerve repair outcomes in patients. First, little is known about the in vivo cellular and molecular mechanisms that control the regenerative microenvironment of the distal nerve segment in humans. Second, assessments that are sensitive and responsive to sub-clinical changes in the tissue microenvironment are awaited.

The work presented in this thesis has made progress towards addressing these unmet clinical needs of regenerative neuroscience. Studying the exposure of human nerve samples retrieved from reconstructive nerve procedures to chemical and physical factors of the surgical environment has enabled this project to go beyond rodent models of nerve regeneration. This has led to new insights into the in vivo cellular and molecular features that underpin human nerve degeneration.

Associated with this theme of characterising human nerve regeneration, this thesis has made the first steps towards validating sensitive and responsive measures of muscle reinnervation.

In summary, this project has made advancements in our understanding of the in vivo biology of human nerve degeneration and investigated sensitive and responsive measures of muscle reinnervation. Together, this work is informing the development of a clinical trial to facilitate the translation of new therapies to improve peripheral nerve repair in humans.

Abbreviations

ALS – Amyotrophic Lateral Sclerosis

ANOVA – Analysis of Variance

ARAT – Action Research Arm Test

AROM – Active Range of Movement

cDNA – Complementary DNA

ChAT – Choline Acetyltransferase

CMAP – Compound Muscle Action Potential

CNAP – Compound Nerve Action Potential

CNS – Central Nervous System

CT – Threshold cycle

CT:c – CT value for calibrator

CT:e – CT value for endogenous control

DAB – 3,3' - Diaminobenzidine

DRG – Dorsal Root Ganglion

DTI – Diffusion Tensor Imaging

EDL – Extensor Digitorum Longus

EMG – Electromyography

FA – Fractional Anisotropy

FFMT – Free Functioning Muscle Transfer

Gd-DPTA – Gadolinium-diethylenetriaminepentaacetate

Gf – Gadofluourine M

GOI – Gene of interest

HIER – Heat-induced epitope retrieval

HKG – Housekeeping gene

HRP – Horseradish peroxidase

IASP – International Association for the Study of Pain

ICC – Intraclass Correlation

IL-1 α – Interleukin-1 α

ITSF – Intermediary Toe Spread Factor

LIF – Leukaemia Inhibitory Factor

MAG – Myelin Associated Glycoprotein

MBP – Myelin Basic Protein

MEP – Motor evoked potential

MRC – Medical Research Council

MRI – Magnetic Resonance Imaging

MRN – Magnetic Resonance Neurography

MU – Motor Unit

MUAP – Motor Unit Action Potential

MUNE – Motor Unit Number Estimation

MUNIX – Motor Unit Number Index

NAP – Nerve Action Potential

NCS – Nerve Conduction Studies

NGF – Nerve Growth Factor

NMJ – Neuromuscular junction

NTC – Negative Controls

NTR – Neurotrophin Receptor

OCT – Optimal Cutting Temperature

OSGE – Oscillating Spin Gradient Echo

PBS – Phosphate Buffered Saline

PDW – Proton Density Weighted

PNI – Peripheral Nerve Injury

PNS – Peripheral Nervous System

PROs – Patient Reported Outcomes

PVF – Peak volitional force

QSART – Sudomotor Axon Reflex Test

REC – Research Ethics Committee

RIN – Ribosomal Integrity Number

RQ – Relative quantification

RT – Reverse transcription

RT-qPCR – Real Time-quantitative Polymerase Chain Reaction

SD – Standard Deviation

SDE – Single Diffusion Encoding

SIP – Surface EMG Interference Pattern

SMA – Spinal Muscle Atrophy

S-MUAP – Surface Motor Unit Action Potential

SMUAP – Single Motor Unit Action Potential

SNAP – Sensory Nerve Action Potential

SPIO – Supra-magnetic Iron Oxide

SSEP – Somatosensory evoked potential

SSI – Static Sciatic Index

STA – Spike Triggered Averaging

STI – Shape Texture Identification Test

STIR – Short Tau Inversion Recovery

T1-w – T1-Weighted

T2-w – T2-weighted

TES – Transcranial Electrical Stimulation

TIRM – Turbo Inversion Recovery Magnitude

TSF – Toe Spread Factor

US – Ultrasound

WEST – Weinstein Enhanced Sensory Test

Contents

Declaration	2
Acknowledgements.....	3
Publications	5
Abstract	9
Impact statement	11
Abbreviations.....	12
Index of figures	20
Index of tables	24
Index of equations	26
Chapter 1: Introduction	27
1.1 Peripheral nerve anatomy.....	27
1.2 Classifications of Peripheral Nerve Injuries.....	29
1.3 Neurobiology of peripheral nerve regeneration	32
1.3.1 Neurapraxia (grade I injury)	32
1.3.2 Biological processes that underpin neural regeneration (grade II – V injuries).....	32
1.3.3 Retrieving human nerve samples for study in the laboratory	37
1.3.4 Changes at the neuromuscular junction and within the muscle	37
1.4 Clinical measurements of nerve injury and regeneration.....	39
1.4.1 Sensibility	40
1.4.2 Pain	41
1.4.3 Motor function	42
1.5 Neurophysiological investigation of peripheral nerve injuries	44
1.5.1 Nerve Conduction Studies	44
1.5.2 Electromyography	45
1.5.3 Timing of neurophysiological assessment.....	48

1.5.4 Determining the extent of neural injury using electro-diagnostic testing .	52
1.5.5 Intra-operative neurophysiology	54
1.5.6 Electrophysiological correlates of the recovery of motor units	56
1.5.7 Quantitative Motor Unit Action Potential (MUAP) analysis.....	60
1.5.8 Motor Unit Number Estimation (MUNE)	61
1.5.9 Electrophysiological correlates of sensory function	65
1.6 Imaging of peripheral nerve injuries.....	67
1.6.1 MRI findings in injured nerves.....	68
1.6.2 MRI findings in denervated muscle	69
1.6.3 Muscle volume changes in denervated muscle and the application of MRI	72
1.6.4 MR neurography	73
1.6.5 MR contrast agents.....	74
1.6.6 MRN to quantify axonal diameter	75
1.6.7 Tractography.....	76
1.6.8 Ultrasound	77
1.7 Conclusions.....	78
Project aims.....	80
Chapter 2: Materials and Methods	82
2.1a) Investigating peri-operative variables that can affect the quality and quantity of RNA isolated from human peripheral nerve samples and 2.1b) Characterising cellular and molecular features of human peripheral nerve degeneration.....	82
2.1.1 RT-qPCR	82
2.1.2 Isolating the effects of antiseptic reagents on RNA yield using a rodent model of peripheral nerve liberation	86
2.1.3 RNA extraction protocol	87
2.1.4 Immunohistochemistry (performed by Dr. Naomi Guppy).....	91
2.1.5 Statistical analysis (nonparametric smoothing linear regression performed by Dr. Simão Larenjeira)	93

2.2 Motor Unit Number Estimation following nerve transfer to reanimate elbow flexion	95
2.2.1 Identification of patients	95
2.2.2 Surgical procedure.....	95
2.2.3 STA MUNE (carried out by Dr. Tom Tidswell)	96
2.2.4 Test-retest repeatability of the STA MUNE protocol.....	99
2.2.5 Statistical analysis (performed by Dr. Simão Laranjeira)	99
2.3 Investigating the relationship of Motor Unit Number Estimation with histological and functional measures of muscle reinnervation	100
2.3.1 Surgical nerve injury models in vivo	100
2.3.2 Nerve and muscle tissue harvest	101
2.3.3 Immunohistochemistry of nerve samples	101
2.3.5 Immunohistochemistry of muscle samples	104
2.3.6 Functional outcomes in vivo.....	105
2.3.7 Statistical analysis.....	109
2.4 Quantitative MRI muscle volume analysis following nerve transfer to reanimate elbow flexion.....	110
2.4.1 Patient selection	110
2.4.2 Quantitative MRI	111
2.4.3 Statistical analysis.....	113
Chapter 3: Investigating peri-operative variables that can affect the quality and quantity of RNA isolated from human peripheral nerve samples	114
3.1 Introduction	114
3.2 Results	116
3.3 Discussion.....	123
Chapter 4: Characterising cellular and molecular features of human peripheral nerve degeneration.....	128
4.1 Introduction	128
4.2 Results	133
4.3 Discussion.....	155

Chapter 5: MUNE following nerve transfer to reanimate elbow flexion	164
5.1 Introduction	164
5.2 Results	166
5.3 Discussion.....	172
Chapter 6: Investigating the relationship between MUNE and histological markers of muscle reinnervation.....	178
6.1 Introduction	178
6.2 Results	182
6.3 Discussion.....	197
Chapter 7: MRI biomarker assessment of reinnervated elbow flexor muscles following nerve transfer.....	202
7.1 Introduction	202
7.2 Results	204
7.3 Discussion.....	214
Chapter 8: Conclusions and future translation	219
8.1 Overall conclusions	219
8.2 Ongoing and future work	220
8.2.1 Relating MUNE and qMRI assessments to clinical assessments of muscular function.....	220
8.2.2 Clinical trial	221
8.2.3 PNI demographic audit	221
References	223
Appendix 1.....	273
Appendix 2.....	275
Appendix 3.....	276

Index of figures

CHAPTER 1

Figure 1.1 - Anatomy of the nerve trunk.

Figure 1.2 - Spontaneous activity recorded upon EMG examination of a denervated biceps muscle.

Figure 1.3 - MUAP recorded from a healthy participant and key morphological features.

Figure 1.4 - A graphical representation of how neurophysiological parameters change in the context of a degenerative nerve lesion.

Figure 1.5 - A summary of changes in the characteristics of MUAPs after nerve injury and at different stages of muscle reinnervation (Smith and Knight, 2011).

Figure 1.6 - T2-weighted MRI scans of uninjured and nerve injured biceps muscles from patient who sustained C5/6 Avulsion.

CHAPTER 2

Figure 2.1 - Experimental setup to record a sample of SMUAPs for the MUNE calculation.

Figure 2.2 - Experimental setup to record a biceps CMAP for the MUNE calculation.

Figure 2.3 - Fascicles of the tibial and common peroneal nerve.

Figure 2.4 - Microchannel neural interface used to stimulate the sciatic nerve.

Figure 2.5 - Single motor unit potentials (SMUAPs) recorded from an uninjured tibialis anterior muscle using an incremental stimulation technique.

Figure 2.6 - Toe spread measurements used to quantify the Static Sciatic Index.

CHAPTER 3

Figure 3.1 - The effect of time between tissue liberation and cryopreservation on RNA yield in human nerve tissue in a surgical environment utilizing standard antiseptic protocols.

Figure 3.2 - The effect of time delays and surgical antiseptic reagents on the quality of RNA isolated from human nerve tissue.

Figure 3.3 - Even when the time delay is minimized/equivalent between samples there is still a large differential in RNA yield due to exposure to surgical antiseptics.

Figure 3.4 - Even when the time delay is minimized/equivalent between samples there is still a large differential in RNA yield due to exposure to surgical antiseptics.

CHAPTER 4

Figure 4.1 - Reconstructive nerve procedures.

Figure 4.2 - Immunohistochemical detection of neurons in healthy and denervated human nerves.

Figure 4.3 - Immunohistochemical and RT-qPCR analysis of Schwann cells in healthy and denervated human nerves.

Figure 4.4 - Immunohistochemistry and RT-qPCR analysis of c-Jun in healthy and denervated human nerves.

Figure 4.5 - Immunohistochemistry and RT-qPCR analysis of P75NTR in healthy and denervated human nerves.

Figure 4.6 - Immunohistochemistry and RT-qPCR analysis of Krox-20 in healthy and denervated human nerves.

CHAPTER 5

Figure 5.1 - The double Oberlin's nerve transfer is commonly deployed to restore elbow flexion.

Figure 5.2 - Percentage recovery of MUNE over time in reinnervated muscles compared to contralateral uninjured muscles post-operatively.

Figure 5.3 - Changes in the mean magnitude of SMUAPs post-operatively as a proportion of CMAPs.

Figure 5.4 - Changes in the magnitude of CMAP in the reinnervated arm post-operatively compared to the uninjured arm.

CHAPTER 6

Figure 6.1 – MUNE and ChAT counts of uninjured tibialis anterior and gastrocnemius muscles.

Figure 6.2 – Relationship between MUNE recordings from the tibialis anterior muscles and ChAT counts from the nerve segment to tibialis anterior.

Figure 6.3 – Relationship between MUNE and NMJ reinnervation of the tibialis anterior muscle following sciatic nerve crush.

Figure 6.4 – Relationship between MUNE, SSI and time following injury.

CHAPTER 7

Figure 7.1 - T1-w, T2-w and PDW signal changes within denervated and reinnervated elbow flexor muscles.

Figure 7.2 - Changes in elbow flexor muscle volume pre- and post-nerve transfer.

APPENDIX 1

Figure 9.1 - Positive controls for immunohistochemistry.

APPENDIX 2

Figure 10.1 - ChAT staining of sural nerve section (negative control).

APPENDIX 3

Figure 11.1 - Quantitative immunohistochemistry analysis of healthy nerves.

Figure 11.2 – Axon counts in healthy nerves.

Figure 11.3 – RT-qPCR data for healthy nerve group.

Index of tables

CHAPTER 1

Table 1.1 - The properties of different nerve fibre types.

Table 1.2 - A summary of the Seddon and Sunderland classification systems and their likely functional outcomes and required surgical intervention.

Table 1.3 - The Medical Research Council (MRC) grading system of muscle power.

CHAPTER 2

Table 2.1 - Demographic of patients and samples included in this study

Table 2.2 - Sequences of forward and reverse primers used in the RT-qPCR assays.

Table 2.3 - MRI imaging parameters used to acquire scans of injured and uninjured elbow flexor muscles.

CHAPTER 4

Table 2.1 - Tabulation of the patient demographic included in this study and details of nerve sample liberated.

CHAPTER 5

Table 5.1 - Tabulation of patient demographics in Chapter 5: MUNE following nerve transfer to reanimate elbow flexion.

Table 5.2 - Test-retest MUNE results for uninjured biceps muscles.

Table 5.3 - Mean MUNE values from uninjured and injured arms.

CHAPTER 7

Table 7.1 - Demographic of patients included in Chapter 7: MRI biomarker assessment of reinnervated elbow flexor muscles following nerve transfer.

Table 7.2 - Scan-rescan, inter- and intra-investigator repeatability of the imaging and segmentation protocol.

Index of equations

CHAPTER 2

Equation 2.1 - Livak method of quantification.

Equation 2.2 - MUNE calculation.

Equation 2.3 - Equation used to determine MUNE.

Chapter 1: Introduction

1.1 Peripheral nerve anatomy

The peripheral nervous system (PNS) consists of neuronal cells, glial cells and stromal cells. Peripheral nerves relay signals from the spinal cord to the rest of the body and from sensory receptors to the central nervous system (CNS). Nerve trunks principally comprise efferent and afferent neurons. Efferent fibres can be made up of motor and autonomic fibres which receive signals from dendrites at the spinal cord primarily through the neurotransmitters acetylcholine, glutamate (e.g from sensory neurons), glycine (inhibitory neurons) and several others. Afferent neurons can be somatic or autonomic in origin and receive a variety of sensory inputs such as from the dendrites of specialised cells such as Pacinian corpuscles located in the skin which detect fine sensation.

Schwann cells, the glial cells of the peripheral nervous system, surround individual axons and have a number of important functions. These cells produce myelin which allows saltatory conduction along myelinated fibres. A α motor fibres represent the most heavily myelinated followed by A β afferent muscle spindle fibres. Both fibres have a conduction velocity of around 30-120m/s. On the contrary, C fibres are unmyelinated and therefore the slowest conducting at 1-2m/s. These fibres relay information from the periphery to the CNS about pain, temperature and also make up the post-ganglionic sympathetic system. The properties of the different fibres in the PNS are summarised in **Table 1.1**.

Non-neuronal cells and connective tissue surrounding the nerve trunk have an important function in providing a structural scaffold for the nerve and adapting it for its function. An endoneurium surrounds individual axons. Groups of axons are surrounded by the perineurium which is a multi-cellular layer composed of specialised perineurial cells with tight junctions forming a fluid barrier. Surrounding this is a layer

of the epineurium which contains a network of cellular, lymphatic and vascular structures which penetrate to deeper layers of the nerve trunk. These are important for the normal functioning of nerves and their response to injury. A visual representation of the nerve trunk and its corresponding microanatomy is shown in **Figure 1.1**. The extent of damage to this network is important in classifying nerve injuries (Geuna et al., 2009).

Fibre Class	Myelin Sheath	Diameter (μm)	Conduction Velocity (m/s)	Spinal Cord Tract	Location	Function
A α	Yes	6-22	30-120	Ipsilateral dorsal column	Efferent to muscles	Motor
A β	Yes	6-22	30-120	Contralateral spinothalamic tract	Afferent from skin and joints	Tactile, proprioception
A γ	Yes	3-8	15-35	Ipsilateral dorsal column	Efferent to muscle spindles	Muscle tone
A δ	Yes	1-4	5-30	Contralateral spinothalamic tract	Afferent sensory nerves	Pain, cold, temperature, touch
B	Yes	1-3	3-15	Preganglionic	Preganglionic sympathetic	A number of autonomic functions
sC	No	0.3-1.3	0.7-1.3	-	Postganglionic sympathetic	A number of autonomic functions
dC	No	0.4-1.2	0.1-2.0	Contralateral spinothalamic tract	Afferent sensory nerves	A number of autonomic functions Pain, warm, temperature, touch

Table 1.1 - The properties of different nerve fibre types (Simon et al., 2016b). Nerve fibres can be classified according to the presence of a myelin sheath, diameter, conduction velocity, spinal cord tract, location and function.

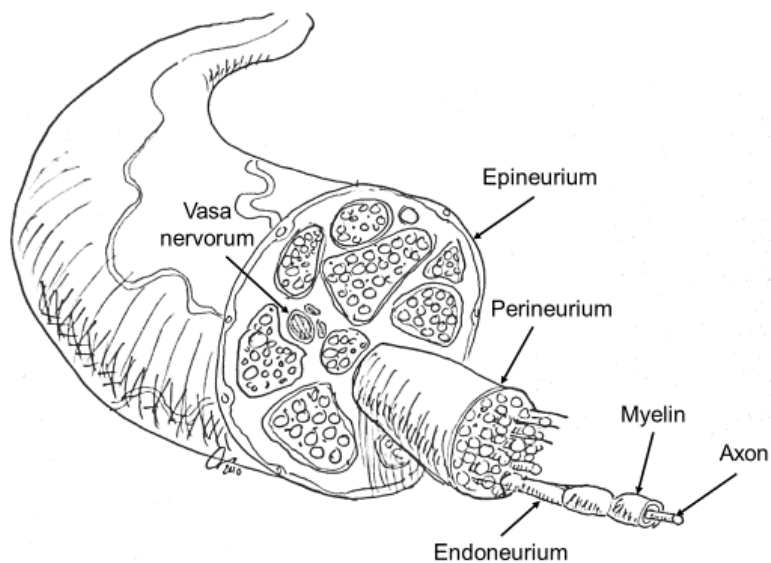


Figure 1.1 - Anatomy of the nerve trunk. Axons are arranged into fascicles surrounded by perineurium. Individual axons are encased by an endoneurium. Illustration by Mr. Tom Quick.

1.2 Classifications of Peripheral Nerve Injuries

Nerve tissue is viscoelastic. Therefore, in closed injuries the severity (grade) of nerve injury largely depends upon the magnitude, rate of application and duration of the forces applied to the nerve trunk. A number of systems exist for the classification of PNI which are based upon the extent of damage to the microanatomy of the nerve trunk. The Seddon and Sunderland classification systems have been widely deployed to assist in determining the severity, prognosis and treatment strategy of PNI (**Table 1.2**) (Seddon, 1943, Sunderland, 1951, Dellon and Mackinnon, 1988). Mackinnon and Dellon modified Sunderland's classification to include a mixed injury type to better reflect clinical practice. Millesi's classification goes one step further to relating the severity of focal nerve injuries requiring reconstruction to the surgical steps necessary to reconstruct these (Millesi, 1985).

Grade I injuries (neurapraxia) may be secondary to a single or persistent event. This type of injury is particularly prevalent in anatomical locations where nerves may be susceptible to stretch or compression such as in osseofascial tunnels and following blunt trauma or stretch injuries. Spontaneous recovery almost always ensues in weeks to months following injury. Neurapraxia can be described as a conduction block which means the nerve is anatomically intact but physiologically broken.

Grade II injuries (axonotmesis), lie within the mild end of the degenerative spectrum. Here, there is discontinuation of the axons but preservation of the surrounding connective tissue usually following blunt trauma. Spontaneous recovery is common and surgical intervention is rarely indicated in the absence of intra-neural scar tissue.

In Grade III-Grade V injuries (Grade III and Grade IV: axonotmesis, Grade V: Neurotmesis) there is more widespread disruption to the anatomy of the nerve trunk. These grades of injuries are more common in blunt, stretch and/or penetrating trauma. The restoration of function is often not possible without surgical intervention.

Whilst these classification systems may be a useful tool in determining the anatomical extent of nerve damage and likely functional outcomes, they are unlikely to reflect the clinical picture. Injuries often do not damage the nerve trunk uniformly meaning that these classification systems most likely do not reflect the heterogenous pathology. It is more likely that nerves demonstrate a mixed classification of nerve injuries (Dellon and Mackinnon, 1988, Mackinnon and Dellon, 1988, Timothy, 2014).

The biological processes that underpin functional recovery depend largely upon the grade of the injury.

Seddon classification	Neuropathology	Sunderland classification	Surgical intervention required?	Likely functional outcome
Neurapraxia	Segmental demyelination	Grade I	Not unless the pathology is persistent	Complete recovery most likely without surgical intervention
Axonotmesis	Transection of the axons but the remaining endoneurium, perineurium and epineurium intact	Grade II	Not likely	Often complete recovery without surgical intervention
Axonotmesis	Transection of axons, endoneurium with preservation of the perineurium and epineurium	Grade III	Maybe	Unlikely complete without surgical intervention
Axonotmesis	Transection of axons, endoneurium, perineurium with preservation of the epineurium	Grade IV	Yes	Poor without surgical intervention
Neurotmesis	Disruption of the entire nerve trunk	Grade V	Yes	Requires surgical intervention
Mixed	Combination of Sunderland Grade I to Grade V	Grade VI	Yes	Requires surgical intervention

Table 1.2 - A summary of the Seddon and Sunderland classification systems and their likely functional outcomes and required surgical intervention (Dellon and Mackinnon, 1988, Mydlarz and Boahene, 2013, Kaya and Sarikcioglu, 2015).

1.3 Neurobiology of peripheral nerve regeneration

An understanding of the biological processes that underpin regeneration and functional recovery in those who have suffered neural trauma is necessary in order to understand and interpret pathological changes on clinical tests.

1.3.1 Neurapraxia (grade I injury)

Pathologically, neurapraxia has a number of potential causes of physiologic dysfunction. The most well characterised is focal demyelination. Degeneration of the myelin sheath impairs conduction of action potentials by changing the mechanical and physical properties of the internodal and paranodal membranes. The capacitance of the membranes increases accompanied by a reduction in the resistance between the paranodal and internodal regions (Bostock and Sears, 1976). The result is a deficiency of current which is able to depolarise the next node of Ranvier. The demyelination of the paranodal segment with the increased exposure of the K^+ channels leads to persistent hyperpolarisation (Smith and Knight, 2011). The activity of the Na^+/K^+ ATPase pump further pushes the resting potential towards the K^+ equilibrium potential (Bostock et al., 1981). The result is the block of conduction leading to clinical signs that are comparable to a lesion that has led to axonal loss.

1.3.2 Biological processes that underpin neural regeneration (grade II – V injuries)

Neural regeneration is a key biological process in those recovering from lesions which have resulted in axonal degeneration. A number of cellular and molecular mechanisms at multiple levels are involved: the CNS, neuron cell body along with the proximal and distal stumps.

Changes at the CNS

The CNS undergoes rapid and long lasting remodelling following PNI. The mechanisms which underpin plasticity and reorganisation in the spinal cord and brain

following axon transection are highly complex and remain poorly understood. Changes within these systems may result in beneficial adaptive functional changes or may cause maladaptive changes which result in symptoms such as neuropathic pain, hyper-reflexia and dystonia. There are currently no effective treatments which can ensure full sensorimotor recovery (Churchill et al., 2001, Hansson and Brismar, 2003, Duff, 2005).

Changes at the cell body and proximal stump

Cellular and molecular changes at the neuronal cell body and the proximal stump are dependent upon a number of factors such as the severity of the injury and the proximity of the lesion to the cell body. At the site of the nerve injury, there is Wallerian degeneration back to the previous node of Ranvier (Waller Augustus and Owen, 1851, Beirowski et al., 2004). In severe injuries, degeneration may extend more proximally and include the cell body in which case the whole proximal segment disintegrates and is phagocytosed. The nerve cell body reacts to injury through a process known as chromatolysis which involves migration of the nucleus to the cell periphery and Nissl granules from the rough endoplasmic reticulum disintegrating and dispersing. Simultaneously, there is proliferation of peri-neuronal glial cells. The glial cell processes extend and interrupt synaptic connections to isolate the nerve as it enters a regenerative phase (Lee and Wolfe, 2000, Severinsen and Jakobsen, 2009).

These events are accompanied by a change in the phenotype of axons and Schwann cells from one that supports myelination and the propagation of action potentials, to one that promotes axonal regeneration and sprouting from the proximal stump (Jessen and Arthur-Farraj, 2019, Jessen and Mirsky, 2019). Axons sprouting from the proximal stump are reduced in diameter especially when functional connections to appropriate end organs are not re-established (Giannini et al., 1989, Ikeda and Oka, 2012). As axonal regeneration and reinnervation of the target end organ ensues,

axonal diameter increases although this rarely returns to pre-injury levels (Giannini et al., 1989, Ikeda and Oka, 2012). The recovery of the axon and the cell body appear to have some symbiosis; the cell body does not fully recover until functional connections are re-established with the target end organ and the final diameter of the regenerating axons depends to a large extent on the recovery of the cell body (Burnett and Zager, 2004, Mar et al., 2014).

Changes at the distal stump

Almost immediately after PNI, there is Wallerian degeneration along a proximo-distal gradient (Waller Augustus and Owen, 1851, Lubinska, 1982). This biological process can be stratified into two distinct stages; a latent phase followed by an aggressive granular phase of neural degeneration (Burnett and Zager, 2004). The time course for complete degeneration of the axons takes around 4-7 days (Chaudhry and Cornblath, 1992, Gaudet et al., 2011, Smith and Knight, 2011). As a result, Schwann cells distal to the injury site lose contact with axons as they degenerate. This represents a radical change in the tissue microenvironment since the key signals that control the phenotype of Schwann cells come from axons (Cattin et al., 2015, Parrinello et al., 2010, Jessen and Arthur-Farraj, 2019). Further stimulus for change is provided by biological factors secreted by immune cells such as macrophages which infiltrate the damaged nerve segment (Rotshenker, 2011, Martini et al., 2008). In response, Schwann cells demonstrate a significant biological response; myelinating and Remak Schwann cells convert to a repair phenotype in order to promote axonal regeneration (Jessen and Mirsky, 2016).

A principal component of this repair phenotype is reversal of myelin differentiation which is marked by the downregulation of genes coding for Krox-20, cholesterol related enzymes and myelin-related proteins such as Myelin Associated Glycoprotein (MAG) and Myelin Basic Protein (MBP) (Boerboom et al., 2017, Jessen and Mirsky,

2016). On the other hand, molecules that characterise developing Schwann cells and mature adult Remak cells such as P75 neurotrophin receptor (P75NTR) are up-regulated (Boerboom et al., 2017, Jessen and Mirsky, 2016). The second component of this response is characterised by the appearance of unique repair-supportive phenotypes. This includes factors that enhance the survival and elongation of injured axons such as Nerve Growth Factor (NGF) and P75NTR (Grothe et al., 2006, Fontana et al., 2012, Brushart et al., 2013). Second, an innate immune response is stimulated which includes upregulation of a plethora of cytokines such as Interleukin-1 α (IL-1 α) and leukaemia inhibitory factor (LIF) which attract macrophages to the injury site (Martini et al., 2008, Rotshenker, 2011) and act on the injured axons to encourage regeneration (Cafferty et al., 2001, Hirota et al., 1996). Thirdly, there is extensive Schwann cell proliferation and elongation as they form aligned columns (Bungner bands) which are critical to guide axons back to their targets (Gomez-Sanchez et al., 2017b). Finally, Schwann cells activate molecular pathways which encourage myelin autophagy (Gomez-Sanchez et al., 2015, Lutz et al., 2017, Jang et al., 2016, Suzuki et al., 2015).

The transcription factor c-Jun plays a critical role in this Schwann cell injury response. c-Jun levels in uninjured nerves are low and are rapidly and strongly up-regulated in injured nerve segments (Shy et al., 1996, De Felipe and Hunt, 1994). When c-Jun upregulation is prevented in c-Jun knockout mice, the regeneration of axons and functional recovery is significantly impaired whilst uninjured nerves retain a normal phenotype (Arthur-Farraj et al., 2012). Together, this suggests that c-Jun is essential for mediating the response of Schwann cells to injury but have a limited role in maintaining normal axonal function (Arthur-Farraj et al., 2012). Studies have since shown that c-Jun indirectly regulates the expression of a number of genes which are implicated in the Schwann cell injury response, de-differentiation of myelin cells and

activation of the repair programme (Arthur-Farraj et al., 2012, Arthur-Farraj et al., 2017).

Animal paradigms of chronic denervation have shown that this response fades over time (Eggers et al., 2010, Hoke and Brushart, 2010). A number of studies have shown that nerve stumps which have suffered a neurotmesis injury demonstrate full or mildly reduced capacity for supporting axonal regeneration for approximately a month (Li et al., 1997, Sulaiman et al., 2002). By two months, the support for regeneration remains unchanged or diminished by up to 50% (Kou et al., 2011, Sulaiman and Gordon, 2000). This further declines over subsequent months to very low levels after six months (Gordon et al., 2011, Li et al., 1997). This loss in the ability to support regenerating axons is particularly pertinent in the context of human nerve injuries where the slow rate of axonal regeneration (around 1mm/day) (Sunderland, 1947) often results in chronic denervation of the distal environment. This deterioration in support for axonal regeneration has been attributed to a number of different mechanisms. For a number of years it was thought that Schwann cell proliferation is critical for successful nerve repair (Hall, 2005, Hall and Gregson, 1977). However, more recent findings have brought this into question (Kim et al., 2000, Yang et al., 2008). It is more likely that the fading of the repair Schwann cell phenotype combined with declining cell numbers are majority contributors to the failure of repair Schwann cells to support regeneration (Jessen and Mirsky, 2019).

Whilst the cellular and molecular mechanisms that underpin the success and failure of this critical Schwann cell response to nerve injury have been extensively studied in rodent models of nerve repair (Jessen and Mirsky, 2019), corresponding studies in humans are not well documented. Addressing this issue would be an important step towards the development of new therapies to improve human peripheral nerve repair and improving the clinical management of patients (Wilcox et al., 2020b, Rayner et

al., 2019). Unfortunately, progress is limited by ethical and practical challenges associated with studying human nerve injury.

1.3.3 Retrieving human nerve samples for study in the laboratory

Investigative methods such as RNA seq (RNA sequencing) and/or RT-qPCR are often deployed in studies to characterise the cellular and molecular mechanisms that underpin the regenerative capacity of the rodent PNS (Bosse, Kury, and Muller 2001; Clements et al. 2017; Jiang et al. 2014; Yi et al. 2017). Whilst it is possible to liberate human nerve tissue for study during reconstructive nerve repair, samples that can be extracted are often small and have varied morphology. Further, nerve samples are exposed to the complex surgical environment, which includes chemical and physical environmental factors, time pressures and other priorities which are not present when sampling animal tissues in a laboratory setting. This affords numerous challenges when optimising protocols for the extraction of RNA with sufficient quantity and quality for quantitative analysis (Wilcox et al., 2019b). Studies that have explored and measured these challenges in detail are needed to develop an optimised protocol for quantitative analysis of mRNA. This will be a pertinent step towards better understanding the cellular and molecular mechanisms that underpin human nerve regeneration.

1.3.4 Changes at the neuromuscular junction and within the muscle

Following neural injury, the neuromuscular junction (NMJ) and the target muscle endure significant changes. The NMJ undergoes extensive remodelling with increases in gutter depth, fragmentation and plate area (Ma et al., 2005). Simultaneously, the muscle begins to atrophy and the diameter of muscle fibres begins to decline with a reduction in muscle fibre conduction velocity (Kraft, 1990). There are also a number of changes at cellular and molecular levels; mRNAs coding for nicotinic acetylcholine receptor synthesis and myogenic regulatory factors are up-

regulated initially followed by a regression back to normal (or subnormal levels) as denervation time increases or reinnervation ensues (Kraft, 1990, Voytik et al., 1993, Adams et al., 1995, Weis et al., 2000, Ma et al., 2005, Ma et al., 2007).

After denervation the overall quantity of muscle fibres has been shown to remain constant for up to one year in animal models (Ashley et al., 2007). However, the individual fibres atrophy and change types altering the distribution and proportion of muscle fibre types (Ashley et al., 2007). The direction and extent of this shift is complex and variable within different muscles (Pette and Vrbova, 1985, Windisch et al., 1998, Kostrominova et al., 2005, Mendler et al., 2007). For example, type IIB and IIC fibres in rat Extensor Digitorum Longus (EDL) and tibialis anterior muscles shift towards type I and IIA slow fibres following denervation (Pette and Vrbova, 1985, Windisch et al., 1998). If reinnervation is achieved, the signal generated by the motor cortex is thought to determine the proportion and distribution of muscle fibre types (Hughes et al., 1993).

For many years, it was thought that changes within the muscle were largely responsible for poor functional outcomes in patients where nerve repair was delayed (Fu and Gordon, 1995). However, animal models have shown that axons still have the capacity to grow into chronically denervated muscle (Fu and Gordon, 1995, Saito and Dahlin, 2008). This suggests that in the absence of intra-neural scar tissue, changes within the chronically denervated distal nerve stump are majority contributors to making the environment increasingly antagonistic to nerve regeneration (Ronchi and Raimondo, 2017).

In summary, considering clinical observations in the light of findings in animal paradigms of reinnervation, it is thought that optimum functional recovery is largely dependent on a sufficient quantity and quality of axons reinnervating the muscle within 1 year following injury (Dellon and Mackinnon, 1988, Mackinnon et al., 2005,

Tung and Mackinnon, 2010). Beyond this time frame, it is thought that phenotypic changes of Schwann cells, axons and irreversible degenerative changes at the motor endplate create an environment that becomes increasingly antagonistic to regeneration (Tung and Mackinnon, 2010, He et al., 2014, Jessen and Mirsky, 2019). Despite significant advancements in surgical interventions for the treatment of PNI, muscle recovery is often seen by the patient as being functionally incomplete (Scheib and Hoke, 2013). A number of treatments have been developed in preclinical models that modulate these biological processes to promote axonal regeneration, preserve denervated muscle and/or modulate complex remodelling of the CNS (Lee and Wolfe, 2000, Faroni et al., 2015). Clinical translation is hindered by the lack of outcome measures that are responsive and/or sensitive enough to detect and quantify the biological changes associated with muscle denervation and reinnervation. The success or failure of these biological events can be monitored to an extent through clinical evaluations of nerve regeneration.

1.4 Clinical measurements of nerve injury and regeneration

Clinical assessments are ultimately an evaluation of function and do not measure nerve regeneration in isolation. The Tinel sign, described over a century ago (1917), measures the advancement of regenerating axons by percussing on the skin along the anatomical course of the nerve (Macdonald, 1918). It is the only test that can monitor the recovery of axons following a degenerative lesion prior to any end-organ reinnervation.

It should be recognised that there is unlikely to be a linear relationship between the quantity and quality of neuronal regeneration and functional recovery. This is because there are many layers of complexity within the regenerating system. For example, within a certain range (down to around 20% of the original number of axons) a denervated muscle can still become fully reinnervated and may still develop pre-injury

peak force. However, it may be reinnervated by axons which were originally from a differing muscle (a process called axonal confusion) (Seitz et al., 2011, Alvarez et al., 2011). This may lead it to function incorrectly or not be under the patient's easy conscious control. As a result, the muscle is likely to have reduced gradeability of force, increased fatigue and co-contract with antagonists. It may also demonstrate decreased proprioception, altered tendon reflex and overall tension. Moreover, the joints the nerve serves may become stiff and the overlying skin may become dry and painful. These peripheral mechanisms are accompanied by parallel central processes demonstrating that there is a highly complex system at play here. The relationship between axonal recovery and subjective measurements of function is also further complicated by psychological and environmental aspects. Normal nerve function in humans allows interaction with our environment through experiences such as pain, touch and temperature. Therefore, it is not surprising that injury to this complex system also results in changes to the way in which one perceives themselves. It follows that clinical assessments should be holistic to mirror the multimodal functions of the PNS. Measures reported by the clinician such as reported pain, sensibility, motor function, electro-diagnostics and imaging should be considered alongside patient reported measures. Some of the commonly deployed and recommended clinical measures of functional recovery are discussed.

1.4.1 Sensibility

Sensibility can be defined as the ability to perceive and assimilate sensation. Detection, discrimination, quantification and identification represent the four levels of sensibility which include all the characteristics of touch, stereognosis and proprioception. This provides some indication as to the integrity of afferent/sensory neurons which receive input from a variety of sources such as free sensory nerve

endings in addition to dendrites from specialised cells such as Pacinian corpuscles among others. This information is then relayed to the somatosensory cortex.

The ability of patients to detect static touch and cutaneous pressure is most commonly determined using the Semmes-Weinstein monofilament test and/or the Weinstein Enhanced Sensory Test (WEST) (Weinstein, 1993, Jerosch-Herold, 2005). These tests have yielded good sensitivity and reliability in detecting changes over time (Jerosch-Herold, 2005). The next level of sensibility is discrimination. The most commonly deployed by clinicians is the two-point discriminatory test which is included in the Medical Research Council (MRC) assessment of sensory recovery providing a measurement of recovery across an 8 point scale. However, a number of studies have raised concerns over the sensitivity of this measure (Chassard et al., 1993, Jerosch-Herold, 2005).

The final component of sensibility is stereognosis which is defined as the ability to recognise an object without any visual cues. The Shape Texture Identification (STI) test is commonly used and has demonstrated good reliability and sensitivity in monitoring outcomes during the recovery of median and ulnar nerves (Rosen and Lundborg, 2003, Jerosch-Herold, 2005).

A complex relationship exists between the communication of afferent neurons with the CNS. By extension, this affords numerous challenges when trying to determine what relationship each of these assessments has to the biological processes associated with nerve regeneration.

1.4.2 Pain

Nociceptive and neuropathic pain are highly prevalent following PNI. The incidence of neuropathic pain following traumatic injuries that involve the brachial plexus in adults has been reported to be as high as 50% (Ciaramitaro et al., 2010). The symptom of pain is measured in clinical practice by using visual or verbal scale of

intensity from 0-10 (Delgado et al., 2018). Other scales exist with written descriptors ranging from “no pain” to “worst pain imaginable” exist (Delgado et al., 2018). The PNI score is a simplified version of this assessment (Birch, 2011a). However, assessment of intensity in isolation is unlikely to reflect the complexity of the lived experience of pain. The International Association for the Study of Pain (IASP) definition of pain is “an unpleasant sensory and emotional experience associated with actual or potential tissue damage” (1986). This definition reflects that pain goes beyond severity alone to better reflect the lived experience of the patients. Outcome measures such as the McGill pain questionnaire which measure pain beyond intensity alone are likely to better reflect this.

In summary, this symptom is likely to have biological effects at multiple levels as well as psychological impacts which can complicate any attempt to establish outcome measures that relate the biological processes of nerve regeneration with patient function and experience.

1.4.3 Motor function

The function of an innervated muscle provides active range of movement (AROM) across a joint. The function of multiple muscles across joints leads to the coordination of movement. The movement across numerous joints allows us to carry out functional tasks. It follows that any assessment of function should reflect each of these components. Measurements of AROM give some indication as to the recovery from paralysis following PNI. The recovery of force often involves measurements of peak volitional force (PVF) as assessed by the Medical Research Council (MRC) grading system of muscle power (**Table 1.3**) from 0-5. The MRC grading system is universally incorporated into manual muscle testing (MMT) which has shown good reliability in distinguishing between nerve injured and uninjured muscles (Aberg et al., 2007). However, the MRC grading system has a number of limitations. Firstly, there is some

subjectivity in the grading as to what is “normal power”. This ambiguity can make distinguishing between MRC grade 4 and 5 challenging (**Table 1.3**). For these reasons, it has been argued that MRC grading of muscle power is an insensitive outcome measure with over 96% of recordings falling within MRC grade 4 (MacAvoy and Green, 2007). This has led to the more widespread use of continuous measurements of PVF using handheld dynamometry (Quick et al., 2016).

Medical Research Council (MRC) score	Muscle response
0	No movement
1	Flicker of movement
2	Movement with gravity eliminated
3	Movement against gravity only (no resistance)
4	Movement against moderate resistance
5	Normal power

Table 1.3 - The Medical Research Council (MRC) grading system of muscle power.

More recently, qualitative studies have refocused attention onto parameters important to patients. Earlier onset of fatigue, increased co-contractibility and pain have been identified as pertinent characteristics of reinnervated muscle by patients (Chammas et al., 1997, Brown et al., 2018). This suggests that assessments of recovered motor function should include objective and subjective measurements beyond that of PVF. It follows that it is important to bear in mind how the entire limb is integrated into daily functional activities. The Sollerman Hand function test and Action Research Arm Test (ARAT) are examples of assessments that measure integrated function in hemiplegic patients (Sollerman and Ejeskar, 1995, Hsueh et al., 2002, McDonnell, 2008, Weng et al., 2010) but they are yet to be validated in a clinical setting of PNI. Patient Reported Outcomes (PROs) are also becoming increasingly utilised globally; resilience and coping strategies are thought to be key predictors of clinical outcomes (Rainey et al., 2014, Jayakumar et al., 2018).

In summary, many clinical measures of nerve regeneration are subjective and do not fully represent the lived patient experience of muscle reinnervation (Brown et al., 2018). By extension, many of these outcome assessments are insensitive and unresponsive to the biological process of nerve regeneration. There is a need to develop objective and subjective metrics that better reflect the lived experience of muscular recovery and what relationship this has to more direct assessments of the biological process of nerve regeneration.

1.5 Neurophysiological investigation of peripheral nerve injuries

Neurophysiological changes are evident long before the onset of clinical signs of muscle reinnervation. Nerve Conduction Studies (NCS) and electromyography (EMG) are indispensable tools in the pre- intra- and post-operative evaluation of PNI. The information provided by these tests can provide invaluable information to the clinician about the anatomical site of the nerve lesion and its severity. Moreover, changes detected using these tests correlate with biological processes of nerve regeneration at multiple levels; the denervated muscle, injured nerve segments and the CNS.

1.5.1 Nerve Conduction Studies

Nerves and muscles are excitable tissues therefore their potentials can be induced and recorded. NCS measure changes in the excitability of nerves and muscles following injury. NCS represent the first line of investigation in the case of suspected PNI requiring minimal patient cooperation. Pertinent parameters that are measured during NCS are:

Compound Muscle Action Potential (CMAP): The summated action potentials of all stimulated motor endplates. It can be obtained by supra-maximal percutaneous stimulation of the trunk of the nerve and recording the response of the muscle. The amplitude of the CMAP can be measured as peak to peak and is largely determined

by the number of functional MUs within a muscle, temporal dispersion, magnitude and duration of single muscle fibre action potentials. The distal latency can be defined as the time between stimulation of the nerve and the onset of the evoked response. The motor conduction velocity can be assessed by the conduction distance divided by the conduction time (Smith and Knight, 2011).

Sensory Nerve Action Potential (SNAP): This represents the response of a sensory nerve following electrical stimulation. Recording is often performed using surface electrodes placed over the skin. The use of needle electrodes may be warranted when examining nerves that are difficult to access due to anatomical reasons (e.g. if the nerve is particularly deep to the skin surface). The magnitude of SNAPs are much smaller than CMAPs. Latency of the SNAP can be determined by the time taken for the initial deflection from baseline following stimulation. The sensory nerve conduction velocity can be calculated as the conduction distance from the stimulating electrode divided by the latency.

1.5.2 Electromyography

The response of the muscle to electrical impulses travelling along the nerves can be characterised using EMG. This involves recording the electrical activity of the affected muscle often through the insertion of a concentric needle electrode. The activity recorded on EMG is dependent to a large extent on patient the patient producing volitional contractions. EMG assessment can provide useful quantitative and qualitative information about Motor Unit Action Potential's (MUAPs). Spatiotemporal recruitment patterns of MUAPs in order to generate movements as well as the presence of denervation and reinnervation can be characterised. In the first step of EMG examination, spontaneous, insertional and volitional activity should be determined:

Insertional activity: The electrical activity recorded upon insertion of the needle electrode.

Spontaneous activity: This describes activity that manifests in denervated muscle such as fibrillations, positive sharp waves (attributable to spontaneously generated action potentials of individual muscle fibres), fasciculations (attributable to spontaneous discharges of individual motor units) and complex repetitive discharges (polyphasic action potentials that demonstrate uniform morphology and frequency of 5-100Hz with abrupt onset and offset) (**Figure 1.2**).

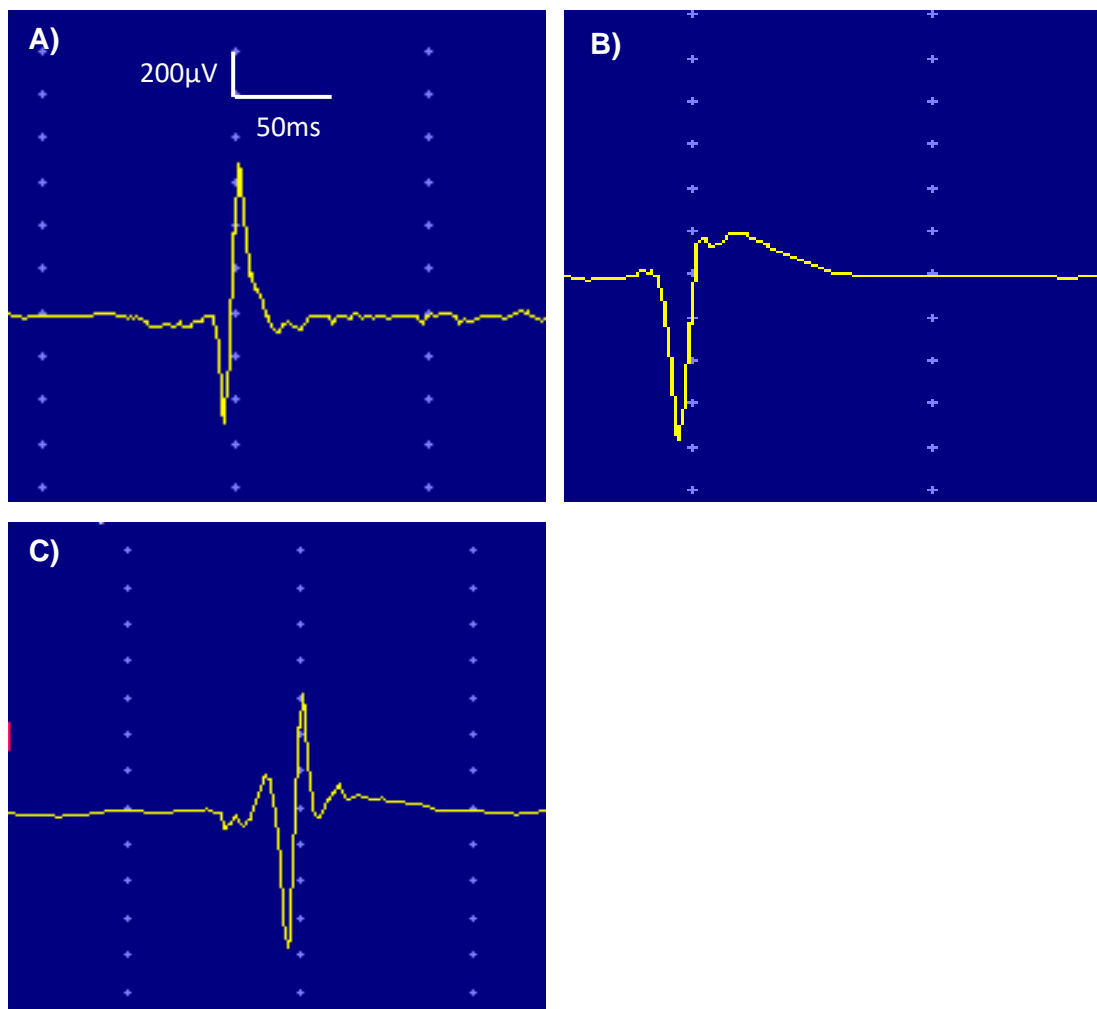


Figure 1.2 - Spontaneous activity recorded upon EMG examination of a denervated biceps muscle. **A)** Fibrillations **B)** Positive sharp wave **C)** Fasciculation.

Once spontaneous and insertional activity has been assessed, the EMG examination can progress onto evaluating different morphological features of MUAPs (**Figure 1.3**) and their firing characteristics. This can provide highly sensitive information about the microanatomy of MUs which can be correlated to biological processes of muscle reinnervation. Specific features of the MUAP and their anatomical correlates are:

Amplitude: Measured from the maximum negative peak to the maximum positive peak. The magnitude of the amplitude has a positive correlation with the quantity and size of muscle fibres within 0.5mm of the tip of the recording electrode (Buchthal et al., 1954a, Buchthal et al., 1954b, Gydkov et al., 1980, Bromberg, 1999).

Duration: Time interval between the initial shift of the MUAP away from baseline until its final return to baseline. The duration has a positive correlation with the number and size of muscle fibres that are within 2.5mm of the tip of the recording electrode (Buchthal et al., 1954a, Buchthal et al., 1954b, Gydkov et al., 1980, Bromberg, 1999).

Area: Calculated as the area under the rectified waveform for its entire duration. This parameter has a positive correlation with the number and size of muscle fibres within 2mm of the tip of the recording electrode (Buchthal et al., 1954a, Buchthal et al., 1954b, Gydkov et al., 1980, Bromberg, 1999).

Number of phases or turns: A phase represents the portion of the MUAP between initially deviating from baseline and returning to baseline. A turn describes a positive or negative peak throughout the duration of the MUAP. The number of phases and turns is positively correlated with the temporal dispersion of action potentials of muscle fibres within 1mm of the tip of the recording electrode (Buchthal et al., 1954a, Buchthal et al., 1954b, Gydkov et al., 1980, Bromberg, 1999). The recording of more than 4 phases is predictive of neurogenic muscle (Bromberg, 1999, Takehara et al., 2004).

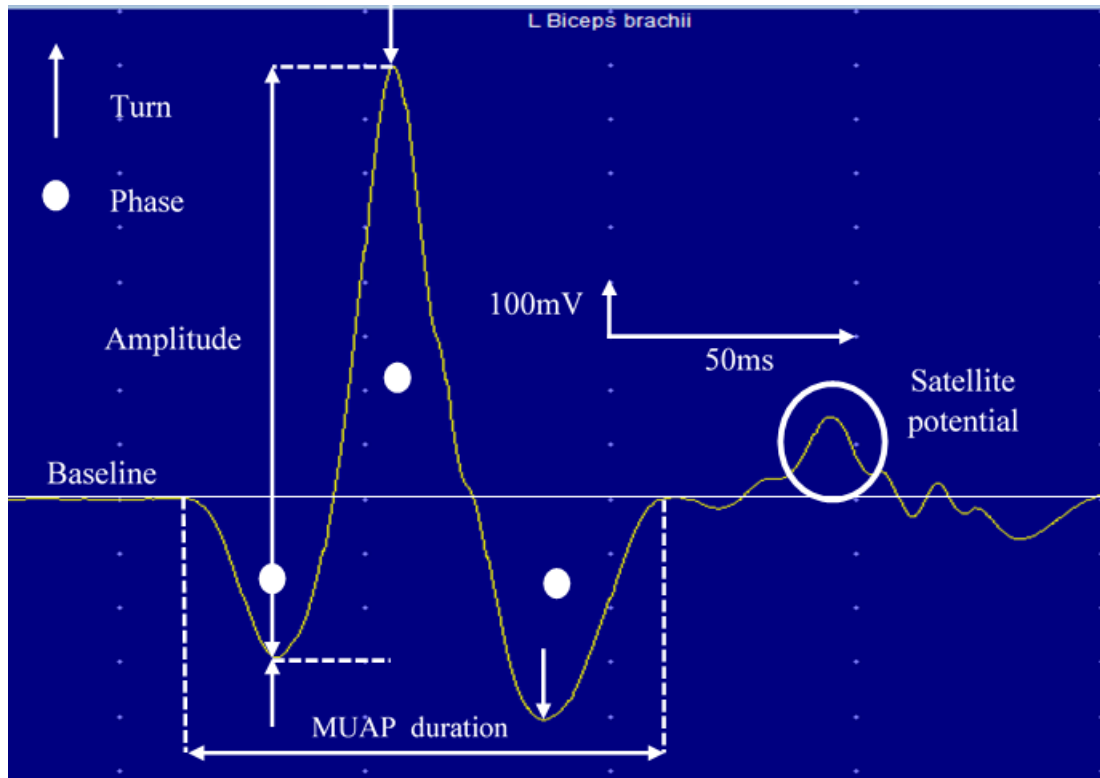


Figure 1.3 - MUAP recorded from a healthy participant and key morphological features.

1.5.3 Timing of neurophysiological assessment

Results from electrodiagnostic studies that accurately characterise the presence or absence of neuropathology associated with PNI depend to a large extent on the timing of investigation. The temporal sequence of electrodiagnostic changes following nerve injury are not linear or immediately apparent following injury (**Figure 1.4**) (Chaudhry and Cornblath, 1992, Smith and Knight, 2011). Moreover, the sequence of changes may be further confused by other factors such as the length of the distal stump with shorter stumps demonstrating an earlier onset of SNAP and/or CMAP abnormality following injury (Chaudhry and Cornblath, 1992, Smith and Knight, 2011). Therefore, the timing of neurophysiological assessment following PNI is critical in order to reach an accurate diagnosis.

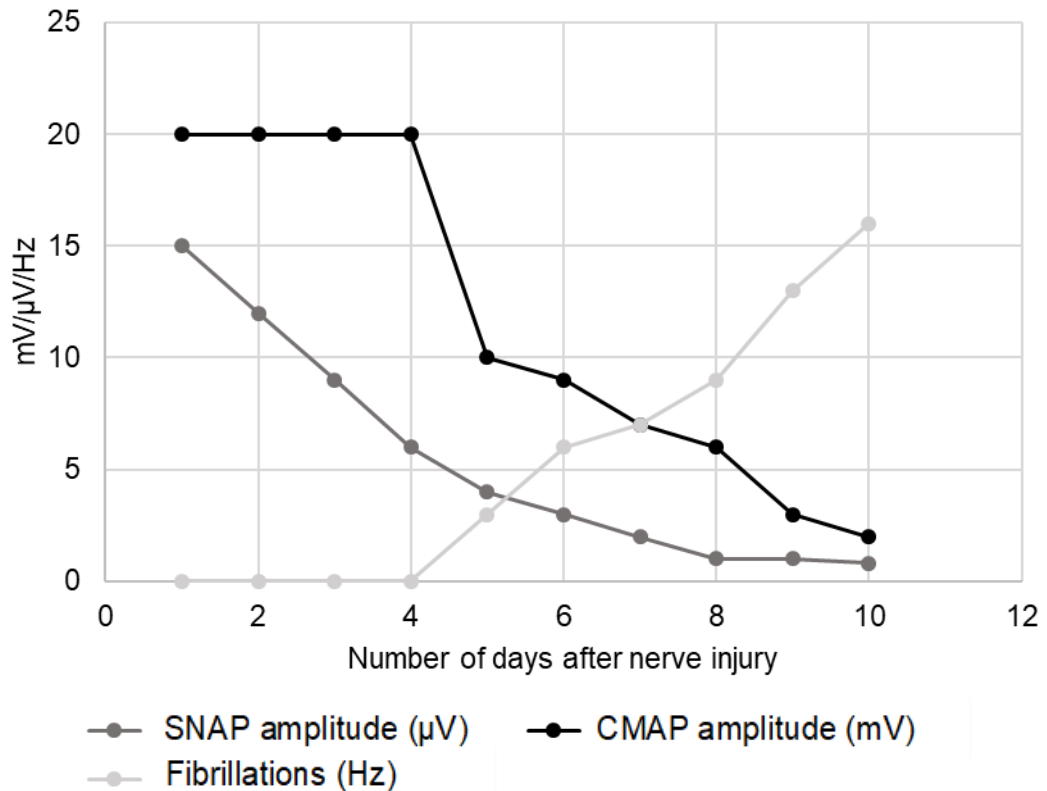


Figure 1.4 - A graphical representation of how neurophysiological parameters change in the context of a degenerative nerve lesion. Based on experimental findings and clinical observations following peripheral nerve injuries (Chaudhry and Cornblath, 1992, Smith and Knight, 2011).

In the context of a non-degenerative nerve lesion (Tinel negative, Grade I injury), myelinated fibres may undergo a pathological process of focal demyelination which results in conduction slowing and/or block. Conduction slowing in isolation does not lead to clinical symptoms unlike conduction block which presents similarly to a degenerative lesion resulting in the loss of sensory and motor function. The CMAP recording can be used to distinguish between a lesion that has caused axonal loss and conduction block; a CMAP that remains close to normal 7 days after the injury suggests that the target muscle has not undergone clinically significant axonal loss (Mallik and Weir, 2005, Smith and Knight, 2011). Considering how the evoked responses of sensory and motor nerve potentials change upon recording from above and below the lesion site can allow a diagnosis to be made with greater certainty. In

conduction block, the CMAP is preserved upon stimulation distal to the injury site and reduced upon stimulation proximally or at the injury site. On the contrary, the CMAP is impaired across the entire course of the nerve where there has been axonal loss.

In a degenerative nerve lesion (Tinel positive, Grade II – V injuries), the CMAP generally remains stable for a few days, declining 3-5 days after the injury before becoming absent over the next 2-4 days (**Figure 1.4**) reflecting the biological process of Wallerian degeneration. Changes in the sensory response tend to precede changes in the CMAP by 2-3 days (Chaudhry and Cornblath, 1992, Smith and Knight, 2011). The time course of these changes is dependent to a large extent on the length of the distal stumps; the onset of abnormalities in NCS recordings is delayed in longer stumps (Miledi and Slater, 1970).

Moving distally to the neuromuscular junction, no changes are evident until 8-20 hours following axonal transection when there is complete failure of neuromuscular transmission (Miledi and Slater, 1970). However, this time interval is dependent to a large extent on the length of the distal stump such that a decrease in the length of the distal stump reduces the time interval between transection and failure of neuromuscular transmission (Miledi and Slater, 1970, Smith and Knight, 2011). A reduction in the resting potential and increased sensitivity to acetylcholine are other changes that occur in response to a degenerative nerve lesion which are also dependent on the length of the distal stump (Smith and Thesleff, 1976). Proliferation of acetylcholine receptors at sites beyond that of the motor endplate are largely responsible for these observations (Miledi and Slater, 1970, Smith and Thesleff, 1976, Smith and Knight, 2011).

The appearance of abnormal spontaneous activity (fibrillations and sharp waves) occurs 1-4 weeks following injury (Smith and Knight, 2011, Chaudhry and Cornblath, 1992). This time interval is dependent on the distance between the injury site and

motor units in the target muscle (Smith and Thesleff, 1976, Chaudhry and Cornblath, 1992). Asynchronous and spontaneous depolarisation of the sarcolemma are responsible for the appearance of fibrillation potentials on EMG (Smith and Thesleff, 1976). This is attributable to ultra-structural changes which result in increased sodium conductance which propagate along the course of the muscle fibre (Smith and Thesleff, 1976, Smith and Knight, 2011). The intensity of fibrillation potentials is associated with the severity of axonal damage; a greater extent of axonal damage leads to more intense fibrillation potentials which regress over time (Smith and Knight, 2011, Wu et al., 2014).

In summary, considering the timing of changes in NCS and EMG recordings in the setting of different degrees of nerve injury, it is widely accepted that electro-diagnostic tests should be carried out between 8 and 10 days following the injury (Chaudhry and Cornblath, 1992, Mallik and Weir, 2005, Campbell, 2008, Smith and Knight, 2011). This optimises the chance for an accurate and timely diagnosis assisting in the clinical management of PNI.

Localising the lesion

The menu of tests on offer to the clinical neurophysiologist allows the examiner to localise the nerve lesion with a high degree of accuracy. First, the lesion can be classified as pre-ganglionic or post-ganglionic by examining SNAPs. In nerve injuries proximal to the dorsal root ganglion (DRG), SNAPs will be preserved as the sensory nerve cell bodies remain intact within the ganglion. This will be accompanied by anaesthesia in the dermatomal region together with impaired motor action potentials. In post-ganglionic lesions, the SNAP will be reduced owing to Wallerian degeneration in post-ganglionic sensory fibres.

1.5.4 Determining the extent of neural injury using electro-diagnostic testing

Further interrogation of features apparent on NCS and EMG recordings following neural injuries can be useful in further stratifying nerve injuries according to their severity.

Conduction block/Neurapraxia

Clinically, conduction block manifests as acute weakness of the limb. Motor NCS demonstrates a CMAP area/amplitude recorded proximal to the nerve lesion is reduced by at least 20% (usually >50%) when compared with the CMAP recorded distal to the nerve lesion (Mallik and Weir, 2005). A focal reduction in conduction velocity is also often reported across the site of the nerve lesion (Mallik and Weir, 2005, Smith and Knight, 2011). The clinical and neurophysiological abnormalities completely reverse upon re-myelination (Smith and Knight, 2011, Menorca et al., 2013). The time to recovery can vary greatly with some clinical studies reporting the reversal of motor paralysis after time periods as long as 6 months although most cases resolve within 3 months following injury (Dumitru et al., 2002). EMG markers of denervation such as spontaneous activity are not classically found in neurapraxic injury since no degenerative changes in the muscle occur. However, this prolongs electrophysiological diagnosis since changes in EMG recordings do not occur for a period of up to 2 weeks following muscle denervation therefore it is not possible to distinguish between conduction block and a more severe axonal degenerative lesion during this time period.

Axonotmesis

In trauma which has resulted in damage of intra-neural structures and axonal degeneration, NCS can give useful information that can assist in the stratification of the severity of the lesion. The disconnected distal segment survives for 4-7 days as Wallerian degeneration ensues along a proximal-distal gradient (Chaudhry and

Cornblath, 1992). As a result, the excitability of the distal stump progressively declines. After this time period, stimulation distal to the nerve lesion results in an absent CMAP. Therefore, the CMAP is initially small or absent proximal to the nerve lesion and preserved distal to the lesion. By the second week of injury, CMAP and SNAP show significant reductions in amplitude distal to the site of injury (Chaudhry and Cornblath, 1992). In addition, EMG examination may reveal fibrillations and positive sharp waves at this time point (Chaudhry and Cornblath, 1992, Campbell, 2008). The time taken for these changes on NCS and EMG examination is largely dependent on the length of the distal stump (Smith and Thesleff, 1976).

Neurotmesis

In neurotmesis, the anatomical disorganisation is so severe that spontaneous regeneration is impossible. After a period of 2 weeks following injury, distinctions between neurotmesis, axonotmesis and lesser degrees of injury are not possible (Chaudhry and Cornblath, 1992, Smith and Knight, 2011). The diagnosis of neurotmesis is only possible with direct visualisation of the nerve but may be suspected in cases of open injury where penetrating trauma may have caused extensive neural damage. For these reasons, early surgical exploration is recommended in order to optimise functional outcomes for the patient (Campbell, 2008, Smith and Knight, 2011). A distinction must be made in the case of suspected iatrogenic nerve injury; early EMG examination within 2-3 days of trauma is recommended since the presence of volitional MUs is predictive of neural continuity despite the presence of clinical signs that may suggest otherwise (Aminoff, 2004).

1.5.5 Intra-operative neurophysiology

A number of indications as determined by clinical examination and/or changes in electrodiagnostic tests for surgical exploration or repair of injured nerves exist (Smith and Knight, 2011):

- Paralysis in the distribution of the injured nerve
- Closed injury with surrounding tissue damage
- Open injury that warrants external reduction and internal fixation
- Nerve injuries that co-present with arterial damage
- Traction injuries to the brachial plexus
- Nerve function that is deteriorating clinically and neurophysiologically after initial diagnosis
- An absence of neurological improvement on clinical examination and electrodiagnostic tests
- Failure of conduction block to improve 6 weeks after injury
- Persistent pain or neuroma formation

The use of neurophysiology intra-operatively has become an indispensable tool for the reconstructive nerve surgeon. A number of neurophysiological techniques have been devised to assist the surgeon in dissection, to isolate the injured region, protect against iatrogenic neural injuries as well as monitor the function of sensory and motor nerves and their more proximal pathways. Nerve action potentials, somatosensory and evoked potentials as well as motor evoked potentials are the most widely reported techniques employed by reconstructive nerve surgeons (Lee et al., 2004, Kline, 2012).

Somatosensory evoked potentials (SSEPs) and Motor evoked potentials (MEPs) can assist in determining the continuity of the corticospinal and somatosensory tracts which, by extension, assists the surgeon in localising the anatomical site of the nerve lesion (Lee et al., 2004, Kline, 2012).

SSEPs have become one of the most commonly deployed modalities of intra-operative neurophysiological investigation of supraclavicular brachial plexus lesions (Sлимп, 2000, Kline, 2012). Recording the SSEP involves direct stimulation of the peripheral nerve distal to the zone of injury. The action potential propagates along the course of the nerve to the dorsal root where it then ascends the dorsal columns in the spinal cord. The dorsal columns synapse at the cervicomedullary junction and decussate as the fibres ascend on to the thalamus and finally to the somatosensory cortex. The SSEP can therefore be recorded at the different sites along this anatomical course (typically the cervical spine and the scalp) to help isolate the location of the nerve lesion. The presence of a central response suggests that the dorsal root is in continuity but it should be noted that only a few hundred fibres need to be present to enable a response to be recorded (Smith and Knight, 2011, Kline, 2012).

MEPs are becoming increasingly utilised to determine the integrity of the descending corticospinal tract and ventral root (Kline, 2012, Sutter et al., 2007, Lee et al., 2004). The motor cortex is stimulated by transcranial electrical stimulation (TES) (through the scalp). The electrical activity travels down the spinal cord and synapses onto the anterior horn cell where the action potential then propagates along the motor nerve to the neuromuscular junction where it causes depolarisation of the muscle which can be recorded using EMG. The presence of an MEP indicates the presence of either continuity or reinnervation of the target muscle. However, it does not prove continuity across the roots; for example where there is discontinuity in one root (such as C5) an

MEP could still be detected in the muscle (such as biceps) due to innervation by an alternative root (such as C6). Moreover, the presence of an MEP is not necessarily predictive of functional reinnervation of muscle.

Once the integrity of the ascending spinothalamic and descending corticospinal tracts has been measured, attention can be focused onto evaluating changes in the PNS as a result of neural trauma.

Assessments of the more distal component of the PNS such as free running EMG can allow more accurate localisation and characterisation of the nerve lesion. Free running and evoked EMG can be used to monitor the function of muscles or motor roots determined to be at risk during surgery. This can be helpful in determining the site of the nerve lesion and its severity. For stimulated EMG, bipolar electrodes are preferred as this minimises the dispersion of current to adjacent nerves (Robert et al., 1995); this is particularly pertinent in brachial plexus surgery.

Nerve action potentials (NAPs) can be recorded directly from the nerve of interest and can determine if there is continuity of the nerve across the site of the lesion. Where a nerve lesion has been isolated to the post-ganglionic region, the presence of a NAP is predictive of several thousand intact axons and is correlated with good functional recovery (Kline and Happel, 1993). This should caution the surgeon against surgical intervention.

Together, these intra-operative neurophysiological assessments can assist the surgeon in determining the severity and location of the nerve lesion. This informs what, if any, surgical intervention is necessary.

1.5.6 Electrophysiological correlates of the recovery of motor units

The rate of regeneration is around 1mm/day across all somatic nerves (Seddon et al., 1943). Depending on the severity of the injury, nerve repair is thought to occur through

two main mechanisms; collateral sprouting and neural regeneration along the course of the nerve fibres (Chen et al., 2007, Menorca et al., 2013). Optimal functional recovery depends on a sufficient quantity and quality of axons re-establishing functional connections with the target muscle within 1 year (Kobayashi et al., 1997, Tung and Mackinnon, 2010). After this time period, molecular and cellular changes in the distal stump and within the muscle are thought to make the environment increasingly antagonistic to successful regeneration (Wu et al., 2014, Jessen and Mirsky, 2019). For these reasons, it is pertinent to carefully monitor patients for neurophysiological signs of reinnervation to inform the surgical management of patients to maximise functional recovery.

Muscle denervation is characterised by abnormal spontaneous activity (fibrillations and positive sharp waves) upon EMG assessment (Smith and Knight, 2011). The intensity of this activity recedes as neural regeneration ensues and function is recovered although these changes are not easily quantifiable (Campbell, 2008, Smith and Knight, 2011). A number of other changes evident on NCS and EMG recordings correlate with early, ongoing and late reinnervation (**Figure 1.5**).

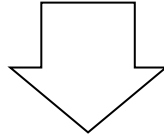
Neural regeneration is the only process through which functional recovery can be achieved following a complete nerve injury. As a result neurophysiological monitoring of regeneration is notoriously challenging until functional neuromuscular junctions have been re-established. The earliest signs of reinnervation are a low number of small unstable MUAPs known as nascent units which can be elicited by volitional effort or evoked potentials distal to the injury site (Smith and Knight, 2011) (**Figure 1.5**). A key characteristic of regenerating nerves is that they require a higher intensity stimulus in order to evoke a response along with reduced conduction velocities until remyelination is complete (Campbell, 2008). Recruitment is diminished and the frequency of MU firing is disproportionately increased when compared with the

number of MUs activated (Campbell, 2008). As the process of reinnervation continues, EMG examination reveals polyphasic MUAPs of longer duration with unstable firing due to the low safety margin at the neuromuscular junction as well as uncoordinated propagation of action potentials along unmyelinated fibres (**Figure 1.5**) (Campbell, 2008, Smith and Knight, 2011). In the later stages of muscle reinnervation, the size of the evoked CMAP increases and conduction velocities regress back towards pre-injury levels (Campbell, 2008, Wu et al., 2014). MUAPs on EMG have larger amplitudes with stable transmission (**Figure 1.5**).

Functional recovery following incomplete nerve injuries that have led to axonal degeneration incorporates a number of biological processes. First, nerve fibres that have been spared injury undergo collateral sprouting and reinnervate adjacent muscle fibres (Hoffman, 1950, Wu et al., 2014, Navarro, 2016). The result is large MUs that have increased duration, amplitude, territory and fibre density (Wu et al., 2014) (**Figure 1.5**). Regeneration of axons that have been injured soon follows (Smith and Knight, 2011). The quantity of reinnervation may be determined by neurophysiological measures such as quantitative MUAP analysis and/or MUNE.

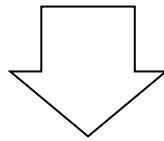
Denervation

Spontaneous activity: fibrillations and sharp waves are evident in *acutely* denervated muscle.



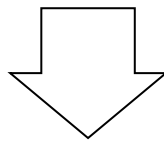
Early muscle reinnervation

MUAPs are normal with a longer duration. This is attributable to the larger innervation ratios of MUs.



Ongoing muscle reinnervation

The amplitude of MUAPs is moderate, polyphasic and of longer duration. The firing characteristics are unstable secondary to unpredictable firing along the course of unmyelinated axonal sprouts.



Chronically reinnervated muscle

The amplitude of MUAPs is increased and demonstrate a stable firing characteristics.

Figure 1.5 - A summary of changes in the characteristics of MUAPs after nerve injury and at different stages of muscle reinnervation (Smith and Knight, 2011).

1.5.7 Quantitative Motor Unit Action Potential (MUAP) analysis

EMG recordings allow analysis of the morphological features of MUAPs which have demonstrated correlations with anatomy and neuro-pathological processes (Krarup et al., 2016). To this end, quantitative analysis of morphological features of MUAPs have been extensively studied to characterise MU remodelling during a number of different neurological diseases (Stalberg and Falck, 1997, Flasar et al., 2017). The concentric needle electrode is reasonably selective and allows examination of the amplitude and area of MUAPs from muscle fibres within 500µm and 200µm of the tip of the electrode respectively (Buchthal et al., 1954a, Buchthal et al., 1954b, Gydkov et al., 1980, Bromberg, 1999). This is particularly useful in assessing the recovery of MUs; it has been shown that changes in MUAP area, duration and amplitude are highly sensitive indicators of early muscle reinnervation in pathologies such as Amyotrophic Lateral Sclerosis (ALS) (Joyce and Carter, 2013). More recently, quantification of changes in the amplitude and duration of MUAPs have demonstrated close associations with reinnervation of facial muscles in a surgical model of hypoglossal facial nerve jump suture (Flasar et al., 2017).

Quantitative MUAP analysis does not provide information about the number of recovering MUs. Therefore, little or no association between quantitative MUAP analysis and functional outcomes has been widely reported. It follows that in order to foster the translation of new therapeutics for the treatment of PNI and to improve clinical management, there is a need for measures that demonstrate improved relationships between the biological process that underpin nerve regeneration and the recovery of functional MUs.

1.5.8 Motor Unit Number Estimation (MUNE)

MUNE is a neurophysiological test that was first coined by McComas to estimate the total number of functional MUs innervating a muscle (McComas et al., 1971a). MUNE is based on the phenomenon that it is possible to observe an increase in the amplitude of the response of a muscle with an increasing proximal nerve stimulus (McComas et al., 1971a). If the intensity of the stimulus is incrementally increased, it is possible to recruit individual MUs (McComas et al., 1971a). Dividing the CMAP by the mean stimulus intensity required to recruit an additional MU yields an estimate of the total MUs innervating the muscle (McComas et al., 1971a). Therefore, it is a technique that has been applied to study the dynamics of a number of different neurological pathologies that lead to the denervation of muscle (Gooch and Harati, 2000, Lawson et al., 2003, Gooch et al., 2014).

A number of different methods have been developed since this original method of “incremental stimulation” first proposed by McComas (de Carvalho et al., 2018). However, all techniques are based on the same principle of obtaining a CMAP and sample of Single Motor Unit Action Potentials (SMUAPs) but can be differentiated by the way in which they record SMUAPs. A recognised limitation of incremental stimulation was the phenomenon of alternation (Brown and Milner-Brown, 1976, Kadrie et al., 1976). Alternation is where two MUs have a similar activation threshold and their individual responsiveness to the same stimulus intensity varies. This is particularly pertinent in the context of muscle reinnervation where the MU pool is more homogeneous with higher innervation ratios (Burnett and Zager, 2004, Faroni et al., 2015, Wu et al., 2014). This led to the development of the Multipoint Stimulation (MPS) technique which overcomes this limitation by stimulating the nerve of interest at multiple sites along the anatomical course until at least 10 SMUAPs are sampled (Brown and Milner-Brown, 1976, Kadrie et al., 1976). However, this method is time

consuming therefore a modified version that combined incremental stimulation and MPS was developed; the investigator stimulated three MUs from at least three different stimulation sites along the course of the nerve to obtain a sample of SMUAPs (Wang and Delwaide, 1995).

Using stimulation to obtain a sample of SMUAPs is not appropriate in proximal nerves. Due to anatomical reasons, it is often not possible to stimulate at a sufficient number of sites to obtain a representative sample of SMUAPs. The digitalisation of EMG recordings drove a number of advancements in MUNE which sought to circumvent these challenges. The spike triggered averaging (STA) technique involves inserting a concentric needle electrode into the muscle of interest to record EMG signals (Bromberg and Abrams, 1995, Power et al., 2012, Gooch et al., 2014). A single MU is isolated and recorded using the needle electrode by the investigator. An amplitude trigger is then used to time lock and average signals from this MU which are recorded using a surface electrode. Different MUs are recruited by isometric contraction of the muscle as well as sampling different locations and depths of the muscle with the electrode to record a representative sample of SMUAPs (Bromberg and Abrams, 1995, Power et al., 2012, Gooch et al., 2014). The CMAP is divided by the averaged amplitude of SMUAPs to obtain MUNE (Bromberg and Abrams, 1995, Power et al., 2012, Gooch et al., 2014). The negative peak area may also be determined for the CMAP and the SMUAP for the MUNE calculation. Using this measure overcomes negative phase cancellation (Bromberg, 2007) which is particularly prevalent when measuring reinnervated muscle where there has been proliferation of acetylcholine receptors (Adams et al., 1995, Ma et al., 2007, Wu et al., 2014). However, a limitation of this method is the issue of patient tolerance to application of the needle electrode. This is of particular importance where multiple measurements are required to study the dynamics of different neurological pathologies.

Efforts have been subsequently made to allow reliable recording of MUNE from proximal muscles whilst also improving patient tolerance. This has informed further developments in techniques to obtain MUNE such as automated incremental stimulation (Galea et al., 2001), F Response method (Wang and Delwaide, 1995), statistical method (Daube, 1995), MUNIX (Motor Unit Index) (Nandedkar et al., 2004) and CMAP scanning (Jacobsen et al., 2018). However, the latter two methods have gained most widespread acceptance as the methods that provide reliable MUNE recordings along with improved patient tolerance when compared with more traditional techniques (such as incremental stimulation and MPS).

In the MUNIX method, the CMAP is recorded by manipulating the location of the electrode to obtain the signal with the amplitude of the greatest magnitude (Nandedkar et al., 2004). The subject is then requested to exert different grades of isometric contraction whilst the surface EMG interference pattern (SIP) is recorded (Nandedkar et al., 2004). A mathematical model is then applied to determine the area of the CMAP and SIP which is used to calculate a motor unit index (Nandedkar et al., 2004). A drawback of this method is that the software required is expensive and this has limited more widespread clinical use.

The CMAP scan method involves increasing the stimulus in small increments and recording the evoked response from the target muscle. The intensity is increased to supramaximal levels in approximately 500 steps (Jacobsen et al., 2018). The differences between each of these successive steps is then quantified after being sorted into an ascending or descending order. The number of largest differences that equate to 50% of the CMAP amplitude is named D-50 (Jacobsen et al., 2018). In the context of muscle reinnervation, this index reduces due to larger innervation ratios. A mathematical model which is available commercially can then be applied to this data to calculate MUNE (Jacobsen et al., 2018). This model simulates the scanning

method and 'fits' it to the recorded results which reduces preferential detection of small and/or large MUs (Jacobsen et al., 2018).

Despite the wealth of advancements that have been made in developing methods to obtain MUNE, there remain a number of limitations. Firstly, MUNE is primarily dependent on the recording of a valid CMAP which is known to show little relationship with muscle size suggesting that it does not provide an accurate representation of the number of MUs (Nandedkar and Barkhaus, 2007, de Carvalho et al., 2018). Moreover, it has been shown that muscle fibres that are located deeper than 15-20mm deep to the recording surface electrodes are not reflected in the CMAP; a limitation that also extends to the surface recording of MUPs (Barkhaus and Nandedkar, 1994, Nandedkar and Barkhaus, 2007). Thirdly, in the context of reinnervated muscle where the motor endplate zone is more diffuse due to proliferation of acetylcholine receptors, identifying an optimal site for recording reliable CMAP recordings is more challenging (Wu et al., 2014, de Carvalho et al., 2018). For these reasons, MUNE remains only an estimate and further work is required to understand what relationship MUNE has to biological correlates of neural regeneration.

Despite these limitations, one of the main benefits of MUNE is good reliability irrespective of which method is used to derive it (Gooch and Harati, 2000, Bromberg, 2007, Gooch et al., 2014). Moreover, MUNE provides a unique assessment of the number of functioning MUs innervating a muscle that complements traditional EMG assessment. For these reasons, MUNE is favoured for quantifying disease progression and has been employed as a primary outcome in trials that have looked at denervating pathologies such as Amyotrophic Lateral Sclerosis (ALS) and Spinal Muscular Atrophy (SMA) (Gooch and Harati, 2000, Bromberg, 2007, Gooch et al., 2014). However, application of MUNE in the inverse physiology, muscle

reinnervation, is awaited perhaps due to limited discussion in the surgical literature. This may be key in aiding the translation of therapies that have demonstrated promising outcomes in preclinical models of nerve injury.

1.5.9 Electrophysiological correlates of sensory function

The regeneration of sensory nerves is closely related to the regeneration of MUs; the return of sensory potentials is widely reported at the same time as the appearance of a low number of unstable MUPs (Smith and Knight, 2011). The return of recordable SNAPs is thought to predict the presence of thousands of moderate-diameter sensory nerves (Kline, 2012). In animal models of PNI, this correlates with clinical recovery of sensory function (Kline, 2012). The recovery of sensory nerves can also be clinically monitored through the Tinel sign (Macdonald, 1918).

Autonomic deficits following PNI should also be considered and included in clinical evaluations. Post-ganglionic sympathetic fibres which traverse in close relationship with the nerve trunk are frequently damaged following PNI leading to loss of sweating, vasomotor tone as well as a reduction in nail growth.

There are a number of neurophysiological quantitative sensory tests that can help determine which fibres have been most severely affected and the extent of damage or recovery.

Quantitative sensory testing

Quantitative sensory testing can quantify the recovery of a number of different components of the sensory and autonomic nervous system.

The sympathetic skin test involves transducing a current between two points on the skin. This stimulates the eccrine sweat glands. The fluid secreted onto the skin surface leads to an increase in resistance between the two points on the skin. This

can provide some indication as to the functioning the sympathetic system (Smith and Knight, 2011).

A similar test is the sudomotor axon reflex test (QSART). This test involves the application of iontophoresed acetylcholine which antidromically stimulates the post-ganglionic sympathetic fibres (Lee et al., 2004, Kline, 2012). This leads to the release of acetylcholine orthodromically which results in sweat secretion. This measure can be quantified and has demonstrated high reliability (Lee et al., 2004, Kline, 2012).

The recovery of larger myelinated A delta (cold threshold) and unmyelinated C (heat threshold) fibres can be determined using a psychophysical test known as thermal thresholds. By measuring the threshold for temperature sensation and applying the “method of limits” algorithm (Lee et al., 2004, Kline, 2012), the recovery of these fibres can be monitored. The “method of limits” method involves applying a thermode to the skin and the temperature of the thermode is incrementally increased until the patient can feel a warm sensation at which point they depress a button. This is defined as the perception threshold. The thermode is then cooled until the participant detects a cool sensation which is termed the disappearance threshold. A number of different cycles have been proposed from which a thermal threshold can be calculated (Yarnitsky and Sprecher, 1994, Hilz et al., 1998, Chong and Cros, 2004).

A number of different methods also exist to detect and quantify vibration sense using the “method of limits” (Chong and Cros, 2004). In this test, the patient is asked to depress a button as soon as they can perceive vibration during incremental increases in vibration intensity (the perception threshold). Similarly, the patient is asked when they can no longer detect the vibration during incremental decreases in the intensity of the vibration (disappearance threshold) (Chong and Cros, 2004).

Electrophysiological correlates of the response of the CNS to PNI

There are a number of changes in the CNS following PNI such as remodelling of the spinal cord. These biological and anatomical changes are associated with a change in crossed spinal reflexes such as the H-reflex (Valero-Cabr  and Navarro, 2001). These reflexes are not widely used in the evaluation of PNI.

In summary, neurophysiological assessments of PNI represent an indispensable tool in determining the location and extent of damage to the PNS. By extension, these tests can provide some indication to what the likely recovery will be. However, sensitive and responsive tests that quantify the biological recovery of MUs have not been well studied in models of nerve injury. This, along with understanding what relationship this has with functional recovery will be key to developing valid outcome measures.

Magnetic Resonance Imaging (MRI) and Ultrasound are other modalities which are indispensable in imaging PNI. Recent advancements have identified opportunities to identify changes associated with the biological processes of nerve regeneration.

1.6 Imaging of peripheral nerve injuries

The mainstay for evaluation of PNI remains clinical examination with supporting NCS and EMG. However, a major restriction associated with these tests is that neurophysiological techniques cannot provide morphological details or demonstrate alterations within the nerve or in adjacent tissues that may have been affected by the injury. In addition, focal lesions are not amenable to neurophysiological evaluation (Koltzenburg and Bendszus, 2004). Whilst imaging is considered invaluable in the work up of patients with disorders of the CNS (Alvarez-Linera, 2008, Murphy and Koh, 2010, Zivadinov et al., 2017), widespread application for disorders of peripheral nerves is awaited (Rayner et al., 2019, Wilcox et al., 2020a). This is despite recent studies demonstrating changes in MRI associated with damaged nerve and skeletal

muscle (Bendszus et al., 2002, Bendszus and Stoll, 2003, Bendszus et al., 2003, Simon et al., 2016a, Kakkar et al., 2018). This may provide opportunities to develop sensitive, responsive and valid outcome measures through which the biological process of nerve regeneration can be monitored and quantified.

In addition, there are a number of practical benefits to imaging; unlike needle electromyography, imaging does not require the active co-operation of the patient and is painless. MRI provides a permanent document of the topographical area studied. Unlike ultrasonography, this does not depend on the experience of the examiner to relocate the area of interest. Focusing on the clinical benefits, there are a number of scenarios which could warrant the use of imaging rather than neurophysiology. For example, in patients who are on anticoagulation or after tissue damage following a traumatic injury where the nerve or muscle may be difficult to reach due to anatomical reasons. In these circumstances, imaging may offer a viable alternative or valuable adjunct to the evaluation of PNI.

Given the potential benefits imaging may have in characterising neural injuries, this section explains how different imaging modalities may be useful in detecting and quantifying changes associated with traumatic PNI.

1.6.1 MRI findings in injured nerves

A normal nerve is found to be isointense or slightly hyperintense on T2-weighted (T2-w) images compared to surrounding muscle. Therefore, it is often challenging to discriminate between muscles and nerves. However, in the context of a degenerative nerve lesion (axonotmesis or neurotmesis), damaged nerves demonstrate a significant increase in T2- relaxation time (they appear bright on T2-w images). In animal models, it has been shown that changes in the signal intensity are apparent within 24 hours after insult and demonstrate a proximo-distal gradient starting at the lesion site (Kullmer et al., 1998, Bendszus et al., 2002, Koltzenburg and Bendszus,

2004, Holzgrefe et al., 2019). If successful nerve regeneration occurs, these signal changes regress back to normal levels over several weeks and are closely associated with the histological and electrophysiological markers of muscle reinnervation (Kikuchi et al., 2003, Wessig et al., 2004). Together, this evidence suggests that there is a close association between MR signal changes and the biological process of peripheral nerve regeneration. Comparative studies in human models of regeneration are needed to realise the benefits this method could have in determining axonal injury, likely prognosis and what relationship these changes have with functional measures of recovery.

A number of reasons for the hyperintense signal on T2-w images of injured nerves have been posited; loss of myelin, an increase in the extracellular space, axonal loss as well as disruption of the axoplasmic transport system are all mechanisms that have been suggested to be at least partially responsible (Titelbaum et al., 1989, Does and Snyder, 1996, Stanisz et al., 2001, Cudlip et al., 2002).

MRI has also emerged as a sensitive tool for the diagnosis of neurapraxia (non-degenerative lesions) such as peroneal nerve compression at the fibular head (Koltzenburg and Bendszus, 2004), thoracic outlet syndrome (Panegyres et al., 1993) and cervical radiculopathy (Dailey et al., 1996).

1.6.2 MRI findings in denervated muscle

Normal muscle tissue can be visualised as an intermediate signal on T1-weighted (T1-w) and T2-w sequences. Clinical reports demonstrate that acutely (<1 month) and sub-acutely (1-6 months) denervated muscle manifests hyperintense signals on MRI sequences that are fluid sensitive including short tau inversion recovery (STIR) and turbo inversion recovery magnitude (TIRM) whilst retaining normal intensity on T1-w images (Polak et al., 1988, Kullmer et al., 1998, Bendszus et al., 2002, Bendszus and Stoll, 2005, Aagaard et al., 2003). In clinical studies, changes in signal intensity have

been reported within 4 days following the injury. In other cases, these changes may evolve over several weeks and persist for several months in denervated muscle (Kamath et al., 2008). As the muscle becomes more chronically denervated (>6 months), there is further atrophy and infiltration of fat, features that can be seen on T1-w and CT images (Clague et al., 1995). The abnormalities in MR signal have been reported to regress back to normal levels within 4-6 weeks following the onset of reinnervation (Viddeleer et al., 2012). Other studies have shown that abnormalities in T2 relaxation time reverse within 10 weeks of the beginning of nerve regeneration (Kamath et al., 2008). Comparable findings have been reported in animal paradigms of PNI with a statistically significant increase in signal on T2-w images of denervated muscles within 48 hours following injury which continues to increase for a further 2-4 weeks (Kamath et al., 2008). If nerve regeneration is successful, the signal regresses back towards normal levels 6-8 weeks post-injury (Kamath et al., 2008). If regeneration fails, muscle atrophy ensues which is accompanied with persistent hyperintense signals on MRI (Kamath et al., 2008).

Focusing on the relationship of MR signal changes with EMG recordings, it has been reported that signal increases on T2-w images of denervated muscle may precede the onset of spontaneous activity in animal and human models of regeneration (**Figure 1.6**) (Wessig et al., 2004). Moreover, the decline of hyperintense signals may also precede the regression of spontaneous activity (Bendszus et al., 2003, Wessig et al., 2004, Simon et al., 2016a). There is also some contrary evidence which suggests that prolongation of the T2 relaxation time and gadolinium enhancement of denervated muscle occur in parallel to the development of spontaneous activity on EMG (Bendszus and Koltzenburg, 2001, Koltzenburg and Bendszus, 2004). Together, this warrants further exploration of the ability of signal changes to predict the likely functional recovery and how they relate to neurophysiological parameters.

The cellular and molecular features that underpin the changes in signal intensities on MRI scans of denervated muscle have not been elucidated. It has been postulated that the signal changes on MR sequences that are fluid sensitive are attributable to an increase in capillary density and/or extracellular space (Koltzenburg and Bendszus, 2004, Wessig et al., 2004, Bendszus and Stoll, 2005). In the subacute denervation period, it is thought that muscle has an increase in the relative amount of fat and extracellular water volume/capillary density (Carlson, 2014, Wu et al., 2014). It is posited that this increase in fat is offset by the increase in extracellular space/capillary density which means that there is no overall change in the T1-relaxation time. For this reason, acutely denervated muscle may be better detected on water sensitive MR sequences. This theory is supported by experimental findings that have shown increased uptake of the extracellular contrast agent Gadolinium-diethylenetriaminepentaacetate (Gd-DPTA) by denervated muscle on T1-w images which closely parallels changes in T2 relaxation time (Bendszus and Koltzenburg, 2001).

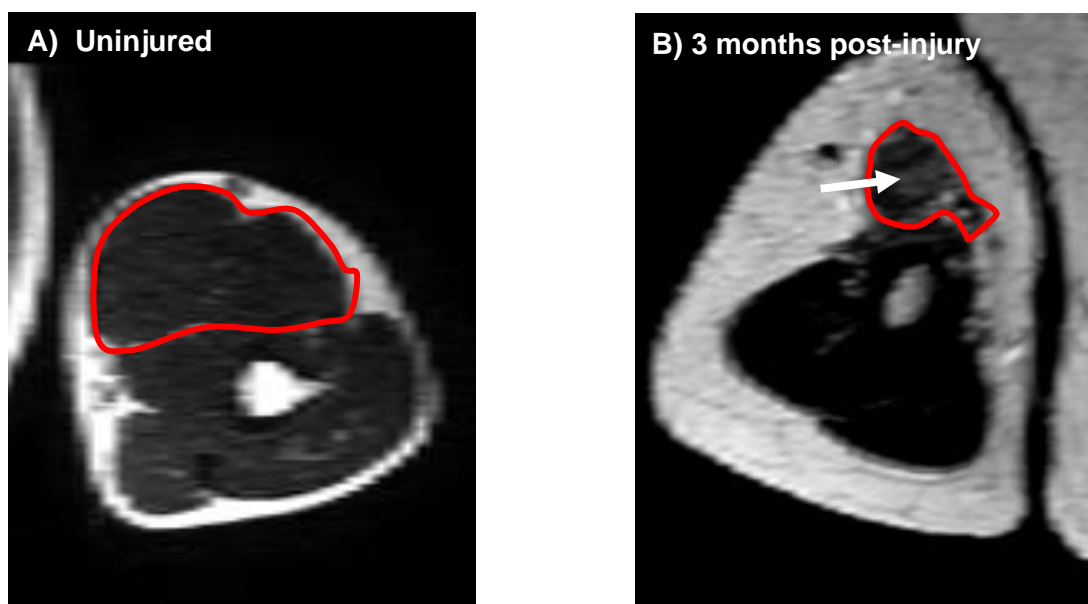


Figure 1.6 - T2-weighted MRI scans of uninjured and nerve injured biceps muscles from patient who sustained C5/6 Avulsion. **A)** Uninjured biceps muscle (uninjured contralateral arm) outlined in red. **B)** Subacutely denervated biceps muscle (3 months following injury) demonstrating increased signal (arrow) and muscle atrophy of biceps muscle (outlined in red) compared to **A)**.

1.6.3 Muscle volume changes in denervated muscle and the application of MRI

The past decade has seen the advent of volumetric assessment from imaging analysis (CT, MRI and Ultrasound). Changes in volumes of organs within the CNS have been utilised as a biomarker to predict the onset and likely prognosis of a number of neurodegenerative conditions (Shen et al., 2011, Maglioni et al., 2018, Petrone et al., 2018, Mitolo et al., 2019). However, application in disorders of the PNS is awaited.

Following nerve transection, it has been shown that rat muscle wet weight demonstrates an initial dramatic decrease in wet weight following denervation. This stabilises at 10-20% of the weight of the healthy, uninjured contralateral side 3-12 months following denervation. The recovery of wet weight can be determined by the size of the nerve gap, severity of nerve damage as well as the time interval between

injury and surgical repair of the damaged nerve. The best recovery of wet weight is when nerve repair is completed within one month following denervation with wet weight recovering to 19%-100% of uninjured contralateral side. When the delay is extended to 3 months or more, the recovery of wet weight is only 10%-20% of the uninjured contralateral side (Wu et al., 2014).

These changes in muscle wet weight have significant clinical relevance in that they can theoretically be applied to predict the likely success or failure of surgical nerve repair (**Figure 1.6**). However, it is impossible to measure muscle wet weight in humans therefore non-invasive imaging techniques such as MRI could theoretically be used to measure volume as a surrogate for wet weight. This could provide a quantitative correlate of neural regeneration which has the capacity to predict likely functional recovery in the setting of neural regeneration. A significant barrier that exists is a limited understanding of what relationship muscle volume has with objective and subjective measures of functional outcomes (Rayner et al., 2019, Wilcox et al., 2020b). Moreover, a standardised model of human peripheral nerve regeneration through which these changes can be quantified is awaited.

1.6.4 MR neurography

Recent decades have seen the advent of novel application of MRI techniques for diagnosing a number of PNS disorders (Dailey et al., 1997, Rose et al., 2010, Baltodano et al., 2014). In the 1990's, magnetic resonance neurography (MRN) was developed which involves the application of a set of MR pulse sequences to distinguish nerves from the surrounding tissues. MRN involves the application of fat-saturated heavily T2-w sequences in order to distinguish the bright nerve signal from the adjacent fat tissue (Howe et al., 1992).

Normal nerves on high-resolution T1-w images appear round in shape and demonstrate a fascicular pattern. A hyper-intense halo often surrounds the nerve

which represents the perineural fat tissue. On fat saturated T2-w images, normal nerves appear isointense or marginally hyperintense compared to the surrounding muscle tissue (a thorough review of the appearance of normal nerves is available elsewhere) (Filler et al., 1993, Moser et al., 2009, Deroide et al., 2010).

Degenerative nerve lesions result in a hyperintense nerve signal in the distal stump that persists for months to years following the lesion (Filler et al., 1996, Kuntz et al., 1996, Dailey et al., 1997, Maravilla and Bowen, 1998, Koltzenburg and Bendszus, 2004). This differs from the hyperintense signal that is evident on MRI images where the T2 signal will regress to normal levels in a proximo-distal gradient once neural regeneration has commenced (Bendszus and Koltzenburg, 2001, Bendszus et al., 2002, Wessig et al., 2004). A further advantage of MRN is that neurotmesis can be directly visualised as discontinuity of the nerve of formation or a neuroma (Filler et al., 1993). This can have important implications on the surgical management of this complex pathology. A limitation of MRN is that signal intensities may return to normal levels in neurotmesis injuries (Koltzenburg and Bendszus, 2004, Bendszus and Stoll, 2005). This means that the clinician cannot distinguish between axonotmesis and neurotmesis. This has promoted the development of novel contrast agents to further characterise and evaluate the nerve lesion.

1.6.5 MR contrast agents

The advent of new contrast agents has enabled remarkable insights into the pathophysiology that underpins neural regeneration and has improved the specificity of MRN. However, no simple association between changes in signal intensity and nerve function has been detailed.

Nerve degeneration and regeneration has been visualised using gadolinium-based MR contrast agents such as gadofluourine M (Gf). This agent selectively accumulates and remains within nerve fibres that are undergoing Wallerian degeneration. This

hyper-intense signal was evident within 48 hours following injury throughout the entirety of the nerve segment that was undergoing Wallerian degeneration. This abnormal hyper-intense signal regressed back to normal levels along a proximo-distal gradient as neural regeneration ensued. However, in nerve fibres which had failed to regenerate, the signal persisted for several weeks after the injury (Bendszus and Koltzenburg, 2001, Bendszus and Stoll, 2005).

Reticuloendothelial contrast agents such as supra-magnetic iron oxide (SPIO) particles have provided novel in vivo, real-time insights into the neuropathology that underpins neural regeneration (Bendszus and Stoll, 2003). The SPIO particles were injected into the systemic circulation 24 hours before MRI at different time points following injury (Bendszus and Stoll, 2003). The SPIO particles were rapidly phagocytosed by macrophages within the reticuloendothelial system located in reticular connective tissue. As a result, a proportion of macrophages became iron-labelled. Their accumulation within tissues can then be closely monitored through increases in signal on T2-w images (Bendszus and Stoll, 2003, Bendszus and Stoll, 2005). This allowed imaging of key biological events such as Wallerian degeneration (Bendszus and Stoll, 2003); a process that commences soon after injury and involves the infiltration of immune cells such as macrophages which clear myelin and other debris which are events thought to be critical in order to permit successful nerve regeneration (Fu and Gordon, 1997, Faroni et al., 2015).

1.6.6 MRN to quantify axonal diameter

MRN has been applied beyond changes in signal intensity. The advent of new sequences has enabled the quantification of axonal diameters (Kakkar et al., 2018). It has been shown that the diameter of axons can vary in health and disease (Cluskey and Ramsden, 2001, Burnett and Zager, 2004, Stassart et al., 2018). Following a nerve injury, axons demonstrate a reduced calibre (Burnett and Zager, 2004,

Sulaiman and Gordon, 2013). As nerve regeneration ensues, the diameters of axons increase towards preinjury levels (Burnett and Zager, 2004, Sulaiman and Gordon, 2013). This change in diameter could theoretically be used as a quantitative marker of nerve regeneration.

The imaging of axon diameters using MRI has been made possible through the application of single diffusion encoding (SDE) spin echo sequences (Jespersen, 2012). More recent studies have used oscillating spin gradient echo (OSGE) sequences which have wider applications in the clinical arena where nerve fibres may have an unknown or dispersed orientation (Parsons et al., 2006, Shemesh et al., 2015, Drobnjak et al., 2016, Jiang et al., 2016, Mercredi et al., 2017). The values for axonal diameter obtained using this method have shown excellent correlations with histological measurements of diameter (Kakkar et al., 2018). Together, this may provide a new sensitive and responsive measure of axonal regeneration.

1.6.7 Tractography

Peripheral nerves are highly anisotropic structures. Diffusion tensor imaging (DTI) with tractography exploits this feature of nerves to image them in health and disease (Jeon et al., 2018). Free water demonstrates random movement of hydrogen nuclei. In nerve tracts, the majority of water diffuses along the longitudinal course of nerves. Following a nerve injury, there is disruption to the microanatomy of the nerve. This permits the diffusion of a higher proportion of water molecules orthogonally to the course of the nerve trunk. Since the pattern of diffusion differs between healthy and injured nerves, this imaging technique can provide a wealth of information that is useful in characterising the nerve lesion.

DTI measures this random diffusion of water and provides quantitative indices which can provide information about the structure and orientation of the nerve. These indices are known as eigenvalues ($\lambda_1, \lambda_2, \lambda_3$), eigenvectors (e_1, e_2, e_3) and fractional

anisotropy (FA) (Li et al., 2013, Boyer et al., 2015, Heckel et al., 2015). Changes in these values are predictive of changes in the microanatomy of the nerve trunk (Morisaki et al., 2011, Heckel et al., 2015, Jeon et al., 2018).

The validation of DTI in evaluating nerve injury has been extensively studied; in particular, FA values demonstrate strong associations with histological markers of denervation and reinnervation (Morisaki et al., 2011, Heckel et al., 2015, Jeon et al., 2018). Animal and human models of nerve injury have shown that FA values are lower in injured nerves when compared to uninjured nerves (Morisaki et al., 2011, Heckel et al., 2015, Jeon et al., 2018, Gallagher et al., 2015). This has been attributed to lower quantities of myelin and anisotropic diffusion of water molecules (Morisaki et al., 2011, Heckel et al., 2015, Jeon et al., 2018). DTI measurements can also assist in determining the stage of nerve regeneration; Wallerian degeneration has been associated with a specific set of changes as has the onset of neural regeneration and muscle reinnervation (Morisaki et al., 2011, Heckel et al., 2015, Jeon et al., 2018).

1.6.8 Ultrasound

Ultrasonography (US) enables real-time in vivo visualisation of peripheral nerves and the surrounding soft tissue with high spatial resolution of up to 400µm using 18MHz transducers (Visser, 2006). In general, the highest available frequency should be used to image peripheral nerves. However, the higher the frequency, the lower the penetration to deeper tissues. Therefore, the use of 18MHz transducers is recommended for the examination of superficial nerves whilst deeper nerves such as the sciatic nerve indicate the use of 10-12MHz transducers (Visser, 2006, Simon et al., 2016a). A normal nerve appears as hyperechoic neuronal fascicles and echogenic surrounding connective tissue. These features enable the differentiation of the nerve from hyperechoic structures surrounding the nerve such as tendons and muscles (Simon et al., 2016a).

In the context of PNI, a number of features can be demonstrated on high-resolution US such as axonal swelling, neuroma formation as well as nerve discontinuity (Kullmer et al., 1998). US has the highest sensitivity for the detection of these features 72 hours after trauma (Kullmer et al., 1998, Simon et al., 2016a). Since US allows rapid examination of long lengths of nerve in a single examination, it has been widely reported as the preferred first-line modality for the investigation of PNI (Tagliafico et al., 2010). Unlike neurophysiology, US can distinguish between neurotmesis and severe axonotmesis long before reinnervation (Kullmer et al., 1998, Simon et al., 2016a).

There has been much written on the sensitivity and specificity of ultrasound in the diagnosis of neuralgic amyotrophy (brachial neuritis) an inflammatory nerve injury which has recently been characterised as having a diagnostic torsional appearance on ultrasound (Abraham et al., 2016, Seror, 2017, van Rosmalen et al., 2019).

Whilst US may provide a number of benefits for the management of PNI in the acute and subacute setting, there are a number of drawbacks to this technique; it is user dependent and contrast resolution is often disappointing (Ohana et al., 2014). As a result, US provides a limited scope for the quantification and prospective evaluation of neuropathological processes underlying PNI when compared to MRI and neurophysiology (Holzgreffe et al., 2019).

1.7 Conclusions

A number of issues must be addressed in order to drive the clinical translation of new therapies for the treatment of PNI.

Experimental protocols must be developed and optimised in order to study the cellular and molecular features of human peripheral nerve regeneration. Effective translation of the wealth of animal data into a better understanding of human nerve injury will

benefit the development of new therapeutics to enhance nerve regeneration and functional outcomes.

Secondly, there is a need for outcome measures that are sensitive and responsive to the biological process of nerve regeneration. The relationship of these measures to objective and subjective measures of muscular function must also be characterised to ensure that these parameters reflect the lived experience of nerve injury.

Therefore, this PhD developed a series of aims and objectives in order to address these issues.

Project aims

The overall aim of this PhD was to advance the available therapeutic options for nerve injury. This led to the development of the following aims:

- 1) Investigate peri-operative variables that can affect the quality and quantity of RNA isolated from human peripheral nerve samples.
- 2) Characterise cellular and molecular features of human peripheral nerve degeneration.
- 3) Quantify MU recovery in reinnervated elbow flexor muscles following nerve transfer using a modified STA MUNE technique in humans.
- 4) Investigate the relationship of MUNE with histological and functional measures of muscle reinnervation in a controlled rodent model of muscle reinnervation.
- 5) MRI biomarker assessment of reinnervated elbow flexor muscles following nerve transfer.

Little is known about the cellular and molecular features which underpin nerve regeneration in humans. Whilst it is possible to retrieve human nerve samples from some reconstructive procedures, peri-operative variables often afford significant challenges to the study of these samples in the laboratory. Therefore, this thesis aimed to optimise surgical handling of nerve samples in order to overcome some of these challenges in **Chapter 3**. This enabled further investigation of some of the cellular and molecular features which underpin human nerve regeneration in **Chapter 4**. Continuing with this theme of human nerve injury characterisation, the remaining Chapters aimed to investigate clinical outcome measures following peripheral nerve repair using human and animal scenarios of muscle reinnervation. **Chapter 5** investigates the responsiveness of MUNE to the temporal process of human muscle reinnervation. **Chapter 6** further explores the relationship of MUNE with the biological

process of muscle reinnervation using a standardised animal model of nerve repair. In order to understand how these changes relate to changes within the muscle, **Chapter 7** investigates the responsiveness of quantitative MRI parameters to the temporal process of muscle reinnervation.

Chapter 2: Materials and Methods

2.1a) Investigating peri-operative variables that can affect the quality and quantity of RNA isolated from human peripheral nerve samples and 2.1b) Characterising cellular and molecular features of human peripheral nerve degeneration.

Informed consent was obtained using the guidelines detailed in the UK Human Tissue Act (2004). Ethical approval for this project was provided by the UCL Biobank Research Committee (REC 15.15). Thirty-nine patients who underwent reconstructive nerve procedures (nerve transfer, Free Functioning Muscle Transfer (FFMT) and nerve autograft) were included (**Table 2.1**). The innervation status of all nerve samples was determined by intra-operative neurophysiology; if a Compound Nerve Action Potential (CNAP) and muscle twitch was absent, the nerve was judged to be denervated. Nerve samples were obtained during the course of the surgical procedure, then processed for immunohistochemistry and/or RT-qPCR analysis. Since many of the patients had suffered global plexus injuries, healthy nerve samples were only included if they were retrieved from sites external to the injury site (the affected upper limb) to ensure the sample was not damaged.

2.1.1 RT-qPCR

2.1a) Investigating peri-operative variables that can affect the quality and quantity of RNA isolated from human peripheral nerve samples.

In order to investigate peri-operative variables that can affect the quality and quantity of RNA isolated from human peripheral nerve samples, 12 denervated and three healthy human nerve samples harvested from 12 different patients were used to investigate the effects of time delays and surgical antiseptics on the yield of RNA (**Table 2.1**).

Samples harvested were often heterogeneous in size, morphology and innervation, so they were dissected into sections measuring 0.5cm +/- 0.2cm in the longitudinal orientation. The dimensions of the samples were chosen to allow comparisons with other RT-qPCR studies of rodent nerve samples which used similar dimensions (Jiang et al., 2014).

Nerve samples were stratified into 3 experimental groups (shown in **Table 2.1**) based on the time that elapsed between surgical dissection of the nerve sample and exposure to surgical antiseptics. Samples were stratified into two different time groups whereby the time between excision of the nerve sample and cryopreservation was less than three minutes or between three and 20 minutes. These time groups were chosen based on experiences within the surgical environment which revealed that surgical handling of the excised nerve sample could defer cryopreservation by at least 3 minutes ranging up to 20 minutes. The inclusion of additional time groups was not feasible in the present study due to the ethical and practical challenges associated with retrieving human nerve samples.

Group 1: Samples whereby the time between sample liberation and cryopreservation was less than 3 minutes.

Group 2: Samples where the time interval between surgical liberation of the nerve sample and cryopreservation was greater than 3 minutes ranging up to 20 minutes.

Since RNA yields from nerve samples remained lower than that reported in rodent studies following optimisation of handling times, the exploration of other peri-operative variables was necessitated. This informed the development of a third experimental group to explore the effect of minimising the exposure of nerve samples to antiseptic reagents.

Experimental Group or Case Number	Age Range (Gender)	Mechanism of Injury	Intraoperative findings	Reconstructive Nerve Procedure	Details of nerve liberated (denervated unless otherwise stated)	Sample used for histology, RT-qPCR or optimisation of RNA isolation?	Denervation Period (Days)
Group 1	20-30 (M)	Motorbike accident	N/A	Below the knee amputation	Tibial	Optimisation of RNA isolation	321
Group 1	20-30 (M)	Motorbike accident	Right C5/6 Avulsion	Oberlin's nerve transfer	Biceps branch of musculocutaneous	Optimisation of RNA isolation	132
Group 1	20-30 (M)	Fall on to sharp cast iron railing	Axonotmesis of superficial peroneal nerve	Excision of nerve	Superficial common peroneal nerve	Optimisation of RNA isolation	145
Group 1	20-30 (M)	Motorbike accident	Left C6-T1 root avulsion	Somsak's nerve transfer	Medial head of triceps branch of the radial nerve	Optimisation of RNA isolation	156
Group 2	30-40 (M)	Iatrogenic nerve injury secondary to humeral fracture repair	Neurotmesis of the axillary nerve	Somsak's nerve transfer	Axillary	Optimisation of RNA isolation	211
Group 2	20-30 (M)	Car v Tree	Right C4 – C7 avulsion	Oberlin's nerve transfer	Biceps branch of musculocutaneous	Optimisation of RNA isolation	132
Group 2	30-40 (M)	Motorbike accident	Right C5/6 Avulsion	Oberlin's nerve transfer	Biceps branch of musculocutaneous	Optimisation of RNA isolation	146
Group 2	20-30 (M)	Car v Lorry	Axonotmesis of the accessory nerve	Fascicle of C7 transfer to accessory nerve	Fascicle of C7 to pectoralis muscles to accessory nerve	Optimisation of RNA isolation	54
Group 2	20-30 (M)	Motorbike accident	C5/6/7 Avulsion	Double Oberlin's nerve transfer	Biceps branch of musculocutaneous	Optimisation of RNA isolation	64
Group 3	30-40 (M)	Iatrogenic nerve injury secondary to left neck lymph node biopsy	Neurotmesis of the spinal accessory nerve	Supraclavicular nerve transfer to spinal accessory	Supraclavicular and Spinal accessory	Optimisation of RNA isolation	52
Group 3	20-30 (F)	Trampoline accident	Neurotmesis of the ulnar nerve	Sural nerve autograft to ulnar	Ulnar and Sural	Optimisation of RNA isolation	124
Group 3	20-30 (M)	Moped v Lampost	C5-7 Avulsion	Intercostal nerve transfer to triceps division of radial nerve	Radial and Intercostal	Optimisation of RNA isolation	156
Case number 1	20-30 (M)	Motorbike accident	Rupture	Right spinal accessory nerve transfer to suprascapular	Distal stump of suprascapular	RT-qPCR	4
Case number 2	30-40 (M)	Fall and laceration	Rupture and Laceration	Medical cutaneous nerve of arm autograft to ulnar	Distal stump of ulnar	RT-qPCR	8

Experimental Group or Case Number	Age Range (Gender)	Mechanism of Injury	Intraoperative findings	Reconstructive Nerve Procedure	Details of nerve liberated (denervated unless otherwise stated)	Sample used for histology, RT-qPCR or optimisation of RNA isolation?	Denervation Period (Days)
Case number 3	30-40 (M)	Motorbike accident	Neurotmesis	Spinal accessory nerve transfer to suprascapular	Distal stump of suprascapular	RT-qPCR	12
Case number 4	20 -30 (F)	Trampoline accident	Neurotmesis	Sural nerve graft to ulnar	Sural (innervated) and distal stump of ulnar	RT-qPCR	40
Case number 5	30-40 (M)	Motorbike accident	C5-7 Avulsion	Spinal accessory nerve transfer to suprascapular transfer and Double Oberlin's nerve transfer	Distal stump of biceps branch of musculocutaneous and distal stump of suprascapular	RT-qPCR	42
Case number 6	20-30 (M)	Motorbike accident	C5-T1 Avulsion	Right intercostal nerve transfer to long thoracic nerve	Distal stump of long thoracic nerve	RT-qPCR	110
Case number 7	30-40 (M)	Glass Laceration	Laceration	Resection of left common peroneal nerve	Distal stump of common peroneal nerve	RT-qPCR	116
Case number 8	20-30 (M)	Moped v Lampost	C5-8 Avulsion	Intercostal nerve transfer to radial nerve	Intercostal (innervated) and distal stump of radial nerve	RT-qPCR	119
Case number 9	40-50 (M)	Motorcycle v car and bus	C5/6 Avulsion	Spinal accessory nerve transfer to suprascapular	Distal stump of suprascapular nerve	RT-qPCR	119
Case number 10	20-30 (M)	Car v Tree	C5/6/7 Avulsion	Oberlin's nerve transfer	Distal stump of biceps branch of musculocutaneous	RT-qPCR	170
Case number 11	20-30 (M)	Motorbike accident	C5/6 Avulsion	Oberlin's nerve transfer	Distal stump of biceps branch of musculocutaneous	RT-qPCR	180
Case number 12	30-40 (M)	Fall and laceration	High ulnar nerve laceration	Anterior interosseous nerve transfer to ulnar nerve	Distal stump of Ulnar nerve	RT-qPCR	182
Case number 13	50-60 (M)	Mechanical fall	C5/6 Avulsion	Right anterior interosseous nerve transfer to ulnar	Distal stump of ulnar nerve	RT-qPCR	270
Case number 14	50-60 (M)	Iatrogenic - left sided neck lymph node biopsy	Neurotmesis	Spinal accessory nerve transfer to suprascapular	Distal stump of suprascapular	RT-qPCR	375
Case number 15	40-50 (M)	Road Traffic Accident	C5-T1 Avulsion	Spinal accessory nerve transfer to suprascapular	Distal stump of suprascapular	RT-qPCR	478
Case number 16	40-50 (M)	Car v Lorry	Axonotmesis	C7 fascicle to spinal accessory nerve	Distal stump of spinal accessory	RT-qPCR and Histology	540
Case number 17	20-30 (M)	Stab wound to the neck	C5/6 Neurotmesis	Oberlin's nerve transfer	Distal stump of C6	Histology	3
Case number 18	20-30 (M)	Motorbike v Car	C5/6 Avulsion	Oberlin's nerve transfer	Distal stump of biceps branch of musculocutaneous	Histology	30

Experimental Group or Case Number	Age Range (Gender)	Mechanism of Injury	Intraoperative findings	Reconstructive Nerve Procedure	Details of nerve liberated (denervated unless otherwise stated)	Sample used for histology, RT-qPCR or optimisation of RNA isolation?	Denervation Period (Days)
Case number 19	20-30 (M)	Motorbike v Truck	Axonotmesis	Double Oberlin's nerve transfer	Distal stumps of biceps and brachialis branches of musculocutaneous	Histology	42
Case number 20	50-60 (F)	Mechanical Fall	C4/5/6/7 Avulsion	Double Oberlin's nerve transfer	Distal stumps of biceps and brachialis branches of musculocutaneous	Histology	58
Case number 21	20-30 (M)	Motorbike v Tree	Axonotmesis	Oberlin's nerve transfer	Distal stump of biceps branch of musculocutaneous	Histology	107
Case number 22	20-30 (M)	Seizure whilst driving	Axonotmesis	Oberlin's nerve transfer	Distal stump of biceps branch of musculocutaneous	Histology	172
Case number 23	20-30 (M)	Road Traffic Accident	C5/6 Avulsion	Free functioning muscle transfer to restore elbow flexion	Distal stump of biceps branch of musculocutaneous	Histology	4745
Case number 24	30-40 (M)	Road Traffic Accident	C5-C8 Avulsion	Free functioning muscle transfer to restore elbow flexion	Intercostal (innervated)	RT-qPCR	6432
Case number 25	20-30 (M)	Stab wound the neck	Neurotmesis	Subclavian nerve transfer to spinal accessory nerve	Distal stump of spinal accessory	Histology	62
Case number 26	20-30 (M)	Motorbike v Car	Axonotmesis	Nerve to long head of triceps nerve transfer to axillary nerve	Distal stump of axillary nerve	Histology	294
Case number 27	30-40 (M)	Motorbike accident	C5/6 Avulsion	Double Oberlin's nerve transfer	Distal stumps of biceps and brachialis branches of musculocutaneous	Histology	115

Table 2.1 - Tabulation of the patient demographic included in this study.

Group 3: Samples liberated and cryopreserved within 3 minutes but utilising a 'clean change' of surgical gloves and surgical equipment for harvest and handling of the sample to minimise exposure to antiseptic reagents. This group included healthy nerve samples in addition to denervated nerves.

2.1.2 Isolating the effects of antiseptic reagents on RNA yield using a rodent model of peripheral nerve liberation

Standard international operating protocols dictate that iodine and/or chlorhexidine based antiseptic reagents should be used to prepare the site of surgical incision as detailed by the World Health Organisation (2016). In order to investigate the effects

of these reagents on RNA, a rodent model of surgical nerve liberation was utilised in an environment that was otherwise absent of antiseptic reagents. All animal use was performed according to the UK Animal Scientific Procedures Act 1986 / the European Communities Council Directives (86/609/EEC) and approved by the UCL Animal Welfare and Ethics Review Board. A total of 9 Sprague Dawley rats (6 female and 3 male) were culled using CO₂ inhalation and had their sciatic nerves excised. The nerves were then sharply dissected into 0.5cm sections (to reflect the size of samples harvested from human patients). The sections were then randomised into 2 groups:

Control group: Samples were processed before any of the experimental samples to minimise the risk of contamination of the experimental environment.

Experimental group: 100 µl of one of the following commonly used surgical antiseptic reagents were applied by pipette: 10% iodine/water, 10% iodine/EtOH (Ethanol) or 2% chlorhexidine gluconate. Within 30 seconds of the nerve samples being excised, the nerve sample and antiseptic reagent was allowed to stand for 30 seconds and then immediately snap-frozen.

2.1.3 RNA extraction protocol

The 15 nerve samples (12 denervated and three healthy) retrieved for optimisation of RNA yield were used to optimise surgical handling and processing (detailed in **Chapter 3**) of the additional 20 nerve samples collected for RT-qPCR analysis to investigate cellular and molecular features of nerve degeneration (**Table 2.1**). All nerve samples underwent RNA isolation using the following protocol:

All materials (Cole-Palmer® LabGEN 125 tissue homogenizer, Cole-Parmer LabGEN® Rotor-Stator Generator, Fine, 75 mm × 5 mm and the Tecan™ Infinite 200 PRO multimode reader) used in this process of RNA isolation were treated with RNase Zap (Invitrogen). Rodent and human nerves were placed into a 5ml tube and snap frozen in liquid nitrogen. The time between tissue isolation and freezing was

monitored as well as the interaction of samples with antiseptic surgical reagents. RNA was isolated from all nerve samples using the Qiagen RNeasy® Fibrous Tissue Mini Kit. The total volume of eluted RNA for each sample was 40µl.

The quantity of RNA was determined using a Tecan™ Infinite 200 PRO multimode reader. Quality of RNA was measured using a NanoDrop™ spectrophotometer to ascertain 260/280 ratios for each sample. Samples were also analysed using Bio-rad Experion™ RNA analysis kits to assess Ribosomal Integrity Number (RIN), obtain electropherogram data and automated agarose gel readings from samples using the Experion™ Automated Electrophoresis System.

The results obtained from this study were used to inform and enable quantitative mRNA analysis of nerve samples retrieved from reconstructive nerve surgery.

Only those samples collected to characterise cellular and molecular features of human peripheral nerve degeneration were processed for downstream mRNA quantification. Samples collected to optimise RNA yield were not used.

2.1b) Characterising cellular and molecular features of human peripheral nerve degeneration.

2.1.3 RNA to cDNA synthesis

In order to convert RNA to complementary DNA (cDNA), the Qiagen whole genome reverse transcription (RT) kit was utilised. The isolated RNA in solution was thawed on ice (within 1 week of RNA isolation from the nerve sample). A minimum of 10ng of RNA (in 1-5µl of RNase free water) was added to a microcentrifuge tube. The resulting volume of RNA was adjusted to equate to 5µl by adding RNase free water. The RT mix was then prepared using the T-Script Buffer and T-Script enzyme in a ratio of 4:1 respectively. A total of 5µl of this RT mix was added to the 5µl solution of RNA. This mix was then placed into a thermocycler (Applied Biosystems SimpliAmp™

Thermal Cycler) and incubated at 37°C for 30 minutes. After this time period, the reaction was terminated by incubating the mix at 95°C for 5 minutes followed by cooling to 22°C.

The ligation mix was then prepared using Ligation Buffer, Ligation Reagent, Ligation Enzyme 1 and Ligation Enzyme 2 in a ratio of 6:2:1:1 respectively (and added in this chronology). A total of 10µl of this mix was added to the resultant RT mix and then vortexed. This mixture was then incubated in the thermocycler at 22°C for 2 hours. The amplification mix was then prepared by mixing REPLI-g Midi Reaction Buffer and REPLI-g Midi DNA Polymerase in a ratio of 29:1 respectively. A total of 30µl of this reaction mix was added to the ligation mix by vortexing and centrifuging briefly. This mixture was then incubated in the thermocycler at 30°C for 8 hours (high-yield reaction). After this time period, the reaction was terminated by incubating the mixture at 95°C for 5 minutes. The resultant cDNA was then diluted in RNase free water in a ratio of 1/250 (2µl of cDNA added to 500µl of RNase free water) and stored at -20°C until required for downstream RT-qPCR.

RT-qPCR reaction mix

Primers for each gene of interest (GOI) and housekeeping gene (HKG) were designed based on the sequences validated at the Harvard Primerbank (Spandidos et al., 2008, Wang and Seed, 2003) and supplied by Sigma-Aldrich. The sequences for the forward and reverse primers are shown for each gene in **Table 2.2**. All assays were optimised such that the efficiency of the RT-qPCR reactions was between 90%-110% in concordance with published guidelines (Bustin et al., 2009, Rogers-Broadway and Karteris, 2015).

All reaction components were thawed on ice then mixed and briefly centrifuged until the reagents were at the bottom of the tubes. To set up the RT-qPCR reactions a MasterMix was made up of 10µL of PowerUp™ SYBR™ Green MasterMix (2X), 2.5µL

of each forward and reverse (100mM solution) primer and 5µL of DNA template diluted in RNase free water (20 µL/well). Sufficient MasterMix was made to run assays for GOI and HKG for each sample in triplicate. MasterMix was made up as n+1 to allow for pipetting errors. This mixture was transferred into a 96-well optical plate (Thermofisher AB-0800).

Gene	Forward Sequence	Reverse Sequence
c-Jun	TCCAAGTGCCGAAAAGGAAG	CGAGTTCTGAGCTTTCAAGGT
P75NTR	TGAACGACCCCAACAATGTGG	GGCTTTTGCTGATACGCTCG
Krox-20	TCTTCCCAATGATCCCAGACT	TTACGGATTGTAGAGAGTGGAGT
SOX10	AGGCTGCTGAACGAAAGTGACAAG	ACTTGTAGTCCGGGTGGTCTTTCT
18S (Housekeeping gene)	CGCGTTTCTATTTTGTGGT	CGGTCCAAGAATTCACCTC

Table 2.2 - Sequences of forward and reverse primers used in the RT-qPCR assays.

In all reaction well plates, no template negative controls (NTC) were run along with 2 control samples (sural and two intercostal nerve samples from case numbers 4, 8 and 24 respectively shown in **Table 4.3**). For the NTC reactions, 5µl of RNase free water was added to the well instead of cDNA template. The optical well plate was sealed with a MicroAmp™ Adhesive Optical Cover and briefly centrifuged to ensure reagents were collected at the bottom of the plate. The plate was then transferred into the Applied Biosystems (Thermofisher QuantStudio™ 3 System) to run the RT-qPCR assay using the following thermocycling parameters: an initial denaturation stage to 94°C for 2 minutes followed by 40 cycles of heating to 94°C for 15 seconds (denaturation), 60 °C for 1 minute (annealing, extension and read fluorescence).

The Livak (Livak and Schmittgen, 2001) method of quantification was used to determine the relative gene expression by characterising the differential between threshold cycle (C_T) values for the endogenous control (18S) ($C_{T:e}$) and the calibrator (sural/intercostal nerve) sample ($C_{T:c}$) (**Equation 2.1**). 18S was selected as the HKG

as it has been shown to be consistently expressed across different human Schwann cell phenotypes (Gambarotta et al., 2014).

$$\text{Relative Quantification (RQ)} = 2^{-\Delta\Delta C_T}$$

with

$$\Delta\Delta C_T = \Delta C_T - C_{T:c}$$

and

$$\Delta C_T = C_T - C_{T:e}$$

Equation 2.1 – Livak method of quantification.

2.1.4 Immunohistochemistry (performed by Dr. Naomi Guppy)

Immunohistochemistry staining protocols (processed by Dr. Naomi Guppy)

Some of the nerve samples liberated from reconstructive surgical nerve procedures were immediately fixed in 10% formalin and then embedded orthogonally in paraffin wax. Serial cross-sections were cut (3 μ m) using a microtome and immunostaining for Neurofilament, SOX10, c-Jun, P75NTR and Krox-20 performed.

All staining was carried out using the Leica Bond III automated immunostaining platform, using Leica Bond Polymer Refine Detection with a 3,3'-Diaminobenzidine (DAB)/horseradish peroxidase (HRP) chromogen (Leica, DS9800), with incubations at ambient temperature unless otherwise specified.

Dewax was carried out on-board using Leica Bond Dewax solution (Leica, AR9222). Washes were performed between each step using Leica Bond Wash (Leica, AR9590). DAB was enhanced using 0.5% copper sulphate following application for 10 minutes.

After on-board heat-induced epitope retrieval (HIER) with Leica Epitope retrieval solution 2 (Leica ER2, high pH, AR9640) for 20 minutes at 99°C, primary antibodies were applied using the following dilutions (using Leica Bond Primary Antibody Diluent (Leica, AR9352)) at ambient temperature: c-Jun (rabbit monoclonal 16A8, Cell Signalling Technologies #9165, 1:500 for 30 minutes), Krox-20 (goat polyclonal, AbCam ab63943, 1:200 for 15 minutes), Neurofilament (NF200 mouse monoclonal N52.1.7, Leica Biosystems PA0371, applied as supplied for 15 minutes). For the SOX10/P75NTR co-stain, the SOX10 primary antibody was added first (rabbit monoclonal EP268, CellMarque 383R-15, 1:200 for 15 minutes) followed by P75NTR (rabbit polyclonal, Novus Biologicals NBP1-85769, 1:400 for 30 minutes). The Leica Bond Polymer Refine Detection system (Leica, DS9800) was used for post-primary treatment of all the sections. For the SOX10/P75NTR co-stain, the Leica Bond Polymer Refine Red detection system (Leica Biosystems, DS9390) was utilised in addition.

All immunohistochemistry protocols were validated using positive controls (documented in **Appendix 1, Figure 9.1**).

Image Capturing and Quantification

Micrographs were captured using the Leica ATC2000. The total cell count was quantified by manually counting the total number of haematoxylin positive cells within each fascicle using ImageJ software (Rueden et al., 2017). This provided a value for the number of cells per mm². Similarly, the total number of SOX10 positive cells within each fascicle was also calculated to quantify the number of Schwann cells per mm².

In order to assess the presence of c-Jun, P75NTR and Krox-20 immunoreactivity in Schwann cells, double-stained sections or adjacent serial sections were quantified in the same way and related to the number of Schwann cells per mm². The number of

neurofilament positive fibres within each fascicle was also determined to calculate the axon density (axons per mm²) for each nerve sample.

2.1.5 Statistical analysis (nonparametric smoothing linear regression performed by Dr. Simão Larenjeira)

2.1a) Investigating peri-operative variables that can affect the quality and quantity of RNA isolated from human peripheral nerve samples.

Statistical analysis was performed using the SPSS software package (version 19; IBM Corp., Armonk, New York). All data are expressed as a median, mean, and one standard deviation unless otherwise stated. A two-tailed Student's t-test and one-way analysis of variance (ANOVA) test were used to determine statistical significance where appropriate. A p-value of < 0.05 was considered significant.

2.1b) Characterising cellular and molecular features of human peripheral nerve degeneration and Section 2.2) Motor Unit Number Estimation following nerve transfer to reanimate elbow flexion.

The aim of **Chapter 4** and **Chapter 5** was to understand the trends in the data available. Trends are commonly uncovered by fitting polynomials of different orders to data. However, for small data sets this may result in an over fit, not least as the variance in the data is not accounted for. Here, therefore, nonparametric smoothing linear regression was implemented (Härdle and Schimek, 2013). This method groups data points into bins and then performs a linear regression to the points in each bin. The size of the bins (termed bandwidth) is a key parameter choice to ensure the data are well represented without biases. To this effect, a cross-validation method was implemented: the data were randomly sampled into two sets; a range of bandwidth values were tested over several randomly sampled sets of the data. The bandwidth was chosen as that which attained the smallest least mean square error on average for all the prediction data sets. After identifying the optimal bandwidth, the robustness

of the model was tested. This was achieved through a bootstrap methodology, which involved generating thousands of random data samples with the same size as the source data, and applying the linear smoothing algorithm with the bandwidth established over all these samples. From this a mean and standard deviation of all the resulting curves was calculated. Through this method, data trends were more clearly illustrated to facilitate discussion and interpretation.

2.2 Motor Unit Number Estimation following nerve transfer to reanimate elbow flexion

Associated with this theme of characterising human nerve injury, this PhD set out to quantify the number of MUs reinnervating a muscle using MUNE.

This study received full ethical approval (REC reference 17/WM/0438, IRAS ID 231428) and all patients were recruited after fully informed written consent.

2.2.1 Identification of patients

A retrospective and prospective review of the patient database at the Peripheral Nerve Injury Unit, Royal National Orthopaedic Hospital was performed to identify candidates who underwent double Oberlin's nerve transfer between August 2017 and March 2019. Patients were then assessed against the following inclusion criteria: patients had to be over 18 years of age; speak fluent English; able to participate verbally with the process. Patients were excluded if they had impaired cognitive functioning or had difficulties in verbal communication and those who had suffered a birth-related brachial plexus injury. A total of 27 patients met the inclusion criteria and all were sent an invitation to participate in the study by telephone and letter. Those who did not respond, received a follow up phone call. A total of 15 patients were subsequently identified. The demographics of patients included are shown in **Table 5.1**.

2.2.2 Surgical procedure

The surgical procedure was standardised as follows: a neurotomy in the longitudinal orientation was performed along donor median and ulnar nerves. Using low amplitude stimulation, a fascicle (no greater than 1/8th the size of the donor nerve) that demonstrated predominantly wrist flexor activity (FCU/FCR) was identified. Other fascicles were subsequently stimulated to ensure that wrist flexion would be

maintained following donor harvest. Fascicles that demonstrated intrinsic hand function upon stimulation were avoided. The fascicles were dissected to allow long working length and transected distally to allow a direct coaptation end to end under no tension (tested through a full range of elbow movement). This was held with microsuture or fibrin glue as surgeons preference.

2.2.3 STA MUNE (carried out by Dr. Tom Tidswell)

MUNE was performed in nerve injured and contralateral biceps muscles by a single investigator (Dr. Tom Tidswell) who was blinded to the reinnervation time of each patient. A modified STA method was used to determine MUNE using previously published protocols (Boe et al., 2004, Bromberg and Abrams, 1995, Gooch et al., 2014). The skin was prepared using Skin Prep Gel (Nuprep, Weaver and Company) at the electrode placement sites to minimise impedance from the skin. Neurology surface electrodes were used to obtain surface EMG recordings (Ambu® Neuroline Cup, 72610-M/10) and were prepared with electrode paste prior to placement (Ten20® Conductive Neurodiagnostic Electrode Paste, Weaver and Company) in order to improve conductivity. The reference electrode was placed over the acromion, ground electrode on the lateral epicondyle of the humerus (**Figure 2.1**) and the recording electrode over the belly of the biceps muscle (**Figure 2.2**). The placement of the electrodes was determined and optimised in concordance with other biceps MUNE studies and the SENIAM project (Boe et al., 2007, Piasecki et al., 2018, Power et al., 2012, Hermens et al., 1999).

The Synergy UltraPro 3 Channel System was used to record MUNE from the biceps muscles. This involved recording a CMAP by percutaneous stimulation of the motor point of the musculocutaneous nerve located at the axilla (**Figure 2.2**).

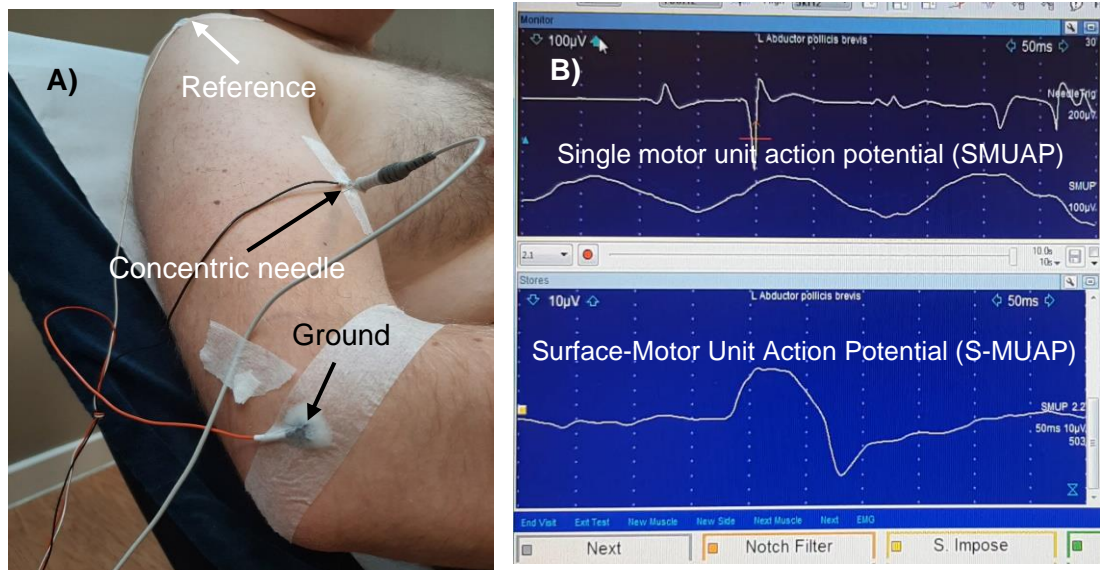


Figure 2.1 - Experimental setup to record a sample of SMUAPs for the MUNE calculation. **A)** Placement of surface electrodes and intramuscular concentric needle in order to record MUNE using a modified STA method. **B)** Isolated single motor unit recorded from intramuscular concentric electrode used to trigger and record a S-MUAP.

In order to record a sample of SMUAPs for the MUNE calculation, a concentric needle (Ambu® Neuroline Concentric 25 x 0.30 mm (1"x30G), 74025-30/25) was introduced into the biceps muscle distal to the recording electrode (**Figure 2.1**). This was utilised to isolate the triggering motor unit spike potentials generated by weak voluntary isometric muscular contractions (**Figure 2.1**). The resulting S-MUAPs (Surface Motor Unit Potentials) were concurrently recorded from the recording surface electrode (**Figure 2.1**) and averaged around 250 times. The concentric needle was inserted at different locations (medial, central and lateral) and depths in order to record a minimum of 15 different SMUAPs. A SMUAP was discarded if it was identical in morphology and amplitude to the previously recorded potential or if it was less than 25µV in amplitude. This technique is thought to allow representative samples of SMUAPs to be obtained from proximal muscle for the MUNE calculation (Bromberg and Abrams, 1995).

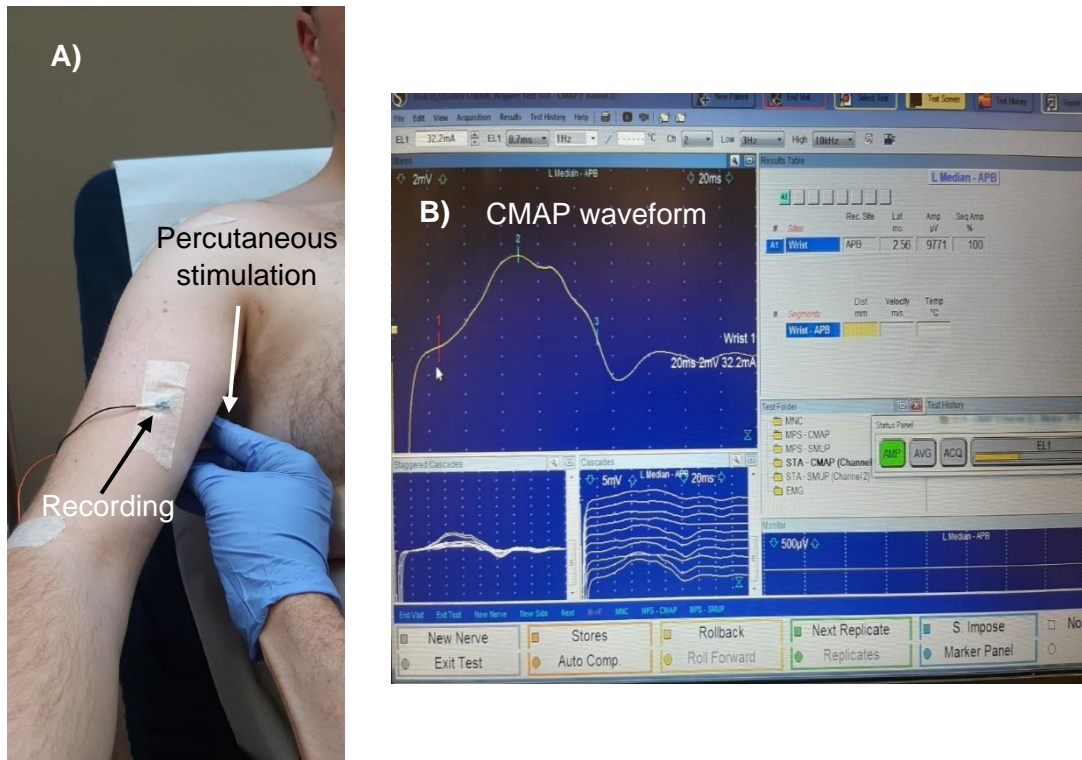


Figure 2.2 - Experimental setup to record a biceps CMAP for the MUNE calculation. **A)** Percutaneous stimulation site of the motor point of the biceps muscle and position of the recording electrode. **B)** Typical CMAP waveform recorded from the biceps muscle.

MUNE was calculated as the negative peak area of the CMAP divided by the mean negative peak area of the population of SMUAPs (**Equation 2.2**).

$$MUNE = \frac{\text{Negative peak area of the CMAP}}{\text{Mean negative peak area of SMUAPs}}$$

Equation 2.2 - MUNE calculation.

This was calculated for the injured arm and the reinnervated arm which allowed the percentage recovery of MUs in the injured arm compared to the reinnervated arm to be quantified. If a patient refused MUNE in their uninjured arm due to poor tolerance of the intramuscular concentric needle electrode, the mean uninjured biceps MUNE value from the other patients was used to calculate percentage recovery of MUNE. Additionally, in cases where CMAPs and S-MUPs were not recordable, estimates of

the number of MUs was obtained using needle EMG and compared with MUNE from the contralateral side.

2.2.4 Test-retest repeatability of the STA MUNE protocol

Four patients and one healthy volunteer underwent test-retests of their uninjured elbow flexor muscles in order to estimate the test-retest repeatability of the STA MUNE protocol. After the initial MUNE assessment, all electrodes were removed and the participant was asked to rest for 5 – 10 minutes. The electrodes were then re-attached and MUNE was repeated using the same protocol.

2.2.5 Statistical analysis (performed by Dr. Simão Laranjeira)

All data are presented as mean, median and interquartile ranges (IQRs) unless otherwise stated. Further information on the non-parametric linear regression implemented to better visualise trends in the data is provided in **section 2.1.5**. In order to determine test-retest repeatability, a two-way random effects model was used to determine the Intraclass Correlation (ICC). ICC values are presented with 95% confidence intervals unless otherwise stated.

2.3 Investigating the relationship of Motor Unit Number Estimation with histological and functional measures of muscle reinnervation

2.3.1 Surgical nerve injury models in vivo

All surgical procedures were performed in accordance with the UK Animals (Scientific Procedures) Act (1986), the European Communities Council Directives (86/609/EEC) and approved by the UCL Animal Welfare and Ethics Review Board. Nine adult female Wistar rats (250-300g) were included in the study. The rats were assigned randomly into groups housed in cages with soft bedding with free access to food and water. Each animal was deeply anaesthetised by inhalation of isoflurane, and the left sciatic nerve was exposed at mid-thigh level. This was done by making an incision around 3cm parallel to the femur between the knee and hip followed by separation of the muscle layers to expose the nerve. Under the microscope (Zeiss CL 1500 ECO) the sciatic nerve and its branches were released from the surrounding tissue. MUNE was then performed in the tibialis anterior and gastrocnemius muscles before performing the crush injury (**Section 2.4.3**).

The crush injury was achieved by application of consistent pressure with a pair of sterile TAAB tweezers type 4 fully closed fully on the same point of the nerve (10mm distal to the hip joint) for 15 seconds. This was repeated an additional two times in the same location with the tweezers positioned perpendicular to the nerve and rotated through 45° between each crush application. The injury site was marked with a 10/0 epineurial suture (Ethicon).

All animals received the same level of interaction throughout the study. They were handled prior to surgery and throughout the study for training and completion of functional testing. All animals were given 5 minutes resting time before functional measurements were recorded. The following protocols were deployed at seven (n=3), 21 (n=5), 31 (n=5) and 42 (n=5) days post-crush (n=3 in each group). The first three

rodents in the seven days, 21 days and 42 days were used to determine the repeatability of MUNE in tibialis anterior and gastrocnemius muscles. The time points were chosen on the basis of previously published experimental evidence which measured NMJ changes in reinnervated tibialis anterior muscles (Magill et al., 2007).

2.3.2 Nerve and muscle tissue harvest

At the end point of the experiment, animals were culled using a Schedule 1 method (CO₂ asphyxiation) according to local regulations. The injured nerves were excised under an operating microscope and sectioned as required for analysis.

An incision was made in both hind legs from the hip down to the paw. The gastrocnemius and tibialis anterior muscles were exposed by an incision in the muscle plane. The gastrocnemius muscle was then separated from the soleus muscle by peeling back the muscle and gently freeing the plane. The tibialis anterior was liberated from the anterior aspect of the hindlimb.

The harvested muscle from each leg was then immediately placed in 4% PFA. The muscle was removed from the 4% PFA and excess fluid removed within 15 minutes of harvesting and weighed. Muscle samples were then stored at 4°C in Phosphate Buffered Saline (PBS).

2.3.3 Immunohistochemistry of nerve samples

Cryosectioning

Following fixation, nerve samples were divided into tibial and common peroneal branches for sectioning. Each nerve segment was immersed in 30% sucrose overnight at 4°C. All segments were snap frozen in Optimal Cutting Temperature (OCT) using liquid nitrogen cooled isopentane. Transverse sections that were 10µm thick were taken from the distal segment of the common peroneal and tibial nerve using a cryostat (Leica CM1860). Sections were adhered to glass slides (Superfrost™ Plus, Thermo Fisher Scientific) for immunofluorescence staining.

Immunofluorescence staining

All washes and dilutions were performed using immunostaining buffer (PBS containing 0.002% sodium azide and 0.3% Triton-X). Slides were heated to 37°C for 20 minutes to induce antigen retrieval and then blocked with 5% horse serum for 40 minutes then incubated in primary antibodies (Neurofilament 1:500, Eurogentec, SMI-35P-050 and Choline Acetyltransferase 1:50, Millipore, AB144P) overnight at 4°C. After washing, sections were incubated with appropriate DyLight-conjugated secondary antibodies (Anti-mouse 549 1:300 and Anti-goat 488 1:300 both from Vector Laboratories at room temperature for 1 hour. Sections were mounted using Vectashield Hardset mounting medium with DAPI (Vector Laboratories). A sample of sural and deep peroneal nerve to tibialis anterior retrieved during the animal surgeries was used as a negative and positive control respectively for ChAT/neurofilament staining (**Appendix 2, Figure 10.1**).

Imaging of motor axons

Fluorescence microscopy (Zeiss Axiolab A1, Axiocam Cm1) was used to capture immunofluorescence images of the nerve sections. Image analysis was conducted using Image J (Rueden et al., 2017). The number of axons (positive for neurofilament) that co-expressed choline acetyltransferase (ChAT) was quantified in each nerve that supplied the gastrocnemius and tibialis anterior muscles (**Figure 2.3**). These fascicles were identified on the basis of previous studies that used retrograde labelling techniques to determine the topographical organisation of the common peroneal and tibial nerves (Badia et al., 2010, Bondok et al., 1990).

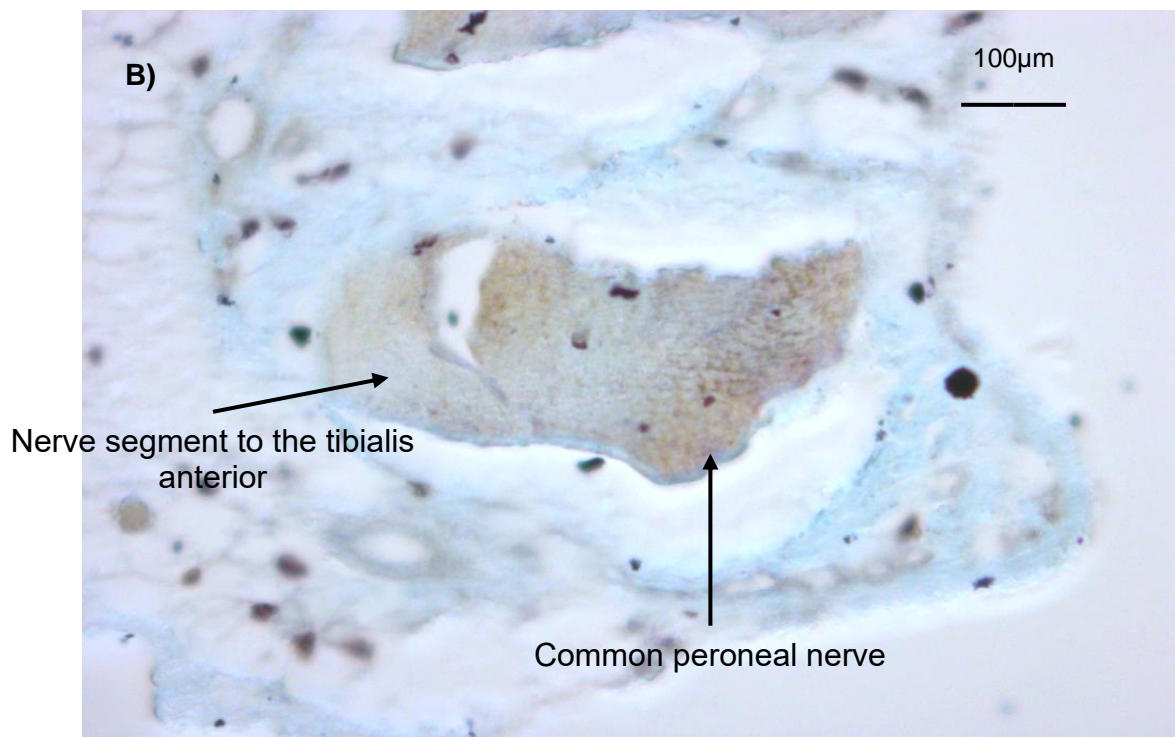
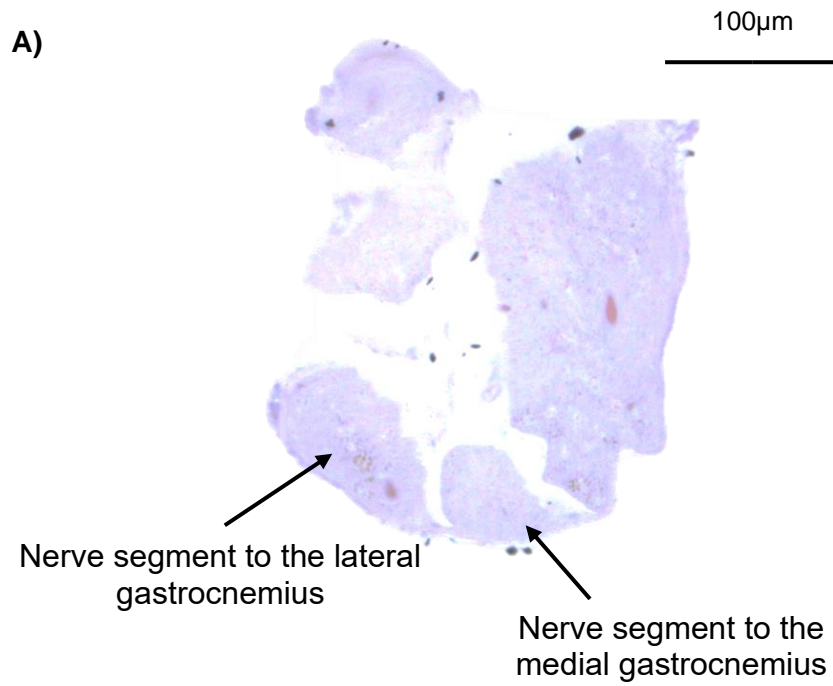


Figure 2.3 - Nerve supply to the gastrocnemius and tibialis anterior muscles. **A)** Tibial nerve with fascicles to the medial and lateral gastrocnemius muscle labelled. **B)** Common peroneal nerve with fascicle to the tibialis anterior muscle labelled.

2.3.5 Immunohistochemistry of muscle samples

Cryosectioning

Following fixation, muscles were immersed in 30% sucrose overnight at 4°C. Samples were then snap-frozen in OCT using liquid nitrogen cooled isopentane. Transverse sections that were 20µm thick were taken at 600µm intervals using a cryostat (Leica CM1860). A minimum of 20 sections from each sample were obtained from the entire cross section of muscle. Sections were adhered to glass slides (Superfrost™ Plus Thermo Fisher Scientific) for immunofluorescence staining.

Immunofluorescence staining

All washes and dilutions were performed using immunostaining buffer (PBS containing 0.002% sodium azide and 0.3% Triton-X). Slides were heated to 42°C for 30 minutes with 20µg/ml proteinase K and then blocked with 10% goat serum for 40 minutes at room temperature. After washing, the sections were incubated in primary antibody (neurofilament, Eurogentec, 1:500). After washing, the sections were incubated with anti-mouse 488 (1:300 Vector Laboratories) and alpha-bungarotoxin (1:1000 Thermofsiher scientific). Sections were mounted using Vectashield Hardset mounting medium with DAPI (Vector Laboratories).

Imaging of the neuromuscular junction

Fluorescence microscopy (Zeiss Axiolab A1, Axiocam Cm1) was used to count the total number of motor endplates (alpha-bungarotoxin) and the number of co-stained reinnervated motor endplates. In addition, the ratio of nerve fibres to NMJs was quantified. For each sample, a minimum of 30 non-overlapping regions of the entire muscle cross-section was analysed. In order to avoid bias, sections were taken 300µm apart.

2.3.6 Functional outcomes in vivo

Compound Muscle Action Potential (CMAP) recording

A reference, ground and recording electrode (Natus) was attached to each animal. The ground was placed into the tail and a reference electrode above the hip bone. A microchannel neural interface (MNI) was placed around the nerve approximately 2mm proximal to the injury site and used to stimulate the nerve. The electrode impedance of the MNI was $27.1 \pm 19.8\text{k}\Omega$ at 1kHz. The MNI was manufactured using a previously documented protocol (Lancashire et al., 2016).

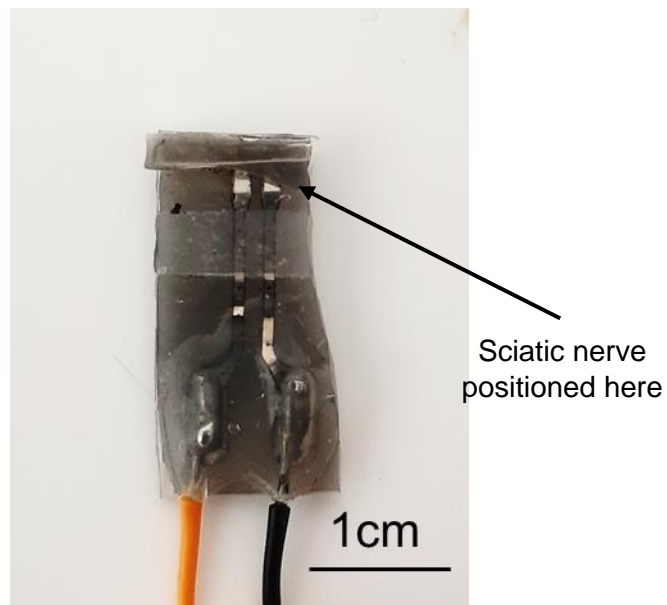


Figure 2.4 - Microchannel neural interface used to stimulate the sciatic nerve.

A monopolar recording needle (Ambu® Neuroline) was inserted into the gastrocnemius or tibialis anterior muscle. The distance between the recording and stimulating electrodes was standardised. The nerve was stimulated with a bipolar voltage configuration and the muscle response recorded. The CMAP was obtained by stimulating the sciatic nerve with square wave pulses of $100\mu\text{s}$ duration and intensity ranging from 1-10mA. The stimulus was increased in 0.2mA steps until the

amplitude of the muscle response no longer increased and was accompanied with a significant twitch of the animal's hindpaw. In order to ensure supramaximal stimulation, the stimulation intensity was increased to around 120% of the intensity used to yield the maximal response and obtain an additional response. If there was no further increase in the magnitude of the CMAP, this response was accepted as the CMAP. The amplitude of the CMAP was measured from peak to peak and recorded. This process was performed in triplicate to ensure the response was reproducible, stable and represented the maximal response.

Mean SMUAP magnitude and MUNE Calculation

A modified version of multipoint MUNE was performed to quantify the number of MUs innervating the tibialis anterior and gastrocnemius muscles (Shefner et al., 2006, Kasselmann et al., 2009, Jacobsen et al., 2018). The mean SMUAP size was determined with a modified multipoint stimulation (MPS) technique as previously reported in other studies (Kasselmann et al., 2009, de Carvalho et al., 2018, Arnold et al., 2015). Incremental responses were obtained by delivering a submaximal stimulation of 100 μ s duration at a frequency of 1Hz while increasing the stimulus intensity in increments of 0.02mA to obtain minimal all or none responses (**Figure 2.5**). The initial response was obtained with a stimulus intensity of between 0.21mA and 0.70mA. If the initial response did not occur between these stimulus intensities, the stimulating electrode was adjusted to increase or decrease the stimulus intensity as required (**Figure 2.5**). Additional increments were evoked by incremental stimulation in increments of 0.02mA to obtain a minimum of four additional increments.

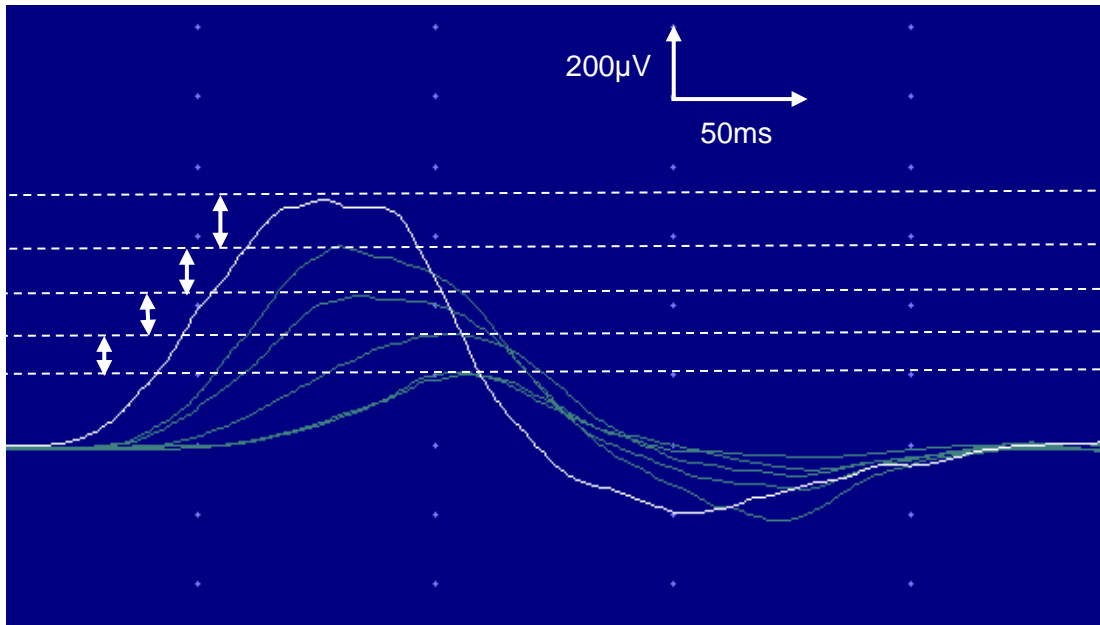


Figure 2.5 - Single motor unit action potentials (SMUAPs) recorded from an uninjured tibialis anterior muscle using an incremental stimulation technique. The white arrows represent the SMUAP size. The mean increment in stimulating current required to recruit an additional motor unit (MU) was quantified and used for the MUNE calculation.

In order for SMUAPs to be accepted for analysis, they had to meet the following criteria (**Figure 2.5**):

- Negative peak should be approximately temporally aligned with the CMAP response.
- Each response stable and unfractionated established by observing duplicate responses.
- Each increment visually distinct and larger compared to the preceding response.
- After each increment is visually confirmed, the amplitude difference between each additional increment was at least 25µV. If the difference was smaller than 25µV, the response was re-recorded.

- After recording all responses, the increments were assessed to ensure that the peak to peak amplitude of the responses was not greater than 1/3 of the total value of all the increments recorded at a site.

The position of the stimulating electrode and the location of the recording electrode was changed to allow the recording of SMUAPs from a different site of the muscle. This process was repeated at least three times in order to obtain a representative sample of at least 12 SMUAPs and to avoid alternation. The mean incremental value was calculated for each site to give an estimate of the mean SMUAP size. MUNE was calculated by dividing the CMAP amplitude (peak-to-peak) by the mean SMUAP amplitude (peak-to-peak) (**Equation 2.3**):

$$MUNE = \frac{CMAP \text{ amplitude (peak - to - peak)}}{Mean \text{ SMUP amplitude (peak - to - peak)}}$$

Equation 2.3 - Equation used to determine MUNE.

Static sciatic index

Functional recovery was measured using the static sciatic index (SSI). The hindpaw of each rat was imaged (a minimum of three images were obtained using a Samsung Galaxy A5 camera with the animal placed in an elevated Perspex box) at one and seven days following the crush injury then every three to four days until the endpoint of the experiment. Images were analysed using Image J (Rueden et al., 2017) to obtain the following parameters (**Figure 2.6**):

Toe Spread Factor (TSF) – the distance between the first and the fifth toe.

Intermediary Toe Spread Factor (ITSF) – the distance between the second and the fourth toe.

These values were then used to calculate the SSI using the following equation:

$$\text{SSI} = (108.44 \times \text{TSF}) + (31.85 \times \text{ITSF}) - 5.49$$

$$\text{TSF} = \text{TS}_{\text{injury}} - \text{TS}_{\text{control}}$$

$$\text{ITSF} = \text{ITS}_{\text{injury}} - \text{ITS}_{\text{control}}$$

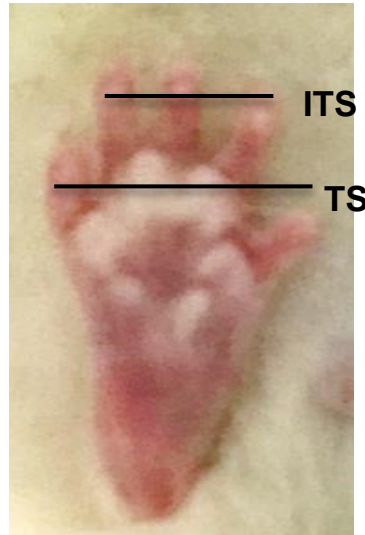


Figure 2.6 - Toe spread measurements used to quantify the SSI.

2.3.7 Statistical analysis

Statistical analysis was performed using the SPSS software package (version 19; IBM Corp., Armonk, New York). All data are expressed as a median, mean, and one standard deviation unless otherwise stated. A two-tailed Student's t-test and one-way ANOVA test were used to determine statistical significance where appropriate with post-hoc Bonferroni correction. A p-value of < 0.05 was considered significant. A power analysis was conducted based on the variance of MUNE from a pilot experiment on uninjured Sprague-Dawley rats and an effect size of 30%. According to the power analysis, five animals per experimental group were required to reach statistical significance $\alpha = 0.05$ and 80% power.

2.4 Quantitative MRI muscle volume analysis following nerve transfer to reanimate elbow flexion

Changes in the number of MUs supplying a muscle are associated with changes in muscle mass and volume (Wu et al., 2014). Therefore, this part of the PhD aimed to quantify the recovery of elbow flexor muscle volume following nerve transfer to reanimate elbow flexion. This study received full ethical approval (REC reference 17/YH/0413, IRAS ID 235012) and all patients were recruited after fully informed written consent.

2.4.1 Patient selection

A retrospective and prospective review of the institute database was performed to identify candidates who underwent nerve transfer to reanimate elbow flexion between August 2017 and March 2019. The operation was performed as described in **section 2.2.1**. Patients were assessed against the following inclusion criteria: patients had to be over 18 years of age; speak fluent English; able to participate verbally with the process. Patients were excluded if they had impaired cognitive functioning or had difficulties in verbal communication and those who had suffered a birth-related brachial plexus injury. A total of 53 patients were screened against the inclusion criteria and all were sent an invitation to participate in the study by telephone and letter. Those who did not respond, received a follow up phone call. All patients were requested to attend MRI and neurophysiological assessment of their injured arms. Invites for additional follow-up appointments were sent every three months following the previous appointment. Patients were withdrawn from the study if they no longer wished to attend additional assessments.

2.4.2 Quantitative MRI

Image acquisition

All imaging was obtained on a 3-Tesla MRI Philips scanner (Achieva, Philips, The Netherlands) using phased array coils. All patients were imaged utilising a standardised protocol with the arm in the supine position (**Table 2.3**). The injured arm was imaged in all 25 patients whilst the uninjured arm was imaged for comparison in six healthy male volunteers.

Imaging parameter	Coronal T1-w Spin Echo	Coronal STIR	Sagittal T2-w Fast Spin Echo	Axial PDW Fast Spin Echo	Axial Fast Spin PDW Fast Spin Echo
Field of view	270x190mm ²	270x190 mm ²	270x190 mm ²	200x200 mm ²	200x200 mm ²
Repetition time	643	4000	3000	3000	3000
Echo time	20	80	100	30	30
Slice thickness	3mm	3mm	3mm	4mm	4mm
Interslice gap	0.3mm	0.3mm	0.3mm	0.4mm	0.4mm
Matrix	364x225	192x127	320x201	288x254	288x274
Bandwidth	361.5	1033	291.5	331	361

Table 2.3 - MRI imaging parameters used to acquire scans of injured and uninjured elbow flexor muscles.

Bias field correction

Images were corrected for intensity non-uniformity using a nonparametric nonuniform intensity normalization model (Sled et al., 1998).

Segmentation protocol to quantify elbow flexor muscle signal and volume

The NiftyView software package (UCL, London, UK) was used to perform segmentation as well as signal intensity and volume measurements. Uninjured and injured elbow flexor muscles were manually segmented using previously documented protocols which demonstrated high repeatability and reliability (O'Brien et al., 2009, Sanchis-Moysi et al., 2012, Vidt et al., 2012). Proximally, segmentation was

commenced at the unification of the long and short heads of the biceps tendon. Once the distal part of the medial condyle of the humerus became visible, segmentation was terminated. The volume and mean signal intensity of the elbow flexor muscles was recorded. The shaft of the humerus was segmented and used to calculate the ratio of elbow flexor muscle signal intensities to the signal intensity of the humeral shaft for T1-w, Proton Density Weighted (PDW) and T2-w images. To provide some standardisation for differences in elbow flexor muscle volume that may arise due to environmental factors, BMI measurements were recorded from participants at each MRI scan appointment. BMI has been shown to be positively correlated ($R^2 > 0.7$) in a number of studies with measurements of muscle volume and upper arm diameter (Benítez Brito et al., 2016, Kumar et al., 2019). Therefore, the elbow flexor muscle volume per unit BMI was determined.

Scan-rescan, inter- and intra-investigator repeatability of the segmentation protocol

One patient and three healthy volunteers underwent scan-rescan tests of their injured and healthy arms (on the dominant side) respectively to determine scan-rescan reproducibility of the qMRI measurements. After the initial scan, patients were asked to get off the scanner table, rest for 5-10 minutes and then get back on to the table again for the second scan with the same imaging protocol. For the assessment of inter- and intra-investigator repeatability assessment, the first 20 MRI scans to be acquired in the study were each manually segmented by an investigator (Matthew Wilcox) and a PhD student (Dr. Kununya Pimolbutr) to quantify the ratio of elbow flexor muscle signal intensity to the signal intensity of the humeral shaft and the elbow flexor muscle volume per unit BMI acquired from T1-w, PDW and T2-w images. The ICC was used to quantify the scan-rescan, inter- and intra-investigator agreement of the segmentation protocol.

2.4.3 Statistical analysis

All data is presented as mean, median and standard deviation unless otherwise stated. Two-tailed Student's t-test was used to determine statistical significance where appropriate. A p-value of <0.05 was considered significant. A two-way random effects model was used to determine the ICC. ICC values are presented with 95% confidence intervals unless otherwise stated.

Chapter 3: Investigating peri-operative variables that can affect the quality and quantity of RNA isolated from human peripheral nerve samples

3.1 Introduction

The extraction of RNA in sufficient quantity and quality is a critical step towards obtaining valid RT-qPCR/RNA seq results (Abasolo et al., 2011, Atz et al., 2007, Popova et al., 2008). A minimum concentration of 5 ng/ μ l is often used for the synthesis of single stranded complementary DNA (cDNA) (Fox et al., 2012, França et al., 2012) and in the quantitative and qualitative assessments of RNA yields; a critical step towards valid RT-qPCR and/or RNA seq results (Bastard et al., 2002, Fleige and Pfaffl, 2006, Wilkes et al., 2010). The quality of RNA can be determined using quantitative and qualitative assays; 260/280 ratios and electropherograms respectively (Mee et al., 2011, Samadani et al., 2015, Walker et al., 2016, Yockteng et al., 2013). When optimising RNA extraction protocols to attain yields sufficient for RT-qPCR assays, it is necessary to consider the tissue that is being processed; a review of the literature highlights differentials in the yield of RNA isolated from different tissues (Grinstein et al., 2018, Ruettinger et al., 2010, Walker et al., 2016).

Based on experiences within our research unit and others, there appears to be a differential between the RNA extraction ratio (mean total RNA (μ g) divided by initial tissue sample mass (mg)) of healthy and denervated nerve liberated from rats. Typical values range from 0.09 μ g/mg for healthy sciatic nerve and 0.27 μ g/mg for denervated sciatic nerve (Weng et al., 2018, Yamamoto et al., 2012). This differential is perhaps attributable to the presence of higher numbers of proliferating cells in denervated tissue. Moreover, the degradation of connective tissue during Wallerian degeneration is likely to make denervated tissue more amenable to complete lysis. In comparing peripheral nerve to other tissues, the reported RNA extraction ratios are considerably lower than those reported for RNA isolated from tissues such as liver,

kidney and spleen which have mean extraction ratios of 1.56µg/mg, 0.50µg/mg and 0.41µg/mg respectively (Yamamoto et al., 2012). The lower RNA yields reported from nerve samples are at least partially attributable to the fact that nerves are invested by fibrous connective tissue particularly in the epineurium (Thomas, 1963). The biomechanical properties of this tissue are antagonistic to total cellular disruption and lysis of nerve tissue which is an imperative step in RNA isolation (Bastard et al., 2002, Guan and Yang, 2008). This is an indication for the application of specialist RNA extraction kits which include a broad spectrum serine protease such as proteinase K to facilitate optimal digestion of tissue and lysis of cells (Amini et al., 2017, Peeters et al., 2016, Yockteng et al., 2013).

Accepting that the concentration of RNA that can be isolated from peripheral nerve tissue is likely to be lower than other tissues, it is pertinent to optimise surgical protocols in order to conserve whatever RNA is available. One variable that has been shown to be predictive of the quality and quantity of RNA extracted from samples is the time interval between sample liberation and cryopreservation (Borgan et al., 2011, Caboux et al., 2013, Hatzis et al., 2011), a variable that is difficult to control in the surgical environment due to intra-operative priorities and handling limitations. It has been shown that delays of hours between sample liberation and cryopreservation impairs RNA isolated from cancerous samples (Borgan et al., 2011, Caboux et al., 2013, Hatzis et al., 2011). However, corresponding time frames using human nerve samples have not been reported.

While a number of past studies of other surgically liberated tissues for qPCR analysis have been optimised by manipulating variables such as time delays and RNA extraction protocols (Borgan et al., 2011, Caboux et al., 2013, Hatzis et al., 2011), the exploration of other peri-operative variables that could impact on RNA yields, such as the chemical environment, have not been reported. The liberal application of

antiseptic compounds in a surgical setting may influence RNA yields although this has not been reported previously. The most common constituents of these reagents globally are chlorhexidine and iodine (Hirsch et al., 2010a, Hirsch et al., 2010b). Despite in vitro experimental evidence demonstrating chlorhexidine and iodine based surgical antiseptic reagents can be cytotoxic to human SH-SY5Y neuroblastoma cells and rat RSC96 Schwann cell populations (Doan et al., 2012), their effects on RNA yield and quality have not been well characterised.

Protocols that detail how human nerve samples should be handled to optimise RNA yields for subsequent RT-qPCR and RNA seq analysis are not documented. This study aimed to explore the time course of RNA degradation in nerve tissue in order to establish an ideal time frame for the liberation of human nerve samples and cryopreservation (snap-freezing in liquid nitrogen). Additionally, this study aimed to investigate for the first time the effect of exposure of human nerve samples to surgical antiseptic reagents. Together, this has the capacity to allow downstream quantitative analysis of cellular and molecular features of human peripheral nerve regeneration.

3.2 Results

The effect of time between tissue extraction and freezing on the yield of RNA isolated from human nerve samples was investigated (Group 1 and Group 2). **Figure 3.1** demonstrates that the optimal yield of RNA isolated from samples cryopreserved within 3 minutes of surgical liberation (Group 1) is approximately 3.6-fold higher than that from samples frozen after more than 3 minutes (Group 2) ($p < 0.01$). Importantly, the latter group had an RNA yield approximately equivalent to the minimum threshold value required for acceptable analysis and cDNA synthesis (Bastard et al., 2002, Fleige and Pfaffl, 2006, Fox et al., 2012, França et al., 2012, Wilkes et al., 2010).

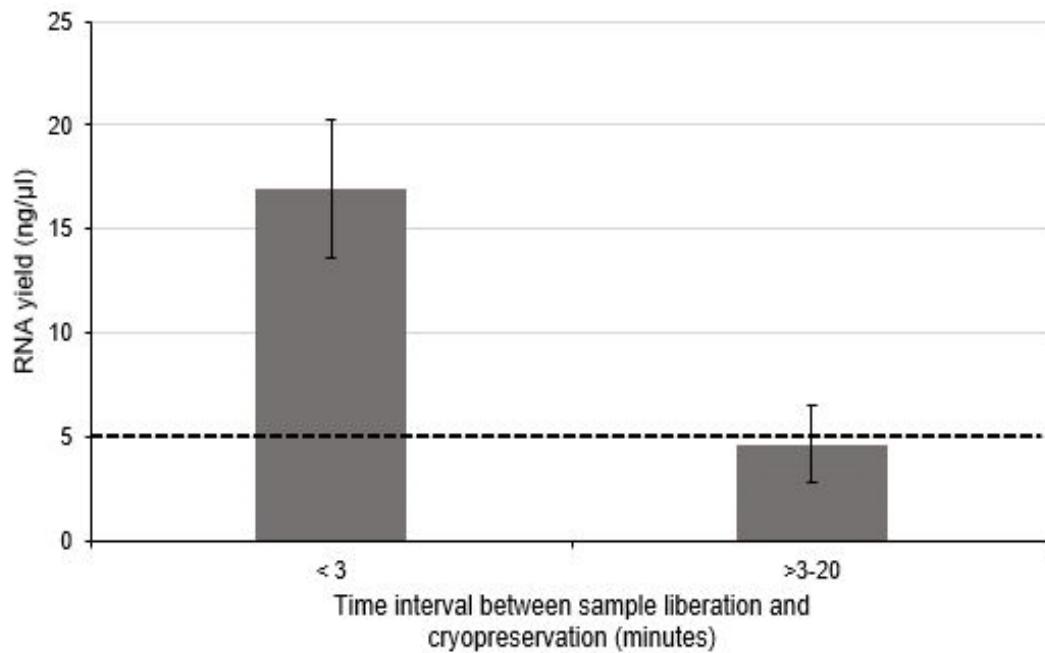
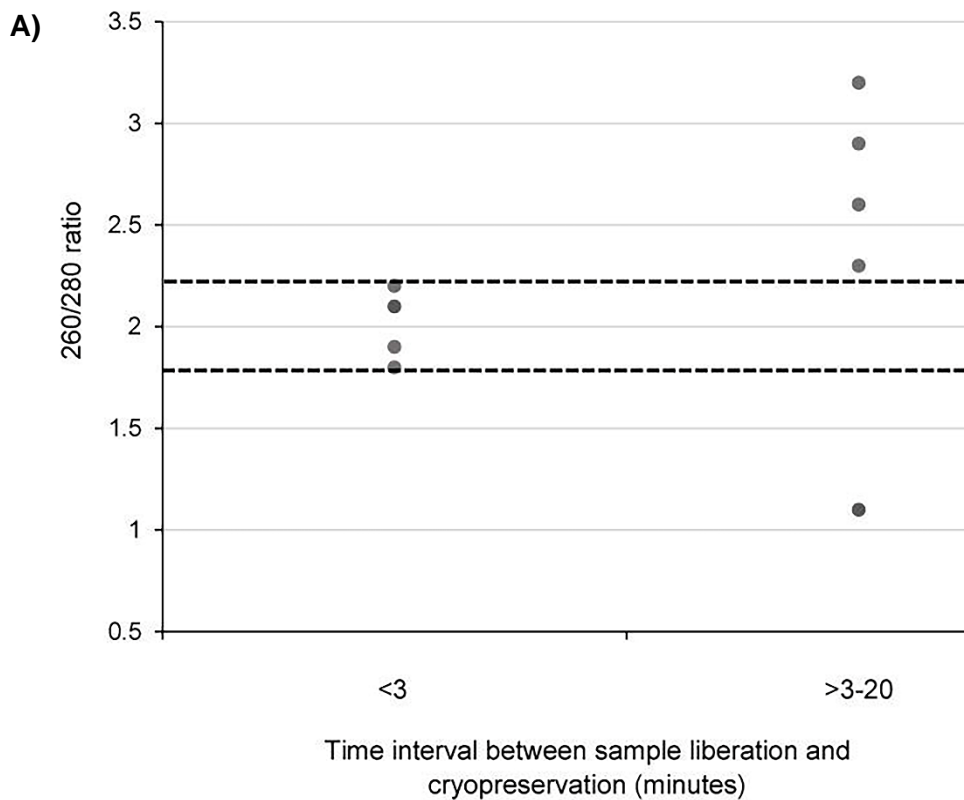


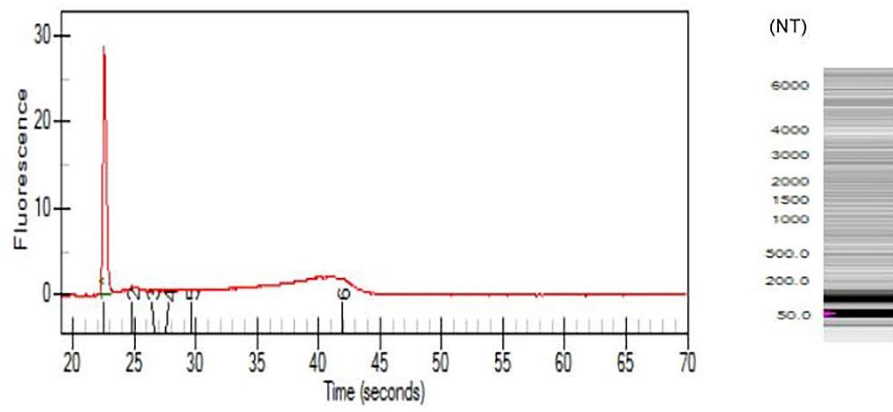
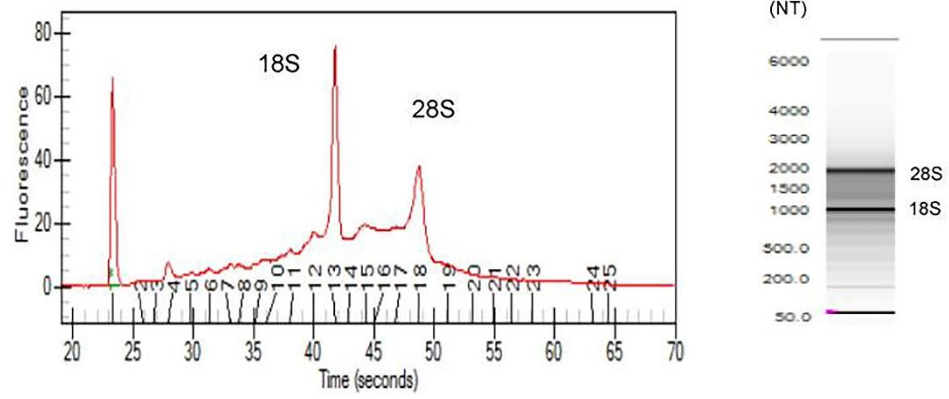
Figure 3.1 - The effect of time between tissue liberation and cryopreservation on RNA yield in human nerve tissue in a surgical environment utilizing standard antiseptic protocols. The duration between nerve tissue removal and freezing was monitored and samples were grouped according to whether the delay was more than (n = 5) or less than 3 min (n = 4). There was a statistically significant difference between each group ($p < 0.01$ two tailed t-test). The dotted black line represents the minimum concentration of RNA often cited (Bastard et al., 2002; Fleige and Pfaffl, 2006; Wilkes et al., 2010; Fox et al., 2012; França et al., 2012) required for downstream RT-qPCR/RNA seq.

The quality of RNA extracted from these nerve samples was concurrently determined quantitatively using 260/280 absorbance ratios (**Figure 3.2A and C**) and semi-quantitatively by analysing the ratio of ribosomal RNA bands in agarose gels and changes in electropherogram morphology (**Figure 3.2B and D**). Nucleic acids have an absorbance maximum at 260nm. The ratio of this to the absorbance at 280nm is used to determine the purity of DNA and RNA. A ratio of 1.8-2.2 is predictive of high quality RNA (Desjardins and Conklin, 2010). An electropherogram describes a chart that is produced when electrophoresis is used as an analytical technique.

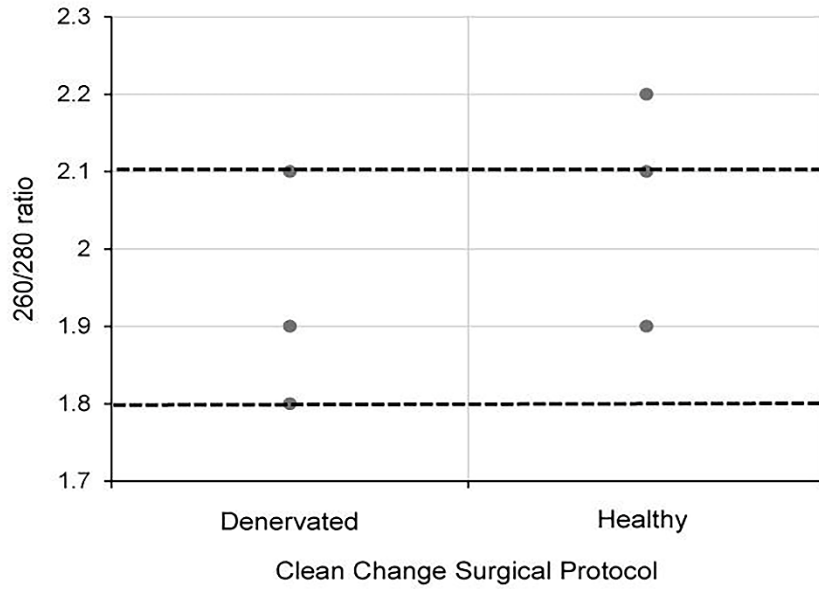
The distribution of 260/280 ratios assessed for samples cryopreserved within 3 minutes (Group 1) is shown in **Figure 3.2A**, all of which fall within the optimal range (1.8-2.2). In addition, two distinct ribosomal RNA bands at 28S and 18S with a ratio of around 2.0 can be seen in the agarose gels (**Figure 3.2B**) indicating high quality RNA isolated from samples processed within 3 minutes. **Figure 3.2B** demonstrates how this ratio is lost in samples exposed to time delays of up to 20 minutes (Group 2 samples). An electropherogram was also assessed to illustrate the overall size of the ribosomal peaks and to further characterise the differential in RNA quality between samples processed within 3 minutes and those exposed to time delays (**Figure 3.2B**).



B)



C)



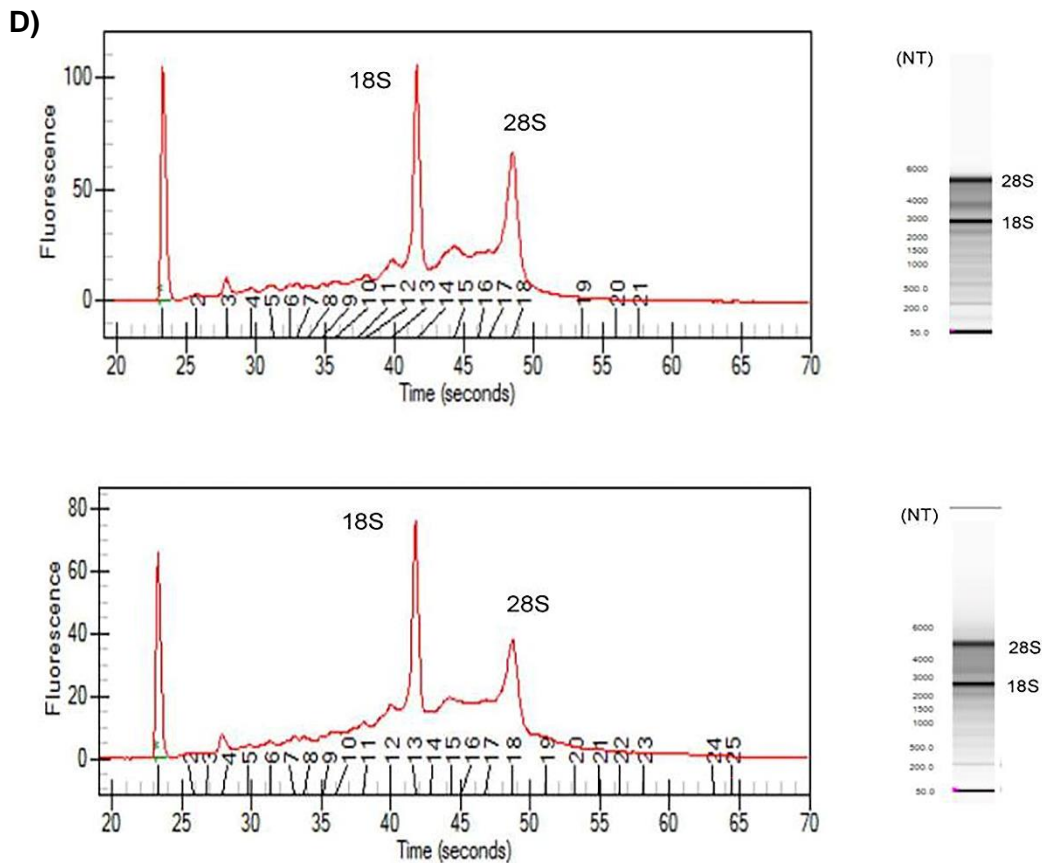


Figure 3.2 - The effect of time delays and surgical antiseptic reagents on the quality of RNA isolated from human nerve tissue. **A)** scatter plot to demonstrate the distribution of 260/280 ratios yielded from RNA isolated from denervated human nerve samples surgically liberated and cryopreserved within 3 min (experimental Group 1) compared to those that were not cryopreserved within this timeframe (experimental Group 2). The two dotted black lines represent the range of 260/280 ratios that is predictive of high quality RNA (1.8–2.2). **B)** Electropherograms (left) and agarose gels (right) digitally produced by the Experon™ Automated Electrophoresis System to assess quality of RNA isolated from denervated human nerve samples. The electropherogram is displayed with fluorescence on the y-axis and time of the fragment on the x-axis. The upper electropherogram/agarose gel represents a denervated sample cryopreserved within 3 min (Group 1) and the lower electropherogram/agarose gel represents a denervated sample that was exposed to a time delay of 20 min (Group 2). **C)** A scatter plot to represent the 260/280 ratios yielded from healthy and denervated samples liberated under a “clean change” surgical protocol (Group 3). **D)** Electropherogram (left) and agarose gels (right) to assess the quality of RNA isolated from healthy and denervated samples liberated under a “clean change” surgical protocol. The upper electropherogram/agarose gel

represents a denervated sample (Group 3) and the lower electropherogram/agarose gel represents sural nerve (Group 3). All samples that yielded 260/280 ratios of between 1.8 and 2.2 were assessed to have Ribosomal Integrity Numbers (RIN) of between 7 and 10 (predictive of high quality RNA).

Using the data from the electropherogram reports, a Ribosomal Integrity Number (RIN) ranging from 1 to 10 (with 10 being predictive of high quality RNA) was assigned to each sample. RIN is generated using an algorithm that selects features from the electropherograms and constructs regression models based on Bayesian learning techniques. This assessment has been validated in a number of studies and has been shown to be highly predictive of RNA quality (Imbeaud et al., 2005, Mueller O, 2004, Schroeder et al., 2006). It was found that all samples with 260/280 ratios between 1.8 and 2.2 (considered optimal) had RIN of between 7 and 10. Moreover, samples that did not have a ratio of between 1.8 and 2.2 had a RIN lower than 7. This provides further evidence that this RNA is of high quality and suitable for RT-qPCR and/or RNA seq analysis.

Since RNA yields from human denervated tissue remained lower than those reported from rodent studies (Weng et al. 2018; Yamamoto et al. 2012), this necessitated further exploration of peri-operative variables. Specifically, the effect of surgical antiseptics on RNA yield. **Figure 3.3** suggests that samples liberated using the “clean change” surgical protocol (Group 3) yielded RNA in concentrations 2.8 times higher than those extracted under standard conditions ($p < 0.01$) (Groups 1 and 2). In comparing denervated tissue to healthy nerve samples, the concentration of RNA isolated from healthy nerve samples was significantly lower than that from denervated tissue ($p < 0.05$) (**Figure 3.3**). Assessments of RNA quality (260/280 absorbance ratios, ratio of ribosomal RNA bands in agarose gels and changes in electropherogram morphology) suggested that the RNA was of high quality (**Figure**

3.2C and D) similar to the quality of RNA from nerve samples cryopreserved within 3 minutes (**Figure 3.2B and C**).

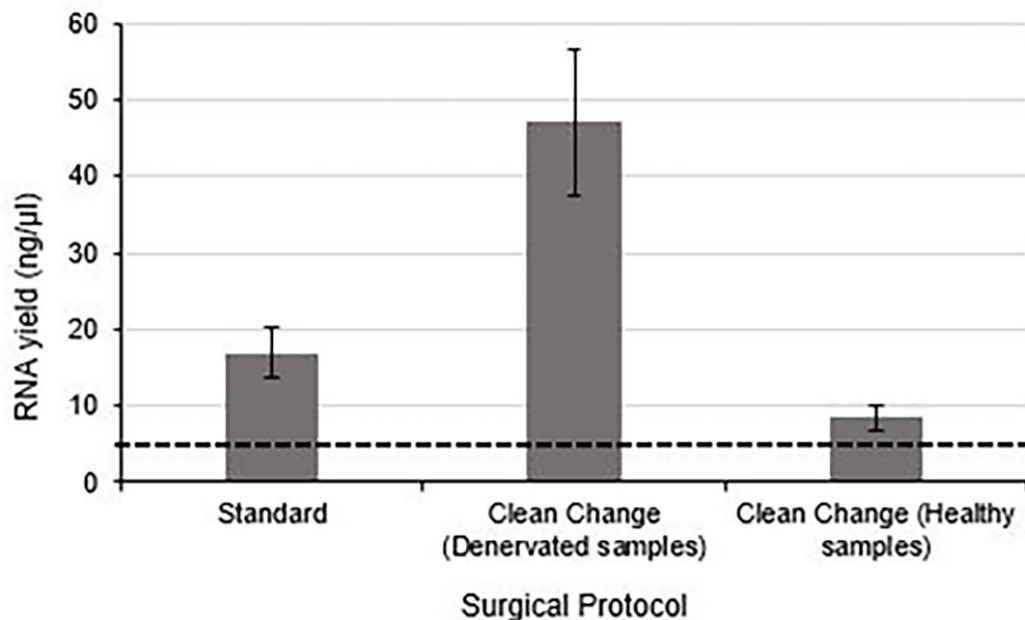


Figure 3.3 - Even when the time delay is minimized/equivalent between samples there is still a large differential in RNA yield due to exposure to surgical antiseptics. Denervated samples were liberated under a standard (n = 4) and “clean change” (n = 3) surgical protocol. Samples liberated in a surgical environment where the “clean change” surgical protocol was implemented yielded RNA concentrations significantly higher than those liberated under standard conditions ($p < 0.01$, two tailed t-test). Healthy nerve samples were also liberated under a “clean change” protocol (n = 3) which yielded significantly lower concentrations of RNA compared to denervated samples ($p < 0.001$ two tailed t-test). The dotted black line represents the minimum concentration of RNA often required for downstream RT-qPCR/RNA seq.

Using nerve tissue freshly harvested from rats under carefully controlled environmental conditions enabled the effects of antiseptic reagents to be studied in isolation. A significant decrease in the yield of RNA (approximately 8.3 fold lower in exposed nerves compared to the Untreated group) ($p < 0.01$) was detected following exposure of rodent nerve samples to each of the different antiseptic reagents (**Figure 3.4**).

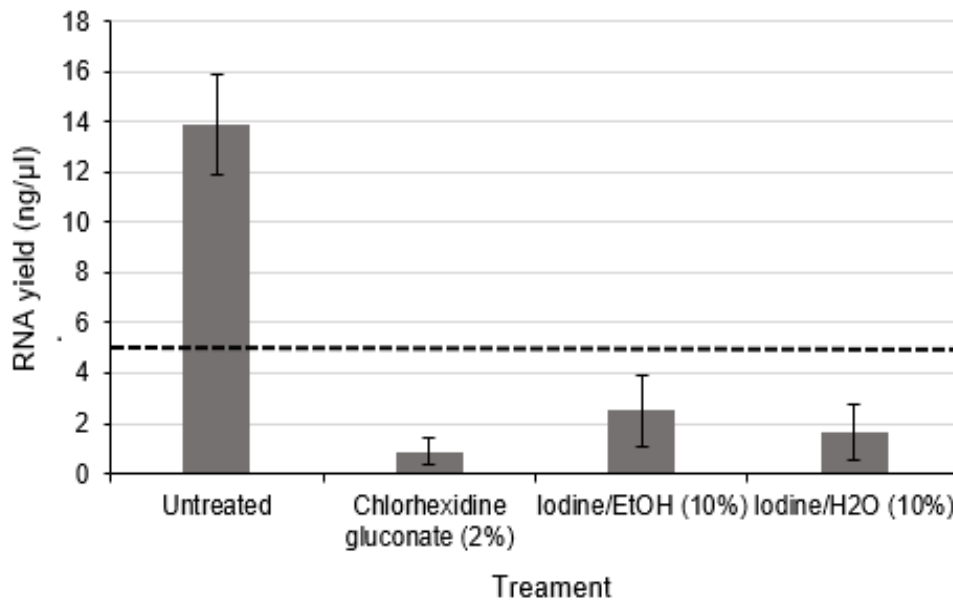


Figure 3.4 - Even when the time delay is minimized/equivalent between samples there is still a large differential in RNA yield due to exposure to surgical antiseptics. Denervated samples were liberated under a standard (n = 4) and “clean change” (n = 3) surgical protocol. Samples liberated in a surgical environment where the “clean change” surgical protocol was implemented yielded RNA concentrations significantly higher than those liberated under standard conditions ($p < 0.01$, two tailed t-test). Healthy nerve samples were also liberated under a “clean change” protocol (n = 3) which yielded significantly lower concentrations of RNA compared to denervated samples ($p < 0.001$ two tailed t-test). The dotted black line represents the minimum concentration of RNA often required for downstream RT-qPCR/RNA seq.

The results presented in this section were utilised to inform the development of methods to allow quantitative analysis of mRNA expression in human nerve samples.

3.3 Discussion

In order to establish a protocol for the reliable extraction of RNA from human nerve samples, this PhD set out to characterise peri-operative variables predictive of RNA yield. The effect on RNA yield of time delays between liberation of the nerve sample and snap freezing was investigated and results suggested that nerve samples should be snap frozen within 3 minutes to preserve RNA quantity and quality. This time

interval is considerably shorter than that cited in other studies that have extracted RNA from surgical specimens which have shown that time delays of several hours between surgical liberation of a sample and cryopreservation is detrimental to RNA quantity and quality (Mee et al., 2011, Patel et al., 2017, Samadani et al., 2015). Studies of surgically harvested tissue have largely been limited to the study of non-fibrous cancerous tissues such as breast and prostate (Mee et al., 2011, Patel et al., 2017, Samadani et al., 2015). These studies achieved optimal yields of RNA (sufficient for RT-qPCR and RNA seq analysis) largely through the optimisation of RNA extraction protocols alone. This is perhaps attributable to the fact that the cancerous tissues explored in these studies have higher cellular densities than nerve tissue and thus more RNA that can be isolated, perhaps diminishing the impact of time delays and/or exposure of samples to antiseptic reagents on the quantity and quality of isolated RNA. Another major difference between nerve samples and other organs is that the nerve trunk contains bundles of axons, together with Schwann cells, fibroblasts, endothelial cells, perineurial cells and other associated cells, but the cell bodies of the neurons are not present since they are located within the CNS or adjacent ganglia. Therefore the RNA which is obtained from excised nerve samples will be predominantly derived from Schwann cells and other non-neuronal cells rather than neurons.

Even when delay was minimised, RNA yields from human nerves in this study remained lower than those reported in rodent studies of denervated nerve tissue (Weng et al., 2018, Yamamoto et al., 2012). Therefore, the exploration of other peri-operative variables such as the interaction of samples with antiseptic surgical reagents such as chlorhexidine and iodine was necessitated. This study showed for the first time that exposure of nerves to surgical antiseptic reagents had detrimental effects on the quantity of RNA that was isolated from the samples. Chlorhexidine and povidone-iodine based antiseptic reagents are cytotoxic to prokaryotic and eukaryotic

cells (Sebben, 1983, Kaoutzanis et al., 2015, Reichman and Greenberg, 2009). Chlorhexidine works by binding to the cell membrane causing it to rupture (Sebben, 1983). On the other hand, povidone-iodine has a broader spectrum of antimicrobial activity (Sebben, 1983). It works by crossing the cell membrane and destroying microbial proteins as well as DNA (Sebben, 1983). It follows that these reagents may have acute cytotoxic effects within the nerve samples thus impair RNA yield.

It was evident that healthy nerve samples yield significantly lower quantities of RNA than that from denervated tissue, which concurs with rodent studies (Weng et al., 2018, Yamamoto et al., 2012) even when the exposure of nerve samples to antiseptic reagents was minimised and the time delay was limited to 3 minutes. The differential observed in both species is likely to be due to the biological mechanisms that underpin nerve regeneration. Evidence from rodent and human models of nerve injury have shown that Wallerian degeneration starts soon after nerve injury, involving a complex cascade of events including degradation of the fibrous connective tissue (Rotshenker, 2011). This may make denervated tissue more amenable to lysis and cellular disruption leading to higher yields of RNA compared to intact health nerve tissue. Furthermore, Wallerian degeneration involves proliferation of Schwann cells and infiltration and proliferation of other non-neuronal cells (such as macrophages and other immune system cells) (Rotshenker, 2011), potentially contributing to increased RNA content in denervated nerve tissue. This finding highlights the pertinence of considering the innervation status of nerve tissue in order to optimise RNA yield.

In order to isolate and further investigate the effects of exposure to antiseptic reagents, this study used a rodent model of peripheral nerve liberation which showed that these antiseptic reagents reduced RNA yields significantly. Chlorhexidine and iodine based reagents can be found in abundance in operating theatres around the

world where they are often deployed for preoperative skin preparation. This finding, together with experimental evidence that has shown iodine and chlorhexidine based reagents to have cytotoxic effects on *in vitro* populations of human neuronal cells and rodent Schwann cells (Doan et al. 2012), necessitates further work to characterise the effect of these reagents on the regenerative capacity of the peripheral nervous system. This could potentially inform the modification and development of surgical tissue handling protocols more generally, beyond just the focus here on obtaining nerve tissue RNA for research.

In addition to influencing RNA extraction, iodine and chlorhexidine based reagents may have downstream effects on qPCR assays. These reagents have been shown to inactivate the Human Immunodeficiency Virus through a mechanism thought to be at least partially attributable to the ability of these reagents to manipulate the viral DNA reverse transcriptase (Harbison and Hammer, 1989, Samadani et al., 2015). This enzyme is analogous to the RNA to cDNA reverse transcriptase step used in RT-qPCR and RNA seq assays, providing an additional reason to avoid the contamination of samples intended for downstream qPCR and RNA seq assays.

In summary, this part of the project reports new experimental evidence from human and animal studies that reveals the effects of time delays and surgical antiseptics on the RNA yield obtained from nerve tissue. This information can help to inform the development of improved methodology, specifically limiting time delay between sample liberation and cryopreservation to less than 3 minutes whilst utilising a “clean change” surgical protocol to reduce antiseptic exposure. These findings provide new information about the response of fresh nerve tissue following isolation, including differences between healthy and denervated samples. This understanding has enabled the effective use of valuable human nerve tissue samples in the next section

to characterise cellular and molecular features that underpin human nerve regeneration.

Chapter 4: Characterising cellular and molecular features of human peripheral nerve degeneration

4.1 Introduction

The cellular and molecular mechanisms that underpin nerve regeneration have been investigated extensively in animal models demonstrating that the plasticity of Schwann cells and their ability to switch to a repair-supportive differentiation state after injury is one of the key reasons for strong regenerative capacity observed in the PNS (Scheib and Höke, 2016, Jessen and Mirsky, 2019, Jessen and Arthur-Farraj, 2019, Jopling et al., 2011, Boerboom et al., 2017).

In rodent models, it has been shown that the failure of motor recovery after chronic denervation (greater than six months) is associated with substantially reduced capacity of the distal nerve to support growth of axons (Fu and Gordon, 1995, Saito and Dahlin, 2008, Wu et al., 2014). After injury, progressive deterioration of denervated nerve and muscle make conditions increasingly antagonistic for regeneration, decreasing the chance of functional recovery (Sulaiman and Gordon, 2000). Rodent studies have established that this can largely be attributed to adverse changes in Schwann cells and their associated basal laminae, including reduced expression of repair-supportive molecules and decreasing Schwann cell numbers (Hoke, 2006, Li et al., 1997, Terenghi et al., 1998). Although this process is thought to be a major obstacle to effective nerve repair, this progressive loss of regeneration support has not been investigated in detail in humans.

Clinical reports have suggested that optimal functional recovery is dependent upon a sufficient number and quality of axons reaching their target within one year following injury (Oberlin et al., 1994, Tung and Mackinnon, 2010, Isaacs and Cochran, 2019). After this time period, functional outcomes are poor (Mackinnon et al., 2005, He et al., 2014, Tung and Mackinnon, 2010). This same pattern of strong initial regeneration

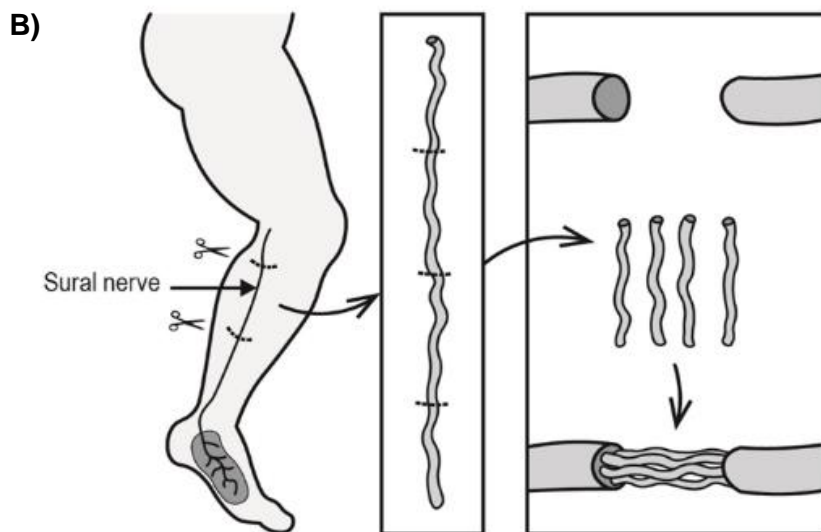
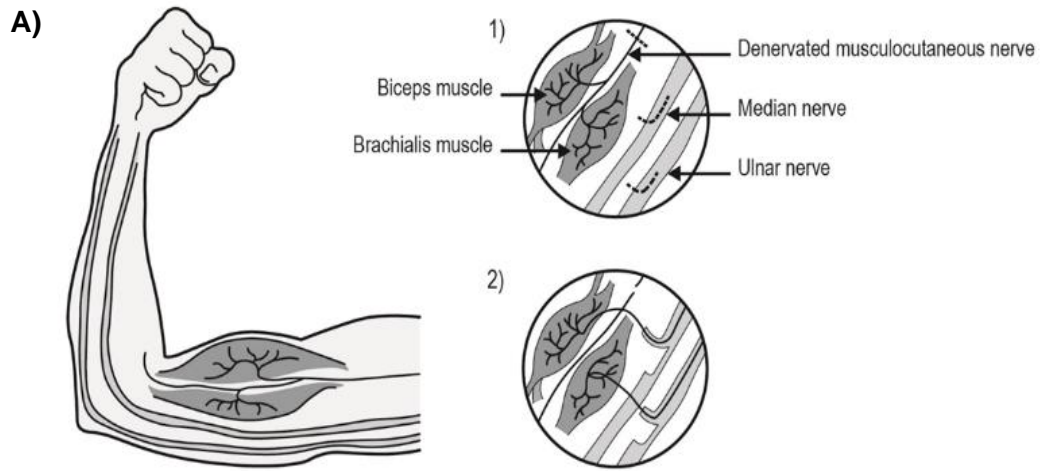
potential followed by declining regenerative capacity during chronic denervation and poor functional outcomes from repair of proximal injuries suggests that the basic biology is likely to be comparable between rodents and humans.

Effective translation of the wealth of animal model data into a human paradigm of nerve regeneration would be of great benefit in the development of improved clinical treatments for nerve injury, but progress is limited by ethical and practical challenges associated with studying human nerve injury as highlighted in **Chapter 3** (Wilcox et al., 2019b, Hewitt et al., 2008). Moreover, the intricate anatomy and diverse range of injuries make PNI a heterogeneous pathology to study.

To address this challenge, this study retrieved nerve samples from patients undergoing treatment for nerve injuries at a range of times from injury from acute to chronic. Many nerve samples were retrieved from nerve transfer surgeries. This procedure is deployed by the reconstructive nerve surgeon following complex proximal nerve injuries or those where there has been a significant delay from injury to treatment. The damaged nerves were identified and characterised using intra-operative neurophysiological monitoring to record (CNAPs. In line with current practice (Herrera-Perez et al., 2015, Slimp, 2000), the nerve was assumed to be denervated if a CNAP and muscle twitch were absent. The surgeon identified and isolated a suitable donor fascicle and creates a neurotmesis injury in order to redirect previously uninjured axons to grow into the chronically denervated stump. The Oberlin's procedure is an example of a nerve transfer which is commonly used to reanimate elbow flexion (**Figure 4.1**) (Oberlin et al., 1994, Leechavengvongs et al., 2006, Leechavengvongs et al., 1998). A nerve autograft is another surgical technique which can be deployed to reconstruct a nerve gap where the timing and local tissue conditions allow. For this the medial cutaneous nerve of the arm or the sural nerve are commonly utilised as the donor (**Figure 4.1**) (Ray and Mackinnon, 2010).

In cases where significant time (greater than 1 year) has passed since the initial nerve injury, a Free Functioning Muscle Transfer (FFMT) is often the only technique to restore movement (Ray and Mackinnon, 2010). This involves identifying a suitable donor muscle as well as its neurovascular bundle and grafting it in order to restore a function considered to be more pertinent to the quality of life of the patient. All of these surgical protocols liberate excess tissue (both healthy and denervated samples) for study in the laboratory, that would otherwise be disposed of. Across our cohort, samples from various time points during chronic denervation were harvested, allowing the time course of any phenotypic changes in denervated nerve tissue to be explored for the first time. In rodent models, Schwann cells reprogram to a transient pro-regenerative phenotype, the 'repair Schwann cell'. Therefore, in the present study we analysed key markers linked with the transition to the repair Schwann cell phenotype, c-Jun, P75NTR and Krox-20, in addition to a pan-Schwann cell marker, SOX10.

Upregulation of the transcription factor c-Jun in Schwann cells follows nerve injury and amplifies a cascade of downstream changes in expression associated with the phenotypic shift of Schwann cells from a normal myelinating or Remak phenotype to a repair phenotype (Arthur-Farraj et al., 2012). Other well-characterised changes associated with Schwann cell reprogramming following injury in rodents include upregulation P75NTR and downregulation of the transcription factor Krox-20 which is associated with myelination (Jang et al., 2010, Mirsky et al., 2008, Jessen and Mirsky, 2008, Kamholz et al., 1999).



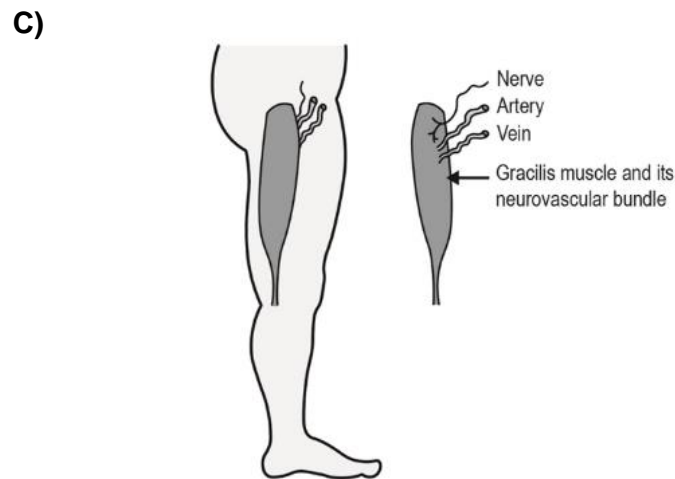


Figure 4.1 - Reconstructive nerve procedures (Wilcox et al., 2020c). **A)** The double Oberlin's nerve transfer is commonly deployed to restore elbow flexion. The surgeon identifies suitable donor fascicles of the ulnar and median nerve that supply wrist flexor muscles. The fascicles are divided and redirected to grow into the denervated musculocutaneous nerve to biceps and brachialis. **B)** Nerve autograft is deployed in larger nerve gaps. The sural nerve is often harvested as the donor nerve and grafted to restore continuity across the damaged nerve trunk. **C)** Free functional muscle transfer (FFMT) is deployed in chronic nerve injuries. This involves identifying a suitable donor muscle and its neurovascular bundle (such as the gracilis) and grafting it to the injured site of nerve damage (often to the upper limb to restore elbow flexion).

SOX10 is a transcription factor constitutively expressed in Schwann cells and has a crucial role in neural crest development, glial cell development and myelin formation and maintenance (Bremer et al., 2011, Finzsch et al., 2010, Miettinen et al., 2015, Nonaka et al., 2008). It serves as a marker to specifically identify Schwann cells in nerve samples (Britsch et al., 2001, Liu et al., 2015, Finzsch et al., 2010). Therefore, this study set out to measure the quantity and distribution (using immunohistochemistry and RT-qPCR) of these four markers in uninjured and injured nerve samples retrieved from reconstructive nerve procedures at a range of acute and chronic time points following injury. By comparing how the expression of these four markers changes over time in denervated samples with uninjured nerve samples,

this study aimed to characterise some of the key cellular and molecular features of human peripheral nerve degeneration.

4.2 Results

Thirty four denervated and five healthy nerve samples were included in the study, from 26 males and one female. The mean patient age at the time of surgery was 34 (± 6) years. The median time between injury and surgery was 116 days (ranging from 4 to 6432 days). A total of 64 nerve samples were retrieved from surgery over a 3 year period. The demographics of patients included in this study are shown in **Table 2.1**. However, 25 samples (39%) were rejected from the study due to one of the following reasons:

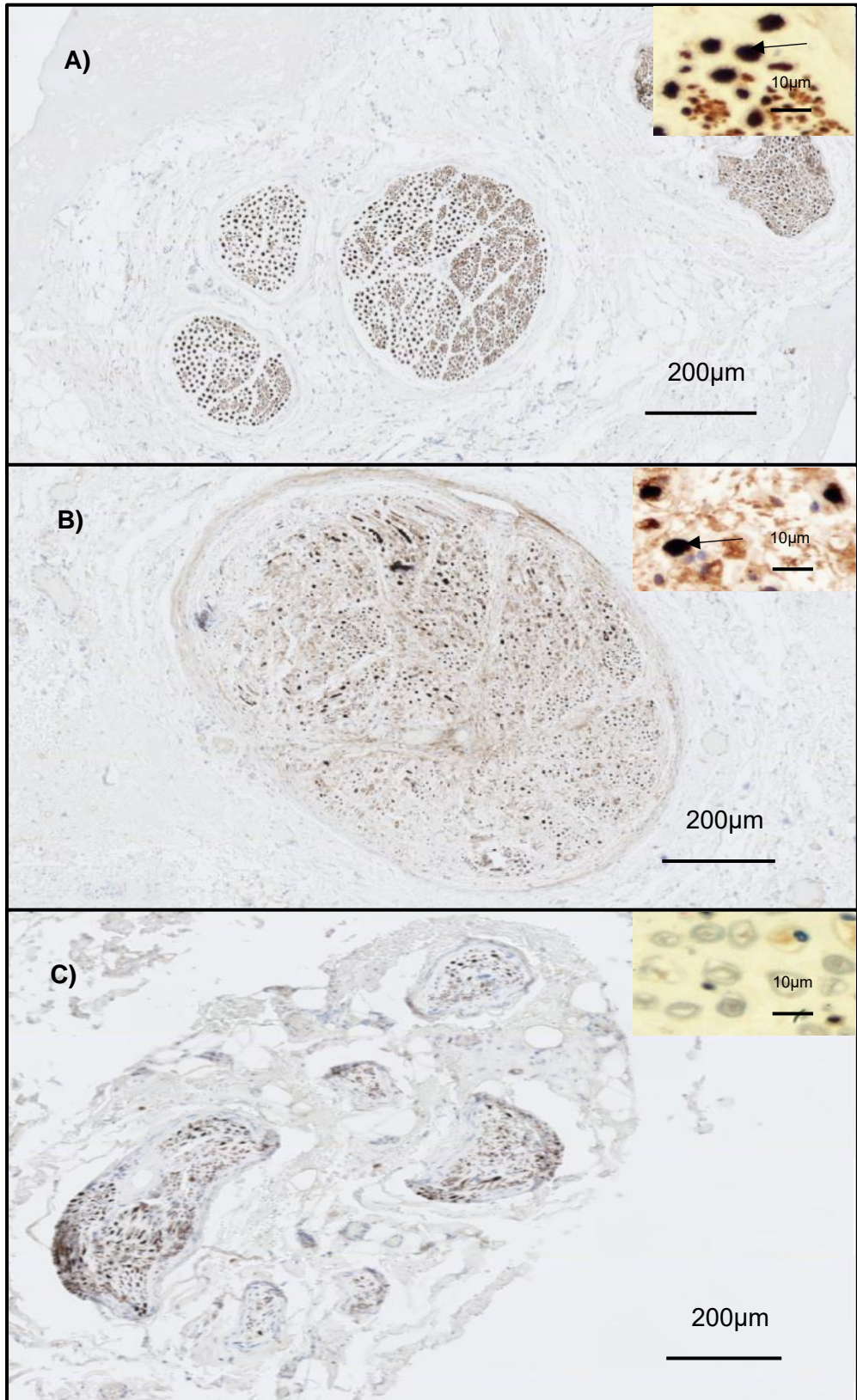
- 1) Fourteen samples yielded insufficient quantity and/or quality of RNA for RT-qPCR analysis.
- 2) Seven of the samples were of insufficient quantity for sectioning.
- 3) Four of the samples presented an inappropriate morphology for sectioning.

For immunohistochemistry, a total of two independent nerve samples with no known pathology were retrieved as a baseline (Case number 4 and 8 as described in **Table 2.1**). The size of the intercostal nerve sample from Case number 24 (**Table 2.1**) was insufficient for immunohistochemical analysis.

Quantification of immunohistochemistry suggested that across the two healthy nerve samples, the density of SOX10 cells as well as expression levels of each of the phenotypic markers c-Jun, P75NTR and Krox-20 was similar ($1872 \pm 258/\text{mm}^2$, $193 \pm 19/\text{mm}^2$, $76 \pm 14/\text{mm}^2$ and $1555 \pm 45/\text{mm}^2$ respectively) (**Appendix 3, Figure 11.1**). Moreover, axon density was similar in sural ($35680/\text{mm}^2$) and intercostal ($33465/\text{mm}^2$) nerve samples ($34,567 \pm 1107/\text{mm}^2$) (**Appendix 3, Figure 11.2**).

For RT-qPCR, a total of three independent nerve samples with no known pathology were retrieved as baseline controls (one sample of sural nerve (Case number 4) and two samples of intercostal nerve (Case number 8 and 24) as shown in **Table 2.1**). The mean relative gene expression in these control samples (where $\Delta C_T = C_T - C_{T,e}$) of the SOX10, c-Jun, P75NTR and Krox-20 (**Appendix 3, Figure 11.3**) was relatively similar across the healthy nerve samples (13.26 ± 1.89 , 10.78 ± 0.42 , 12.55 ± 1.62 , 8.96 ± 0.81 respectively). Immunohistochemical detection of axons in the damaged samples using neurofilament antibodies revealed that the large majority of samples contained fewer than 10 axons beyond 40 days of denervation (**Figure 4.2 A-E**).

Immunohistochemistry followed by quantitative analysis of micrographs showed how the number and phenotype of Schwann cells within the denervated samples varied according to denervation time, compared with normal healthy nerve controls. To account for variations in the dimensions of nerves between individuals, cross-sections were quantified in terms of the intra-fascicular density of cells, expressed as immunoreactive cells per mm^2 cross-sectional area. It is clear from **Figure 4.3A-E** that the total cell density (haematoxylin positive cells) increased after injury to reach a peak after about 90–100 days of denervation. Compared to healthy control nerves, cell density was elevated in samples that were denervated for up to 200 days then this density decreased to lower than healthy controls in the more chronically denervated samples.



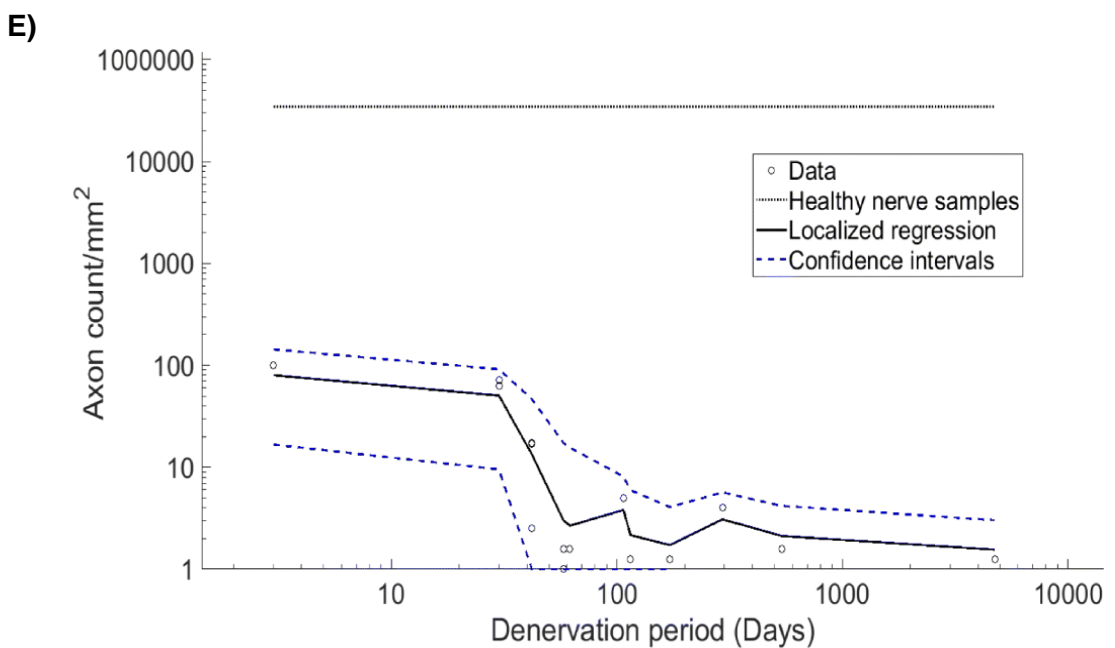
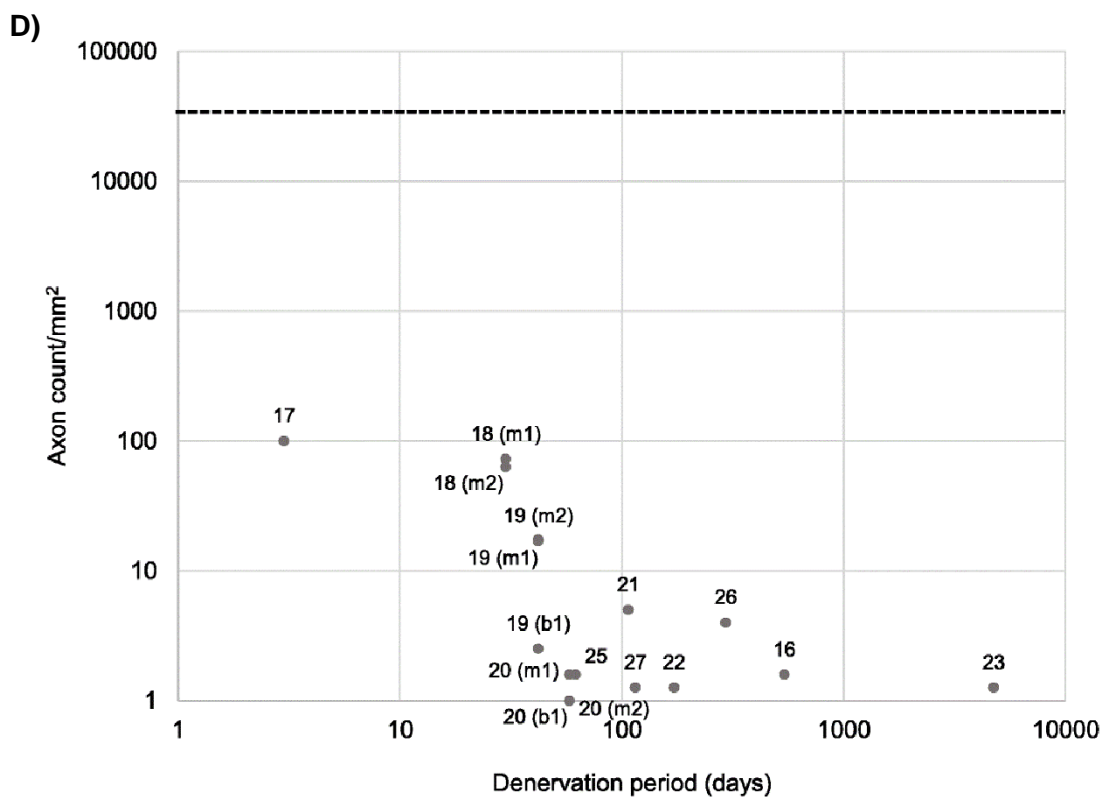
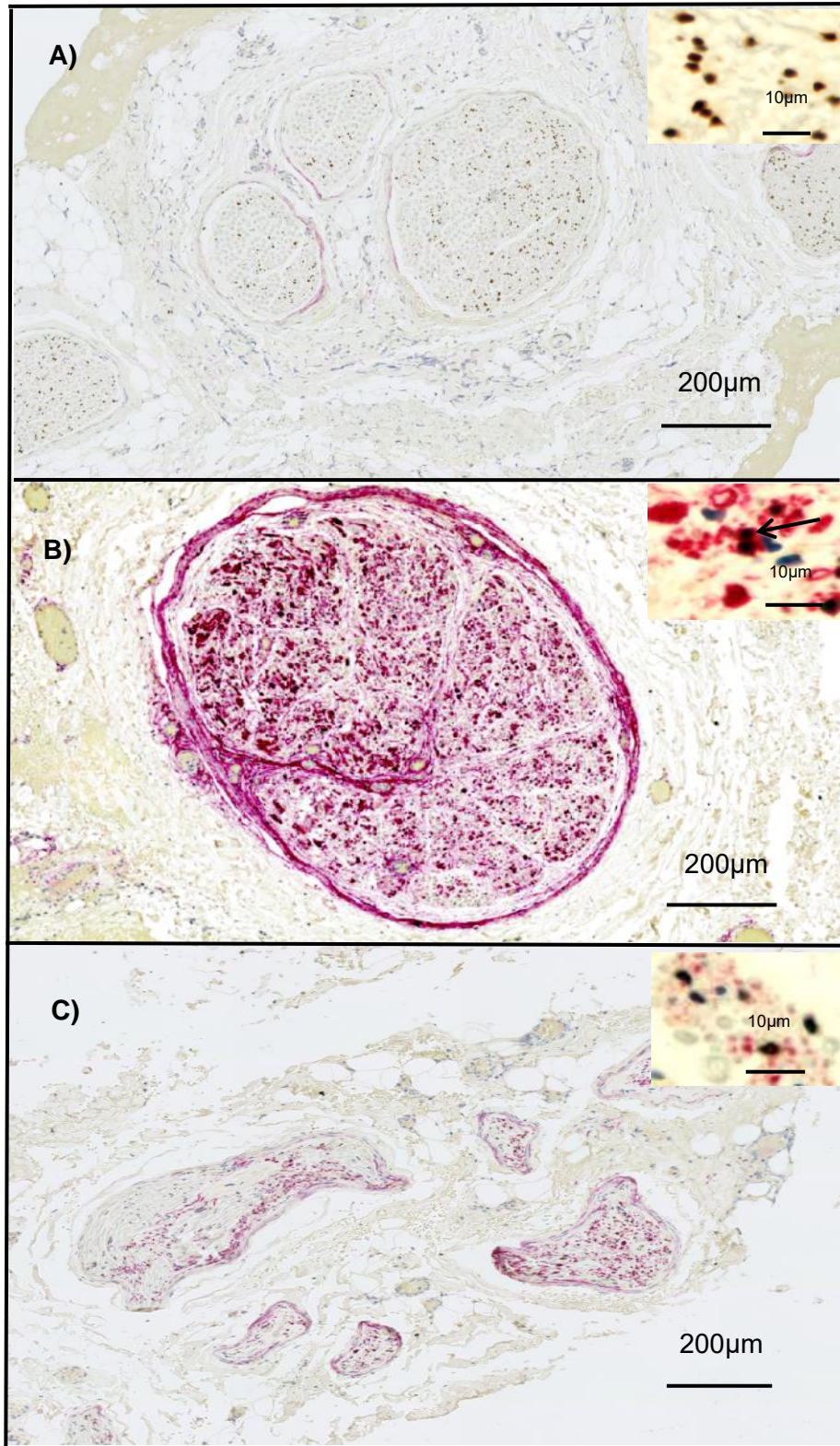


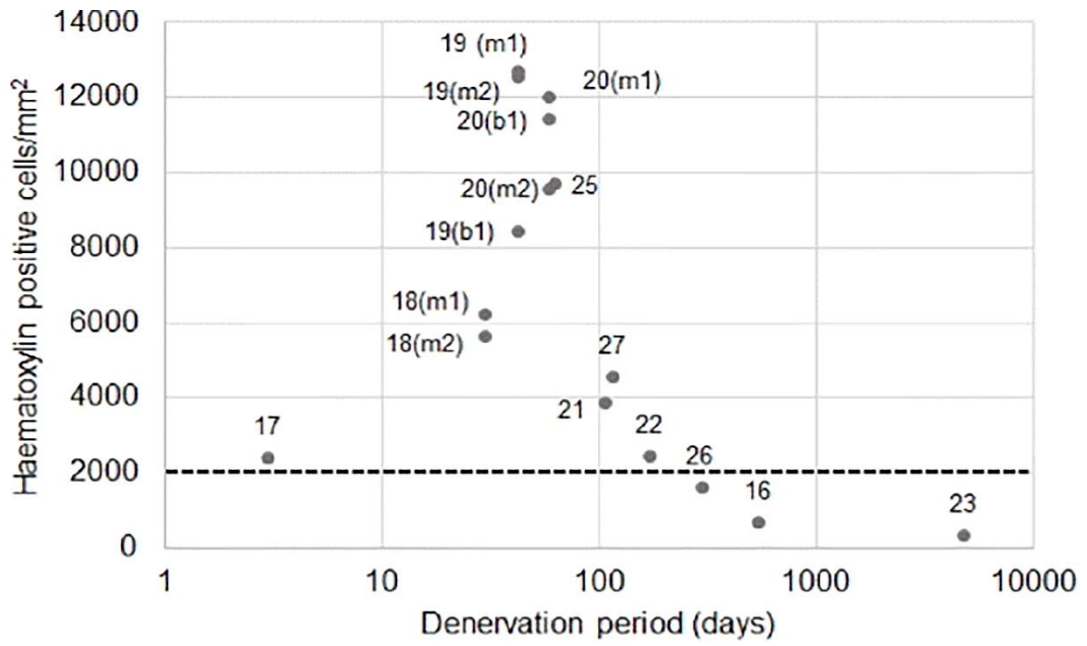
Figure 4.2 - Immunohistochemical detection of neurons in healthy and denervated human nerves. **A) – C)** represent nerve cross sections stained for neurofilament (brown) with haematoxylin and eosin stain. The black arrow in the micrograph

represents positive neurofilament staining. In **D)** and **E)** the black dotted line represents the mean number of axons detected in healthy nerve samples (case number 4 and 8). The x-axis is Log(denervation time in days) **A)** Healthy sural nerve. **B)** Biceps branch of the musculocutaneous nerve denervated for 30 days. **C)** Axillary nerve denervated for 294 days with deteriorated morphology. **D)** A scatter plot to represent $\text{Log}(\text{axon count}/\text{mm}^2)$ against denervation time. **E)** Nonparametric smoothing linear regression of the $\text{Log}(\text{axon count}/\text{mm}^2)$ against denervation time. Case numbers are attached to each data point for reference to **Table 2.1** with descriptors of whether the sample was collected proximally or distally: *m1* - Proximal part of the denervated stump of the biceps branch of musculocutaneous nerve, *m2* - Distal part of the denervated stump of the biceps branch of musculocutaneous nerve, *b1* - Proximal section of the denervated stump of the brachialis branch of musculocutaneous nerve, *s1* - Denervated stump of suprascapular nerve, *sa1* - Proximal section of the denervated stump of the spinal accessory nerve, *sa2* - Distal section of the denervated stump of the spinal accessory nerve.

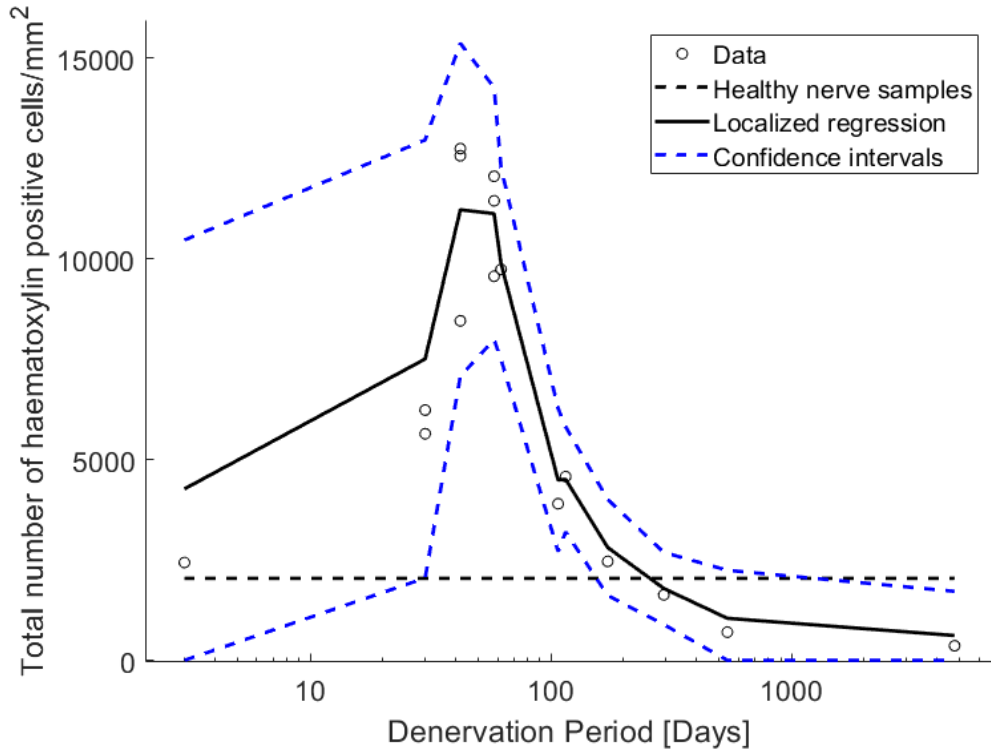
SOX10 positive Schwann cells represented approximately half of the total number of haematoxylin positive cells in most cases (**Figure 4.3F and G**). The density of SOX10-positive cells also peaked at 90–100 days and then decreased as seen using haematoxylin labelling. In contrast to that seen in injured nerves, the large majority of cells in healthy nerve samples were found to be SOX10 positive. However, RT-qPCR analysis of SOX10 mRNA expression did not mirror the injury-induced increases in cell density at 90–100 days described above. Instead, SOX10 was upregulated above baseline in all but two of the denervated samples. A trend towards decreasing SOX10 levels was, however, seen after 100 days of denervation (**Figure 4.3H and I**).

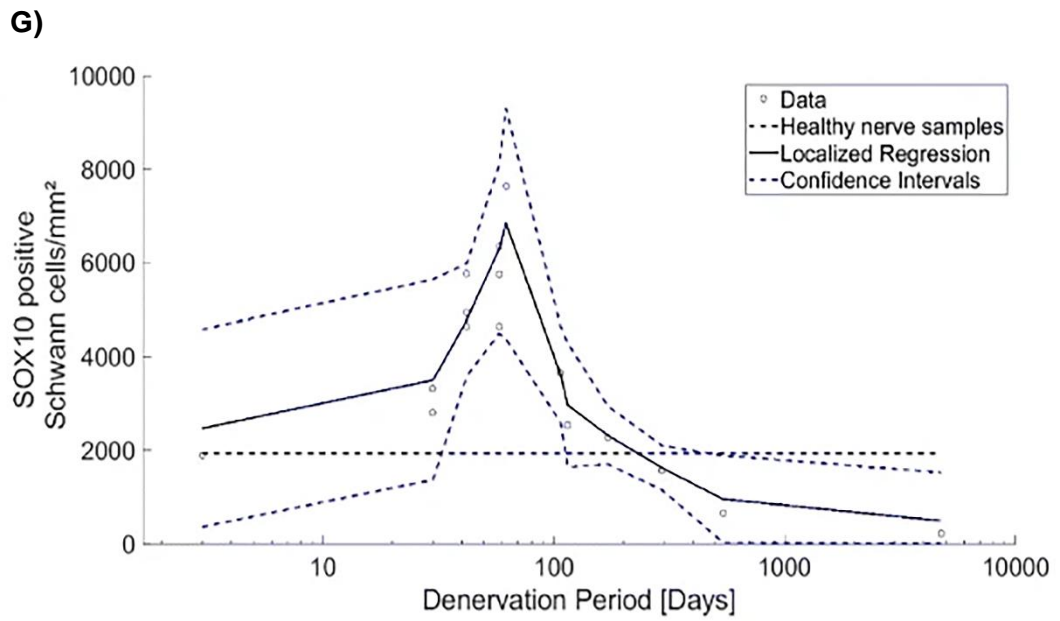
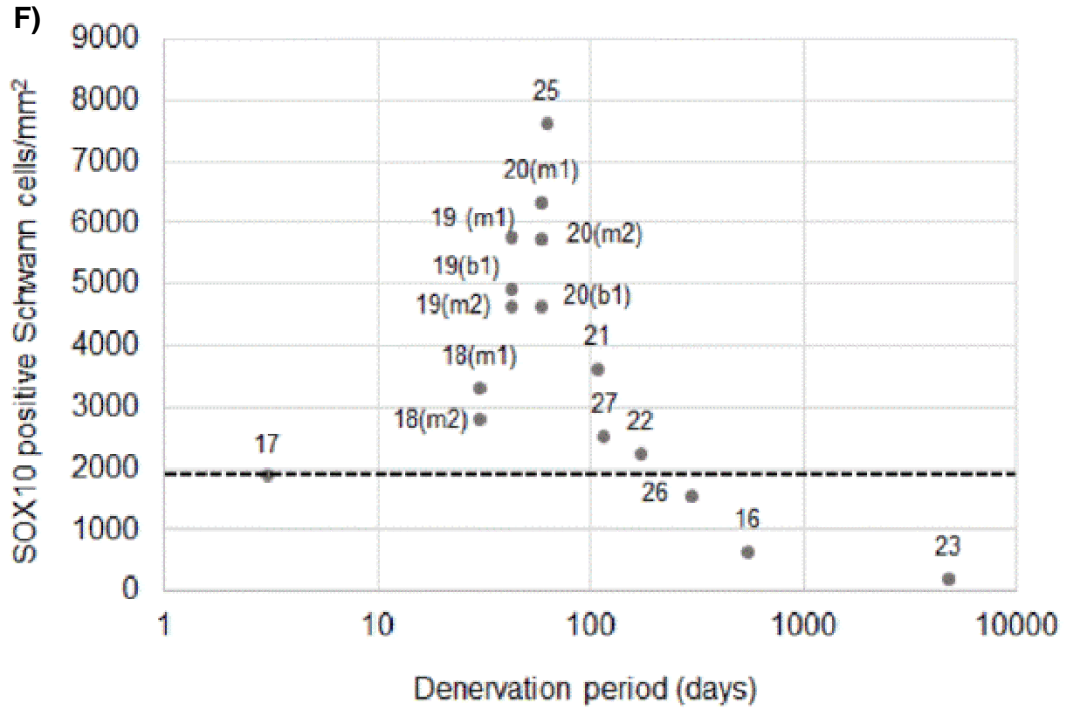


D)



E)





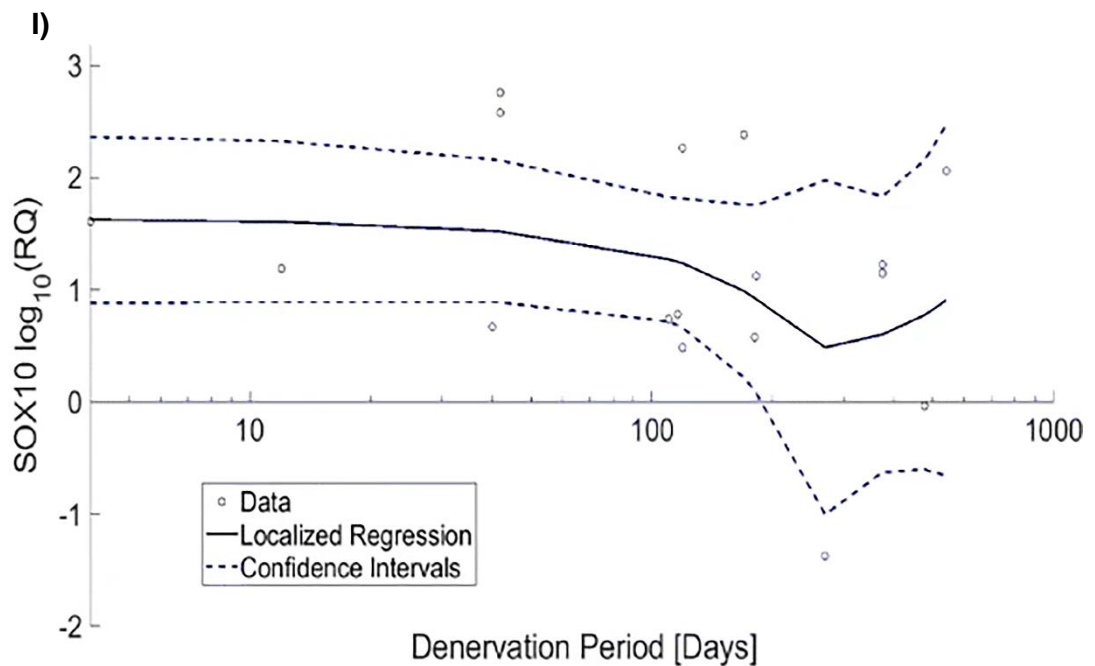
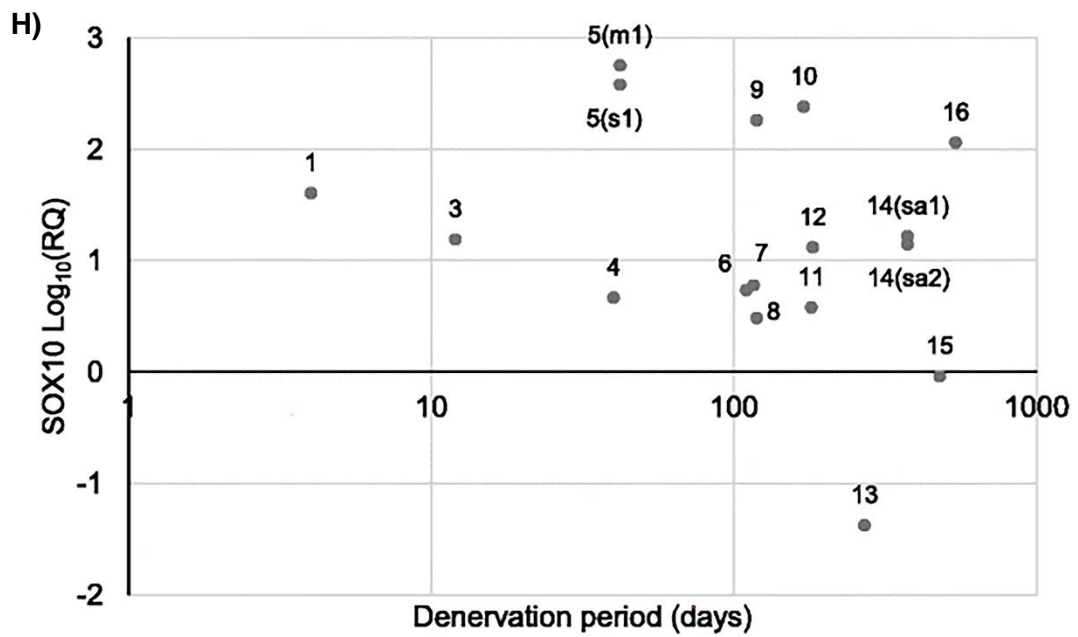
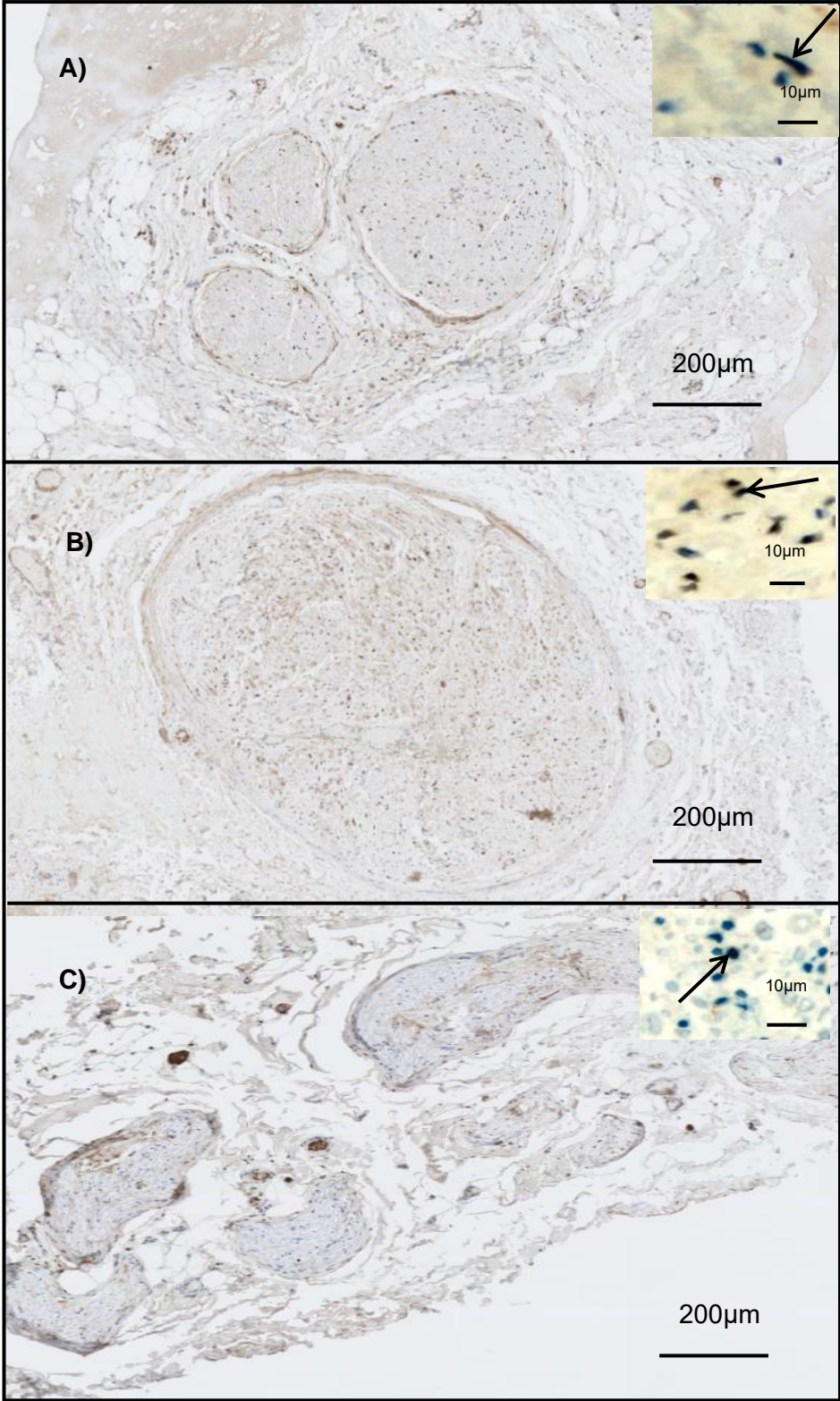


Figure 4.3 - Immunohistochemical and RT-qPCR analysis of Schwann cells in healthy and denervated human nerves. **A-C** represent nerve cross sections immunostained for SOX10 (brown) and P75 (red) along with haematoxylin and eosin stain. The black arrow in the micrographs indicates a SOX10/P75NTR positive Schwann cell. **D-I** the x-axis represents Log(denervation time in days). In **D-G**, the horizontal black dotted line represents the mean value obtained for the healthy nerve

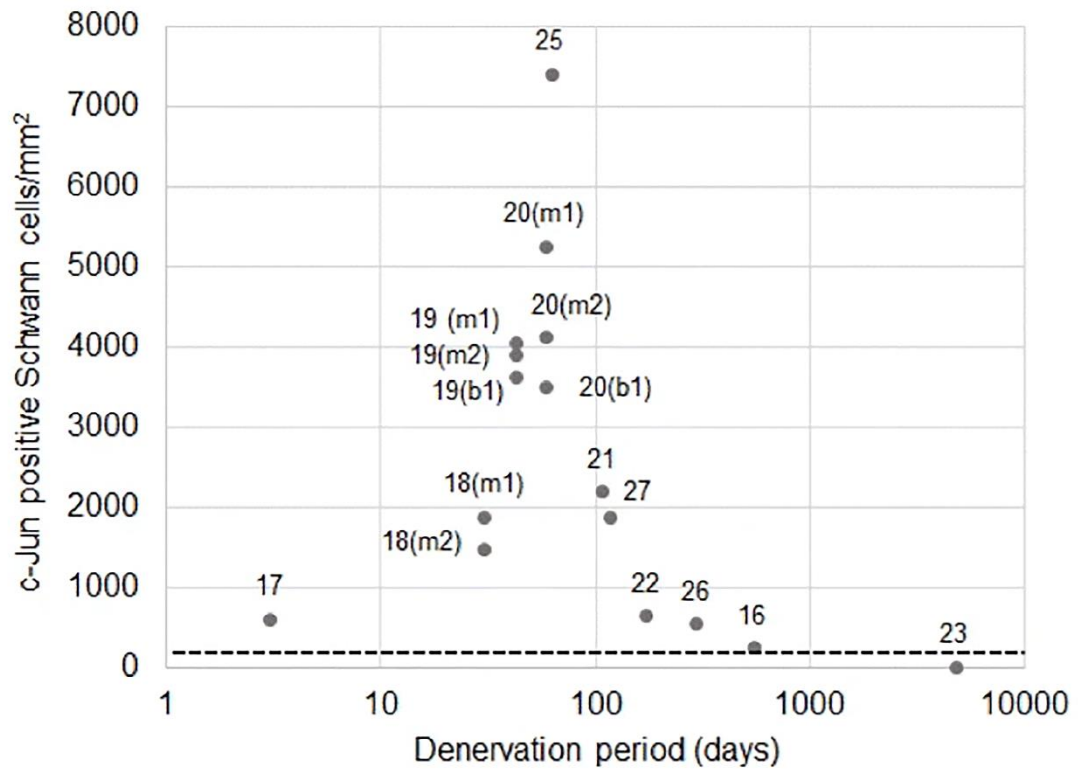
group. **A**) Healthy sural nerve. **B**) Biceps branch of the musculocutaneous nerve denervated for 30 days. The brown staining represents a SOX10 positive nucleus whilst the red cytoplasmic staining represents P75NTR positive staining. **C**) Axillary nerve denervated for 294 days with deteriorated morphology. **D**) Scatter plot to represent the total number of haematoxylin positive cells/mm² in denervated samples. **E**) Nonparametric smoothing linear regression of the total number of haematoxylin positive cells/mm² in denervated samples. **F**) Scatter plot to represent the total number of Schwann cells/mm² across denervated samples. **G**) Nonparametric smoothing linear regression of the total number of SOX10 positive Schwann cells/mm². **H**) RT-qPCR analysis of SOX10 mRNA expression across denervated samples. **I**) Non-parametric smoothing linear regression of the SOX10 RT-qPCR data. Case numbers are attached to each data point for reference to **Table 2.1** with descriptors of whether the samples were collected proximally or distally: *m1* - Proximal part of the denervated stump of the biceps branch of musculocutaneous nerve. *m2* - Distal part of the denervated stump of the biceps branch of musculocutaneous nerve. *b1* - Proximal section of the denervated stump of the brachialis branch of musculocutaneous nerve. *s1* - Denervated stump of suprascapular nerve. *sa1* - Proximal section of the denervated stump of the spinal accessory nerve. *sa2* - Distal section of the denervated stump of the spinal accessory nerve.

With immunohistochemistry analysis, the number of Schwann cells per mm² showing positive expression of nuclear c-Jun was elevated in the denervated nerves, particularly between 10 and 100 days denervation (**Figure 4.4A -E**). Peak expression was seen at 90–100 days co-incident with the peaks of total cell density and density of SOX10 positive cells. The level of Schwann cell c-Jun expression declined to levels similar to or lower than that of uninjured nerves by around 500 days of denervation (**Figure 4.4D and E**). The RT-qPCR data were comparable, showing that c-Jun expression was increased approximately 140-fold in the samples with the shortest denervation period (4–50 days) and was also increased (to a slightly lesser extent) in most samples up to 200 days (**Figure 4.4F and G**). Beyond this time point c-Jun expression declined, and there was a trend for some of the nerve samples to have c-Jun expression levels lower than the healthy nerve baseline (**Figure 4.4F and G**).

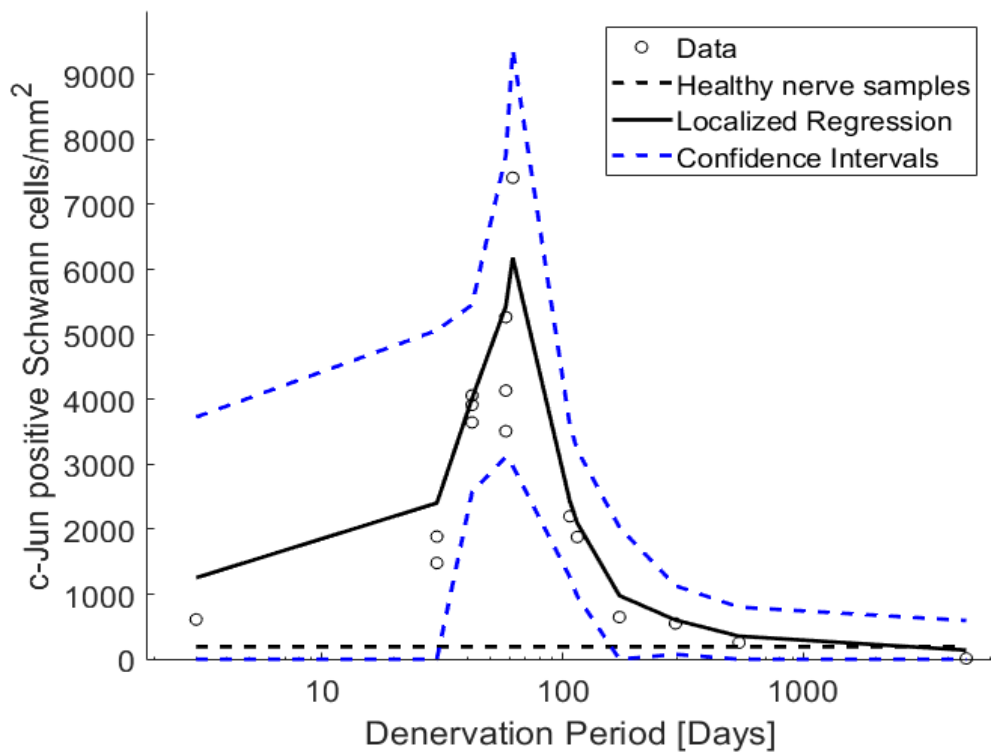
P75NTR demonstrated a similar trend, with immunohistochemistry analysis showing the number of P75NTR positive Schwann cells per mm² to be elevated particularly between 10 and 100 days of denervation followed by a decline after more than around 80 days of denervation (**Figure 4.5A–E**). The RT-qPCR data were comparable, showing that samples denervated for between 4 and 170 days demonstrated an increase in P75NTR mRNA expression of 10- to 100-fold compared to uninjured nerves. P75NTR expression in most samples that had been denervated for longer declined towards and eventually below baseline (**Figure 4.5F and G**). Moreover, it was found from the immunohistochemistry and RT-qPCR results that samples collected more distally yielded lower levels of c-Jun and P75NTR than those harvested more proximally (**Figure 4.4D and F, Figure 4.5D and F**).



D)



E)



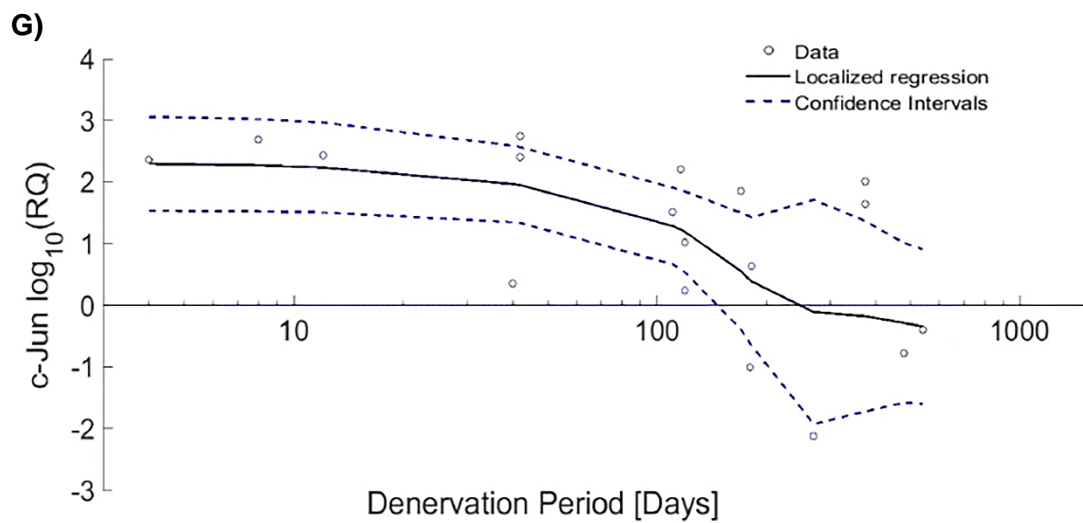
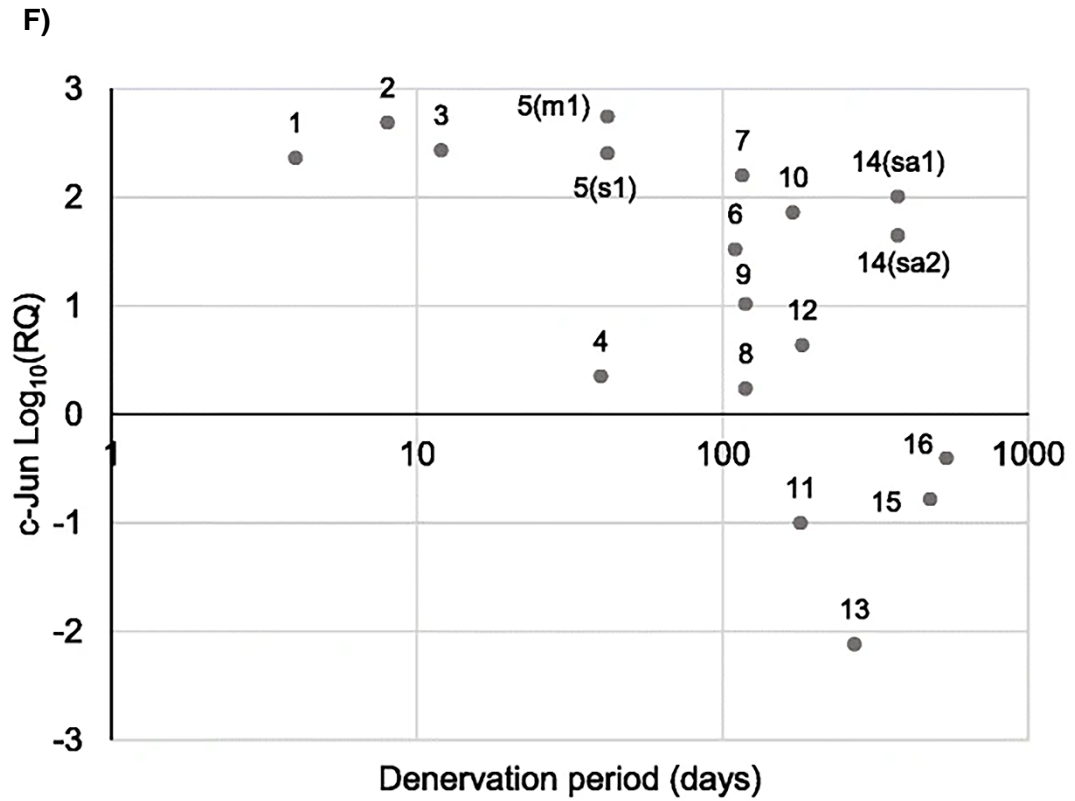
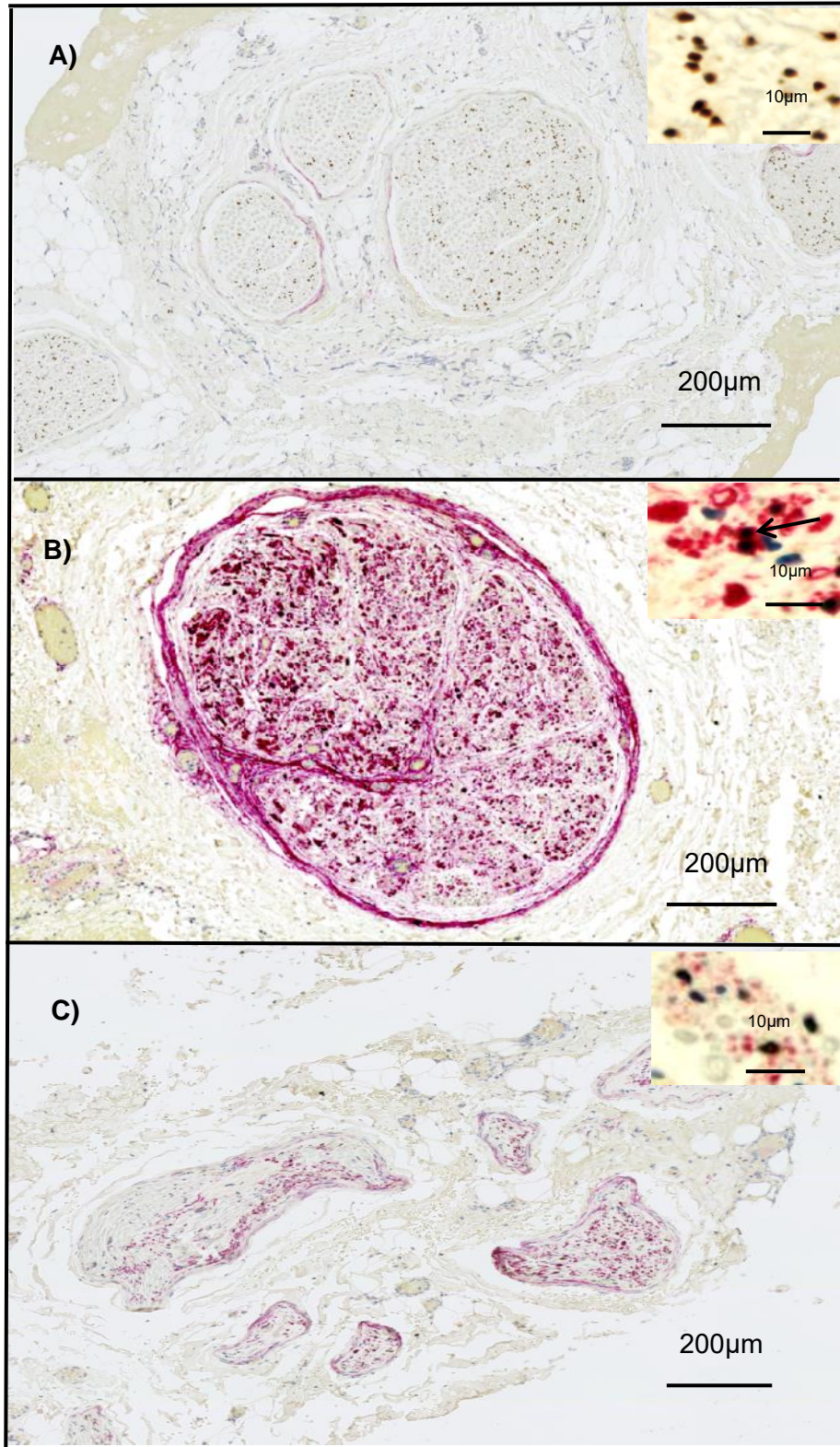
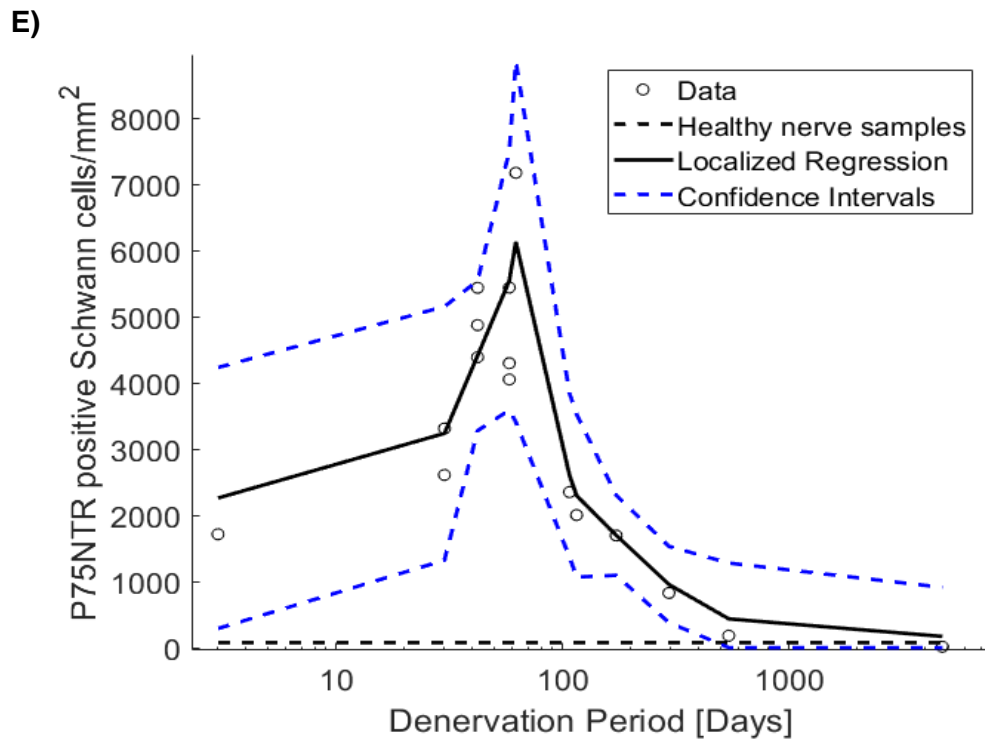
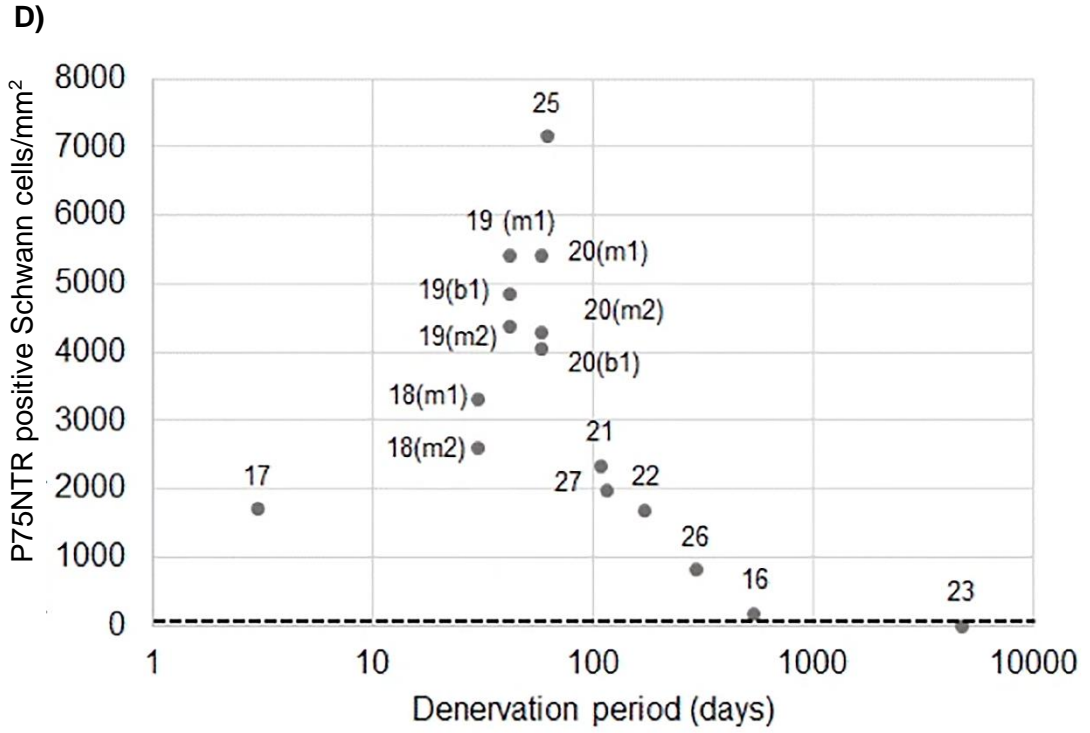


Figure 4.4 - Immunohistochemistry and RT-qPCR analysis of c-Jun in healthy and denervated human nerves. **A) - C)** represent nerve cross sections immunostained for c-Jun (brown) along with haematoxylin and eosin stain. The black arrow in the micrographs indicates a c-Jun positive Schwann cell. The x-axis in **D) - G)** represents Log(denervation time in days). In **D)** and **E)** the horizontal black dotted line represents the mean value obtained for the healthy nerve group. **A)** Healthy sural nerve. **B)**

Biceps branch of the musculocutaneous nerve denervated for 30 days. **C)** Axillary nerve denervated for 294 days with deteriorated morphology. **D)** A scatter plot to represent the total number of c-Jun positive Schwann cells/mm² in denervated samples. **E)** Nonparametric smoothing linear regression of the total number of c-Jun positive Schwann cells/mm². **F)** RT-qPCR analysis of c-Jun mRNA expression across denervated samples. **G)** Nonparametric smoothing linear regression of the c-Jun RT-qPCR data. Case numbers are attached to each data point for reference to **Table 2.1** with descriptors of whether the samples were collected proximally or distally: *m1* - Proximal part of the denervated stump of the biceps branch of musculocutaneous nerve, *m2* - Distal part of the denervated stump of the biceps branch of musculocutaneous nerve, *b1* - Proximal section of the denervated stump of the brachialis branch of musculocutaneous nerve, *s1* - Denervated stump of suprascapular nerve, *sa1* - Proximal section of the denervated stump of the spinal accessory nerve, *sa2* - Distal section of the denervated stump of the spinal accessory nerve.

Krox-20 expression identified using immunohistochemistry was lower than baseline in nearly all samples, as expected from the involvement of this transcription factor in myelination (**Figure 4.6A–E**). Beyond 1 month of denervation, the proportion of Krox-20 positive Schwann cells demonstrated an overall decrease until reaching almost 0 by around 500 days denervation (**Figure 4.6D and E**). RT-qPCR demonstrated a similar trend with most samples demonstrating down-regulation of Krox-20 mRNA, by 3000-fold in some cases (**Figure 4.6F and G**).





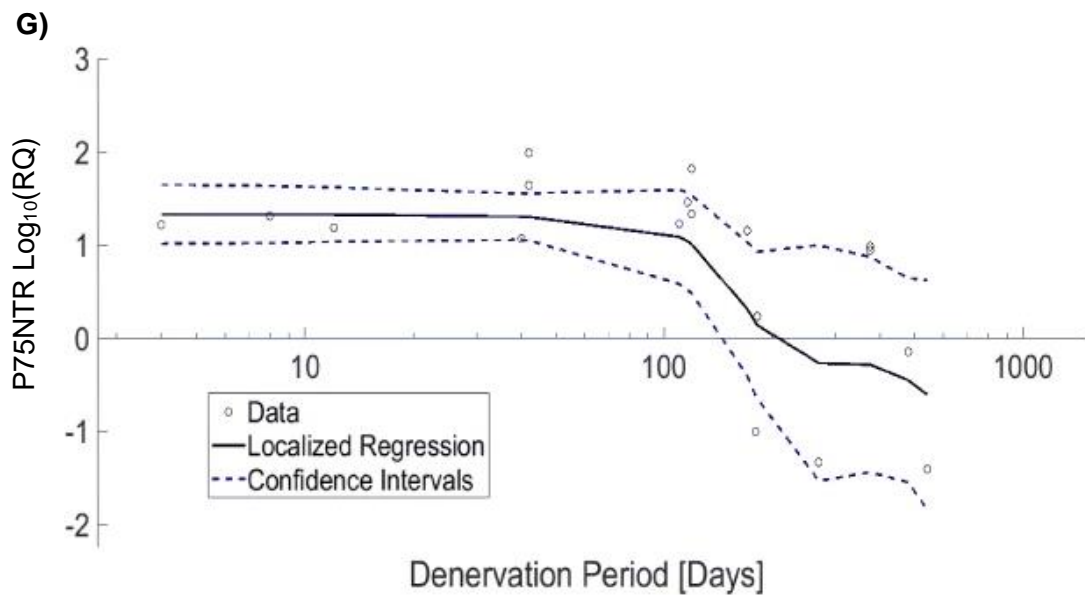
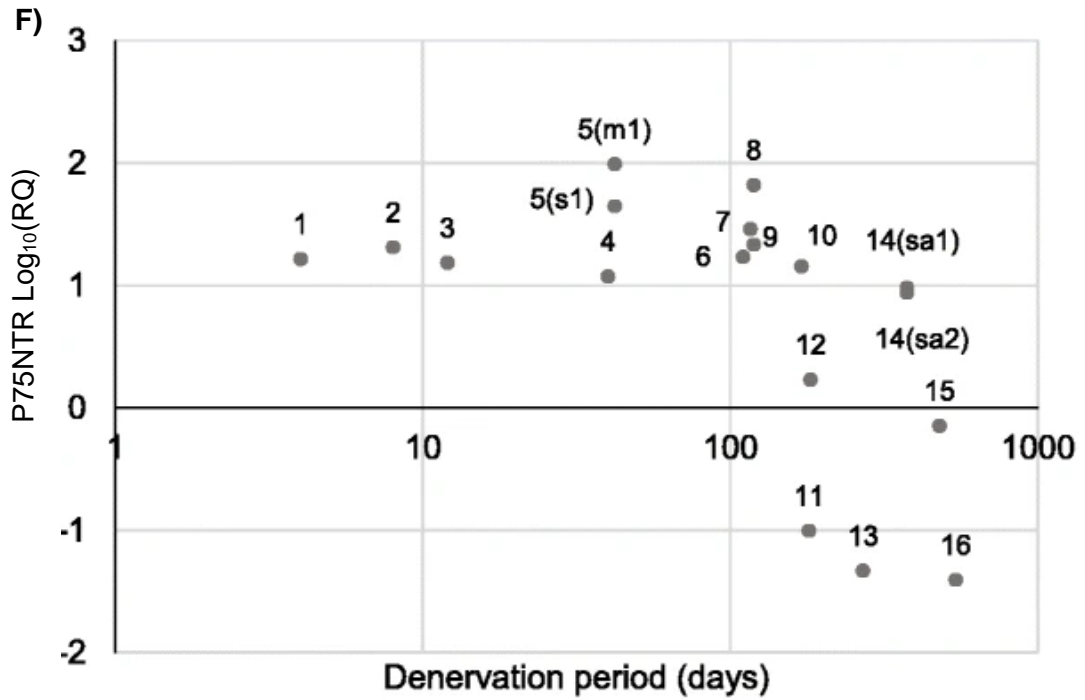
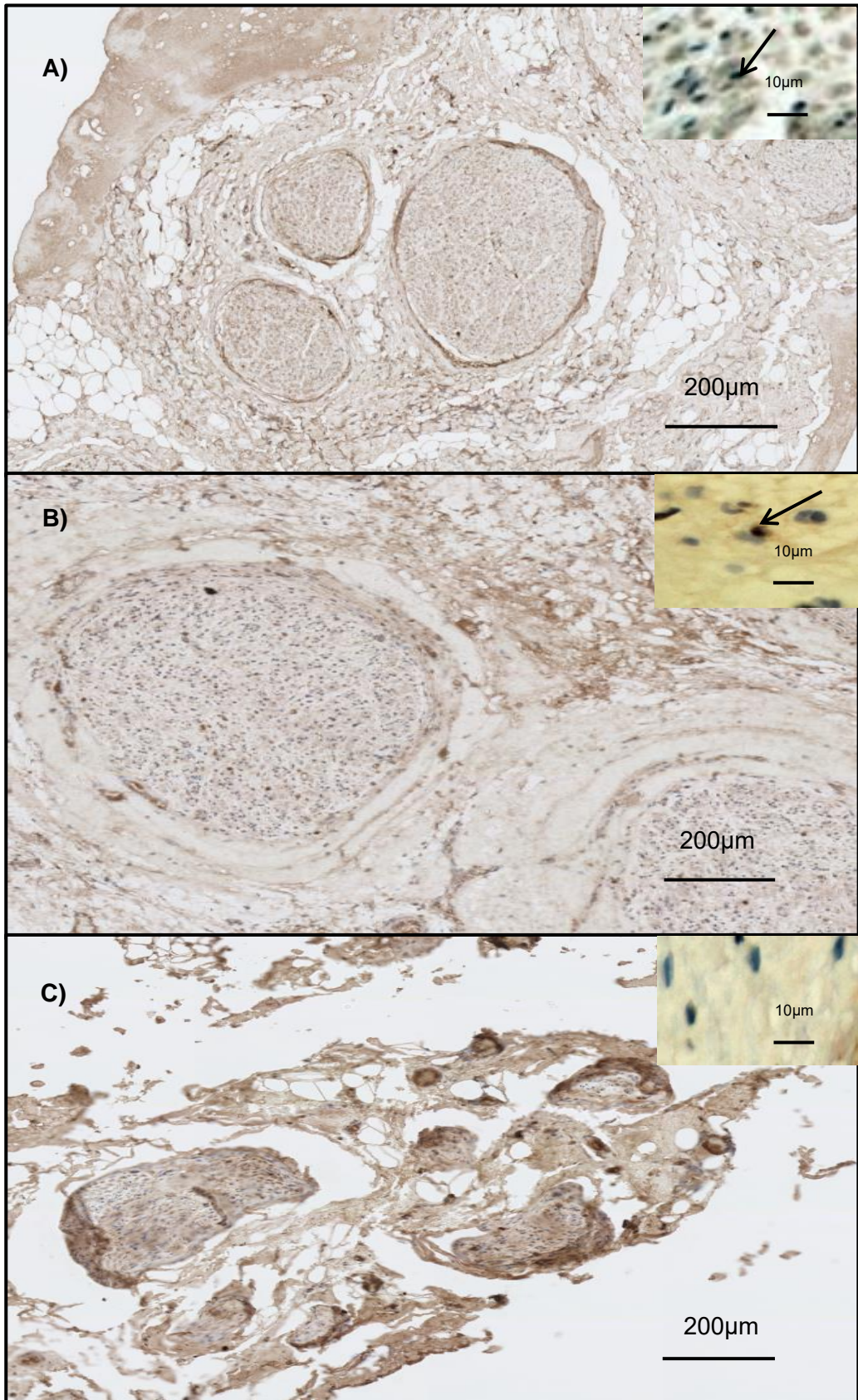
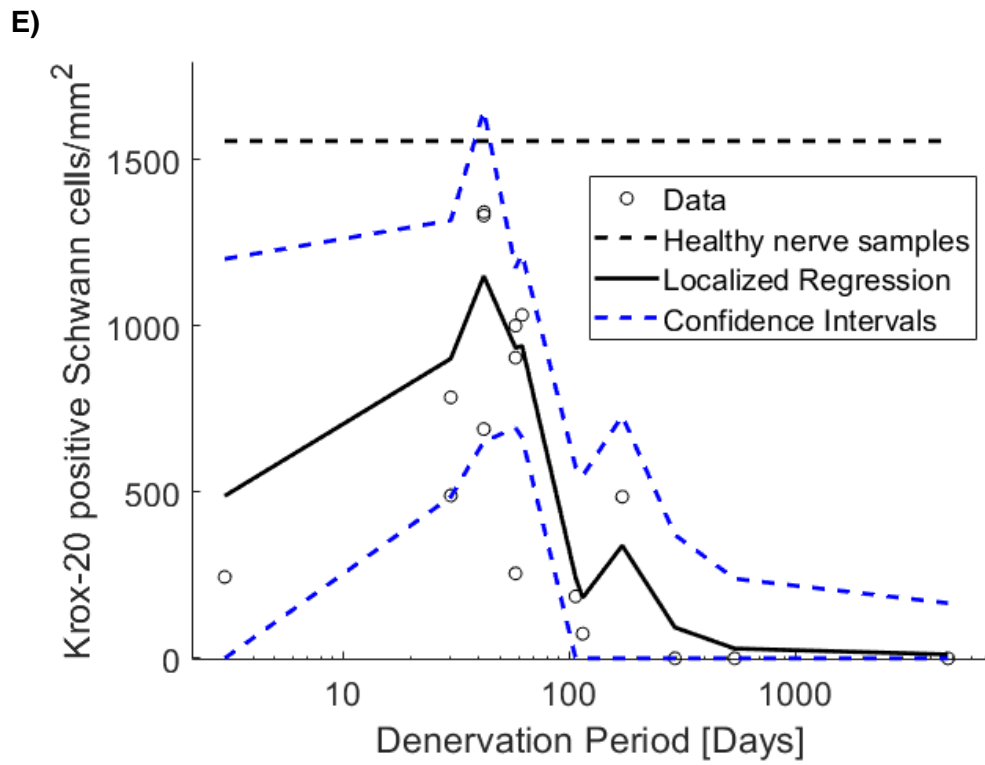
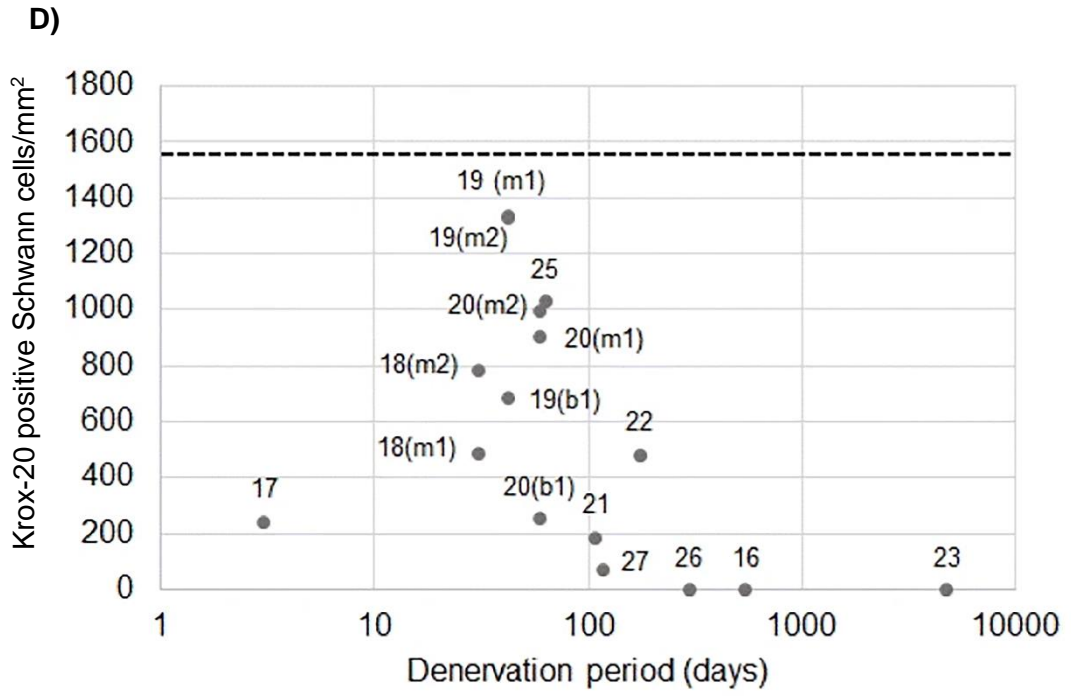


Figure 4.5 - Immunohistochemistry and RT-qPCR analysis of P75NTR in healthy and denervated human nerves. **A) - C)** represent nerve cross sections immunostained for SOX10 (brown) and P75 NTR (red) along with haematoxylin and eosin stain. The black arrow in the micrographs indicates a SOX10/P75NTR positive Schwann cell. The x-axis in **D) – G)** represents Log(denervation time in days). In **D)** and **E)** the horizontal black dotted line represents the mean value obtained for the healthy nerve group. **A)** Healthy Sural nerve **B)** Biceps branch of the musculocutaneous nerve denervated for 30 days **C)** Axillary nerve denervated for 294 days with deteriorated

morphology. **D)** A scatter plot to represent the total number of P75NTR positive Schwann cells/mm² in denervated samples. **E)** Nonparametric smoothing linear regression of the total number of P75NTR positive Schwann cells/mm². **F)** RT-qPCR analysis of P75NTR mRNA expression across denervated samples. **G)** Nonparametric smoothing linear regression of the P75NTR RT-qPCR data. Case numbers are attached to each data point for reference to **Table 2.1** with descriptors of whether the samples were collected proximally or distally: *m1* - Proximal part of the denervated stump of the biceps branch of musculocutaneous nerve, *m2* - Distal part of the denervated stump of the biceps branch of musculocutaneous nerve, *b1* - Proximal section of the denervated stump of the brachialis branch of musculocutaneous nerve, *s1* - Denervated stump of suprascapular nerve, *sa1* - Proximal section of the denervated stump of the spinal accessory nerve, *sa2* - Distal section of the denervated stump of the spinal accessory nerve.





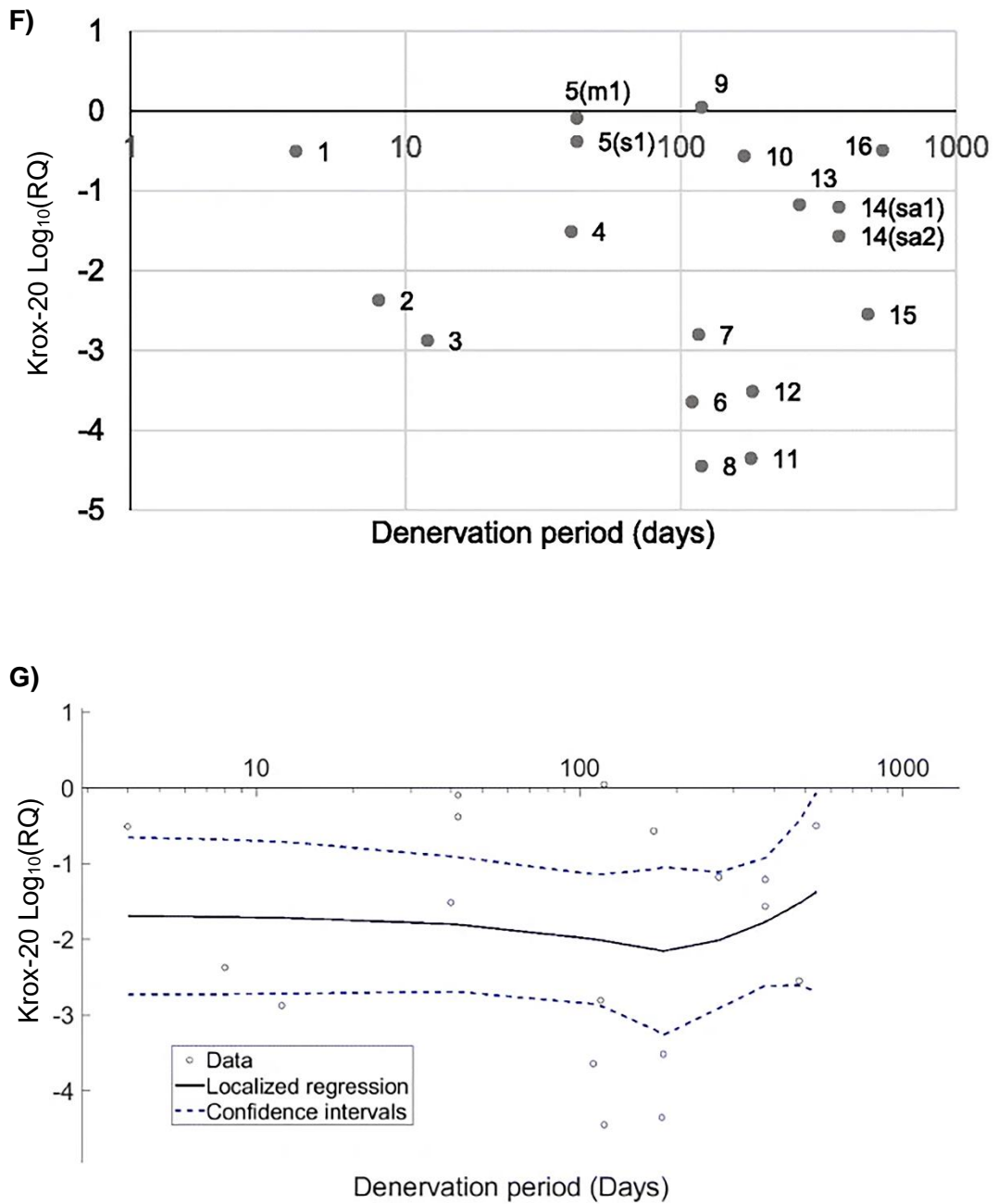


Figure 4.6 - Immunohistochemistry and RT-qPCR analysis of Krox-20 in healthy and denervated human nerves. **A) - C)** represent nerve cross sections immunostained for Krox-20 (brown) along with haematoxylin and eosin stain. The black arrow in the micrograph indicates a Krox-20 positive Schwann cell. The x-axis in **D) - G)** represents Log(denervation time in days). In **D)** and **E)** the horizontal black dotted line represents the mean value obtained for the healthy nerve group. **A)** Healthy sural nerve. **B)** Biceps branch of the musculocutaneous nerve denervated for 30 days. **C)** Axillary nerve denervated for 294 days with deteriorated morphology. **D)** A scatter

plot to represent the total number of Krox-20 positive Schwann cells/mm² in denervated samples. **E)** Nonparametric smoothing linear regression of the total number of Krox-20 positive Schwann cells/mm². **F)** RT-qPCR analysis of Krox-20 mRNA expression across denervated samples. **G)** Nonparametric smoothing linear regression of the Krox-20 RT-qPCR data. Case numbers are attached to each data point for reference to **Table 2.1** with descriptors of whether the samples were collected proximally or distally: *m1* - Proximal part of the denervated stump of the biceps branch of musculocutaneous nerve, *m2* - Distal part of the denervated stump of the biceps branch of musculocutaneous nerve, *b1* - Proximal section of the denervated stump of the brachialis branch of musculocutaneous nerve, *s1* - Denervated stump of suprascapular nerve, *sa1* - Proximal section of the denervated stump of the spinal accessory nerve, *sa2* - Distal section of the denervated stump of the spinal accessory nerve.

4.3 Discussion

To help bridge the gap between the extensive studies of rodent Schwann cells in regenerating nerves and their counterparts in injured human nerves, damaged human nerves for key markers and regulators associated with the rodent Schwann cell injury response were examined. Particular attention was paid to events that take place during chronic denervation of distal nerve stumps, since both in rodents and humans, the deterioration of this tissue during long-term denervation is considered to be an important obstacle to effective nerve repair. For the first time, the markers SOX10, c-Jun, P75NTR and Krox-20 have been explored in denervated samples. Moreover, exploration of the markers SOX10, P75NTR and Krox-20 in healthy human nerve has been quantified for the first time.

To achieve this objective, this study utilised standardised surgical protocols of human nerve liberation, nerve transfer, autograft and FFMT. Almost 40% of the total samples retrieved from surgery were rejected from the study due to the tissue being unsuitable for RT-qPCR and/or immunohistochemistry analysis. This reflects the significant

challenges associated with retrieving human nerve samples from the surgical environment for study in the laboratory (Caboux et al., 2013, Wilcox et al., 2019b). The majority of samples were rejected on the basis of insufficient quantities and quality of RNA. This prompted a recent study to optimise handling of samples in the surgical environment (Wilcox et al., 2019b).

The data on gene and protein expression obtained from the healthy control nerve population in the present study concurs with the rodent literature, and the axon densities are similar to those reported in studies of human sural nerve samples extracted from cadavers (Jacobs and Love, 1985, Ochoa and Mair, 1969). In addition, there was little variation between samples in the expression of the markers of interest (SOX10, c-Jun, P75NTR and Krox-20) between healthy nerve samples from different individuals, assessed using quantitative RT-qPCR and immunohistochemistry analysis suggesting that this was a suitable control group.

Rodent studies have shown that nuclear SOX10 immunoreactivity serves as a specific Schwann cell marker, since in peripheral nerves this transcription factor is selectively and constitutively expressed in Schwann cells (Bremer et al., 2011, Finzsch et al., 2010). Whilst SOX10 has also been examined in human Schwann cells, this has been largely limited to the study of pathologies such as Schwannoma (Karamchandani et al., 2012, Nonaka et al., 2008). The present results show that in healthy human nerve Krox-20, c-Jun and P75NTR are expressed in SOX10 positive cells.

Focusing on immunohistochemical detection of axons, it was found that most samples that were denervated beyond 10 days had fewer than 10 axons present. This is consistent with Wallerian degeneration and concurs with neurophysiological reports which have shown that the CMAP declines to subnormal and un-recordable levels

over 10 days following a nerve injury which has led to the transection of axons (Campbell, 2008, Smith and Knight, 2011).

In comparing the density of Schwann cells (SOX10 positive cells) between healthy controls and denervated samples, it was found that nerves that had been denervated for about a month showed approximately 4-fold higher densities of Schwann cells compared to baseline levels. This is consistent with the well documented injury-induced proliferation of Schwann cells in rodent nerves (Hoke, 2006, Terenghi et al., 1998, Li et al., 1997). Classically, Schwann cell proliferation has been considered important for regeneration, although this has been called into question by more recent results (Kim et al., 2000, Yang et al., 2008).

In human nerves denervated for longer periods, we observed and quantified another notable aspect of repair Schwann cell biology previously studied in rodents, namely the steady and dramatic reduction of Schwann cell numbers in the denervated stump. Eventually, at 5-7 months, the number of cells fell to levels below even those in uninjured nerves. This decline in cell density during chronic denervation was seen both counting total number of cells positive for haematoxylin and counting SOX10 positive cells only. However, a smaller proportion of the total cell population was SOX10 positive in the chronically denervated samples. This is likely due to an increase in the non-Schwann cell population associated with Wallerian degeneration such as the infiltration of other cells such as macrophages and other immune cells (Bosse et al., 2001, Jung et al., 2014, Menorca et al., 2013, Liu et al., 2019), which could be investigated in future studies using additional immunohistochemical markers. The gradual loss of Schwann cells from denervated distal stumps is considered to be a major contributor to the creation of an environment that becomes increasingly antagonistic to regeneration over time (Li et al., 1997, Terenghi et al., 1998, Sulaiman and Gordon, 2000, Hoke, 2006, Jessen and Mirsky, 2016). Contrary

to the histological analysis, SOX10 mRNA remained elevated in all but two of the denervated samples. This discrepancy could be attributable to the use of different nerve samples for RT-qPCR and histology as well as alteration of post-translational regulation of SOX10 in the Schwann cells found in injured nerves.

Focusing on markers of Schwann cell phenotype in injured nerves, the expression of all markers was variable between individuals in contrast to that seen in uninjured control nerves, but there were some overall trends. Some of the variability between individuals could be caused by the number of different mechanisms of injury included in the present study (such as avulsions as well as ruptures and lacerations). Age differences between participants (mean age of 34 (\pm 6) years) could also affect the results, since rodent data show that the Schwann cell injury response is subdued in aging animals (Painter, 2017).

From animal models it is known that upregulation of c-Jun is a global amplifier of the reprogramming events that take place in Schwann cells following denervation and are critical for successful nerve regeneration (Arthur-Farraj et al., 2012, Fontana et al., 2012, Jessen and Mirsky, 2016). A key component of this reprogramming is the appearance of a novel set of phenotypes that constitute part of a repair programme, and upregulation of markers that characterise pre-myelinating Schwann cells. P75NTR is one such marker and at the protein level P75NTR has been shown to be regulated by c-Jun. c-Jun and P75NTR are upregulated within hours following injury and continue to increase for a further 7-10 days (Gomez-Sanchez et al., 2017a, Sulaiman and Gordon, 2013). During chronic denervation, the expression of these markers in the distal stump then steadily declines. As c-Jun levels decline, functional outcomes become less favourable, while genetic restoration of c-Jun levels in transgenic mice restores regeneration (Jessen et al., 2017, Sulaiman and Gordon, 2000, Hoke et al., 2002, Scheib and Hoke, 2013). While the role of P75NTR in

regeneration is not clear (Reichardt, 2006, Chao, 2003, Gonçalves et al., 2019), the drop in P75NTR expression during chronic denervation has been used as a marker of repair Schwann cell deterioration (Gomez-Sanchez et al., 2017a, Sulaiman and Gordon, 2013).

For the first time, this study has shown that a similar pattern of regulation is seen in human nerve regeneration. c-Jun and P75NTR increase in acutely damaged samples (within the first month) and decline in chronically denervated samples. This finding provides new information that can inform the clinical management of nerve-injured patients. Clinical studies suggest that optimal muscle reinnervation is dependent upon a sufficient quantity and quality of motor units being established at the target organ within 1-year following injury (Aydin et al., 2004, Mackinnon et al., 2005). This time-frame has been largely based on the understanding of degenerative changes at the motor endplate and within the denervated muscle (Mackinnon et al., 2005, He et al., 2014, Tung and Mackinnon, 2010, Dahlin, 2006, Noaman et al., 2004). Importantly, the present study provides new evidence suggesting that the repair phenotype of Schwann cells also fades over a shorter time period of around 100 days following injury, resulting in an environment increasingly less supportive of regeneration. Moreover, the results show that in human Schwann cells, c-Jun and P75NTR expression are associated, as previously seen in rodents, suggesting that the basic molecular features which underpin nerve regeneration in humans and rodents are comparable.

The changes in the mRNA reported here may also mirror changes at the level of the spinal cord. Animal models have shown that shortly after neural trauma, injury-induced excitation signals are transduced retrogradely from neuronal and non-neuronal cells to their own injured cell body (Liu and Wang, 2020). An array of molecular responses have been identified leading to the dysregulation of neurotrophic

factors, neurotrophic receptors, neuropeptides and transcription factors (Liu and Wang, 2020). Specifically, the upregulation of c-Jun and P75NTR and down-regulation of Krox-20 represent key changes in the creation of a neuronal phenotype that is supportive of regeneration, which fades over time leading to the reduced regenerative capacity of chronically axotomised axons (Liu and Wang, 2020).

The nonparametric linear regression analysis of Schwann cell numbers and c-Jun, P75NTR and Krox-20 expression during chronic denervation summarises key temporal changes in repair Schwann cells after injury. With further data this could become a useful tool in assessing and predicting changes associated with denervation in PNI patients. It is notable that the magnitude of the expression fold changes in gene expression between control and damaged human nerves, presented in the RT-qPCR data, are significantly larger than those reported in rodent studies (Arthur-Farraj et al., 2012, Chan et al., 2014, Tomita et al., 2007, Yi et al., 2017). To accommodate this range, the present data are displayed as $\text{Log}_{10}(\text{RQ})$ changes, rather than $\text{Log}_2(\text{RQ})$ changes which are reported in a number of rodent studies (Arthur-Farraj et al., 2012, Chan et al., 2014, Tomita et al., 2007, Yi et al., 2017).

Where a sample had been collected and dissected into proximal and distal sections from the same nerve (case 14, 18, 19 and 20), samples which were collected more distally expressed lower quantities of repair Schwann cell markers (c-Jun and P75NTR) than their more proximal counterparts. This observation, whilst based on a limited number of samples, suggests that Schwann cell phenotype becomes less supportive of regeneration in more distal nerve segments, an observation that warrants further exploration.

Down-regulation of the molecular pathways associated with myelination is another key component of the repair programme that is governed by c-Jun in rodents (Jessen and Mirsky, 2016, Jessen and Mirsky, 2008, Parkinson et al., 2004, Parkinson et al.,

2008). Krox-20 is a marker of myelination and its absence or malfunction has been linked with a number of myelinopathies (Jang et al., 2010, Kamholz et al., 1999). The expression of Krox-20 was down-regulated in all denervated samples presented in this study, indicating reversal of myelin differentiation. This suggests that after injury the molecular machinery of myelination in human Schwann cells is regulated in a similar way to that in rodents.

This study should be interpreted in light of its limitations. Although samples were assumed to be denervated based on intra-operative neurophysiology, a few samples demonstrated some positive neurofilament staining. This is perhaps attributable to neurofilament positive autonomic/afferent fibres. Such axons would not have been detected in the functional screening and would therefore not have been excluded from the study. To a small degree, the presence of these axons may have influenced the local cellular environment, meaning that not all of the Schwann cells will have shifted towards a repair phenotype. In addition, only a small number of healthy nerve samples were used for comparison with denervated samples (three samples for RT-qPCR and two samples for histology). This limitation reflects the ethical and practical challenges associated with obtaining healthy nerve samples. Even when it is possible to retrieve small samples of healthy nerve during surgical procedures, the yield of RNA is often reduced to levels sub-optimal for quantification (Wilcox et al., 2019b). In addition, the small size and morphology of these samples can make them inappropriate for histological analysis when complete transverse sections cannot be obtained. A further limitation was that this study only obtained a small number of acutely denervated samples (three samples retrieved less than 30 days following the initial injury). In the general trauma population, nerve injuries often occur secondary to severe vehicular collisions (McAllister et al., 1996, Ciaramitaro et al., 2010) which is reflected in the present study, accounting for 18 out of 27 of injuries (67%). As a result, many patients present with co-morbidities that require treatment before

investigation of a suspected nerve injury, leading to a substantial delay between the initial injury and reconstructive nerve surgery where the samples can be retrieved. In addition, patients are often observed for 3 to 6 months for spontaneous functional recovery following blunt trauma before surgical repair is considered (Birch, 2011b). For these reasons, the retrieval of acutely denervated (less than 10 days between injury and surgery) samples was challenging. This study would also benefit from the inclusion of more samples at standardised time points. However, this is challenging due to the heterogeneous nature of PNI, the rarity of the injuries as well as the practical and ethical challenges associated with harvesting human nerve tissue for study in the laboratory (Hewitt et al., 2008, Wilcox et al., 2019b). Lastly, only one sample from a female was retrieved in the present study (case number 4). This sample was found to have lower quantities of the c-Jun and p75NTR mRNA compared to males at a similar denervation time period (**Fig. 4F** and **Fig. 5F**). This suggests that the repair Schwann cells in this sample are less supportive to neuronal regeneration. This contradicts evidence from rodent models that suggests females exhibit a faster rate of neuronal regeneration compared to males (Kovacic et al., 2004, Stenberg and Dahlin, 2014). It has been shown that this differential may be attributable to a repair Schwann cell phenotype in the distal stump that is sustained for a longer period of time following injury in females compared to males (Kovacic et al., 2004, Stenberg and Dahlin, 2014). This warrants studies of additional female nerve samples to compare the time course of repair Schwann cell deterioration to the findings presented here.

In summary, this study provides new insights into some of the key cellular and molecular features that underpin the regenerative capacity of the human PNS, providing additional explanations for clinical observations and reports. It was found, first, that two major genes associated with repair Schwann cells in rodents, c-Jun and P75NTR, are also up-regulated in acutely injured human nerves, an observation that

encourages the view that rodent models are relevant for learning about human nerve injury. Second, as in rodents, the expression of both of these genes declines during long-term denervation. In rodents, diminishing c-Jun and P75NTR levels mark the general deterioration of repair cells during chronic denervation, a process thought to be a major obstacle to effective nerve repair. The down-regulation of c-Jun and P75NTR reported here provides the first molecular evidence that also in humans, repair cells deteriorate during chronic denervation, and provides markers with which this critical process can be monitored.

Chapter 5: MUNE following nerve transfer to reanimate elbow flexion

5.1 Introduction

A major obstacle to the trial of new therapies for the treatment of nerve injuries is the absence of sensitive and responsive measurements of nerve regeneration. NCS and spontaneous activity on EMG are the current gold standard for the clinical assessment and characterisation of nerve injuries (Smith and Knight, 2011). However, changes on these neurophysiological tests over time are difficult to quantify which limits their application as outcome measures of nerve regeneration.

MUNE is a neurophysiological test that approximates the quantity of Motor Units (MUs) innervating a muscle (Clifton L Gooch et al. 2014; McComas et al. 1971; Shefner 2001). Originally described by McComas et al. in 1971 (McComas et al. 1971), MUNE is based upon the phenomenon that incremental stimulation of a nerve results in an increase in the amplitude of the muscle response. Dividing the maximal CMAP by the mean increase in muscle action potential recorded from the recruitment of single motor units yields an estimate of the number of MUs innervating a muscle.

MUNE is a valid test in clinical trials to quantify distal muscle denervation and predicting likely functional outcomes in pathologies such as Amyotrophic Lateral Sclerosis (ALS) and Spinal Muscular Atrophy (SMA) (Boe, Stashuk, and Doherty 2007; C L Gooch and Harati 2000). However, MUNE has not been explored in muscle reinnervation and there is limited discussion in the surgical literature.

A common surgical challenge following traumatic injury to the upper cervical roots, upper trunk, lateral cord or musculocutaneous nerve is loss of elbow flexion. The double Oberlin's nerve transfer is often deployed by reconstructive nerve surgeons in order to reanimate elbow flexion (**Figure 5.1**). Suitable donor fascicles from the ulnar and/or median nerves are identified by the surgeon and transferred into motor branches of the denervated muscles.

This standardised surgical procedure provides a model to monitor the recovery of MUs as a confirmed denervated muscle is reinnervating and followed up at a range of acute and chronic time points post-operatively.

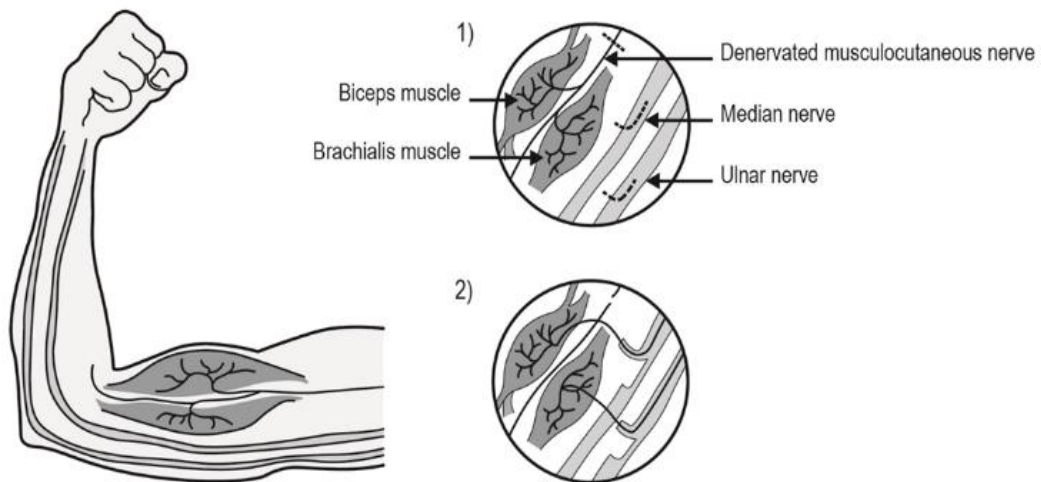


Figure 5.1 - The double Oberlin's nerve transfer is commonly deployed to restore elbow flexion (Wilcox et al., 2020c). The surgeon identifies suitable donor fascicles of the ulnar and median nerve that supply wrist flexor muscles. The fascicles are divided and redirected to grow into the denervated musculocutaneous nerve to biceps and brachialis.

A number of different methods have been reported for MUNE in proximal muscles such as the biceps (Boe, Stashuk, and Doherty 2007; Calder et al. 2005; Clifton L Gooch et al. 2014; Lewis et al. 2003; Shefner 2001). Many of these studies have reported practical challenges in stimulating a proximal nerve such as the musculocutaneous at enough sites in order to obtain a representative sample of SMUAPs (de Carvalho et al., 2018). This is due to the musculocutaneous nerve being relatively deep and short in length affording challenges to achieving stable and repetitive electrical stimulation. Therefore, a number of studies have deployed a modified MUNE approach using a Spike Triggered Averaging (STA) technique to

obtain MUNE recordings from proximal muscles such as the biceps (Boe et al., 2004, Bromberg and Abrams, 1995, Lewis et al., 2003, Power et al., 2012). Unlike other methods, STA MUNE only requires access to the accessibility to the innervating nerve for the CMAP recording. The recording of a sample of SMUAPs is achieved through incremental increases in isometric contractions of the muscle to recruit additional SMUAPs rather than percutaneous stimulation. This technique has demonstrated good test-retest reliability in uninjured and denervated muscles (Boe et al., 2007, Power et al., 2012). Therefore, this study set out to establish the reproducibility of previously published protocols of the modified STA technique in measuring the number of MUs innervating elbow flexor muscles (Boe et al., 2004, Bromberg and Abrams, 1995, Lewis et al., 2003, Power et al., 2012). Using this protocol, this study aimed to quantify the recovery of MUs at a range of acute and chronic time points following Oberlin's nerve transfer.

5.2 Results

Fifteen patients, 14 male and one female, were included in this study with a median age of 34 (IQR 29 to 53). There were 13 right sided brachial plexus injuries and two that were left sided. All patients sustained their injuries following road traffic accidents (**Table 5.1**). Eleven patients had C5/6 avulsions. Axonotmesis of the musculocutaneous nerve and C5-7 avulsion were each found in two cases. Twelve injuries were on the dominant side and three on the non-dominant side.

The median number of days between injury and surgery was 107 days (IQR 50.5 to 157 days). Patients were invited for MUNE post-operatively at a median time of 381 days (IQR 221 to 644 days).

Case Number	Age Range (Gender)	Mechanism of injury	Number of days between injury and nerve transfer	Intra-operative findings	Number of days between nerve transfer and MUNE	Medical Research Council grading of muscle power
1	20-30 (M)	Motorbike v Car	191	C5/6 Avulsion	190	2
2	20-30 (M)	Motorbike v Car	97	C5/6 Avulsion	209 and 321	2 and 4
3	40-50 (M)	Motorbike v Tree	97	C5/6 Avulsion	276	2
4	30-40 (M)	Motorbike v Car	11	C5-7 Avulsion	577	4
5	20-30 (M)	Motorbike v Car	30	C5/6 Avulsion	529	4
6	20-30 (M)	Motorbike v Car	290	C5/6 Avulsion	689	4
7	20-30 (M)	Motorbike v Tree	107	Axonotmesis of the musculocutaneous nerve	543 and 599	3 and 4
8	30-40 (M)	Motorbike v Lampost	56	C5/6 Avulsion	1698	4
9	20-30 (M)	Motorbike v Car	212	C5/6 Avulsion	1509	4
10	40-50 (M)	Motor bike v Car	146	C5/6 Avulsion	1644	4
11	30-40 (M)	Motorbike v Car	45	Axonotmesis of the musculocutaneous nerve	1189	4
12	30-40 (M)	Motorbike v Car	143	C5/6 Avulsion	113 and 204	0
13	50-60 (M)	Motorbike v Car	141	C5/6 Avulsion	381	0
14	20-30 (M)	Motorbike v Car	15	C5-C7 Avulsion	319	1
15	30-40 (F)	Bicycle v Bus	168	C5/6 Avulsion	155 and 232	0 and 1

Table 5.1 - Tabulation of patient demographics in Chapter 5: MUNE following nerve transfer to reanimate elbow flexion.

Test-retest studies revealed that the STA MUNE protocol had an ICC of 0.97 (0.71-1.00) (**Table 5.2**). Uninjured contralateral biceps MUNE values were obtained from 11 of the patients for comparison to the injured arm.

Intraclass correlation	Confidence Interval
0.97	0.71-1.00

Table 5.2 - Test-retest MUNE results for uninjured biceps muscles. This was performed on the uninjured arms of one healthy volunteer and four patients (case numbers 4, 7 and 8 (**Table 5.1**)).

The mean uninjured biceps MUNE value was 370 (± 59) (**Table 5.3**). Four patients (case numbers 3, 11, 13 and 14 (**Table 5.1**)) refused MUNE assessment of their uninjured arm due to poor tolerance of the intramuscular concentric needle electrode. In these patients, the mean biceps MUNE value from the 11 other patients (**Table 5.3**) was used to calculate the percentage MUNE recovery in the nerve injured arm. In addition, CMAPs and SMUAPs were not recordable from the injured arm in five cases (case numbers 12 (113 and 204 days post-operatively), 13, 14 and 15 (**Table 5.1**)). This is because only a small number of MUs (2-4 MUs) were detectable with needle EMG. In these cases, the number of MUs was quantified with needle EMG and compared with MUNE on the uninjured side.

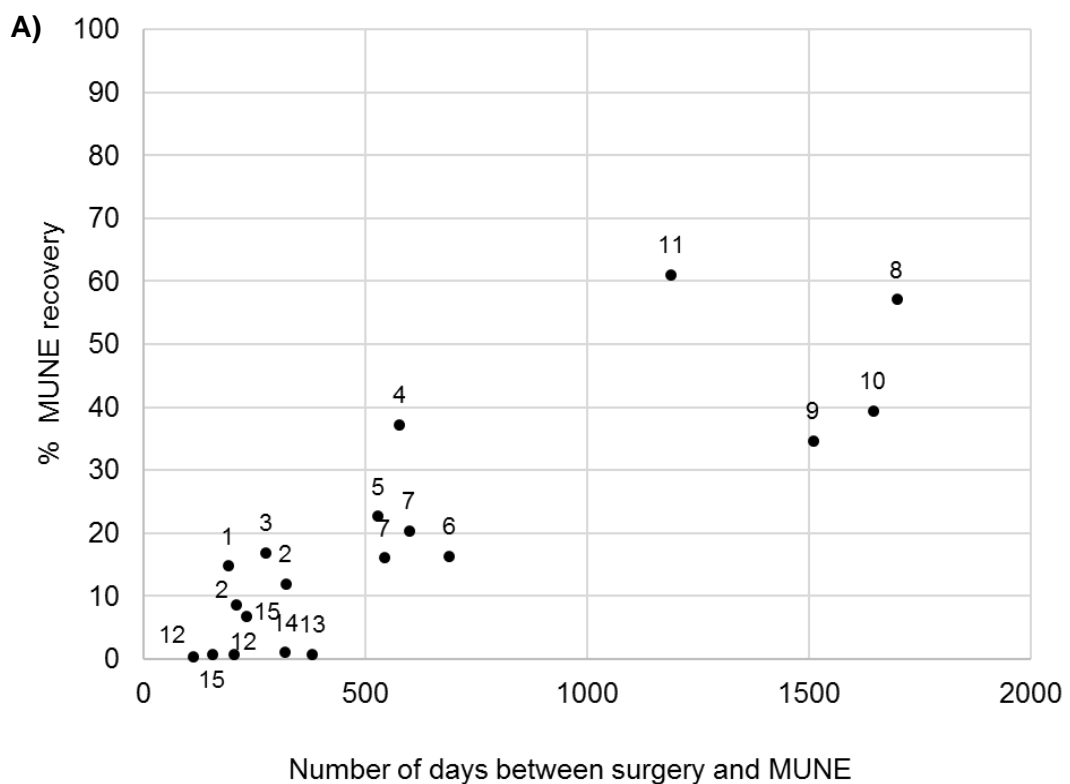
Arm	Mean MUNE (± 1 Standard deviation)	Range
Uninjured (n=15)	370 (± 59)	207 – 435
Injured (n=14)	72.35 (± 73.41)	1 - 262

Table 5.3 - Mean MUNE values from uninjured and injured arms. Fifteen recordings were obtained from uninjured elbow flexor muscles. Four patients (case numbers 3, 11, 13 and 14 (**Table 5.1**)) refused MUNE assessment of their uninjured arm due to poor tolerance of the intramuscular concentric needle electrode. Fourteen MUNE recordings were obtained from injured arms. In the remaining 6 recordings, (case numbers 12 (113 and 204 days post-operatively), 13, 14 and 15 (**Table 5.1**)) only 2-4 MUs were detected using needle EMG which were did not elicit S-MUPs that were sufficient for the MUNE calculation.

Figure 5.2 shows that MUNE recovered over time post-operatively. MUNE reached around 50% of the uninjured side in the most chronically reinnervated muscles (>800 days post-operatively) (**Figure 5.2**).

The magnitude of SMUAPs in sub-acutely reinnervated muscles (around 200 days post-operatively) was around 2-fold larger than that of uninjured muscle (**Figure 5.3**). Beyond this time period, the magnitude of SMUAPs declined towards that of uninjured muscles between 200 and 600 days post-operatively (**Figure 5.3**). In more chronically reinnervated muscles (beyond 1000 days post-operatively), the magnitude of SMUAPs was found to be within the range of uninjured muscles (**Figure 5.3**).

Lastly, the recovery of the CMAP demonstrated an increase over time, reaching 70 – 85 % of uninjured muscles in patients assessed after 1000 days (**Figure 5.4**).



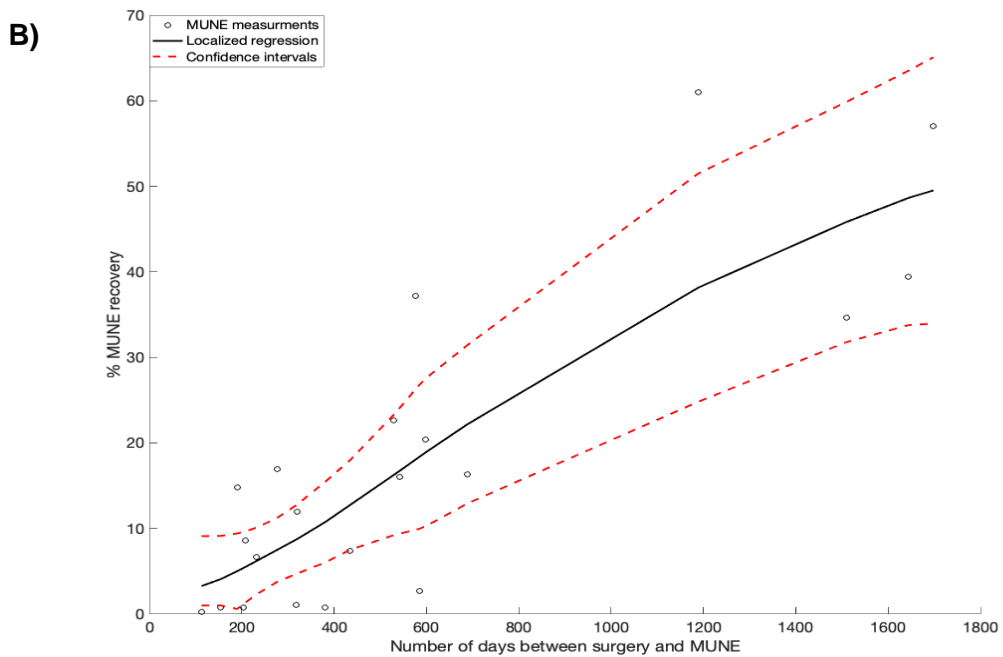
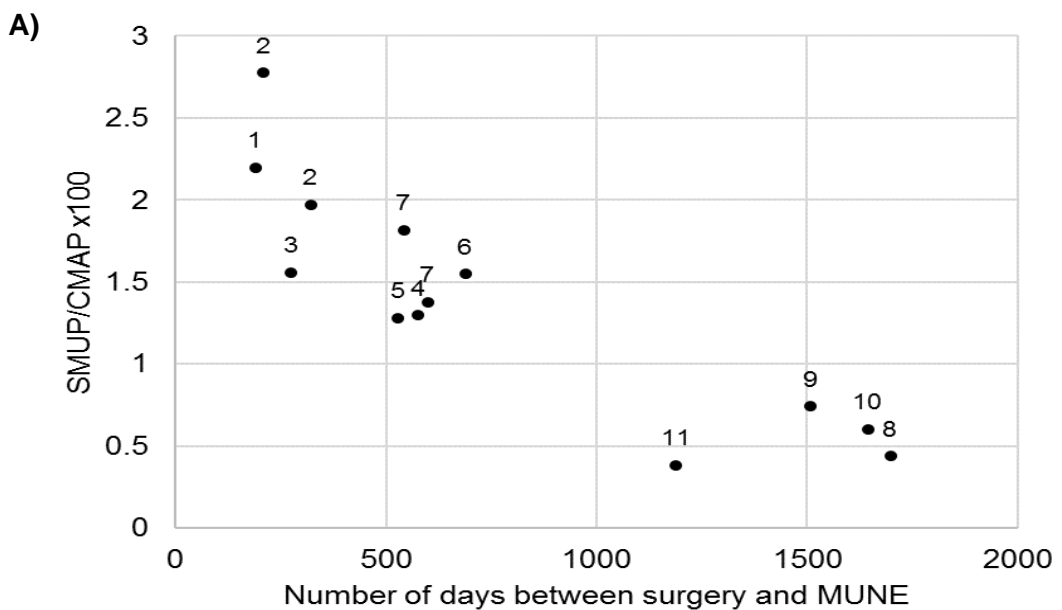


Figure 5.2 - Measurements of MUNE over time in reinnervated muscles compared to contralateral uninjured muscles post-operatively. **A)** MUNE in reinnervated muscles as a proportion of the contralateral, uninjured arm against the number of days between surgery and neurophysiological follow up. Case numbers are attached to each data point for reference to **Table 2.1**. **B)** Application of non-parametric linear regression of the data presented in **A)**.



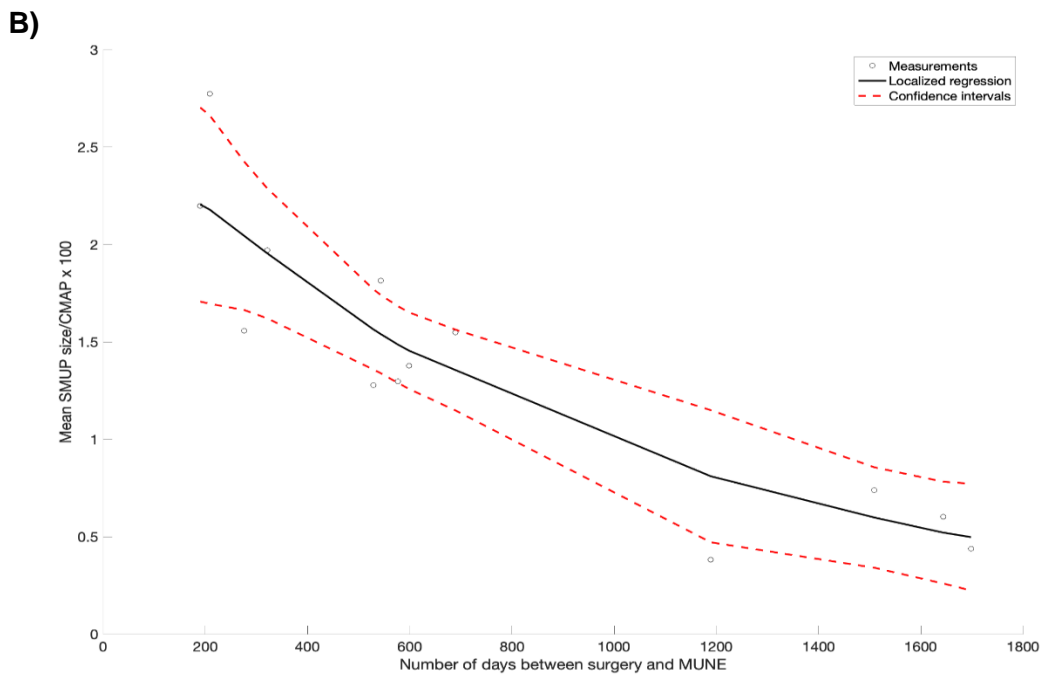
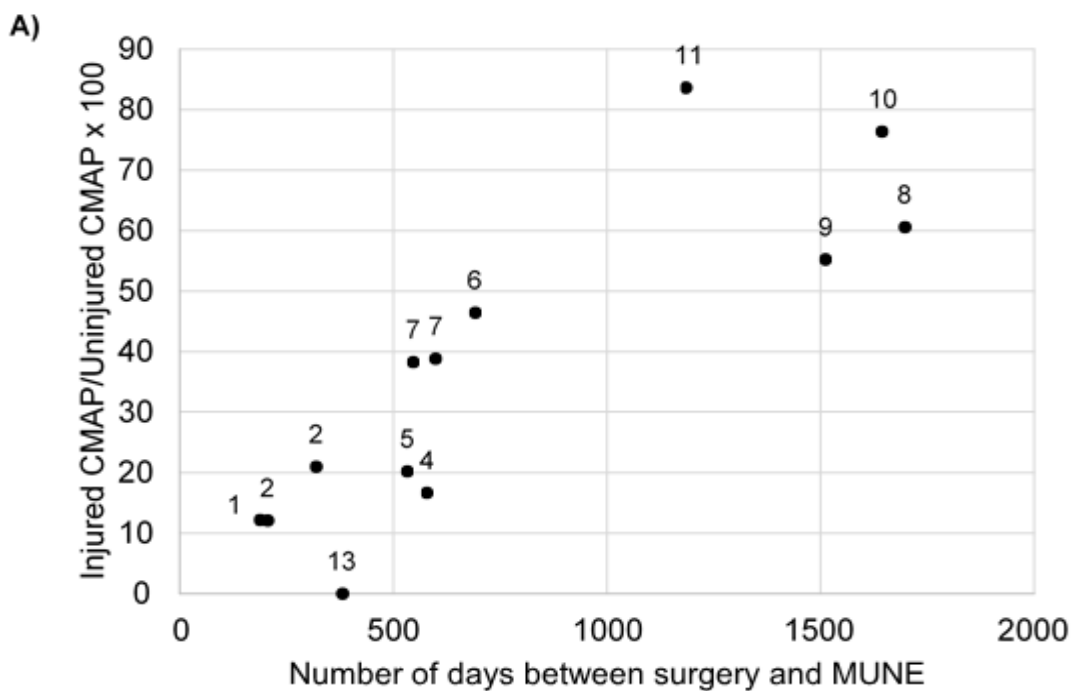


Figure 5.3 - Measurements of the mean magnitude of SMUAPs post-operatively as a proportion of CMAPs. **A)** Measurements of SMUAP magnitude post-operatively as a proportion of CMAP recordings. Case numbers are attached to each data point for reference to **Table 2.1**. **B)** Non-parametric linear regression of the data presented in **A)**.



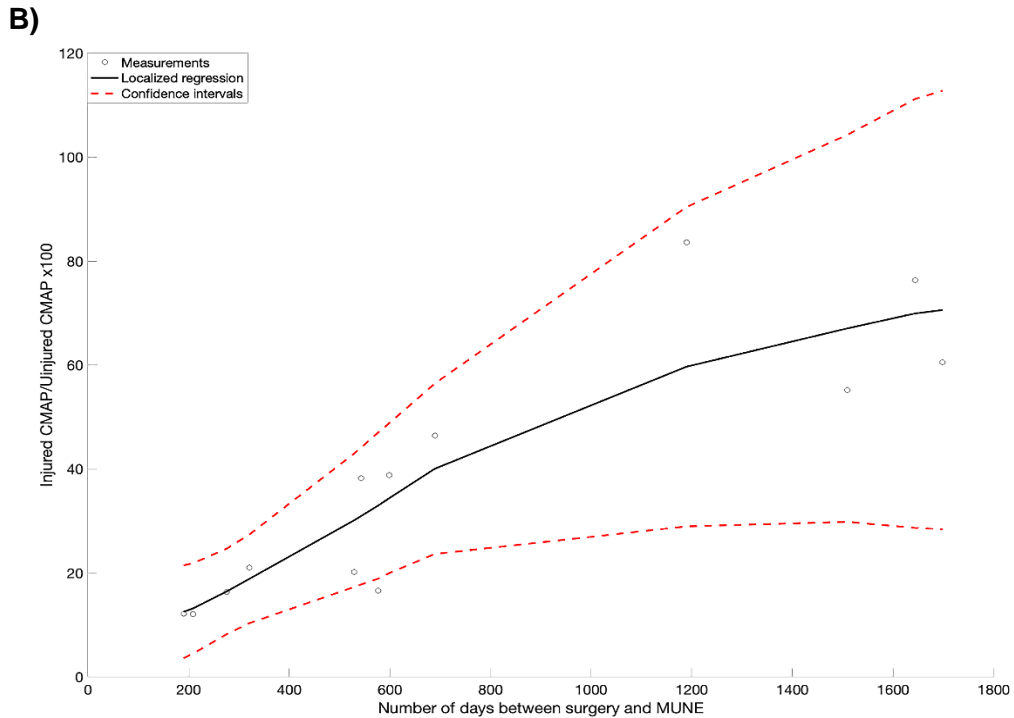


Figure 5.4 - Measurements of CMAP magnitude in the reinnervated arm post-operatively compared to the uninjured arm. **A)** Measurements of CMAP magnitude post-operatively as a percentage of the uninjured contralateral side. Case numbers are attached to each data point for reference to **Table 2.1**. **B)** Non-parametric linear regression of the data presented in **A**).

5.3 Discussion

A major barrier to the trial of new therapies for the treatment of PNI is the absence of sensitive and responsive measures of nerve regeneration and muscle reinnervation. Therefore, this study set out to quantify the recovery of MUs following nerve transfer to reanimate elbow flexion using a modified STA MUNE technique. This technique has previously been deployed to monitor changes in the number of MUs in proximal muscles such as the biceps (Boe et al., 2007, Boe et al., 2004, Bromberg and Abrams, 1995, Power et al., 2012).

Valid outcome measures must demonstrate high reliability in order to detect minimal clinically important differences (Mohtadi, 2016, Rayner et al., 2019). Obtaining repeatable MUNE recordings is dependent to a large extent on selecting an

appropriate method to record reliable and representative samples of SMUAPs (de Carvalho et al., 2018, Shefner, 2001). In comparing the biceps MUNE values reported in this study to methods that used percutaneous stimulation to obtain a representative sample of SMUAPs for the MUNE calculation (Shefner, 2001), it was found that test-retest repeatability was higher in this study. This supports the findings of other studies which support the use of STA MUNE in proximal muscles such as the biceps in order to improve reliability (Boe et al., 2004, Bromberg and Abrams, 1995, de Carvalho et al., 2018). This reflects the practical challenges associated with stimulating a proximal nerve at a sufficient number of sites to yield a repeatable and representative sample of SMUAPs.

The method used to quantify the magnitude of the CMAP and SMUAPs can also have significant consequences on the accuracy of MUNE recordings. In comparing the uninjured biceps MUNE values to other studies that employed a similar modified STA MUNE technique, a number of similarities and differences can be found. In studies that quantified the mean magnitude of CMAPs and SMUAPs using peak-to-peak amplitude, MUNE values trended to be higher than those reported in the present study (Strong et al., 1988, Brown et al., 1988). However, in studies that used the mean negative peak area to quantify the magnitude of CMAPs and SMUAPs, values were comparable to the findings presented in this study (Power et al., 2012, Boe et al., 2004, Bromberg and Abrams, 1995, Lawson et al., 2003). In addition, the latter MUNE values demonstrate closer associations with histological MU estimates from cadaveric samples of the musculocutaneous nerve (Isla and Pozuelos, 2011, Chiarapattanakom et al., 1998). This differential in the MUNE values is at least partially attributable to temporal dispersion of the action potential at the post-synaptic membrane leading to reduced peak-to-peak amplitude but increased negative peak area (Sander and Oh, 2006, Olney et al., 1987). This feature is further accentuated in the context of reinnervated muscle where there is proliferation of post-synaptic

acetylcholine receptors in the temporal orientation (Wu et al., 2014). Together, this suggests that quantifying the negative peak area of CMAPs and SMUAPs leads to more accurate quantification of MUs in healthy and reinnervated muscles using the STA MUNE technique.

With regards to the recovery of MUNE in reinnervated muscle, it was found that the number of MUs was greater in patients at later time points post-operatively. Implementation of the non-parametric linear regression revealed that the fastest apparent rate of recovery of MUs took place between around 200 and 900 days post-operatively. The increase in MUNE over time appears to suggest that the process of muscle reinnervation can be monitored in a predictable fashion using this technique. With further data from individuals at standardised post-operative follow up time, valuable information about prognosis and likely functional recovery may be revealed. By extension, this would benefit the clinical management of this complex pathology. Together, this suggests that MUNE is a suitable marker for monitoring the chronic process of muscle reinnervation, which is consistent with the findings of other studies that found MUNE is a useful measure of chronic muscle denervation (Gooch et al., 2014, Gooch and Harati, 2000).

Secondly, MUNE was found to increase even in the most chronically reinnervated muscle (> 2 years post-operatively) when compared with MUNE recordings obtained in approximately the first two-years post-operatively. In a nerve transfer, a suitable donor fascicle that is proximal to the denervated recipient is identified. The donor is dissected and the axons are transferred to regenerate into the denervated stump. This procedure minimises regeneration distances to <4cm. Given that human nerves regenerate at a rate of approximately 1mm/day (Sunderland, 1947), it can be inferred that the majority of the neurites will reach the muscle within 9 months (± 3 months). Therefore, the findings in the present study suggest that MUNE is not directly related

to the anatomical number of MUs reinnervating the elbow flexor muscles. This is likely to be attributable to re-modelling at the neuromuscular junction during the chronic process of muscle reinnervation (Wu et al., 2014, Magill et al., 2007). Animal models have shown that the ratio of neurites to motor endplates remains elevated compared to uninjured muscles long after they have reached their targets (Wu et al., 2014). Over time, this ratio regresses towards uninjured levels (Wu et al., 2017). In addition, the myelin coating neurites takes time to mature after they have reinnervated the motor endplate (Smith and Knight, 2011). Together, these findings suggest that higher stimulation intensities may be needed to recruit individual MUs even when neurites have reached their targets leading to a lower MUNE. As the neuromuscular junction and the myelin sheath around innervating neurites matures, the mean SMUAP size becomes smaller leading to a corresponding increase in MUNE. Support for this hypothesis is provided by the pattern of changes in SMUAPs found in reinnervated elbow flexor muscles.

It was found that acutely and sub-acutely reinnervated muscles (0 – 200 days post-operatively) demonstrated SMUAPs with magnitudes around 2-fold larger than uninjured muscles. As the time between surgery and MUNE increased, the magnitude of SMUAPs returned towards levels similar to that of uninjured muscles by around 1000 days post-operatively. This finding correlates with animal models of nerve regeneration which have shown that sub-acutely reinnervated muscle demonstrates poly-innervation of the motor-endplate with 2:1 innervation ratios (Magill et al., 2007, Vannucci et al., 2019, Wu et al., 2014). This is associated with larger SMUAP magnitudes on EMG assessment (Smith and Knight, 2011). In more chronically reinnervated muscle, the innervation ratio trends back towards that found uninjured muscles (1:1 innervation ratio) resulting in smaller SMUAP magnitudes (Magill et al., 2007, Smith and Knight, 2011). This suggests that the changes in SMUAP magnitude presented here reflect the extensive re-modelling of the neuromuscular junction

associated with muscle reinnervation. Future work should aim to characterise this relationship between MUNE and histological markers of motor axons and muscle reinnervation (**Chapter 6**).

In contrast, the CMAP was found to increase over time following surgery. The CMAP recovered to around 50% of that of uninjured muscles in the most chronically reinnervated muscles. It is known that the relationship of the CMAP with the volume of uninjured muscles is not well correlated (Barkhaus and Nandedkar, 1994) which is one of the main reasons why MUNE remains an estimate. It is known that changes in the CMAP amplitude and negative peak area are affected by changes in muscle fibre volume and type (Maathuis et al., 2013, Wu et al., 2017). Studies that investigate the relationship of these changes with CMAP in muscle reinnervation will be key to establishing what relationship CMAP has with the biological process of muscle reinnervation.

This study should be interpreted in light of its limitations. Patients were retrospectively identified from the institute database rendering the findings susceptible to selection bias; only 15 out of a potential 27 patients (56%) participated in the present study. Only one female participated in this study. Recent findings from rodent models suggest that the rate of nerve regeneration in females may be faster compared to their male counterparts (Kovacic et al., 2004). Future studies should be conducted to interrogate whether any differential in the rate of MUNE recovery following nerve transfer can be detected between males and females. This study was conducted at a national referral centre for nerve injuries meaning that patients often had to travel from far afield to attend their MUNE appointment. Nine out of the 12 patients (75%) cited this as their reason for non-participation. This self-selection bias may mean that the results presented may not be representative of the broader population. Future studies may be able to circumvent this to some degree through multi-centre studies.

This will require investigation of the inter- and intra- investigator repeatability of the MUNE method presented here. Secondly, the sample size was relatively small compared to other studies that have investigated MUNE in neurological pathologies associated with muscle denervation (Lawson et al., 2003, Lewis et al., 2003, Boe et al., 2007). Sample size is a significant challenge when studying brachial plexus injuries since it is a rare pathology (Kaiser et al., 2020, Midha, 1997). There are also broader challenges associated with research using trauma patients since the follow up rate can be as low as 2% among this patient demographic (Hansen et al., 2014, Leukhardt et al., 2010). Future studies should also seek to quantify MUNE in the donor nerve pre-operatively to allow for more meaningful comparisons to be made between pre- and post-operative MUNE recovery. Further, this study would have benefited from following-up individual patients longitudinally to better monitor changes in MUNE over time. Lastly, the STA MUNE technique is dependent on the use of a concentric needle to isolate a single MU. This was found to reduce the tolerance of the test in some of the patients. Newer methods such as MUNIX (Motor Unit Number Index) may offer non-invasive alternatives to quantify MU numbers (Nandedkar et al., 2004).

In summary, this study has established that MUNE is a measure that has the potential to monitor the chronic process of muscle reinnervation. Future work should investigate the relationship of MUNE with histological markers of muscle reinnervation and motor axons. In addition, the relationship between MUNE and subjective as well as objective measures of muscular function must be delineated in order to determine the validity of MUNE as an outcome measure in muscle reinnervation. This will help drive the clinical translation of new therapeutics for PNI.

Chapter 6: Investigating the relationship between MUNE and histological markers of muscle reinnervation

6.1 Introduction

In **Chapter 5**, MUNE demonstrated the capacity to track the recovery of MUs following nerve transfer to reanimate elbow flexion. In order to further investigate the validity of MUNE as an outcome measure of muscle reinnervation, this Chapter aims to interrogate the link between MUNE, the biological process of muscle reinnervation and a measurement of motor function in a controlled animal model of nerve injury. Characterisation of this relationship will inform power calculations for future clinical trials which hope to enhance peripheral nerve repair (Rayner et al., 2019, Wilcox et al., 2020a).

Methods used to acquire MUNE principally differ in the way they measure a representative sample of SMUAPs. Early studies used an incremental MUNE technique in distal muscles (e.g. thenar muscles) to reveal information about the dynamics of a number of neuromuscular diseases in humans (McComas et al., 1971b, Gawel et al., 2015, Wang and Delwaide, 1995, Jagtap et al., 2014, Stein and Yang, 1990, Carleton and Brown, 1979, Hansen and Ballantyne, 1978). Animal models of neuromuscular disease were subsequently developed to reveal new information about anatomical correlates of MUNE (Reaume et al., 1996, Shefner et al., 1999). However, challenges are encountered when applying an incremental methodology in proximal human muscles such as the biceps (Boe et al., 2004, Bromberg and Abrams, 1995, Brown et al., 1988). Percutaneous stimulation of a proximal nerve trunk (such as the musculocutaneous nerve) at a sufficient number of sites to record a response from a representative sample of SMUAPs is often onerous for the patient and clinical investigator leading to low repeatability of MUNE measurements (Bromberg and Abrams, 1995, Shefner, 2001, Gooch et al., 2014, de

Carvalho et al., 2018). This stimulated studies to investigate the ability of modified STA technologies to capture a representative sample of SMUAPs (Power et al., 2012, Bromberg and Abrams, 1995, Shefner, 2001) (such as that described in **section 2.2.3**). These techniques rely on the co-operation of the patient to perform graded voluntary isometric contractions of the muscle being studied to determine the mean magnitude of SMUAPs. A drawback of this method is that it is not feasible for animals to execute voluntary isometric muscle contractions affording challenges to studies which aim to learn more about anatomical correlates associated with the STA technique in controlled animal models. However, it has been shown that remarkably similar MUNE values can be obtained irrespective of the technique used provided that the well-defined assumptions and criteria to identify SMUAPs associated with each method are fulfilled (de Carvalho et al., 2018, Bromberg and Abrams, 1995, Shefner, 2001). This suggests that although it may not be possible to use an identical MUNE method to that presented in **section 2.2.3** in controlled animal models of nerve injury, it is possible to use an alternative technique such as incremental stimulation to reveal information about the relationship of MUNE with the biological process of muscle reinnervation. Irrespective of the MUNE method chosen, the aim of MUNE is to generate a number that accurately estimates the number of MUs innervating a muscle. If this number was anatomically verifiable, MUNE could be compared against this benchmark.

In uninjured muscles, a handful of studies have sought to correlate MUNE with anatomical features in animals and humans. Eisen et al. 1974 performed incremental MUNE studies on uninjured rat soleus muscles and compared these results to the number of large myelinated fibres in the nerve to soleus (Eisen et al., 1974). A later study performed STA MUNE on human thenar muscles and compared these values with the anatomy of recurrent median nerves retrieved from cadavers (Lee et al., 1975). Both studies reported that MUNE correlates with the number of large

myelinated fibres (Eisen et al., 1974, Lee et al., 1975); a finding which has been confirmed by more recent studies which employed a wide variety of MUNE methods such as MPS, statistical methods and CMAP scan (Arasaki et al., 1997, Peyronnard and Lamarre, 1977, Shefner, 2001).

The accuracy of different MUNE methods has also been interrogated in denervated muscles (Reaume et al., 1996, Shefner et al., 1999, Azzouz et al., 1997, Shefner, 2001). Animal models of ALS have shown that MUNE tends to underestimate anatomical approximations of the number of large myelinated fibres in muscle denervation (Reaume et al., 1996, Shefner et al., 1999, Azzouz et al., 1997, Shefner, 2001). This finding has been largely attributed to a phenomenon known as alternation (Shefner, 2001). Techniques that rely on incremental stimulation to measure the mean magnitude of SMUAPs assume that each increase in EMG amplitude resembles the recruitment of an additional MU (DeForest et al., 2018, Bromberg, 2007). This assumption is violated if multiple MUs respond to a given increment in stimulus. Additionally, the activation thresholds of axons often overlap (Burke et al., 2009) therefore an increase in EMG amplitude may reflect the firing of multiple MUs rather than the recruitment of an individual MU. This is a particularly pertinent factor in reinnervated and denervated muscles which have been shown to fashion more homogeneous MU pools when compared to uninjured muscles (Novak and Salafsky, 1967, Albani et al., 1988b, Bagust et al., 1981, Albani et al., 1988a). As a result, it can often be challenging to distinguish between two independent MUs with similar activation thresholds. This has the potential to lead to an overestimation of the magnitude of SMUAPs leading to an underestimation of MUNE in denervated muscles (Shefner, 2001, DeForest et al., 2018). More recent variants of the incremental technique such as MPS (Shefner, 2001, DeForest et al., 2018) have attempted to address this issue but may give rise to other limitations such as the

inability to record a representative sample of SMUAPs (Shefner, 2001, de Carvalho et al., 2018).

The biological process of motor endplate reinnervation can also lead to changes which may influence different components of the MUNE calculation. It has been shown that the recovery of CMAP strongly correlates with the reinnervation of motor endplates (Vannucci et al., 2019). However, detailed investigation of the relationship of other biological aspects of reinnervation such as polyinnervation of the motor endplate (Vannucci et al., 2019) with components of the MUNE calculation is awaited. Regenerating axonal branches that reach the muscle fibre often reinnervate more than one motor endplate (Pavlov et al., 2008, Bischoff et al., 2009, Seitz et al., 2011). This means that one muscle fibre can be reinnervated by more than one motor axon which often have antagonising actions (Pavlov et al., 2008, Bischoff et al., 2009, Seitz et al., 2011). Polyinnervation of motor endplates is considered a major contributor to impaired functional recovery in denervated and reinnervated muscle (Pavlov et al., 2008, Bischoff et al., 2009, Seitz et al., 2011, Vannucci et al., 2019). Establishing the interconnection of polyinnervation of the motor endplate with the MUNE calculation would allow this critical process to be monitored.

Despite these technical issues and biological considerations encountered when studying denervated and reinnervated muscle, it has been shown that a decline in MUNE correlates with axonal loss in animal models of neuromuscular pathologies such as ALS (Reaume et al., 1996, Shefner et al., 1999, Azzouz et al., 1997, Shefner, 2001). Moreover, these changes in MUNE often preceded the onset of clinical signs of axonal loss (Reaume et al., 1996, Shefner et al., 1999, Azzouz et al., 1997, Shefner, 2001) suggesting that MUNE has the capacity to detect sub-clinical changes. Corresponding studies that have investigated the link between MUNE, anatomy and motor function in reinnervated muscle are awaited. Addressing this

issue would represent a key step towards understanding the validity of MUNE as an outcome measure of muscle reinnervation.

A major limitation associated with studies which investigated the link between MUNE and anatomy in healthy as well as denervated muscles is that no clear verification was provided that the axons counted were motor axons (Shefner et al., 2001, Shefner et al., 1999, Reaume et al., 1996). Since the publication of these studies, the discovery of immunohistochemical markers such as ChAT has enabled specific and reliable detection of motor axons (Furness et al., 1984, Furness et al., 1985, Mann et al., 1995, Schemann et al., 1995, Schemann et al., 1993). Investigation of the link between MUNE and ChAT in a controlled animal model of muscle reinnervation would represent an important step forwards in determining the accuracy of MUNE.

Creation of an axonotmesis injury to the rat sciatic nerve is commonly used as an in vivo model of nerve injury by researchers to investigate peripheral nerve regeneration and muscle reinnervation (Haastert-Talini, 2020, Ronchi et al., 2019). The diameter and length of the rat sciatic nerve is the largest when compared to other nerves which makes surgical handling easier (Bozkurt et al., 2011, Sinis et al., 2011). Functional measures such as the SSI which monitor the recovery of hindpaw motor function following sciatic nerve crush have demonstrated validity in determining the efficacy of new therapies which hope to enhance muscle reinnervation (Rayner et al., 2019, Wood et al., 2011a). Therefore, this study aimed to measure the link between MUNE, histological markers of muscle reinnervation and SSI in order to determine the validity of MUNE as an outcome measure of muscle reinnervation.

6.2 Results

Repeatability of MUNE recordings

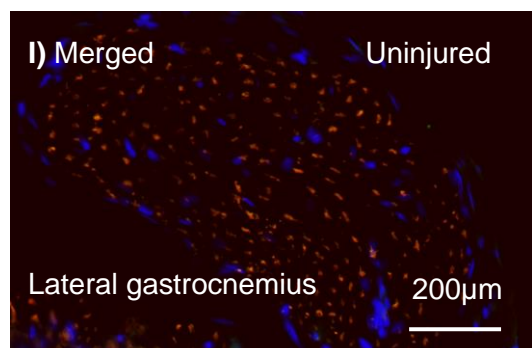
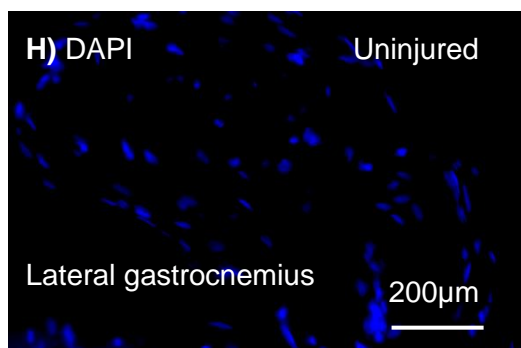
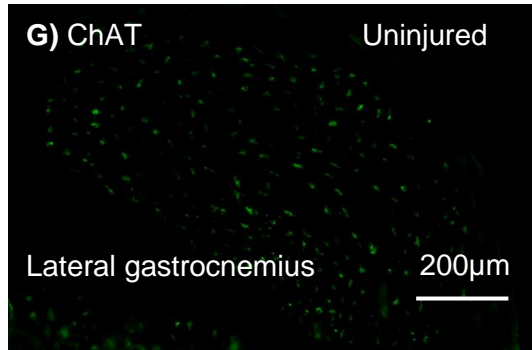
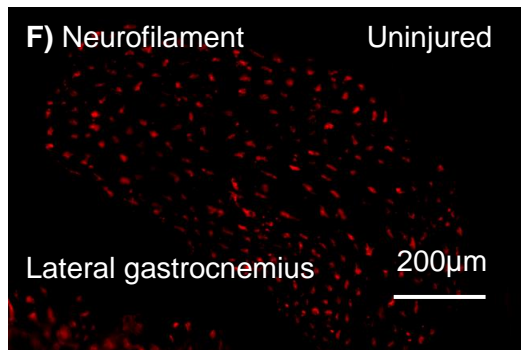
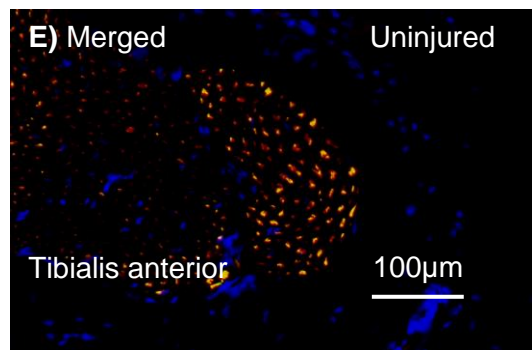
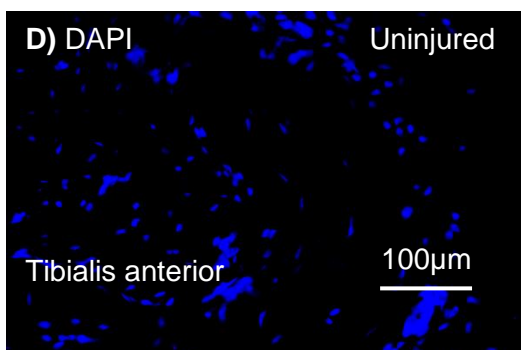
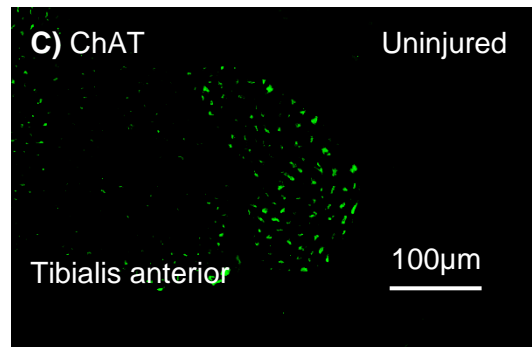
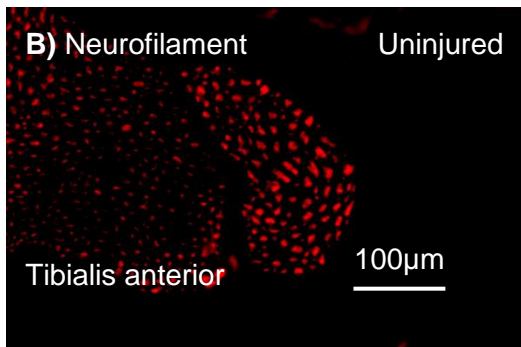
The repeatability of MUNE recordings from the tibialis anterior and gastrocnemius muscles was assessed by comparing pre-crush MUNE recordings with MUNE values

obtained from the uninjured contralateral muscles. The ICC was 0.81 (0.64-0.99) for the tibialis anterior and 0.69 (0.42-0.84) for the gastrocnemius muscle.

Relationship between MUNE and ChAT

The mean MUNE value obtained from uninjured, contralateral tibialis anterior muscles was 80.8 ± 12 whilst the mean number of ChAT positive axons detected was approximately 10% lower; 74 motor axons ± 9.5 (**Figure 6.1A - E**). This was not a statistically significant difference. The mean MUNE value recorded from uninjured, contralateral gastrocnemius muscles was 120 ± 21 whilst the mean number of ChAT positive axons found in the medial and lateral nerve segments to the gastrocnemius was 224 ± 26 (**Figure 6.1A, F - M**). This two-fold differential represents a statistically significant difference ($p < 0.001$). However, it is important to point out that the number of motor axons detected using histology in the nerve segment to the lateral gastrocnemius muscle (115 ± 25 motor axons) was not significantly different to MUNE recordings from the gastrocnemius muscle (120 ± 21) (**Figure 6.3A, F - I**) when compared with the number of motor axons detected in the nerve segment to the medial gastrocnemius (125 ± 31) (**Figure 6.3A, J - M**).





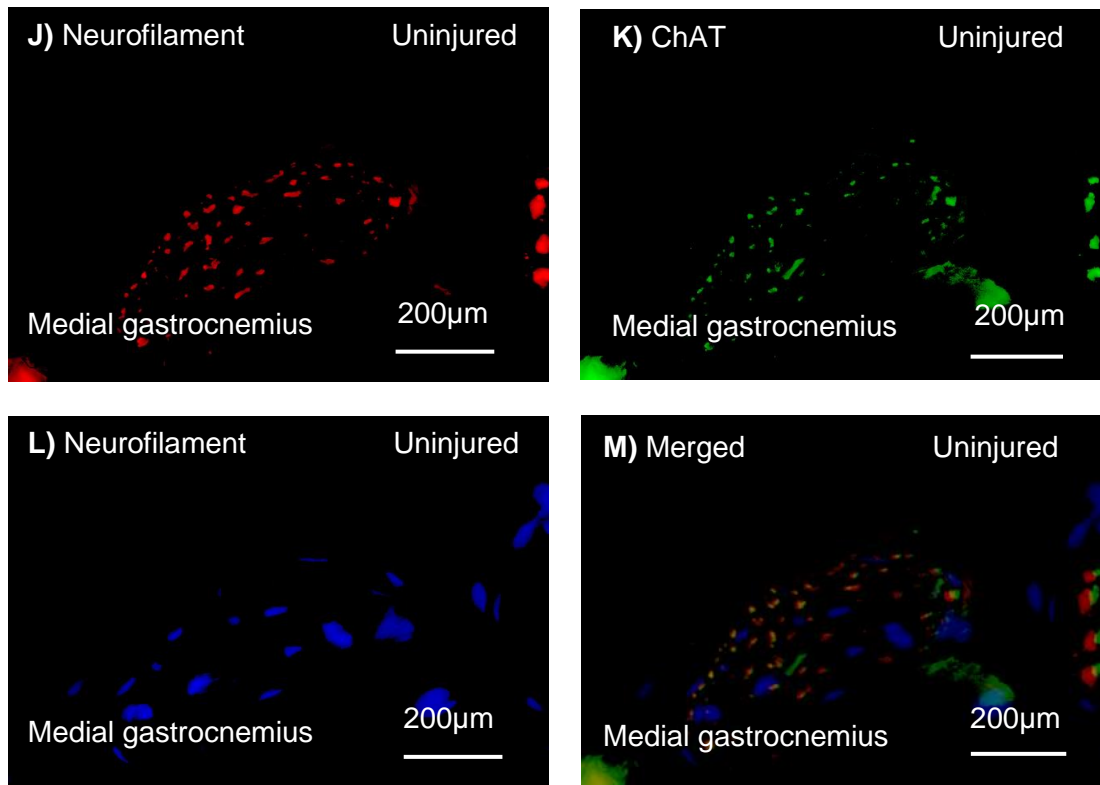
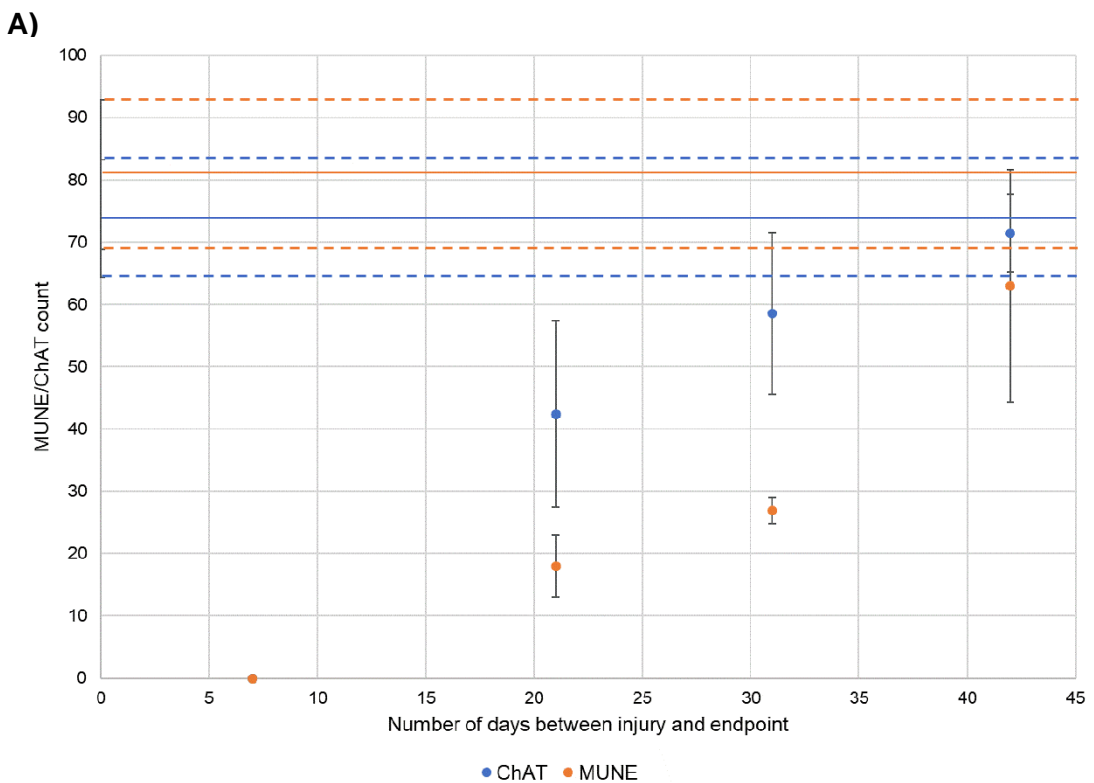


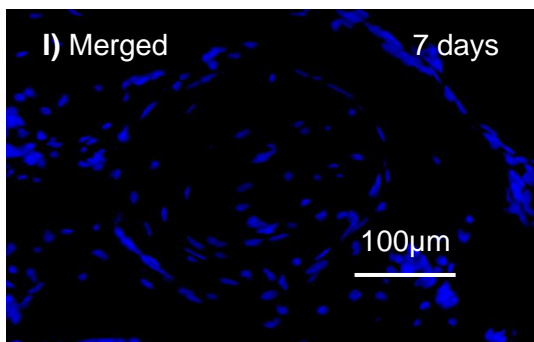
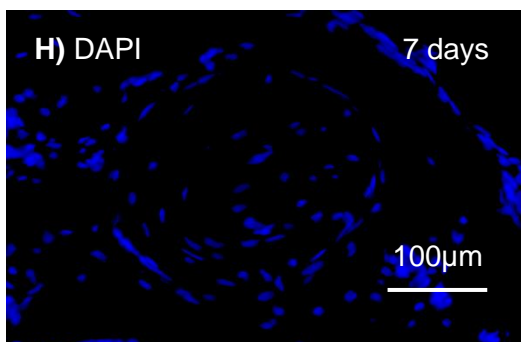
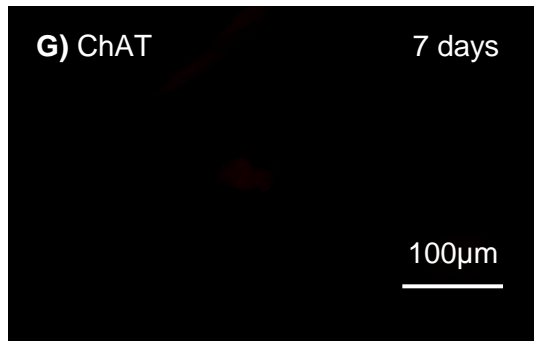
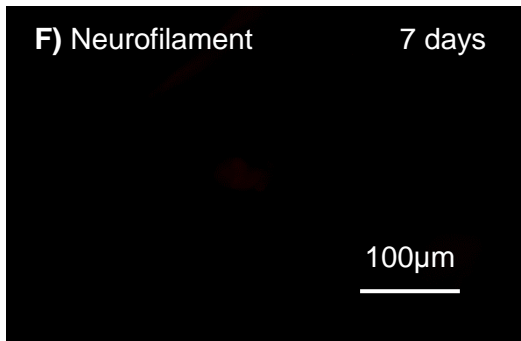
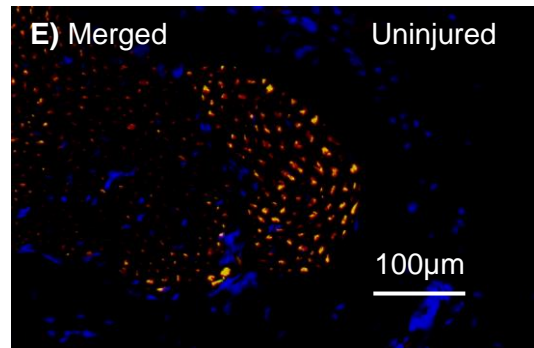
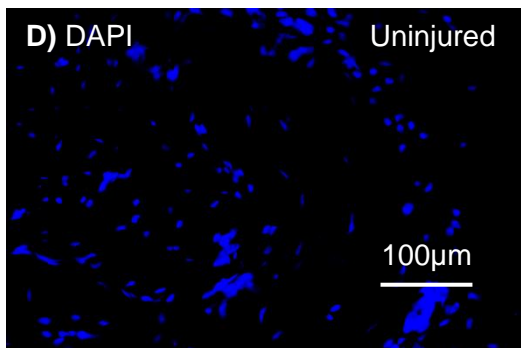
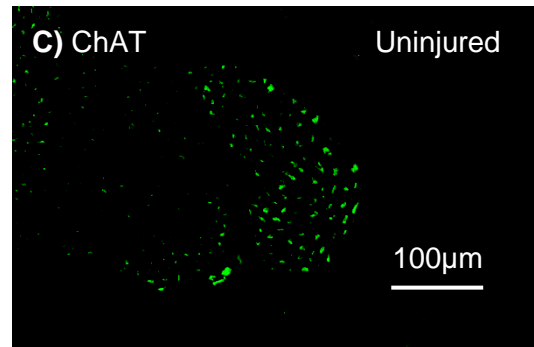
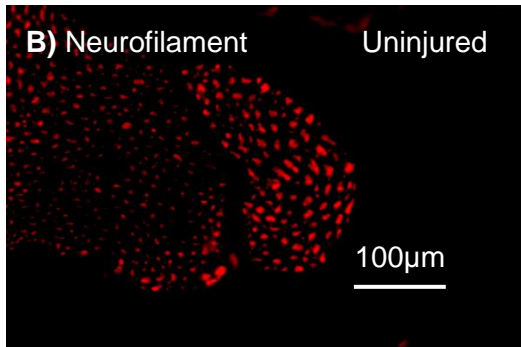
Figure 6.1 - MUNE and ChAT counts of uninjured tibialis anterior and gastrocnemius muscles. **A)** MUNE obtained from uninjured contralateral tibialis anterior and gastrocnemius muscles. The mean value obtained from the uninjured tibialis anterior muscle was 87 ± 12 ($n=18$) compared to 72 ± 10 ($n=18$) ChAT axons detected in the uninjured nerve segment to the tibialis anterior representing a non-statistically significant difference. However, the number of motor axons innervating the gastrocnemius muscle that were detected using MUNE (120 ± 21 , $n=9$) was approximately half the number counted using ChAT counts (224 ± 21 , $n=9$); a statistically significant difference ($p < 0.001$). **B) – E)** are representative images of the nerve segment to tibialis anterior. **F) – I)** are representative images of the nerve segment to the lateral head of the gastrocnemius muscle. **J) – M)** are representative images of the nerve segment to the medial head of the gastrocnemius muscle.

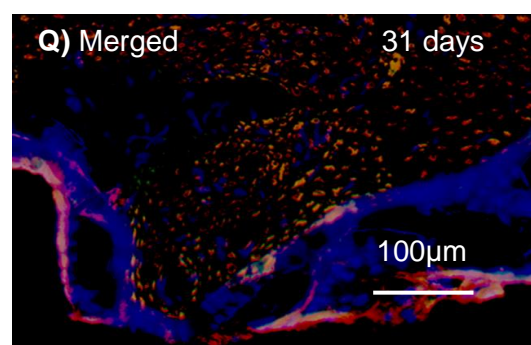
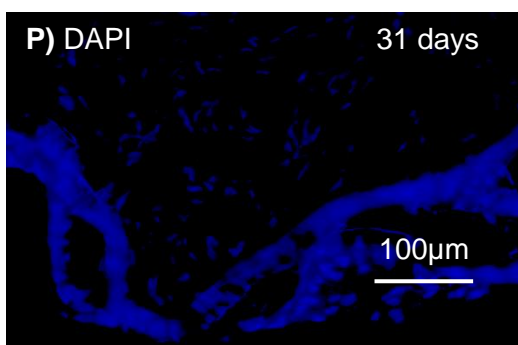
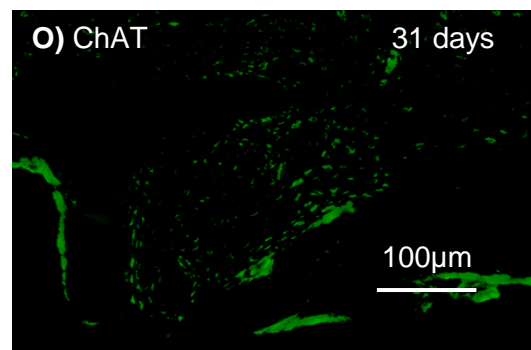
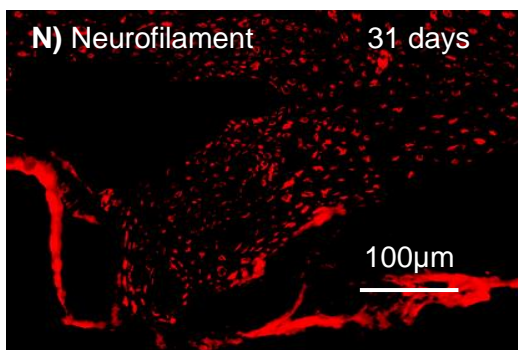
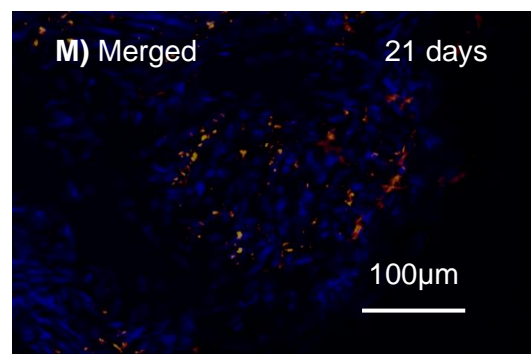
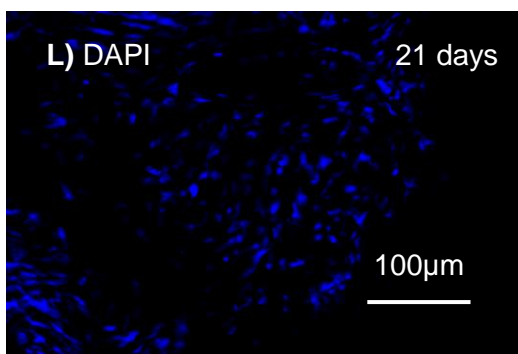
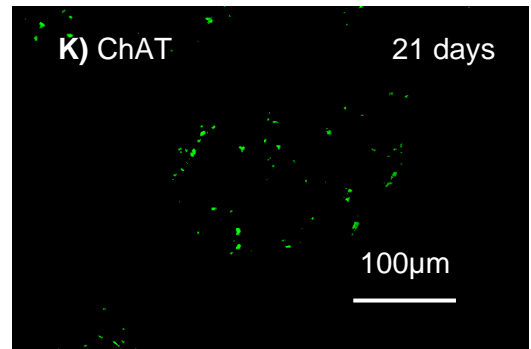
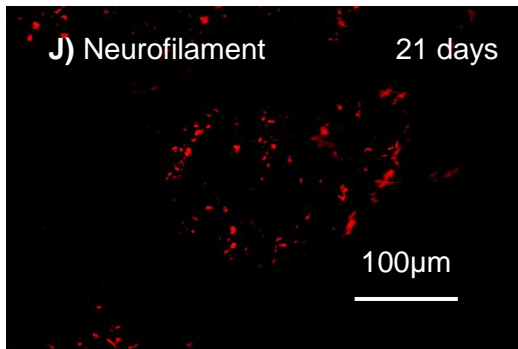
Since MUNE recordings from tibialis anterior muscles were less variable and demonstrated a closer relationship with the number of motor axons detected using histology, reinnervation of the tibialis anterior muscle following sciatic nerve crush

was selected to measure the correspondence between MUNE, ChAT, NMJ innervation and SSI.

With regards to the relationship between MUNE of tibialis anterior and ChAT positive axons in the nerve segment to tibialis anterior following sciatic nerve crush, no axons were detected using physiology or histology seven days following injury (**Figure 6.2A, F - I**). Twenty-one days following injury, the mean MUNE recording was less than half of the number of motor axons detected using histology; 18 ± 5 compared to 42 ± 14 respectively (**Figure 6.2A, J - M**) representing a statistically significant differential ($p < 0.001$). By 31 days, the differential between MUNE (27 ± 2.1) still significantly ($p < 0.01$) underestimated ChAT (54.6 ± 13.7) by around 50% (**Figure 6.2A, N - Q**). Forty-two days following injury, MUNE (64.2 ± 19) and ChAT (71.4 ± 6.2) were not significantly different and recovered to levels similar to uninjured levels (**Figure 6.2A, B - E, R - U**).







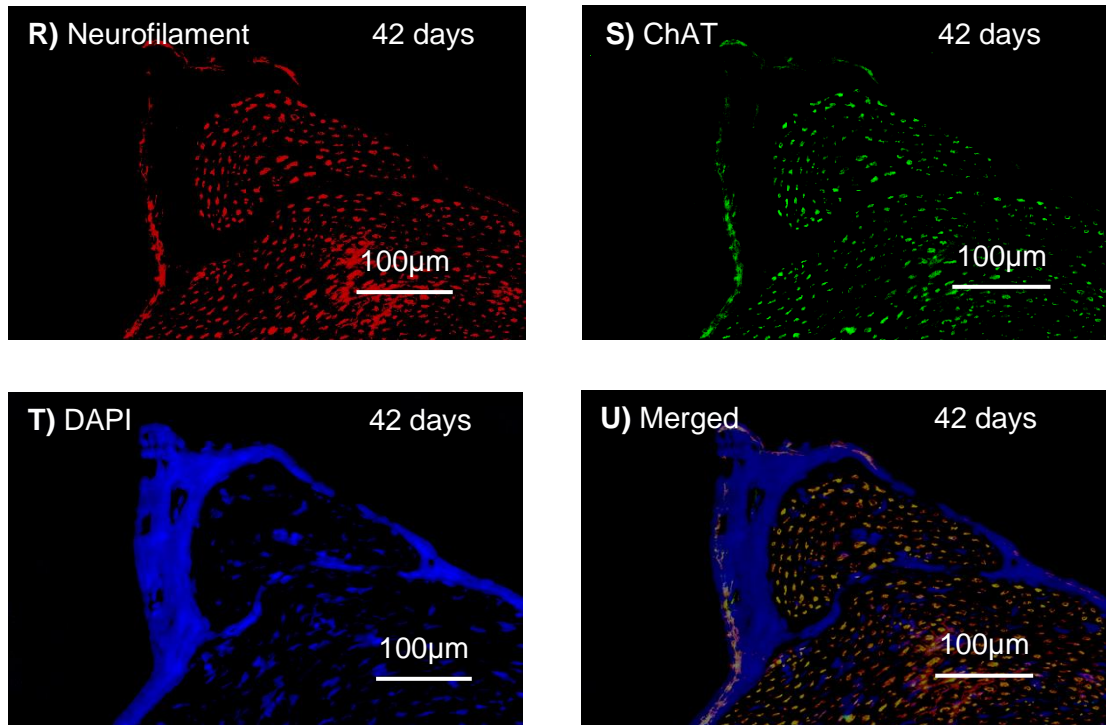


Figure 6.2 - Relationship between MUNE recordings from the tibialis anterior muscles and ChAT counts from the nerve segment to tibialis anterior. **A)** Quantification of the mean MUNE value and ChAT following sciatic nerve crush. Seven days post-injury, MUNE was not recordable ($n=3$) and no motor axons were detected using histology ($n=3$). Twenty-one days post-injury, the mean number of motor axons detected using MUNE (18.6 ± 5.02 , $n=5$) was approximately half the ChAT count (42.4 ± 14.7 , $n=5$) representing a statistically significant difference ($p < 0.001$, two-tailed t-test). By 31 days post-injury, the mean MUNE recording was 26.8 ± 2.1 ($n=5$) compared to 54.6 ± 13.7 ($n=5$) ChAT positive axons; a statistically significant difference ($p < 0.05$, two-tailed t-test). At 42 days post-injury, the mean MUNE recording was 64.1 ± 18.7 ($n=5$) whilst the mean number of ChAT positive axons was not statistically significant (71.4 ± 6.2 , $n=5$). The solid orange line represents the mean MUNE value obtained from uninjured contralateral tibialis anterior muscle (87 ± 12 , $n=18$) and the dashed orange lines represent one standard deviation from the mean. The solid blue line represents the mean ChAT count from nerve segments to the contralateral uninjured tibialis anterior muscles (72 ± 10 , $n=18$) and the dashed blue lines represent one standard deviation from the mean. **B) – U)** are representative images of immunostaining of the nerve segment to tibialis anterior. **B) – E)** represent uninjured nerve segments. **F) – I)** represent nerve segments 7 days following injury. **J) – M)** represent nerve segments 21 days following injury. **N) – Q)** represent nerve segments 31 days following injury. **R) – U)** represent nerve segments 42 days following injury.

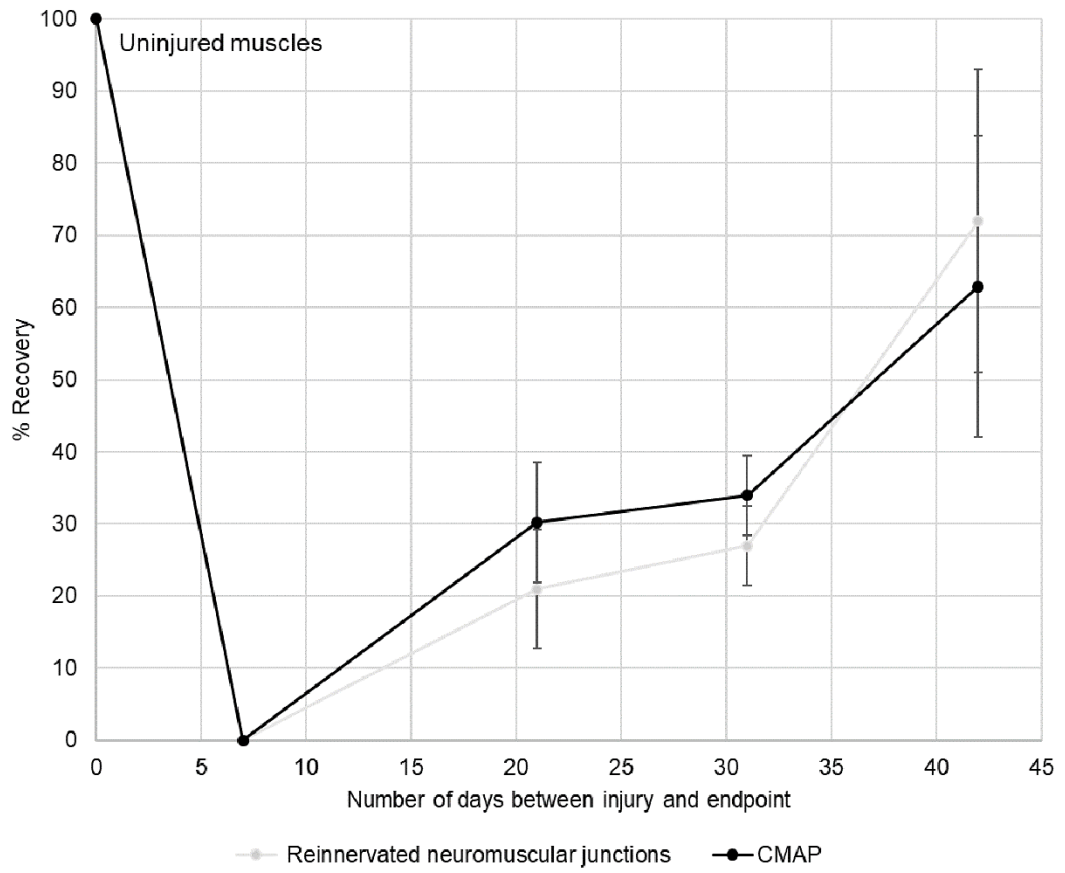
CMAP and NMJ reinnervation

No CMAP could be elicited seven days following crush (**Figure 6.3A**). Beyond this time period, CMAP recovered steadily, increasing to around 60% of the pre-crush CMAP 42 days following injury (**Figure 6.3A**). The proportion of reinnervated NMJs in tibialis anterior muscles following injury compared to contralateral uninjured muscles demonstrated good correspondence with restoration of CMAP ($R^2=0.63$, $p<0.001$) (**Figure 6.3A - Z**).

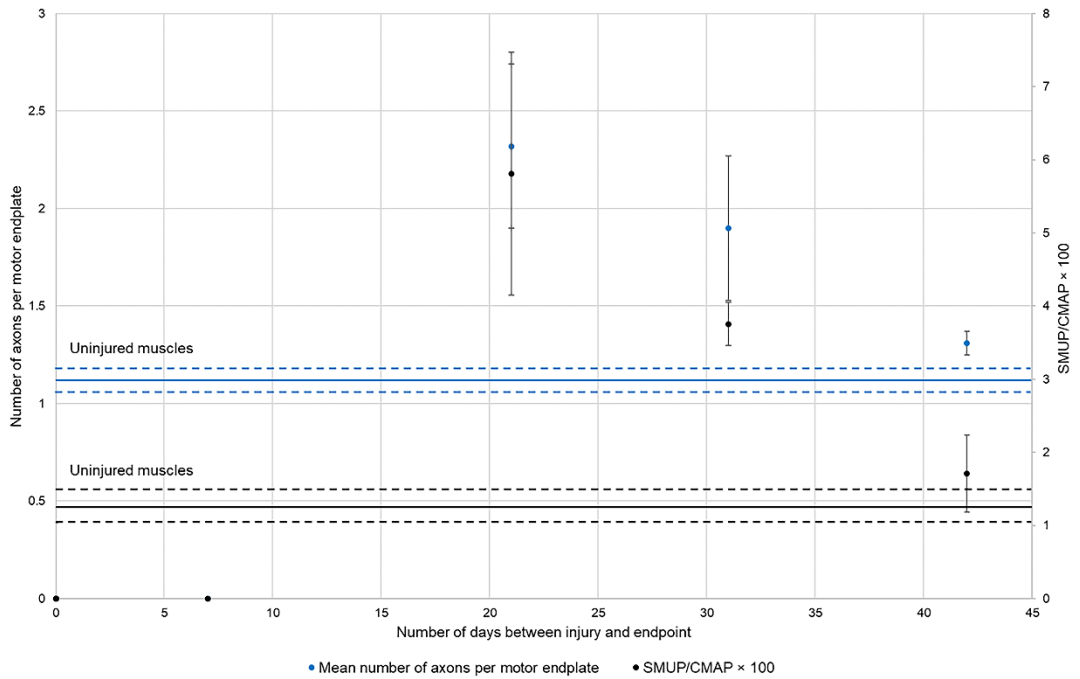
SMUAP/NMJ innervation ratio

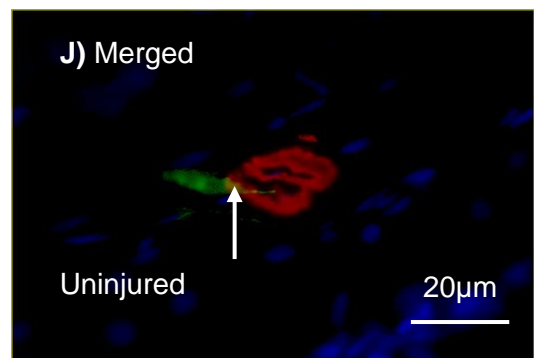
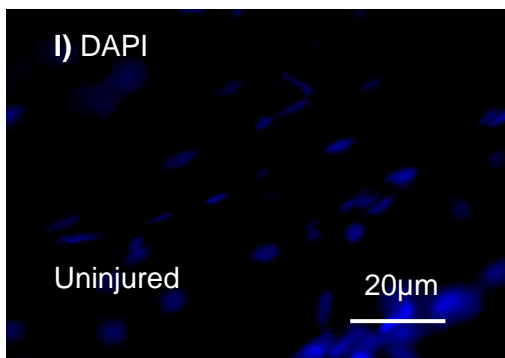
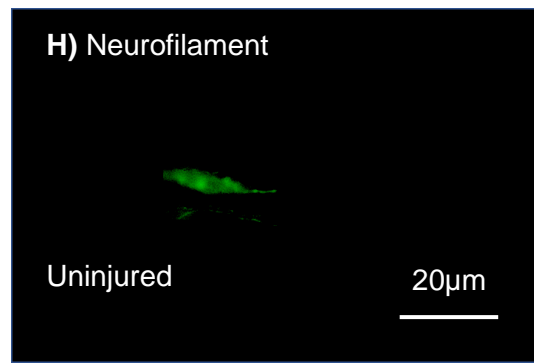
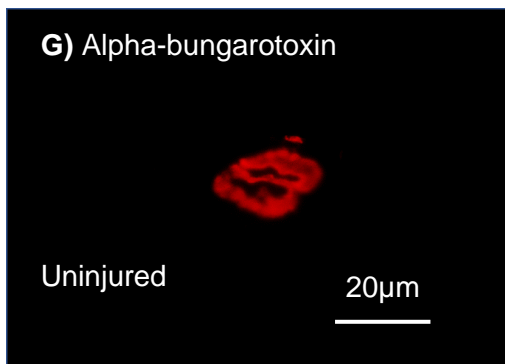
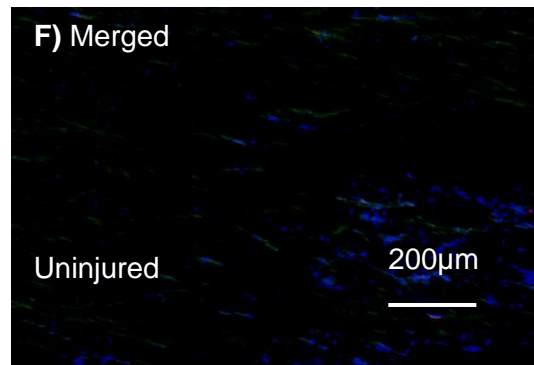
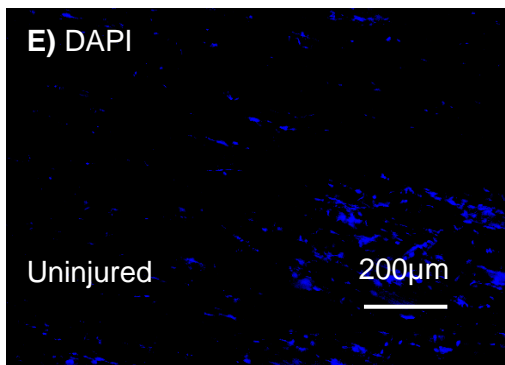
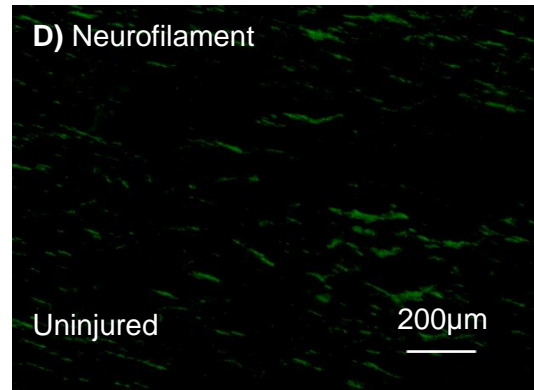
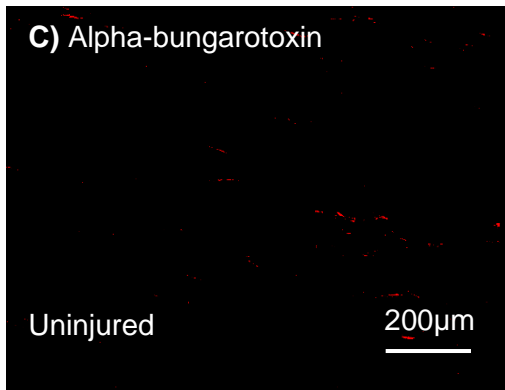
The mean number of axons in uninjured tibialis anterior was approximately one per motor endplate (**Figure 6.3B - J**). All NMJs were denervated one week following injury (**Figure 6.3B, K - R**). Twenty-one days following injury, there were approximately two motor axons per motor endplate (**Figure 6.3B, S - Z**). This corresponded with SMUAP recordings that were around five times larger than those recorded from uninjured muscles (**Figure 6.3B**). The number of axons per motor endplate and magnitude of SMUAPs then started to regress back towards uninjured levels (**Figure 6.3B**). By 42 days following injury, there were in the region of 1.3 motor fibres detected per motor endplate and the magnitude of SMUAPs recovered to less than twice the size of those elicited from uninjured muscles (**Figure 6.3B**).

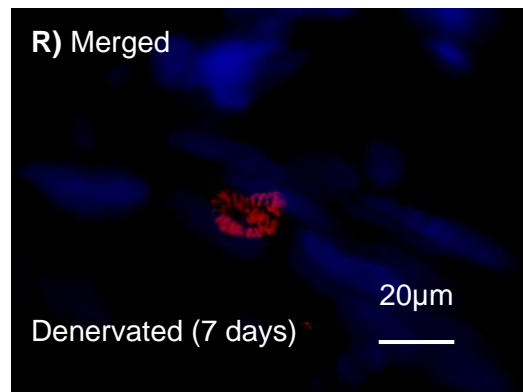
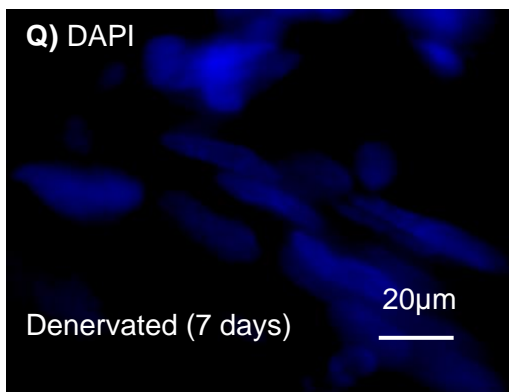
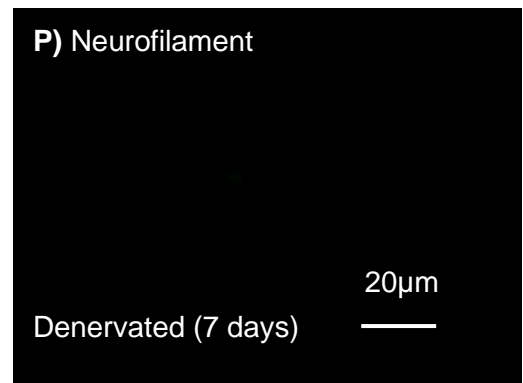
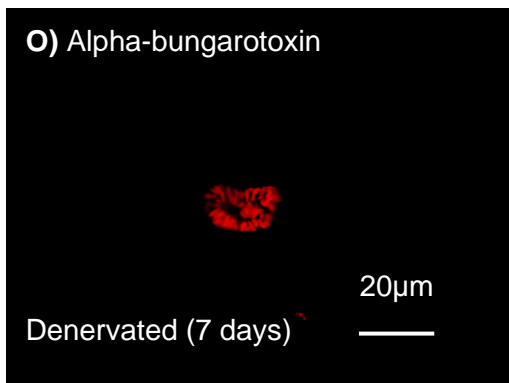
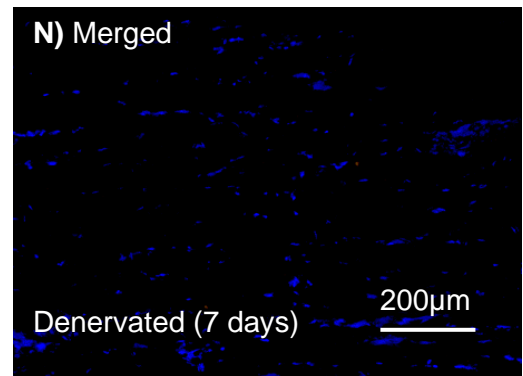
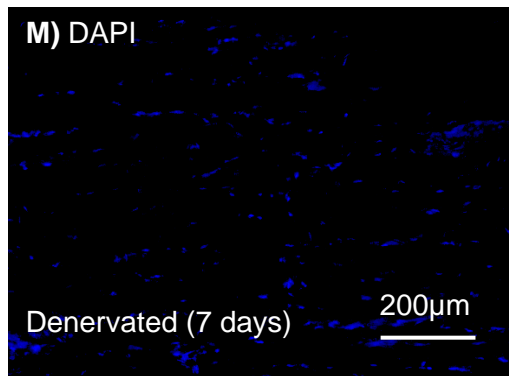
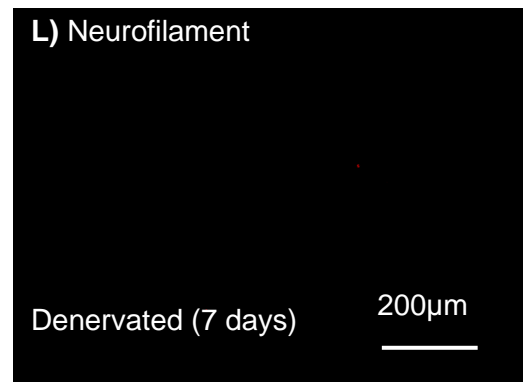
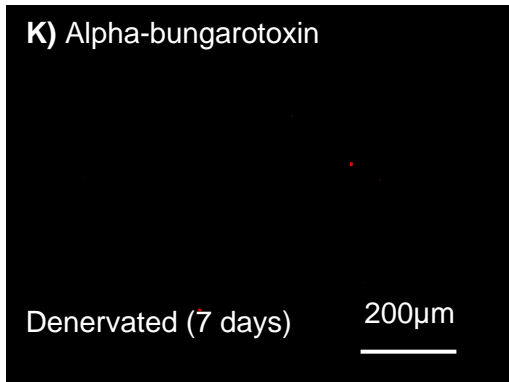
A)



B)







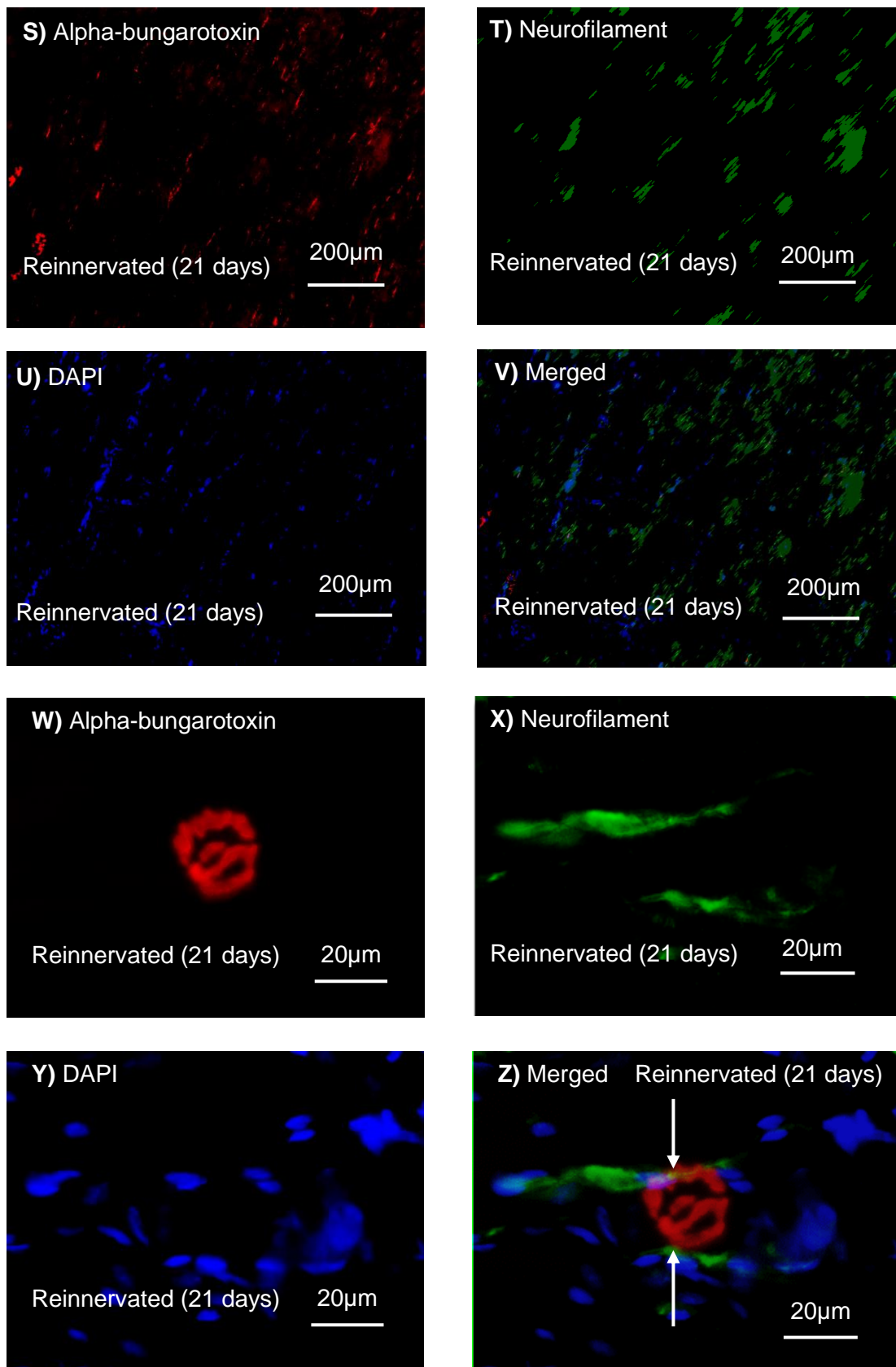


Figure 6.3 - Relationship between MUNE and NMJ reinnervation of the tibialis anterior muscle following sciatic nerve crush. **A)** Quantification of the recovery of

CMAP as a proportion of the pre-injury value and the proportion of reinnervated NMJs detected in the injured muscle. Seven days post-injury no CMAP was recordable and all NMJs were denervated (n=3). Twenty one days following injury CMAP and NMJ reinnervation recovered to 30.2% \pm 8.3 (n=5) and 21% \pm 4 (n=5) respectively. Thirty one days following injury CMAP and NMJ reinnervation recovered to 34% \pm 5.5 (n=5) and 27% \pm 12 (n=5) respectively. By 42 days post-injury, CMAP and NMJ reinnervation increased to 62.9% \pm 21 (n=5) and 72% \pm 14 (n=5) respectively. There was a moderate correlation between CMAP recovery and NMJ reinnervation ($R^2=0.63$, $p<0.001$) **B)** Quantification of the number of axons per motor endplate and the magnitude of SMUAPs recorded. Analysis of uninjured, contralateral muscles revealed a mean number of 1.12 \pm 0.06 (n=5) motor axons per motor endplate and SMUAP magnitude was 1.25% \pm 0.21 (n=5) of the CMAP value. Seven days following injury there were no innervated NMJs and no recordable SMUAPs (n=3). Twenty one days post-injury, there were a mean number of 2.32 \pm 0.42 (n=5) motor axons per motor endplate and the mean SMUAP magnitude was 5.8% \pm 1.7 (n=5) of the pre-crush CMAP value. Thirty one days following injury, the mean number of motor axons per motor endplate was 1.9 \pm 0.37 (n=5) and the mean SMUAP magnitude was 3.75% (\pm 0.3) of the pre-crush CMAP value. By 42 days post-injury, the mean number of motor axons per motor endplate was 1.31 \pm 0.06 (n=5) and the mean SMUAP magnitude was 1.71% \pm 0.5 (n=5) of the pre-crush CMAP value. **C) – F)** Low power images of uninjured tibialis anterior muscle **G) – J)** High power images of uninjured tibialis anterior muscle. The white arrow indicates an innervated NMJ. **K) – N)** Low power images of denervated muscle (7 days following injury). **O) – R)** High power images of denervated tibialis anterior muscle (7 days following injury). **S) – V)** Low power images of reinnervated tibialis anterior muscle (31 days following injury). **W) – Z)** High power images of reinnervated tibialis anterior muscles. The white arrows indicate a reinnervated NMJ.

MUNE and SSI

MUNE could not be recorded seven days following injury. When comparing MUNE recordings from the tibialis anterior muscles following injury with MUNE recorded from the tibialis anterior before injury, it was found that MUNE recovered steadily between seven and 31 days following injury; increasing at a mean rate of around 10% per day (**Figure 6.4**). Beyond this time period, MUNE rapidly recovered to around 80% of pre-

injury levels (**Figure 6.4**). The recovery of SSI followed a similar pattern of change following sciatic nerve crush; 1 day following injury, SSI declined to its lowest level at around -100. This recovered at a steady rate in the first 12 days following injury. Between 12 and 25 days, there was a faster rate of SSI recovery before reaching levels similar to that recorded from uninjured paws beyond 25 days.

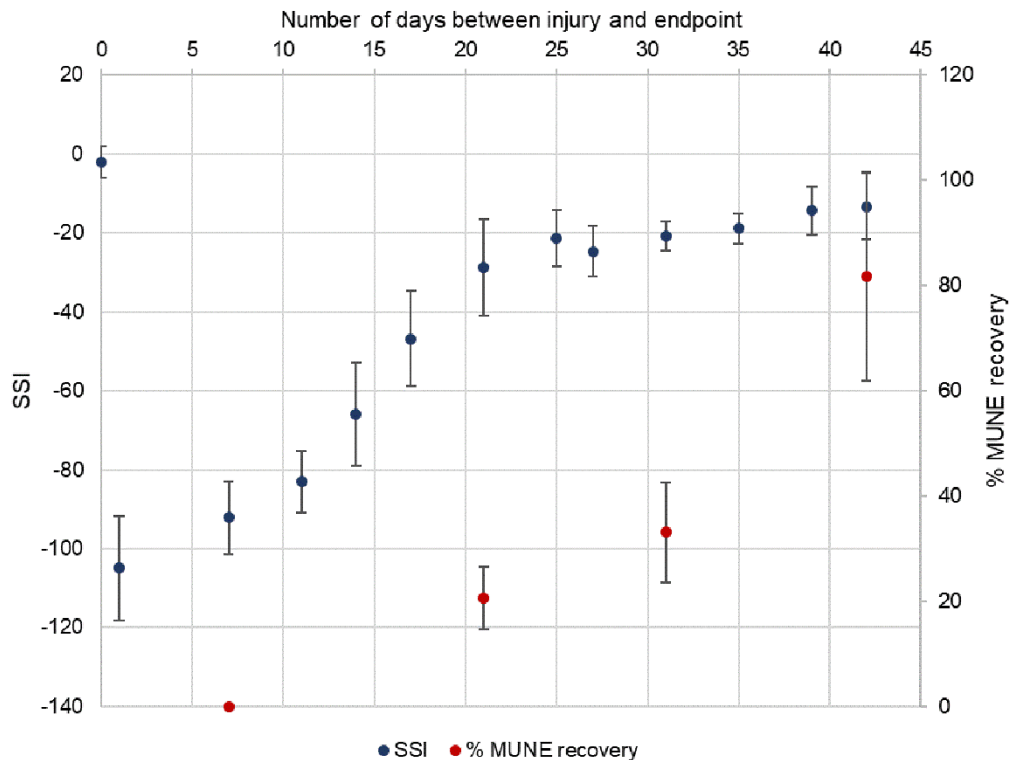


Figure 6.4 - Relationship between MUNE, SSI and time following injury. The recovery of MUNE is expressed as a percentage of the value obtained before the crush injury to the sciatic nerve. Data are means \pm 1 SD. The mean percentage MUNE recovery seven, 21, 31 and 42 days post-injury was 0% (n=3), 20.6% \pm 6 (n=5), 33.2% \pm 9.5 (n=5) and 81.8% \pm 19.82 (n=5) respectively. There was no statistically significant difference between the percentage MUNE recovery at 21 and 31 days post-injury. However, percentage MUNE recovery was significantly higher at 42 days compared to 31 days post-injury as well as at 42 days compared to 21 days ($p < 0.001$, one way ANOVA with Bonferroni correction).

6.3 Discussion

Chapter 5 demonstrated that MUNE is responsive to the temporal process of muscle reinnervation in humans. In order to further interrogate the validity of MUNE as an outcome measure of muscle reinnervation, this study aimed to measure the association between MUNE, histological markers of muscle reinnervation and the recovery of motor function following sciatic nerve crush in rats.

Valid outcome measures should demonstrate high intra-assay repeatability ($R^2 \geq 0.7$) in order to maximise the power of trials which hope to establish the efficacy of new therapies which hope to enhance peripheral nerve repair (Sedgwick, 2015, Mohtadi, 2016). The reproducibility of the MUNE protocol documented in **section 2.3.6** when comparing pre-crush to uninjured contralateral MUNE values was 0.81 (0.64-0.99) for the tibialis anterior muscles and 0.69 (0.42-0.84) for the gastrocnemius muscles; similar to the levels of reproducibility reported by other studies which have investigated the reproducibility of a diverse range of MUNE techniques (Mintz et al., 2016, Arnold et al., 2015, Kasselmann et al., 2009, Barghi and Gladden, 2013). The MUNE values obtained from uninjured tibialis anterior and gastrocnemius muscles are also comparable to other studies (Mintz et al., 2016, Arnold et al., 2015, Kasselmann et al., 2009, Barghi and Gladden, 2013). Together, this suggests that the MUNE protocol documented in this study is reproducible and valid.

Focusing on the relationship between MUNE in uninjured muscles and histological quantification of motor axons (ChAT staining) in healthy nerve samples, no significant difference was found between physiological (MUNE) and ChAT positive axons in uninjured tibialis anterior muscles. This suggests that MUNE accurately registered the number of motor axons innervating uninjured tibialis anterior muscles. However, MUNE in gastrocnemius muscles significantly under-estimated the number of MUs detected using histology. This observation may be attributable to differences in the

anatomy of the gastrocnemius and tibialis anterior muscles. The gastrocnemius is composed of an inner and an outer head supplied by independent nerve segments (Peker et al., 2013, Taborowska et al., 2016). The positioning of the rodent on the operating table made access to the medial aspect of the gastrocnemius muscle challenging meaning that the CMAP recording may only represent the lateral head of the gastrocnemius muscle. The fact that MUNE values obtained from the gastrocnemius muscle correspond with the number of ChAT positive axons found in the nerve segment to the lateral gastrocnemius muscle supports this suggestion. This challenge is not encountered when studying the tibialis anterior which has only one head and is supplied by the deep peroneal nerve (Peker et al., 2013). These findings concur with observations reported in other studies which assessed the link between MUNE and large myelinated fibres innervating uninjured hindpaw muscles (Shefner, 2001, Eisen et al., 1974). For this reason, the reinnervation of tibialis anterior rather than gastrocnemius was selected to measure the relationship between MUNE and anatomy in reinnervated muscle following sciatic nerve crush. Future studies that aim to use rodent models to learn more about anatomical correlates of MUNE, or use MUNE as an outcome measure, should also consider this finding when designing experiments.

With regards to the association between MUNE in reinnervated muscles and ChAT staining of regenerating nerve segments to the tibialis anterior, MUNE significantly underestimated the number of motor axons at 21 and 31 days post-crush. By 42 days there was no significant difference between MUNE and ChAT counts. This finding suggested that MUNE did not provide a direct assessment of motor axons re-establishing functional connections with denervated muscle fibres. These findings could potentially be explained by technical limitations associated with the MUNE technique such as alternation. However, the MUNE protocol employed in the present study was informed by studies which aimed to minimise the impacts of alternation

(DeForest et al., 2018, Kadrie et al., 1976). It is more likely that this differential between MUNE and ChAT in acutely reinnervated muscles is due to other factors. As a result, this study delved deeper into other factors that may influence MUNE recordings such as the biological process of motor endplate reinnervation.

Careful histological assessment of NMJ reinnervation is universally used as a surrogate of functional recovery following injury. It was found that CMAP demonstrated good correlation with the proportion of reinnervated motor endplates. This concurs with other studies which have shown that the recovery of CMAP is highly responsive to the reinnervation of motor endplates (Vannucci et al., 2019, English et al., 2013). Together, this suggests that CMAP provides a useful surrogate for measuring the proportion of reinnervated NMJs.

Focusing on the relationship of motor fibres with motor endplates, it was found that acutely reinnervated muscle (21 days following crush) demonstrated polyinnervated motor endplates (approximately two motor fibres per motor endplate). This regressed back towards a 1:1 relationship over subsequent time points. Polyinnervation of motor endplates is an important biological feature of reinnervated muscle that is thought to be an important contributor to impaired reinnervated muscular function (Pavlov et al., 2008, Bischoff et al., 2009, Seitz et al., 2011, Vannucci et al., 2019). By extension, it is important to uncover physiological correlates in order to identify measures that can monitor this process. This will accommodate trials of therapies which hope to enhance functional recovery of reinnervated muscle. The findings suggest that measurements of SMUAP magnitude may provide a marker through which this critical biological process can be monitored. Future human studies may be able to use this finding to relate biological changes with clinical assessments of muscular function. This will help future studies delineate the biological and clinical efficacy of therapies which hope to enhance human peripheral nerve repair. Understanding the relationship of MUNE

with functional assessments may be a key step towards the development of valid outcome measures (Rayner et al., 2019, Wilcox et al., 2020b). It was found that increased in MUNE corresponded with improvements in SSI measurement suggesting that MUNE is related to an index of motor function. Translation of this finding into humans would enable clinicians to identify cases where surgical intervention may offer clinical benefit. This would also represent an important step towards detecting a meaningful clinical response in clinical trials that aim to determine the effectiveness of therapies that hope to improve peripheral nerve repair. Therefore, future studies should aim to interrogate the relationship of MUNE with objective and subjective measures of muscular function.

This study has a number of limitations. For reasons already discussed in **section 6.1**, it was not possible to perform the same MUNE method used to acquire the data presented in **Chapter 5** in the controlled animal model of nerve injury used here. Future studies should identify practical methods which allow valid MUNE recordings to be obtained in proximal as well as distal muscles in both humans and animals. This will help researchers to use consistent methods to yield MUNE and help to reduce inter-investigator variability. The nerve segments to tibialis anterior and/or gastrocnemius were excised for histology proximally to where they divided into their terminal branches. This means that the ChAT counts provided for reinnervated muscles may represent an overestimation of the total number of MUs innervating the muscle. Future studies may be able to overcome this limitation using retrograde labelling techniques and counting the number of positively stained motor axons in the spinal cord.

In summary, this study has delineated the link between MUNE and different aspects of the biological process of muscle reinnervation. The recovery of CMAP demonstrated responsiveness with reinnervation of NMJs whilst changes in SMUAP

magnitude corresponded with changes in the polyinnervation of motor endplates. These findings suggest that MUNE is a useful metric for monitoring these biological processes which are known to be critical for the restoration of muscular function. Future studies should determine whether MUNE can be used as a way to quantify changes in a meaningful clinical response in clinical trials of therapies which hope to enhance muscle reinnervation.

Chapter 7: MRI biomarker assessment of reinnervated elbow flexor muscles following nerve transfer

7.1 Introduction

Neurophysiological changes associated with muscle reinnervation (**Chapter 5** and **Chapter 6**) are accompanied by volumetric and signal changes evident on MRI scans of reinnervated muscles (Koltzenburg and Bendszus, 2004, Viddeleer et al., 2016, Simon et al., 2016b). However, studies that have investigated the responsiveness of these parameters within a surgical scenario of muscle reinnervation are not well established. Addressing this issue will be an important step towards developing valid outcome measures of muscle reinnervation (Rayner et al., 2019, Wilcox et al., 2020b).

Conventional assessments of reinnervated muscle often measure morphological features of MUAPs and/or spontaneous activity recorded using intramuscular EMG (Smith and Knight, 2011). Changes in these parameters are difficult to quantify and frequently lack responsiveness to the biological process of muscle reinnervation (Koltzenburg and Bendszus, 2004, Smith and Knight, 2011, Wessig et al., 2004). Developing improved outcome measures is important to track change in clinical trials and to identify cases where surgical intervention may offer clinical benefit. However, this is challenging in the context of human muscle reinnervation. The rate of human nerve regeneration is slow, around 1mm/day (Sunderland, 1947), therefore small incremental changes over time may be masked by environmental factors and/or measurement variation. Furthermore, the intricate anatomy and diverse range of injuries make PNI a heterogeneous pathology to study. As a result, there is a need to identify a surgical scenario of human muscle reinnervation in which human nerve regeneration can be monitored.

In rodent models of nerve repair, changes in muscle wet weight associated with denervation and reinnervation have been used to predict functional recovery (Wu et

al., 2014). Additionally, this parameter demonstrates responsiveness to the biological process of nerve regeneration and correlates with functional evaluations (Wu et al., 2014). As a result, muscle wet weight is often utilised as an outcome measure by researchers to establish the efficacy of therapies that hope to improve muscle reinnervation (Wood et al., 2011b, Rayner et al., 2019). Unfortunately, measurement of muscle wet weight in humans is not feasible. However, the advent of quantitative Magnetic Resonance Imaging (qMRI) techniques has enabled researchers to non-invasively identify biomarkers to quantify and monitor biological processes associated with neuromuscular pathologies such as Charcot Marie Tooth (CMT) disease (Rossor et al., 2020, Jenkins et al., 2018, Morrow et al., 2016, Müller et al., 2020). Many of these processes have demonstrated correlation with changes in muscle volume and signal intensities observed using qMRI methods (Rossor et al., 2020, Jenkins et al., 2018, Morrow et al., 2016, Müller et al., 2020). Corresponding studies in a human paradigm of muscle reinnervation are not as well established. A handful have shown that fluid sensitive qMRI sequences are responsive to the biological process of muscle reinnervation (Volk et al., 2014, Viddeleer et al., 2012). However, these studies were conducted in non-standardised surgical scenarios involving patients with traumatic transections of the median or ulnar nerve and facial muscle paralysis. Additionally, they did not investigate other qMRI markers such as volumetric changes and signal changes on T1-w, PDW and T2-w MRI sequences which have shown responsiveness to the biological process of muscle denervation (Rossor et al., 2020, Jenkins et al., 2018, Morrow et al., 2016, Müller et al., 2020). Addressing this issue would represent an important step towards identifying valid outcome measures of muscle reinnervation.

Therefore, using the same surgical scenario of elbow flexor muscles reinnervated by nerve transfer employed in **Chapter 5** and described in **section 2.2.1** the responsiveness of qMRI biomarker assessment using conventional MRI sequences

(T1-w, PDW and T2-w images) was investigated at pre- and post-operative time points.

7.2 Results

Clinical features

Twenty-five patients, 23 males and two females, were included in this study with a median age of 34.5 years (ranging from 23 to 66 years). There were ten right-sided and 15 left-sided brachial plexus injuries; 14 and 11 of which were on the dominant and non-dominant side respectively. Twenty-one of the injuries were due to motorbike accidents, two were following bicycle accidents, one following a car accident and one due to a skiing accident. Intra-operatively, 22 patients were found to have C5/6 avulsion, one had a C5-8 avulsion, one had a C5-7 avulsion and one had axonotmesis of biceps branch of musculocutaneous nerve. Each patient attended for a mean number of 2 MRI scans (± 0.66). Six healthy male volunteers with a median age of 34.5 (ranging from 24 to 52) underwent MRI scans of their elbow flexor muscles on their dominant (four were right-handed and two were left-handed) side for comparison to nerve injured arms (**Table 7.1**).

Case Number	Age range (Gender)	Mechanism of injury	Intra-operative findings	Operation details	Number of days between injury and surgery	Number of days between surgery and MRI scan
1	30-39 (M)	Motorbike accident	C5-8 Avulsion	Right double Oberlin's, spinal accessory to suprascapular	15	28 and 213
2	30-39 (M)	Motorbike accident	C5/6 Avulsion	Right spinal accessory to suprascapular and right Oberlin's	173	45 and 239
3	20-29 (M)	Motorbike v tree	Axonotmesis of biceps branch of musculocutaneous nerve	Left Oberlin's	121	292 and 485
4	20-29 (M)	Motorbike v car	C5/6 Avulsion	Left spinal accessory to suprascapular and double Oberlin's	30	70 days pre-operatively, 47 and 136 days post-operatively
5	20-29 (M)	Motorbike v Car	C5/6 Avulsion	Left spinal accessory to suprascapular and Oberlin's	76	338 and 513
6	50-59 (M)	Motorbike accident	C5/6 Avulsion	Left Oberlin's	323	35, 87 and 580
7	40-49 (M)	Bicycle v Car	C5/6 Avulsion	Right double Oberlin's and Somsak's	44	539
8	50-59 (F)	Motorbike accident	C5/6 Avulsion	Left Oberlin's	242	193, 336 and 533
9	30-39 (F)	Car v Lorry	C5/6 Avulsion	Right Oberlin's	45	1419
10	20-29 (M)	Motorbike accident	C5/6 Avulsion	Right Oberlin's	92	1626
11	20-29 (M)	Bicycle v Bus	C5/6 Avulsion	Right Oberlin's and Somsak's	433	1371
12	20-29 (M)	Motorbike v car	C5/6 Avulsion	Right Oberlin's and suprascapular to spinal accessory	97	1145
13	30-39 (M)	Motorbike accident	C5/6 Avulsion	Right Oberlin's	168	58 and 226
14	30-39 (M)	Motorbike v Lamppost	C5/6 Avulsion	Left Oberlin's	356	41 and 267

Case Number	Age range (Gender)	Mechanism of injury	Intra-operative findings	Operation details	Number of days between injury and surgery	Number of days between surgery and MRI scan
15	30-39 (M)	Motorbike v car	C5/6 Avulsion	Left Oberlin's	143	86 days pre-operatively and 162 days post-operatively
16	40-49 (M)	Motorbike accident	C5/6 Avulsion	Left spinal accessory to suprascapular, Oberlin's and Somsak's	278	114 and 196
17	20-29 (M)	Motorbike accident	C5/6 Avulsion	Left spinal accessory nerve to suprascapular and Oberlin's	107	64 and 248
18	60-69 (M)	Skiing accident	C5/6 Avulsion	Left Oberlin's	141	223 and 388

Table 7.1 - Demographic of patients included in Chapter 7: MRI biomarker assessment of reinnervated elbow flexor muscles following nerve transfer.

Scan-rescan, inter- and intra-investigator reproducibility of the MRI segmentation protocol

The imaging protocol demonstrated high scan-rescan reproducibility when quantifying signal intensity on T1-w (ICC=0.96 (0.62 - 1.00)) images. This reproducibility was less consistent for PDW (ICC=0.91 (0.18 - 0.99)) and T2-w (ICC=0.88 (0.13 - 1.00)) images. Similar results were obtained for volumetric measurements obtained from T1-w (ICC=0.95 (0.50 - 0.93)), PDW (ICC=0.97 (0.72 - 1.00)) and T2-w (ICC=0.94 (0.17 - 1.00)) images (**Table 7.2**).

With regards to the inter-investigator reproducibility agreement of the segmentation protocol, high reproducibility was found for signal intensity quantification of T1-w (ICC=0.92 (0.80 - 0.97)), PDW (ICC=0.96 (0.90 - 0.99)) and T2-w (ICC=0.96 (0.87 - 0.98)) images. Volumetric assessments demonstrated similar reproducibility across

T1-w (ICC=0.98 (0.98 -1.00)), PDW (ICC=0.86 (0.63 - 0.95)) and T2-w (ICC=0.98 (0.95 - 0.99)) images (**Table 7.2**).

Finally, analysis of the intra-investigator reproducibility of the segmentation protocol revealed high reproducibility across T1-w (ICC=0.99 (0.97 - 1.00)), PDW (ICC=0.92 (0.78 - 0.97)) and T2-w (ICC=0.79 (0.49 - 0.93)) images. Volumetric measurements yielded similar reproducibility across T1-w (ICC=0.99 (0.98 - 1.00)), PDW (ICC=0.98 (0.95 - 0.99)) and T2-w (ICC=0.99 (0.98 - 1.00)) images (**Table 7.2**).

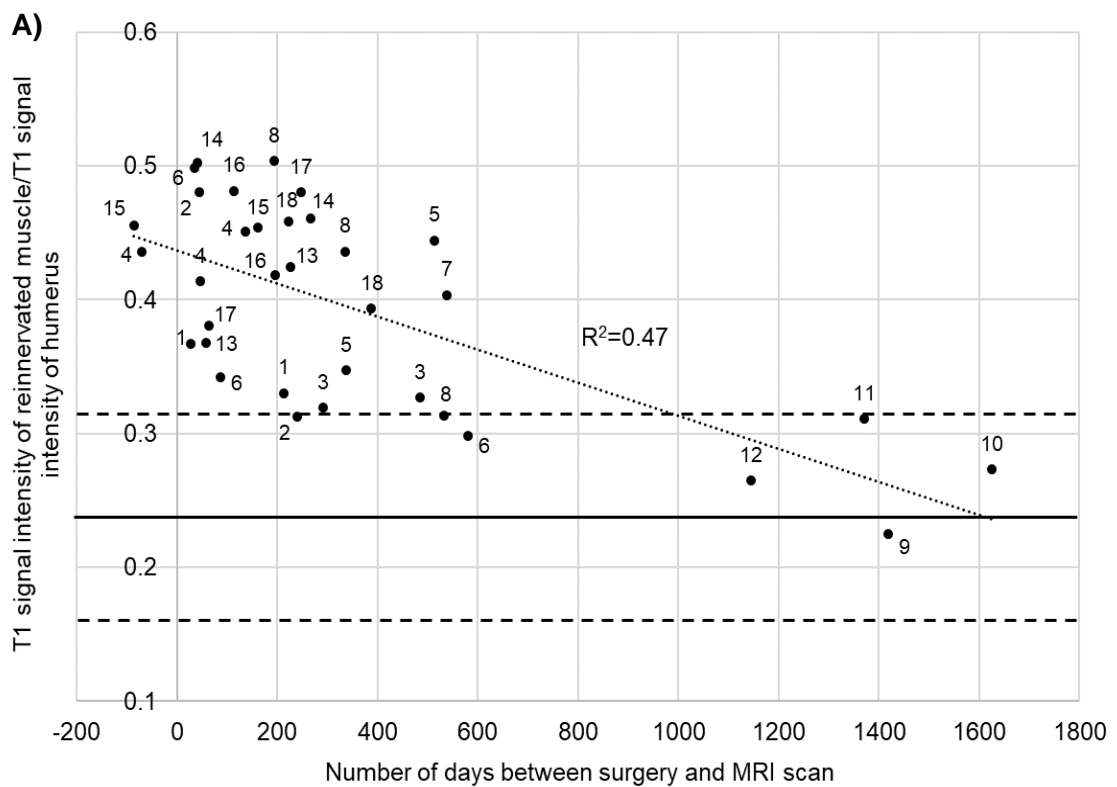
Since volumetric measurements ascertained from T1-w scans yielded the highest overall scan-rescan, inter- and intra-investigator reproducibility, T1-w images were used to quantify elbow flexor muscle volume (**Table 7.2**).

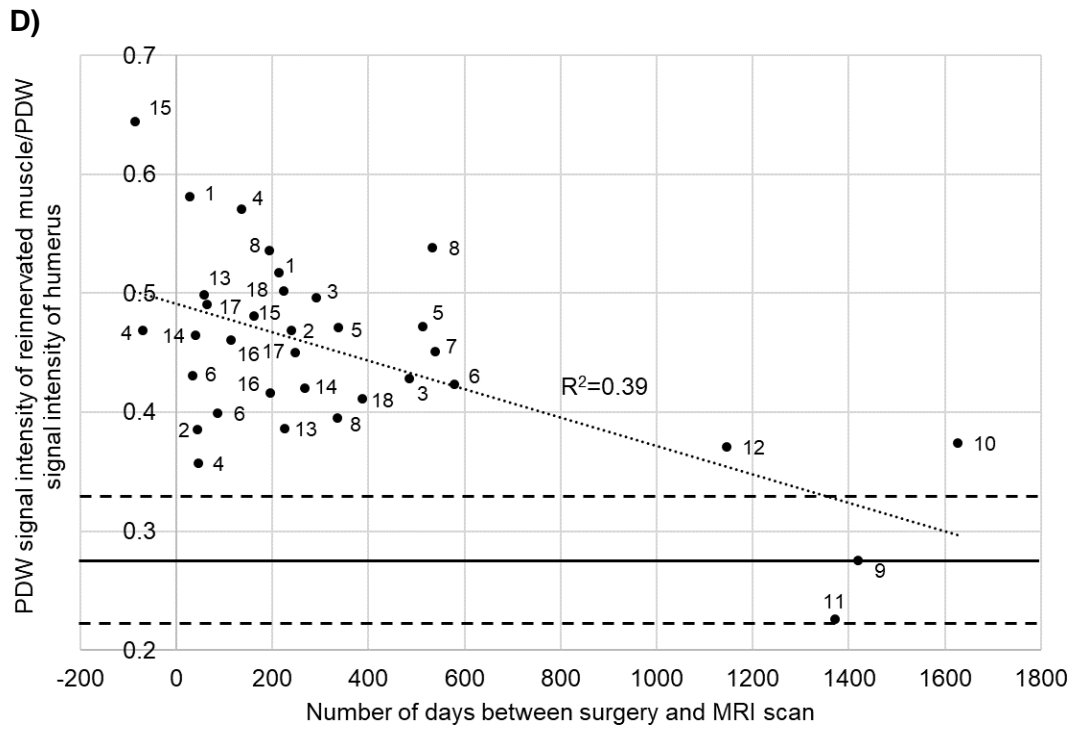
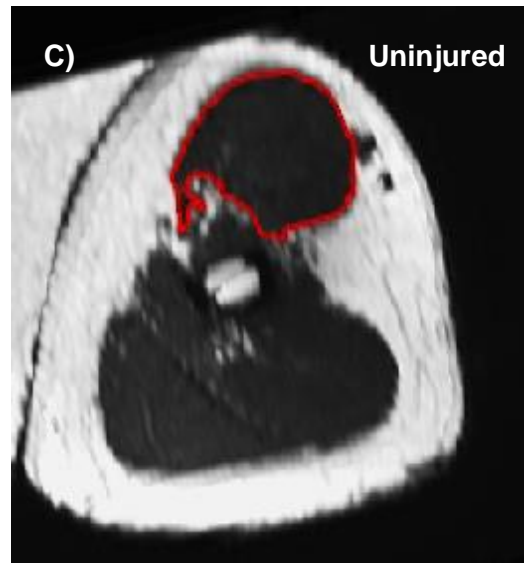
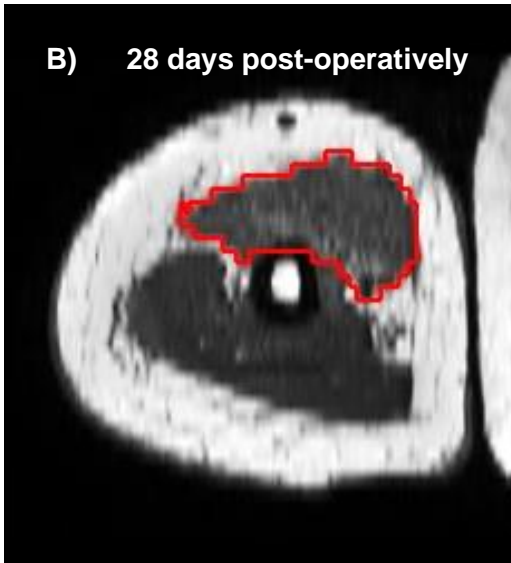
Quantitative MRI parameter	Scan-rescan reproducibility	Inter-investigator reproducibility	Intra-investigator reproducibility
T1-w signal	0.96 (0.62 - 1.00)	0.92 (0.80 - 0.97)	0.99 (0.97 - 1.00)
PDW signal	0.91 (0.18 - 0.99)	0.96 (0.90 - 0.99)	0.92 (0.78 - 0.97)
T2-w signal	0.88 (0.13 - 1.00)	0.96 (0.87 - 0.98)	0.79 (0.49 - 0.93)
T1-w volume	0.95 (0.50 - 0.93)	0.98 (0.98 - 1.00)	0.99 (0.98 - 1.00)
PDW volume	0.97 (0.72 - 1.00)	0.86 (0.63 - 0.95)	0.98 (0.95 - 0.99)
T2-w volume	0.94 (0.17 - 1.00)	0.98 (0.95 - 0.99)	0.99 (0.98 - 1.00)

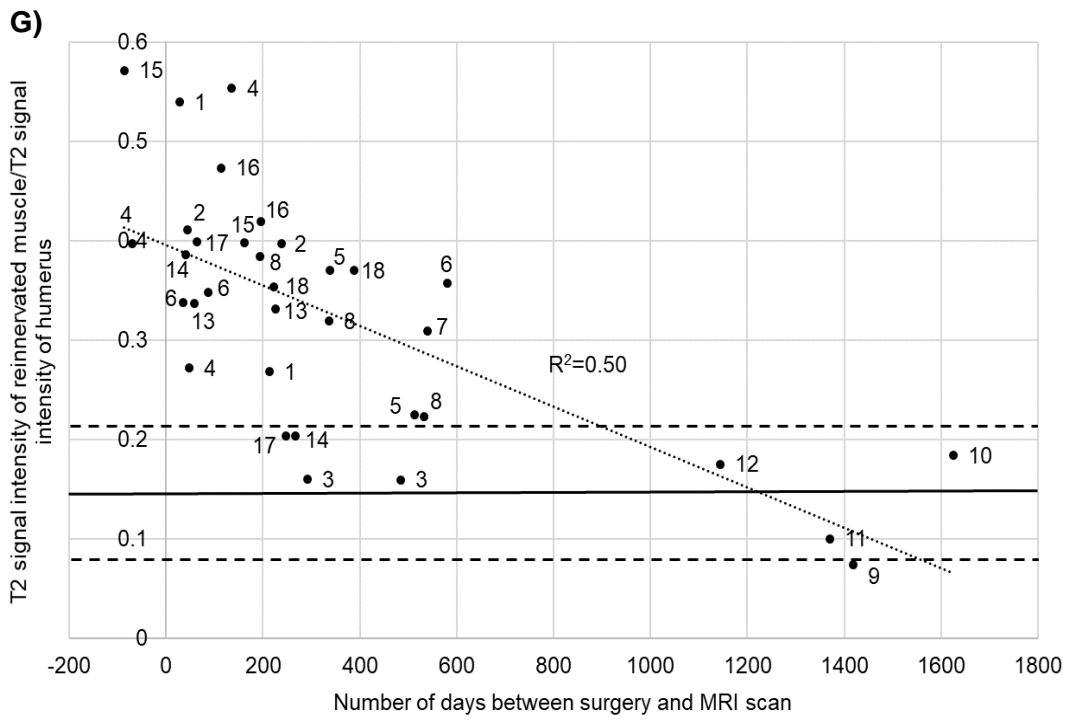
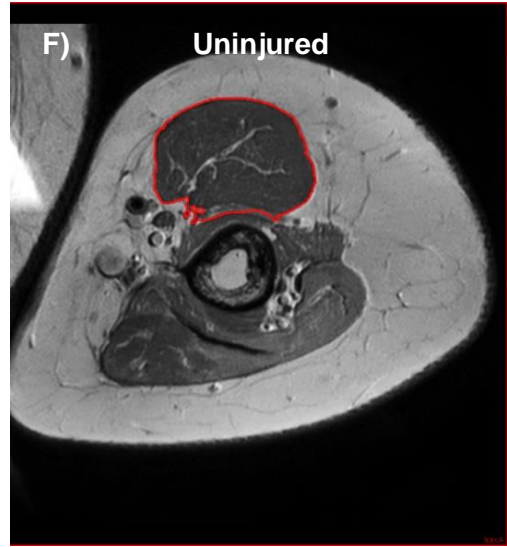
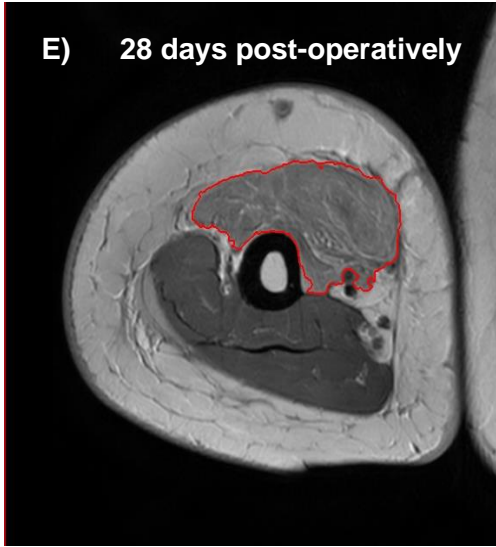
Table 7.2 - Scan-rescan, inter- and intra-investigator reproducibility of the imaging and segmentation protocol. Scan-rescan was performed on the dominant arm of three healthy volunteers and the injured arm from case number 6 (**Table 7.1**). Inter- and intra-investigator reproducibility was determined from the first 15 MRI scans saved to the research database (case numbers 1-12 (**Table 7.1**) and the dominant arm of three healthy volunteers). Values represent the ICC value with a 95% confidence interval in brackets.

Quantitative analysis of T1-w, PDW and T2-w signal changes

The mean ratio of T1-w signal intensity of uninjured elbow flexor muscles to signal intensity of the humerus was 0.24 (\pm 0.08). Overall, there was a weak to moderate negative linear correlation between changes in the ratio of T1-w signal intensities with pre- and post-operative time points ($R^2=0.47$, $p<0.001$) (**Figure 7.1A**). T1-w signal intensity of elbow flexor muscles in the first 200 days was around two-fold higher than uninjured elbow flexor muscles (**Figure 7.1A-C**). Approximately 3-years post-operatively, the T1-w signal intensity of reinnervated elbow flexor muscles normalised towards levels similar to that of uninjured muscles (**Figure 7.1A-C**).







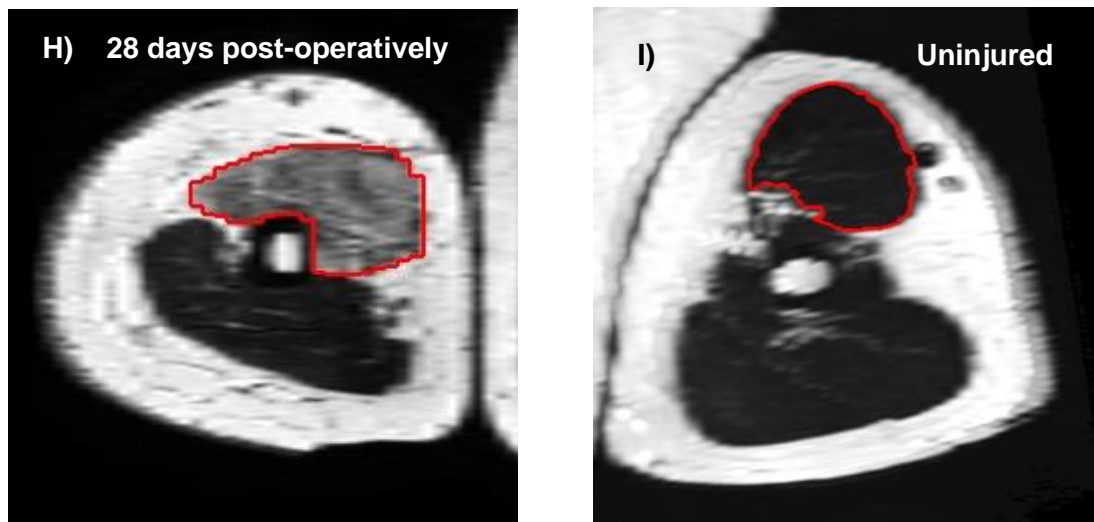


Figure 7.1 - T1-w, T2-w and PDW signal changes within denervated and reinnervated elbow flexor muscles. In **A**), **D**) and **G**) the solid black line represents the mean signal intensity of uninjured elbow flexor muscles (n=6) and the dashed black lines represent \pm one standard deviation from the mean. The dotted black linear regression lines were calculated using Spearman's rank correlation coefficient. Case numbers are attached to each data point for reference to **Table 7.1**. In **B**), **C**), **E**), **F**), **H**) and **I**), the red line envelops the elbow flexor muscles. **A**) Quantification of T1-w signal change at pre- and post-nerve transfer time points. **B**) T1-w image of biceps-brachialis muscle 28 days following nerve transfer (case number 1). **C**) T1-w image of uninjured biceps-brachialis muscle (dominant side). **D**) Quantification of PDW signal change at pre- and post-nerve transfer time points. **E**) PDW image of biceps-brachialis muscle 28 days following nerve transfer (case number 1). **F**) PDW image of uninjured biceps-brachialis muscle (dominant side). **G**) Quantification of T2-w signal change at pre- and post-nerve transfer time points. **H**) T2-w image of biceps-brachialis muscle 28 days following nerve transfer (case number 1). **I**) T2-w image of uninjured biceps-brachialis muscle (dominant side).

The mean ratio of PDW signal intensity of uninjured elbow flexor muscles to PDW signal intensity of the humerus was $0.28 (\pm 0.05)$ (**Figure 7.1D**). Changes in the ratio of PDW signal intensities yielded a weak to moderate negative linear correlation with pre- and post-operative time points ($R^2=0.39$, $p<0.001$) (**Figure 7.1D**). In the first 200 days post-operatively, reinnervated elbow flexor muscles demonstrated a ratio of PDW signal intensity that was around two-fold higher than uninjured muscles (**Figure**

7.1D, E). The ratio of signal intensities returned towards uninjured levels by approximately 3 years post-operatively (**Figure 7.1D-F**).

The mean ratio of T2-w signal intensity of uninjured elbow flexor muscles to T2-w signal intensity of the humerus was 0.14 (± 0.07) (**Figure 7.1G**). Changes in the ratio of T2-w signal intensity demonstrated a moderate negative linear correlation with pre- and post-operative time points ($R^2=0.50$, $p<0.001$) (**Figure 7.1G**). In the first 200 days post-operatively, T2-w signal intensity of reinnervated elbow flexor muscles was approximately two-fold higher compared to uninjured muscles (**Figure 7.1G-I**). In some cases (case numbers 17, 14 and 3), the ratio of T2-w signal intensities of reinnervated muscles were found to be similar to that of uninjured muscles within one-year post-operatively (**Figure 7.1G**). After around 3-years following nerve transfer, the ratio of T2-w signal intensities returned towards to similar levels as that of uninjured muscles (**Figure 7.1G-I**).

Volumetric analysis

The mean muscle volume per unit BMI of uninjured elbow flexor muscles was 10.76ml per unit BMI (± 1.42) (**Figure 7.2A, B**). The volume per unit BMI of elbow flexor muscles demonstrated a strong positive linear correlation with pre- and post-operative time points ($R^2=0.73$, $p<0.001$) (**Figure 7.2A**).

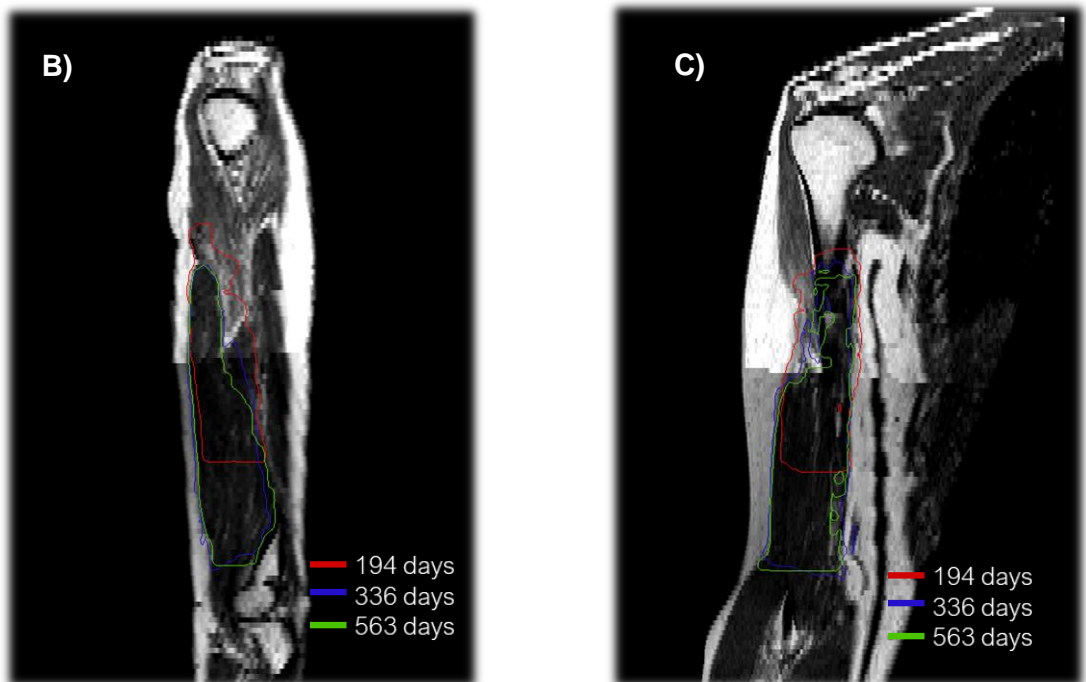
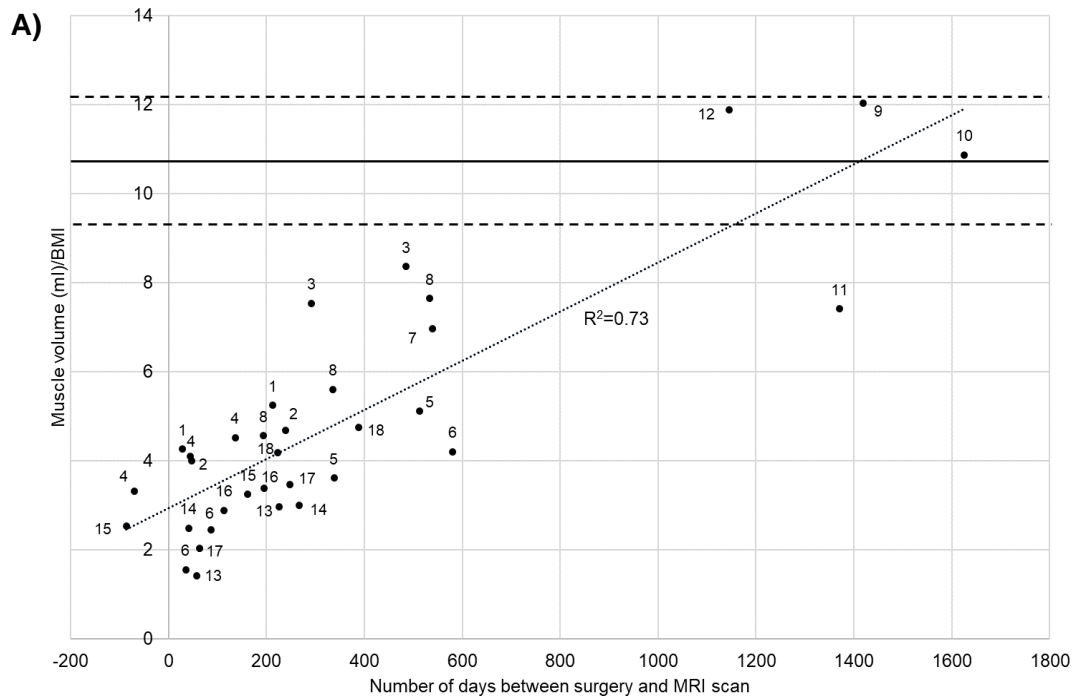


Figure 7.2 - Changes in elbow flexor muscle volume pre- and post-nerve transfer. **A)** Quantification of elbow flexor muscle volume at pre- and post-nerve transfer time points. The solid black line represents the mean uninjured elbow flexor muscle volume (n=6) and the dashed black lines represent \pm one standard deviation from the

mean. The dotted black linear regression line was calculated using Spearman's rank correlation coefficient ($R^2=0.73$, $p<0.001$). Case numbers are attached to each data point for reference to **Table 7.1. B)** and **C)** Represent deformable registration of elbow flexor muscle segmentations from case number 8 at 194, 336 and 563 days post-operatively (**Table 7.1. B)** Sagittal plane. **C)** Coronal plane.

7.3 Discussion

Studies that have investigated the validity of qMRI parameters as outcome measures of neuromuscular diseases have provided methods that are responsive to the biological process of muscle denervation. However, corresponding studies in a clinical scenario of muscle reinnervation are not well established. To address this issue, the present study investigated the responsiveness of qMRI biomarkers within a surgical scenario of muscle reinnervation.

Traumatic brachial plexus injuries represent a relatively rare pathology with surgical treatment based at national referral centres across the globe. This affords significant challenges to the recruitment of patient cohorts for clinical trials with sufficient statistical power to determine the efficacy of new therapies to improve peripheral nerve repair. Therefore, future studies are likely to involve multicentre trials which has the potential to introduce significant inter-investigator variance in outcome measurement. Developing assessments that demonstrate high inter- and intra-investigator reliability ($ICC \geq 0.7$) represents an important step towards addressing this challenge. The findings show that the segmentation protocol deployed in this study to measure elbow flexor muscle signal and volumetric changes demonstrated excellent inter- and intra- investigator reproducibility (Sedgwick, 2015). This concurs with other studies that have used qMRI techniques to quantify biological changes associated with neuromuscular pathologies such as CMT (Rossor et al., 2020, Jenkins et al., 2018, Morrow et al., 2016, Müller et al., 2020).

Quantitative analysis of signal changes on T1-w, PDW and T2-w images demonstrated only weak to moderate responsiveness to pre- and post-operative time points. However, there were some overall trends. Acutely (first 30 days post-operatively) and sub-acutely (30-100 days post-operatively) reinnervated muscles demonstrated higher T1-w and PDW signal intensities which were approximately double that of uninjured muscles. The signal intensity then regressed over time towards uninjured levels in the most chronically reinnervated muscles (>1000 days post-operatively). This suggests that acutely reinnervated muscles had higher fat content compared to uninjured muscles which regressed back towards uninjured muscles over time (Aagaard et al., 2003, Kamath et al., 2008, Wessig et al., 2004). This concurs with the findings from case studies and small case series which have shown that T1-w signal intensities increased in denervated thenar, hypothenar and facial muscles which returned back towards uninjured levels within six months following the onset of muscle reinnervation (West et al., 1994, Wessig et al., 2004). More recent qMRI techniques such as the 3-point Dixon method exploit the phase difference between water and fat to separate these two components (Morrow et al., 2016, Grimm et al., 2018). As such, they can give a quantitative measure of the signal fraction of both water and fat (Morrow et al., 2016, Grimm et al., 2018, Rossor et al., 2020). This approach has been used as a biomarker by investigators to sensitively measure intramuscular fat accumulation associated with a number of neuromuscular pathologies (Morrow et al., 2016). The findings presented here warrant future studies to investigate whether these techniques demonstrate validity in muscle reinnervation.

Analysis of changes in the intensity of elbow flexor muscle on T2-w images revealed a similar trend. T2-w signal intensity was increased in (first 30 days post-operatively) and sub-acutely (30-100 days post-operatively) to around three times that of uninjured muscles. In some cases, the T2-w signal of muscles regressed back towards uninjured levels as early as approximately 200-600 days post-operatively. This finding

concur with animal studies which have shown that fluid sensitive qMRI parameters regress back towards pre-injury levels faster than fat sensitive measures following sciatic nerve injury (Simon et al., 2016b, Bendszus et al., 2002, Koltzenburg and Bendszus, 2004, Kullmer et al., 1998). Together, this suggests that fat sensitive sequences may be a more sensitive measure of chronically reinnervated muscle compared to fluid sensitive sequences. The cellular and molecular mechanisms responsible for this difference remain largely unknown. Future studies should address this to better understand the relationship between the changes evident within these qMRI parameters and the biological process of muscle reinnervation.

Quantification of reinnervated elbow flexor muscle volume per unit BMI demonstrated the greater receptiveness to the biological process of muscle reinnervation compared to signal changes evident on T1-w, PDW, and T2-w sequences. Volumetric assessment may provide a more direct appraisal of functional reinnervation by MUs when compared to signal change measurements (Wu et al., 2014). Whilst signal changes are receptive to changes in fat and/or water content, their relationship with the biological process of muscle reinnervation remains unclear (Wu et al., 2014). Future studies should address the relationship between reinnervated muscle volume and clinical assessments of muscular function. This will be an important step towards detecting a meaningful clinical response in clinical trials that aim to establish the efficacy of new therapies to improve peripheral nerve repair.

The findings of this study must be interpreted in light of its limitations. Only four scan-rescans were performed to measure intra-assay reproducibility providing an explanation for some of the large confidence intervals. Obtaining additional scan-rescans was challenging due to the long acquisition time and limited scanning time available. Future studies should address this in order to better understand the intra-assay variation. This will be an important step towards undertaking multicentre clinical

trials. Future studies should also consider comparing signal intensity and volume against the contralateral uninjured arm of each patient which may provide improved standardisation for genetic and environmental factors that may lead to differences in muscle volume between individuals (O'Brien et al., 2009, Sanchis-Moysi et al., 2012, Vidt et al., 2012). This was not possible in the present study due to insufficient funding. Additionally, the effect of the time interval between injury and surgery was not considered. An incremental increase in time between injury and surgery leads to a tissue microenvironment that becomes increasingly antagonistic to axonal regeneration and muscle reinnervation as demonstrated by the findings presented in **Chapter 4** (Tung and Mackinnon, 2010, Wilcox et al., 2020c, Jessen and Mirsky, 2019). Phenotypic changes within the proximal and distal stump as well as the denervated muscle are thought to be at least partially responsible (Jessen and Mirsky, 2019, Wilcox et al., 2020c). Future studies should investigate this further to establish an optimum time window for surgical nerve repair in order to optimise functional outcomes. In addition, the data would have benefited from standardised MRI follow-up time points with a larger cohort of patients. This was challenging since this study was conducted at a national referral centre meaning patients often had to travel from far afield which may have antagonised follow-up. Additionally, brachial plexus injury is a relatively rare pathology (accounting for around 1% of all trauma cases (Midha, 1997)) which restricted the recruitment of a larger cohort of patients. There was also a shortage of data between approximately 600 and 1100 days post-operatively. In agreement with current guidelines, patients were evaluated for discharge from clinic around 2-years following nerve transfer affording challenges to the long term follow-up of these patients (Isaacs and Cochran, 2019). This is characteristic of studies involving trauma with follow-up rates reported to be as low as 2% (Hansen et al., 2014). Finally, only two female (8%) patients were included in this study. Based on animal models, females are thought to exhibit faster rates of axonal regeneration

since their repair Schwann cell phenotype is maintained for a longer time period compared to their male counterparts (Kovacic et al., 2004, Stenberg and Dahlin, 2014). Future studies should explore whether this difference is also present in humans and can translate into faster rates of muscle volume recovery.

In summary, this study has evaluated the responsiveness of qMRI biomarkers to track the recovery of muscle following nerve transfer. Volumetric assessments of reinnervated elbow flexor muscle demonstrated the greatest responsiveness to the biological process of muscle reinnervation. This suggests that volumetric MRI is a suitable candidate as an outcome measure of muscle reinnervation.

Chapter 8: Conclusions and future translation

8.1 Overall conclusions

This thesis has successfully contributed to translational research in PNI by providing new insights into some of the molecular features and signals which control human nerve regeneration and degeneration. In addition, important steps towards the development of valid outcome measures of muscle reinnervation have been made. Together, the findings have assisted the advancement of therapeutic options for peripheral nerve repair.

In **Chapter 3**, some of the challenges associated with the retrieval of human nerve samples from the surgical environment for study in the laboratory were successfully circumvented. This allowed **Chapter 4** to go beyond rodent models of nerve repair to provide important insights into cellular and molecular features that underpin human peripheral nerve regeneration. This data will inform the development of new therapies to improve nerve repair and provides valuable information which may help clinicians optimise the timing of surgical nerve repair.

Continuing with this theme of characterisation of human nerve injury, the remaining Chapters focused on developing approaches to enhance clinical translation of new therapies which hope to improve human peripheral nerve repair. **Chapter 5** identified a method to monitor changes in the number of elbow flexor MUs over time using STA MUNE. In order to better understand the validity of MUNE as an outcome measure of muscle reinnervation, the relationship of MUNE with histological and functional markers of muscle reinnervation in rats was explored in **Chapter 6**. Together, the findings suggest that MUNE is a method that demonstrates responsiveness to the biological process of muscle reinnervation and correlates with the recovery of motor function.

Finally, **Chapter 7** investigated volumetric and signal changes evident on MRI scans of reinnervated muscle that parallel neurophysiological parameters of reinnervation. It was found that changes in muscle volume per unit BMI were correlated with pre- and post-operative time. Future work will be focused on establishing whether MUNE and qMRI have the capacity to act as outcome measures that can detect a meaningful clinical response evoked by new therapies to improve peripheral nerve repair.

8.2 Ongoing and future work

8.2.1 Relating MUNE and qMRI assessments to clinical assessments of muscular function

Future work is being planned to explore the validity of other potential outcome measures of muscle reinnervation. qMRI technologies have enabled investigators to precisely measure the accumulation of intramuscular fat in denervated muscles. This measure has demonstrated validity as an outcome measure within neuromuscular pathologies (Morrow et al., 2016, Grimm et al., 2018, Gawel et al., 2015). Application of these qMRI protocols to reinnervated muscle may reveal improved methods to measure the recovery of muscular function.

Outcome measures of muscle reinnervation (such as MUNE and volumetric MRI) can show validity through correlation with clinical assessments of muscular function (Sedgwick, 2015). Addressing this issue would represent an important step towards detecting a meaningful clinical response in clinical trials of therapies which hope to enhance human peripheral nerve repair. However, clinical assessment of reinnervated muscular function is complex. Conventionally, the recovery of muscular function is often assessed through PVF measurements using the MRC grading system and/or HHD (Quick et al., 2016, Bhandari et al., 2009, Sturma et al., 2018, Wali et al., 2017). Studies by our research unit and others have shown that patient reported impairments of reinnervated muscle are not associated with the recovery of

PVF (Brown et al., 2018). An earlier onset of muscular fatigue, pathologic co-contraction, decreased proprioception and muscle pain have been identified by patients as central themes of muscle reinnervation (Brown et al., 2018, Chammas et al., 1997). This has stimulated our research unit and others to develop experimental protocols which can quantify muscular fatigue and co-contraction around the elbow joint (Wilcox et al., 2019a). These protocols were used to measure muscular fatigue, PVF and co-contraction in the patients presented in **Table 5.1** and **Table 7.1**. Ongoing research with our collaborators at the School of Biomedical Engineering & Imaging Sciences, Kings College London is comparing this data to the volumetric information presented in **Chapter 7** to develop mathematical models which may be able to predict functional recovery following nerve injury. Developing this area of work will help clinicians identify cases where surgical intervention may offer clinical benefit and inform the development of clinical trials.

8.2.2 Clinical trial

There is no drug routinely used to enhance peripheral nerve repair in humans. A major barrier to clinical translation of new therapies has been the absence of clinical outcome measures that are responsive to the biological process of muscle reinnervation. The work presented in this thesis has made some steps towards addressing this issue and will assist future studies in defining a minimal clinically important difference. This has benefited the development of a prospective clinical trial to determine the effectiveness of Ibuprofen in improving nerve regeneration with colleagues within the UCL Centre for Nerve Engineering.

8.2.3 PNI demographic audit

To inform the development of the clinical trial (**section 8.2.2**), a patient demographic audit of the patient database at the Peripheral Nerve Injury Unit, Royal National Orthopaedic Hospital has been undertaken. Ongoing analysis of this database has

been focused on better characterising the demographics of patients who suffer PNI. Additionally, clinical and neurophysiological records are being retrospectively analysed and compared to co-morbidities as well as regular drug prescriptions. This will help identify therapies which may offer clinical benefit in the treatment of PNI. Together, this work will inform the design of the drug trial in **section 8.2.2** and may identify new therapeutic agents to enhance nerve repair.

References

1917. Nerve Wounds Symptomatology of Peripheral Nerve Lesions caused by War Wounds. By J. TINEL, late Chef de Clinique at La Salpêtrière, with Preface by PROFESSOR DEJERINE, translated by FRED. ROTHWELL, revised and edited by CECIL A. JOLL. Pp. xii + 317, with 323 illustrations. London Baillière, Tindal & Cox. 15s. net. *BJS*, 5, 517-517.
1986. Classification of chronic pain. Descriptions of chronic pain syndromes and definitions of pain terms. Prepared by the International Association for the Study of Pain, Subcommittee on Taxonomy. *Pain Suppl*, 3, S1-226.
2004. RE: *Human Tissue Act*.
2016. RE: *WHO Surgical Site Infection Prevention Guidelines*.
- AAGAARD, B. D., LAZAR, D. A., LANKEROVICH, L., ANDRUS, K., HAYES, C. E., MARAVILLA, K. & KLIOT, M. 2003. High-resolution magnetic resonance imaging is a noninvasive method of observing injury and recovery in the peripheral nervous system. *Neurosurgery*, 53, 199-203; discussion 203-4.
- ABASOLO, N., TORRELL, H., ROIG, B., MOYANO, S., VILELLA, E. & MARTORELL, L. 2011. RT-qPCR study on post-mortem brain samples from patients with major psychiatric disorders: reference genes and specimen characteristics. *Journal of psychiatric research*, 45, 1411-1418.
- ABERG, M., LJUNGBERG, C., EDIN, E., JENMALM, P., MILLQVIST, H., NORDH, E. & WIBERG, M. 2007. Considerations in evaluating new treatment alternatives following peripheral nerve injuries: a prospective clinical study of methods used to investigate sensory, motor and functional recovery. *J Plast Reconstr Aesthet Surg*, 60, 103-13.
- ABRAHAM, A., IZENBERG, A., DODIG, D., BRIL, V. & BREINER, A. 2016. Peripheral Nerve Ultrasound Imaging Shows Enlargement of Peripheral Nerves Outside

- the Brachial Plexus in Neuralgic Amyotrophy. *J Clin Neurophysiol*, 33, e31-e33.
- ADAMS, L., CARLSON, B. M., HENDERSON, L. & GOLDMAN, D. 1995. Adaptation of nicotinic acetylcholine receptor, myogenin, and MRF4 gene expression to long-term muscle denervation. *J Cell Biol*, 131, 1341-9.
- ALBANI, M., LOWRIE, M. B. & VRBOVÁ, G. 1988a. Reorganization of motor units in reinnervated muscles of the rat. *J Neurol Sci*, 88, 195-206.
- ALBANI, M., LOWRIE, M. B. & VRBOVÁ, G. 1988b. Reorganization of motor units in reinnervated muscles of the rat. *Journal of the Neurological Sciences*, 88, 195-206.
- ALVAREZ-LINERA, J. 2008. 3T MRI: advances in brain imaging. *Eur J Radiol*, 67, 415-26.
- ALVAREZ, F. J., TITUS-MITCHELL, H. E., BULLINGER, K. L., KRASZPULSKI, M., NARDELLI, P. & COPE, T. C. 2011. Permanent central synaptic disconnection of proprioceptors after nerve injury and regeneration. I. Loss of VGLUT1/IA synapses on motoneurons. *J Neurophysiol*, 106, 2450-70.
- AMINI, P., ETTLIN, J., OPITZ, L., CLEMENTI, E., MALBON, A. & MARKKANEN, E. 2017. An optimised protocol for isolation of RNA from small sections of laser-capture microdissected FFPE tissue amenable for next-generation sequencing. *BMC Molecular Biology*, 18, 22-22.
- AMINOFF, M. J. 2004. Electrophysiologic testing for the diagnosis of peripheral nerve injuries. *Anesthesiology*, 100, 1298-303.
- ARASAKI, K., TAMAKI, M., HOSOYA, Y. & KUDO, N. 1997. Validity of electromyograms and tension as a means of motor unit number estimation. *Electromyography*, 20, 552-560.
- ARNOLD, W. D., SHETH, K. A., WIER, C. G., KISSEL, J. T., BURGHESE, A. H. & KOLB, S. J. 2015. Electrophysiological Motor Unit Number Estimation

- (MUNE) Measuring Compound Muscle Action Potential (CMAP) in Mouse Hindlimb Muscles. *JoVE*, e52899.
- ARTHUR-FARRAJ, P. J., LATOUCHE, M., WILTON, D. K., QUINTES, S., CHABROL, E., BANERJEE, A., WOODHOO, A., JENKINS, B., RAHMAN, M., TURMAINE, M., WICHER, G. K., MITTER, R., GREENSMITH, L., BEHRENS, A., RAIVICH, G., MIRSKY, R. & JESSEN, K. R. 2012. c-Jun reprograms Schwann cells of injured nerves to generate a repair cell essential for regeneration. *Neuron*, 75, 633-647.
- ARTHUR-FARRAJ, P. J., MORGAN, C. C., ADAMOWICZ, M., GOMEZ-SANCHEZ, J. A., FAZAL, S. V., BEUCHER, A., RAZZAGHI, B., MIRSKY, R., JESSEN, K. R. & AITMAN, T. J. 2017. Changes in the coding and non-coding transcriptome and DNA methylome that define the Schwann cell repair phenotype after nerve injury. *Cell reports*, 20, 2719-2734.
- ASHLEY, Z., SUTHERLAND, H., LANMULLER, H., RUSSOLD, M. F., UNGER, E., BIJAK, M., MAYR, W., BONCOMPAGNI, S., PROTASI, F., SALMONS, S. & JARVIS, J. C. 2007. Atrophy, but not necrosis, in rabbit skeletal muscle denervated for periods up to one year. *Am J Physiol Cell Physiol*, 292, C440-51.
- ATZ, M., WALSH, D., CARTAGENA, P., LI, J., EVANS, S., CHOUDARY, P., OVERMAN, K., STEIN, R., TOMITA, H., POTKIN, S., MYERS, R., WATSON, S. J., JONES, E. G., AKIL, H., BUNNEY, W. E., JR. & VAWTER, M. P. 2007. Methodological considerations for gene expression profiling of human brain. *Journal of neuroscience methods*, 163, 295-309.
- AYDIN, M. A., MACKINNON, S. E., GU, X. M., KOBAYASHI, J. & KUZON, W. M., JR. 2004. Force deficits in skeletal muscle after delayed reinnervation. *Plastic and reconstructive surgery*, 113, 1712-1718.

- AZZOUZ, M., LECLERC, N., GURNEY, M., WARTER, J.-M., POINDRON, P. & BORG, J. 1997. Progressive Motor Neuron Impairment in an Animal Model of Familial Amyotrophic Lateral Sclerosis. *In*: TEELKEN, A. & KORF, J. (eds.) *Neurochemistry: Cellular, Molecular, and Clinical Aspects*. Boston, MA: Springer US.
- BADIA, J., PASCUAL-FONT, A., VIVO, M., UDINA, E. & NAVARRO, X. 2010. Topographical distribution of motor fascicles in the sciatic-tibial nerve of the rat. *Muscle Nerve*, 42, 192-201.
- BAGUST, J., LEWIS, D. M. & WESTERMAN, R. A. 1981. Motor units in cross-reinnervated fast and slow twitch muscle of the cat. *The Journal of physiology*, 313, 223-235.
- BALTODANO, P. A., TONG, A. J., CHHABRA, A. & ROSSON, G. D. 2014. The role of magnetic resonance neurography in the postoperative management of peripheral nerve injuries. *Neuroimaging Clin N Am*, 24, 235-44.
- BARGHI, E. & GLADDEN, M. 2013. Motor unit number estimation in normal and parkinsonism model of medial gastrocnemius muscle in rats. *International journal of molecular and cellular medicine*, 2, 72-79.
- BARKHAUS, P. E. & NANDEDKAR, S. D. 1994. Recording characteristics of the surface EMG electrodes. *Muscle & Nerve*, 17, 1317-1323.
- BASTARD, J. P., CHAMBERT, S., CEPPA, F., COUDE, M., GRAPEZ, E., LORIC, S., MUZEAU, F., SPYRATOS, F., POIRIER, K., COPOIS, V., TSE, C. & BIENVENU, T. 2002. [RNA isolation and purification methods]. *Annales de biologie clinique*, 60, 513-523.
- BEIROWSKI, B., BEREK, L., ADALBERT, R., WAGNER, D., GRUMME, D. S., ADDICKS, K., RIBCHESTER, R. R. & COLEMAN, M. P. 2004. Quantitative and qualitative analysis of Wallerian degeneration using restricted axonal labelling in YFP-H mice. *J Neurosci Methods*, 134, 23-35.

- BENDSZUS, M. & KOLTZENBURG, M. 2001. Visualization of denervated muscle by gadolinium-enhanced MRI. *Neurology*, 57, 1709-11.
- BENDSZUS, M., KOLTZENBURG, M., WESSIG, C. & SOLYMOSI, L. 2002. Sequential MR imaging of denervated muscle: experimental study. *AJNR Am J Neuroradiol*, 23, 1427-31.
- BENDSZUS, M. & STOLL, G. 2003. Caught in the act: in vivo mapping of macrophage infiltration in nerve injury by magnetic resonance imaging. *J Neurosci*, 23, 10892-6.
- BENDSZUS, M. & STOLL, G. 2005. Technology Insight: visualizing peripheral nerve injury using MRI. *Nature Clinical Practice Neurology*, 1, 45-53.
- BENDSZUS, M., WESSIG, C., REINERS, K., BARTSCH, A. J., SOLYMOSI, L. & KOLTZENBERG, M. 2003. MR imaging in the differential diagnosis of neurogenic foot drop. *AJNR Am J Neuroradiol*, 24, 1283-9.
- BENÍTEZ BRITO, N., SUÁREZ LLANOS, J. P., FUENTES FERRER, M., OLIVA GARCÍA, J. G., DELGADO BRITO, I., PEREYRA-GARCÍA CASTRO, F., CARACENA CASTELLANOS, N., ACEVEDO RODRÍGUEZ, C. X. & PALACIO ABIZANDA, E. 2016. Relationship between Mid-Upper Arm Circumference and Body Mass Index in Inpatients. *PloS one*, 11, e0160480-e0160480.
- BHANDARI, P. S., SADHOTRA, L. P., BHARGAVA, P., BATH, A. S., MUKHERJEE, M. K., BHATTI, T. & MAURYA, S. 2009. Surgical outcomes following nerve transfers in upper brachial plexus injuries. *Indian journal of plastic surgery : official publication of the Association of Plastic Surgeons of India*, 42, 150-160.
- BIRCH, R. 2011a. Pain. In: BIRCH, R. (ed.) *Surgical Disorders of the Peripheral Nerves*. London: Springer London.

- BIRCH, R. 2011b. *Surgical disorders of the peripheral nerves*, Springer Science & Business Media.
- BISCHOFF, A., GROSHEVA, M., IRINTCHEV, A., SKOURAS, E., KAIDOGLOU, K., MICHAEL, J., ANGELOVA, S., KUERTEN, S., SINIS, N., DUNLOP, S. & ANGELOV, D. 2009. Manual stimulation of the orbicularis oculi muscle improves eyelid closure after facial nerve injury in adult rats. *Muscle & nerve*, 39, 197-205.
- BOE, S. G., STASHUK, D. W. & DOHERTY, T. J. 2004. Motor unit number estimation by decomposition-enhanced spike-triggered averaging: control data, test-retest reliability, and contractile level effects. *Muscle Nerve*, 29, 693-9.
- BOE, S. G., STASHUK, D. W. & DOHERTY, T. J. 2007. Motor unit number estimates and quantitative motor unit analysis in healthy subjects and patients with amyotrophic lateral sclerosis. *Muscle & nerve*, 36, 62-70.
- BOERBOOM, A., DION, V., CHARIOT, A. & FRANZEN, R. 2017. Molecular Mechanisms Involved in Schwann Cell Plasticity. 10.
- BONDOK, A. A., BOTROS, K. G. & GABR, O. M. 1990. Segmental motor and sensory innervation of muscles in anterior leg compartment as revealed by retrograde transport of horseradish peroxidase. *Anat Anz*, 170, 359-65.
- BORGAN, E., NAVON, R., VOLLAN, H. K. M., SCHLICHTING, E., SAUER, T., YAKHINI, Z., LINGJAERDE, O. C., SORLIE, T. & BORRESEN-DALE, A.-L. 2011. Ischemia caused by time to freezing induces systematic microRNA and mRNA responses in cancer tissue. *Molecular oncology*, 5, 564-576.
- BOSSE, F., KURY, P. & MULLER, H. W. 2001. Gene expression profiling and molecular aspects in peripheral nerve regeneration. *Restorative neurology and neuroscience*, 19, 5-18.
- BOSTOCK, H. & SEARS, T. A. 1976. Continuous conduction in demyelinated mammalian nerve fibers. *Nature*, 263, 786-7.

- BOSTOCK, H., SEARS, T. A. & SHERRATT, R. M. 1981. The effects of 4-aminopyridine and tetraethylammonium ions on normal and demyelinated mammalian nerve fibres. *J Physiol*, 313, 301-15.
- BOYER, R. B., KELM, N. D., RILEY, D. C., SEXTON, K. W., POLLINS, A. C., SHACK, R. B., DORTCH, R. D., NANNEY, L. B., DOES, M. D. & THAYER, W. P. 2015. 4.7-T diffusion tensor imaging of acute traumatic peripheral nerve injury. *Neurosurgical focus*, 39, E9-E9.
- BOZKURT, A., SCHEFFEL, J., BROOK, G., JOOSTEN, E., SUSCHEK, C., O'DEY, D., PALLUA, N. & DEUMENS, R. 2011. Aspects of static and dynamic motor function in peripheral nerve regeneration: SSI and CatWalk gait analysis. *Behavioural brain research*, 219, 55-62.
- BREMER, M., FROB, F., KICHKO, T., REEH, P., TAMM, E. R., SUTER, U. & WEGNER, M. 2011. Sox10 is required for Schwann-cell homeostasis and myelin maintenance in the adult peripheral nerve. *Glia*, 59, 1022-1032.
- BRITSCH, S., GOERICH, D. E., RIETHMACHER, D., PEIRANO, R. I., ROSSNER, M., NAVE, K. A., BIRCHMEIER, C. & WEGNER, M. 2001. The transcription factor Sox10 is a key regulator of peripheral glial development. *Genes Dev*, 15, 66-78.
- BROMBERG, M. B. 1999. Electronic myoanatomic atlas for clinical electromyography muscle localization for needle insertion in clinical EMG CD-ROM. Electronic atlas of electromyographic waveforms, EMG on CD. Vol. II, Parts I-IV. *Muscle & Nerve*, 22, 1468-1469.
- BROMBERG, M. B. 2007. Updating motor unit number estimation (MUNE). *Clinical neurophysiology : official journal of the International Federation of Clinical Neurophysiology*, 118, 1-8.

- BROMBERG, M. B. & ABRAMS, J. L. 1995. Sources of error in the spike-triggered averaging method of motor unit number estimation (MUNE). *Muscle Nerve*, 18, 1139-46.
- BROWN, H., JOHNSON, K., GILBERT, A. & QUICK, T. J. 2018. The lived experience of motor recovery of elbow flexion following Oberlin nerve transfer: A qualitative analysis. *Hand Therapy*, 23, 130-138.
- BROWN, W. F. & MILNER-BROWN, H. S. 1976. Some electrical properties of motor units and their effects on the methods of estimating motor unit numbers. *Journal of neurology, neurosurgery, and psychiatry*, 39, 249-257.
- BROWN, W. F., STRONG, M. J. & SNOW, R. 1988. Methods for estimating numbers of motor units in biceps-brachialis muscles and losses of motor units with aging. *Muscle Nerve*, 11, 423-32.
- BRUSHART, T., ASPALTER, M., GRIFFIN, J., REDETT, R., HAMEED, H., ZHOU, C., WRIGHT, M., VYAS, A. & HÖKE, A. 2013. Schwann cell phenotype is regulated by axon modality and central–peripheral location, and persists in vitro. *Experimental neurology*, 247, 272-281.
- BUCHTHAL, F., GULD, C. & ROSENFALCK, P. 1954a. Action potential parameters in normal human muscle and their dependence on physical variables. *Acta Physiol Scand*, 32, 200-18.
- BUCHTHAL, F., PINELL, P. & ROSENFALCK, P. 1954b. Action potential parameters in normal human muscle and their physiological determinants. *Acta Physiol Scand*, 32, 219-29.
- BURKE, D., HOWELLS, J., TREVILLION, L., MCNULTY, P. A., JANKELOWITZ, S. K. & KIERNAN, M. C. 2009. Threshold behaviour of human axons explored using subthreshold perturbations to membrane potential. *The Journal of physiology*, 587, 491-504.

- BURNETT, M. G. & ZAGER, E. L. 2004. Pathophysiology of peripheral nerve injury: a brief review. *Neurosurg Focus*, 16, E1.
- BUSTIN, S. A., BENES, V., GARSON, J. A., HELLEMANS, J., HUGGETT, J., KUBISTA, M., MUELLER, R., NOLAN, T., PFAFFL, M. W., SHIPLEY, G. L., VANDESOMPELE, J. & WITTEWER, C. T. 2009. The MIQE Guidelines: Minimum Information for Publication of Quantitative Real-Time PCR Experiments. *Clinical Chemistry*, 55, 611 LP-622.
- CABOUX, E., PACIENCIA, M., DURAND, G., ROBINOT, N., WOZNIAK, M. B., GALATEAU-SALLE, F., BYRNES, G., HAINAUT, P. & LE CALVEZ-KELM, F. 2013. Impact of delay to cryopreservation on RNA integrity and genome-wide expression profiles in resected tumor samples. *PLoS one*, 8, e79826-e79826.
- CAFFERTY, W. B., GARDINER, N. J., GAVAZZI, I., POWELL, J., MCMAHON, S. B., HEATH, J. K., MUNSON, J., COHEN, J. & THOMPSON, S. W. 2001. Leukemia inhibitory factor determines the growth status of injured adult sensory neurons. *Journal of Neuroscience*, 21, 7161-7170.
- CAMPBELL, W. W. 2008. Evaluation and management of peripheral nerve injury. *Clinical Neurophysiology*, 119, 1951-1965.
- CARLETON, S. A. & BROWN, W. F. 1979. Changes in motor unit populations in motor neurone disease. *J Neurol Neurosurg Psychiatry*, 42, 42-51.
- CARLSON, B. M. 2014. The Biology of Long-Term Denervated Skeletal Muscle. *European journal of translational myology*, 24, 3293-3293.
- CATTIN, A.-L., BURDEN, J. J., VAN EMMENIS, L., MACKENZIE, F. E., HOVING, J. J., CALAVIA, N. G., GUO, Y., MCLAUGHLIN, M., ROSENBERG, L. H. & QUEREDA, V. 2015. Macrophage-induced blood vessels guide Schwann cell-mediated regeneration of peripheral nerves. *Cell*, 162, 1127-1139.

- CHAMMAS, M., MICALLEF, J. P., PREFAUT, C. & ALLIEU, Y. 1997. Fatigue analysis of human reinnervated muscle after microsurgical nerve repair. *Clinical orthopaedics and related research*, 144-149.
- CHAN, K. M., GORDON, T., ZOCHODNE, D. W. & POWER, H. A. 2014. Improving peripheral nerve regeneration: from molecular mechanisms to potential therapeutic targets. *Experimental neurology*, 261, 826-835.
- CHAO, M. V. 2003. Neurotrophins and their receptors: a convergence point for many signalling pathways. *Nat Rev Neurosci*, 4, 299-309.
- CHASSARD, M., PHAM, E. & COMTET, J. J. 1993. Two-point discrimination tests versus functional sensory recovery in both median and ulnar nerve complete transections. *The Journal of Hand Surgery: British & European Volume*, 18, 790-796.
- CHAUDHRY, V. & CORNBLATH, D. R. 1992. Wallerian degeneration in human nerves: Serial electrophysiological studies. *Muscle & Nerve*, 15, 687-693.
- CHEN, Z.-L., YU, W.-M. & STRICKLAND, S. 2007. Peripheral regeneration. *Annual review of neuroscience*, 30, 209-233.
- CHIARAPATTANAKOM, P., LEECHAVENGVONGS, S., WITONCHART, K., UERPAIROJKIT, C. & THUVASETHAKUL, P. 1998. Anatomy and internal topography of the musculocutaneous nerve: the nerves to the biceps and brachialis muscle. *J Hand Surg Am*, 23, 250-5.
- CHONG, P. S. T. & CROS, D. P. 2004. Technology literature review: Quantitative sensory testing. *Muscle & Nerve*, 29, 734-747.
- CHURCHILL, J. D., ARNOLD, L. L. & GARRAGHTY, P. E. 2001. Somatotopic reorganization in the brainstem and thalamus following peripheral nerve injury in adult primates. *Brain Res*, 910, 142-52.
- CIARAMITARO, P., MONDELLI, M., LOGULLO, F., GRIMALDI, S., BATTISTON, B., SARD, A., SCARINZI, C., MIGLIARETTI, G., FACCANI, G. & COCITO, D.

2010. Traumatic peripheral nerve injuries: epidemiological findings, neuropathic pain and quality of life in 158 patients. *J Peripher Nerv Syst*, 15, 120-7.
- CLAGUE, J. E., ROBERTS, N., GIBSON, H. & EDWARDS, R. H. 1995. Muscle imaging in health and disease. *Neuromuscul Disord*, 5, 171-8.
- CLUSKEY, S. & RAMSDEN, D. B. 2001. Mechanisms of neurodegeneration in amyotrophic lateral sclerosis. *Molecular pathology : MP*, 54, 386-392.
- CUDLIP, S. A., HOWE, F. A., GRIFFITHS, J. R. & BELL, B. A. 2002. Magnetic resonance neurography of peripheral nerve following experimental crush injury, and correlation with functional deficit. *J Neurosurg*, 96, 755-9.
- DAHLIN, L. 2006. Nerve injury and repair: from molecule to man.
- DAILEY, A. T., TSURUDA, J. S., FILLER, A. G., MARAVILLA, K. R., GOODKIN, R. & KLIOT, M. 1997. Magnetic resonance neurography of peripheral nerve degeneration and regeneration. *Lancet*, 350, 1221-2.
- DAILEY, A. T., TSURUDA, J. S., GOODKIN, R., HAYNOR, D. R., FILLER, A. G., HAYES, C. E., MARAVILLA, K. R. & KLIOT, M. 1996. Magnetic resonance neurography for cervical radiculopathy: a preliminary report. *Neurosurgery*, 38, 488-92 discussion 492.
- DAUBE, J. R. 1995. Estimating the number of motor units in a muscle. *J Clin Neurophysiol*, 12, 585-94.
- DE CARVALHO, M., BARKHAUS, P. E., NANDEDKAR, S. D. & SWASH, M. 2018. Motor unit number estimation (MUNE): Where are we now? *Clinical neurophysiology : official journal of the International Federation of Clinical Neurophysiology*, 129, 1507-1516.
- DE FELIPE, C. & HUNT, S. P. 1994. The differential control of c-jun expression in regenerating sensory neurons and their associated glial cells. *Journal of Neuroscience*, 14, 2911-2923.

- DEFOREST, B. A., WINSLOW, J. & THOMAS, C. K. 2018. Improved motor unit number estimate when motor unit alternation is addressed. 125, 1131-1140.
- DELGADO, D. A., LAMBERT, B. S., BOUTRIS, N., MCCULLOCH, P. C., ROBBINS, A. B., MORENO, M. R. & HARRIS, J. D. 2018. Validation of Digital Visual Analog Scale Pain Scoring With a Traditional Paper-based Visual Analog Scale in Adults. *Journal of the American Academy of Orthopaedic Surgeons. Global research & reviews*, 2, e088-e088.
- DELLON, A. L. & MACKINNON, S. E. 1988. Basic scientific and clinical applications of peripheral nerve regeneration. *Surgery annual*, 20, 59-100.
- DEROIDE, N., BOUSSON, V., LÉVY, B. I., LAREDO, J. D. & KUBIS, N. 2010. L'imagerie du nerf et du muscle dans les atteintes nerveuses périphériques associée à l'électroneuromyographie : le couple idéal ? *La Revue de Médecine Interne*, 31, 287-294.
- DESJARDINS, P. & CONKLIN, D. 2010. NanoDrop Microvolume Quantitation of Nucleic Acids. *Journal of Visualized Experiments : JoVE*, 2565-2565.
- DOAN, L., PISKOUN, B., ROSENBERG, A. D., BLANCK, T. J. J., PHILLIPS, M. S. & XU, F. 2012. In vitro antiseptic effects on viability of neuronal and Schwann cells. *Regional anesthesia and pain medicine*, 37, 131-138.
- DOES, M. D. & SNYDER, R. E. 1996. Multiexponential T2 relaxation in degenerating peripheral nerve. *Magn Reson Med*, 35, 207-13.
- DROBNJAK, I., ZHANG, H., IANUS, A., KADEN, E. & ALEXANDER, D. C. 2016. PGSE, OGSE, and sensitivity to axon diameter in diffusion MRI: Insight from a simulation study. *Magn Reson Med*, 75, 688-700.
- DUFF, S. V. 2005. Impact of peripheral nerve injury on sensorimotor control. *J Hand Ther*, 18, 277-91.
- DUMITRU, D., ZWARTS, M. J. & AMATO, A. A. 2002. *Peripheral nervous system's reaction to injury*.

- EGGERS, R., TANNEMAAT, M., EHLERT, E. & VERHAAGEN, J. 2010. A spatio-temporal analysis of motoneuron survival, axonal regeneration and neurotrophic factor expression after lumbar ventral root avulsion and implantation. *Experimental neurology*, 223, 207-220.
- EISEN, A., KARPATI, G., CARPENTER, S. & DANON, J. 1974. The motor unit profile of the rat soleus in experimental myopathy and reinnervation. *Neurology*, 24, 878-878.
- ENGLISH, A. W., LIU, K., NICOLINI, J. M., MULLIGAN, A. M. & YE, K. 2013. Small-molecule trkB agonists promote axon regeneration in cut peripheral nerves. *Proceedings of the National Academy of Sciences of the United States of America*, 110, 16217-16222.
- FARONI, A., MOBASSERI, S. A., KINGHAM, P. J. & REID, A. J. 2015. Peripheral nerve regeneration: Experimental strategies and future perspectives. *Advanced Drug Delivery Reviews*, 82-83, 160-167.
- FILLER, A. G., KLIOT, M., HOWE, F. A., HAYES, C. E., SAUNDERS, D. E., GOODKIN, R., BELL, B. A., WINN, H. R., GRIFFITHS, J. R. & TSURUDA, J. S. 1996. Application of magnetic resonance neurography in the evaluation of patients with peripheral nerve pathology. *J Neurosurg*, 85, 299-309.
- FILLER, A. G., KLIOT, M., WINN, H. R., TSURUDA, J. S., HAYES, C. E., HOWE, F. A., GRIFFITHS, J. R., FILLER, A. G., BELL, B. A. & FILLER, A. G. 1993. Magnetic resonance neurography. *The Lancet*, 341, 659-661.
- FINZSCH, M., SCHREINER, S., KICHKO, T., REEH, P., TAMM, E. R., BÖSL, M. R., MEIJER, D. & WEGNER, M. 2010. Sox10 is required for Schwann cell identity and progression beyond the immature Schwann cell stage. *The Journal of cell biology*, 189, 701-712.
- FLASAR, J., VOLK, G. F., GRANITZKA, T., GEIßLER, K., IRINTCHEV, A., LEHMANN, T. & GUNTINAS-LICHIUS, O. 2017. Quantitative facial

- electromyography monitoring after hypoglossal-facial jump nerve suture. *Laryngoscope investigative otolaryngology*, 2, 325-330.
- FLEIGE, S. & PFAFFL, M. W. 2006. RNA integrity and the effect on the real-time qRT-PCR performance. *Molecular aspects of medicine*, 27, 126-139.
- FONTANA, X., HRISTOVA, M., DA COSTA, C., PATODIA, S., THEI, L., MAKWANA, M., SPENCER-DENE, B., LATOUCHE, M., MIRSKY, R., JESSEN, K. R., KLEIN, R. D., RAIVICH, G. & BEHRENS, A. 2012. C-Jun in Schwann cells promotes axonal regeneration and motoneuron survival via paracrine signaling. *Journal of Cell Biology*, 198, 127-141.
- FOX, B. C., DEVONSHIRE, A. S., BARADEZ, M.-O., MARSHALL, D. & FOY, C. A. 2012. Comparison of reverse transcription-quantitative polymerase chain reaction methods and platforms for single cell gene expression analysis. *Analytical biochemistry*, 427, 178-186.
- FRANÇA, A., FREITAS, A. I., HENRIQUES, A. F. & CERCA, N. 2012. Optimizing a qPCR Gene Expression Quantification Assay for *S. epidermidis* Biofilms: A Comparison between Commercial Kits and a Customized Protocol. *PLoS ONE*, 7, e37480-e37480.
- FU, S. Y. & GORDON, T. 1995. Contributing factors to poor functional recovery after delayed nerve repair: prolonged denervation. *The Journal of neuroscience : the official journal of the Society for Neuroscience*, 15, 3886-3895.
- FU, S. Y. & GORDON, T. 1997. The cellular and molecular basis of peripheral nerve regeneration. *Molecular neurobiology*, 14, 67-116.
- FURNESS, J., COSTA, M., GIBBINS, I., LLEWELLYN-SMITH, I., OLIVER, J. J. C. & RESEARCH, T. 1985. Neurochemically similar myenteric and submucous neurons directly traced to the mucosa of the small intestine. 241, 155-163.

- FURNESS, J., COSTA, M., KEAST, J. J. C. & RESEARCH, T. 1984. Choline acetyltransferase-and peptide immunoreactivity of submucous neurons in the small intestine of the guinea-pig. *237*, 329-336.
- GALEA, V., FEHLINGS, D., KIRSCH, S. & MCCOMAS, A. 2001. Depletion and sizes of motor units in spinal muscular atrophy. *Muscle Nerve*, *24*, 1168-72.
- GALLAGHER, T. A., SIMON, N. G. & KLIOT, M. 2015. Diffusion tensor imaging to visualize axons in the setting of nerve injury and recovery. *Neurosurg Focus*, *39*, E10.
- GAMBAROTTA, G., RONCHI, G., FRIARD, O., GALLETTA, P., PERROTEAU, I. & GEUNA, S. 2014. Identification and validation of suitable housekeeping genes for normalizing quantitative real-time PCR assays in injured peripheral nerves. *PLoS one*, *9*, e105601-e105601.
- GAUDET, A. D., POPOVICH, P. G. & RAMER, M. S. 2011. Wallerian degeneration: gaining perspective on inflammatory events after peripheral nerve injury. *Journal of neuroinflammation*, *8*, 110-110.
- GAWEL, M., KOSTERA-PRUSZCZYK, A., LUSAKOWSKA, A., JEDRZEJOWSKA, M., RYNIEWICZ, B., LIPOWSKA, M., GAWEL, D. & KAMINSKA, A. 2015. Motor unit loss estimation by the multipoint incremental MUNE method in children with spinal muscular atrophy--a preliminary study. *Neuromuscul Disord*, *25*, 216-21.
- GEUNA, S., RAIMONDO, S., RONCHI, G., DI SCIPIO, F., TOS, P., CZAJA, K. & FORNARO, M. 2009. Chapter 3: Histology of the peripheral nerve and changes occurring during nerve regeneration. *Int Rev Neurobiol*, *87*, 27-46.
- GIANNINI, C., LAIS, A. C. & DYCK, P. J. 1989. Number, size, and class of peripheral nerve fibers regenerating after crush, multiple crush, and graft. *Brain Research*, *500*, 131-138.

- GOMEZ-SANCHEZ, J. A., CARTY, L., IRUARRIZAGA-LEJARRETA, M., PALOMO-IRIGOYEN, M., VARELA-REY, M., GRIFFITH, M., HANTKE, J., MACIAS-CAMARA, N., AZKARGORTA, M., AURREKOETXEA, I., DE JUAN, V. G., JEFFERIES, H. B. J., ASPICHUETA, P., ELORTZA, F., ARANSAY, A. M., MARTINEZ-CHANTAR, M. L., BAAS, F., MATO, J. M., MIRSKY, R., WOODHOO, A. & JESSEN, K. R. 2015. Schwann cell autophagy, myelinophagy, initiates myelin clearance from injured nerves. *The Journal of cell biology*, 210, 153-168.
- GOMEZ-SANCHEZ, J. A., PILCH, K. S., VAN DER LANS, M., FAZAL, S. V., BENITO, C., WAGSTAFF, L. J., MIRSKY, R. & JESSEN, K. R. 2017a. After Nerve Injury, Lineage Tracing Shows That Myelin and Remak Schwann Cells Elongate Extensively and Branch to Form Repair Schwann Cells, Which Shorten Radically on Remyelination. *The Journal of neuroscience : the official journal of the Society for Neuroscience*, 37, 9086-9099.
- GOMEZ-SANCHEZ, J. A., PILCH, K. S., VAN DER LANS, M., FAZAL, S. V., BENITO, C., WAGSTAFF, L. J., MIRSKY, R. & JESSEN, K. R. 2017b. After nerve injury, lineage tracing shows that myelin and Remak Schwann cells elongate extensively and branch to form repair Schwann cells, which shorten radically on remyelination. *Journal of Neuroscience*, 37, 9086-9099.
- GONÇALVES, N. P., MOHSENI, S., EL SOURY, M., ULRICHSEN, M., RICHNER, M., XIAO, J., WOOD, R. J., ANDERSEN, O. M., COULSON, E. J., RAIMONDO, S., MURRAY, S. S. & VÆGTER, C. B. 2019. Peripheral Nerve Regeneration Is Independent From Schwann Cell p75NTR Expression. 13.
- GOOCH, C. L., DOHERTY, T. J., CHAN, K. M., BROMBERG, M. B., LEWIS, R. A., STASHUK, D. W., BERGER, M. J., ANDARY, M. T. & DAUBE, J. R. 2014. Motor unit number estimation: a technology and literature review. *Muscle & nerve*, 50, 884-893.

- GOOCH, C. L. & HARATI, Y. 2000. Motor unit number estimation, ALS and clinical trials. *Amyotrophic lateral sclerosis and other motor neuron disorders : official publication of the World Federation of Neurology, Research Group on Motor Neuron Diseases*, 1, 71-82.
- GORDON, T., TYREMAN, N. & RAJI, M. A. 2011. The Basis for Diminished Functional Recovery after Delayed Peripheral Nerve Repair. *The Journal of Neuroscience*, 31, 5325.
- GRIMM, A., MEYER, H., NICKEL, M. D., NITTKA, M., RAITHEL, E., CHAUDRY, O., FRIEDBERGER, A., UDER, M., KEMMLER, W., ENGELKE, K. & QUICK, H. H. 2018. Repeatability of Dixon magnetic resonance imaging and magnetic resonance spectroscopy for quantitative muscle fat assessments in the thigh. *J Cachexia Sarcopenia Muscle*, 9, 1093-1100.
- GRINSTEIN, M., DINGWALL, H. L., SHAH, R. R., CAPELLINI, T. D. & GALLOWAY, J. L. 2018. A robust method for RNA extraction and purification from a single adult mouse tendon. *PeerJ*, 6, e4664-e4664.
- GROTHER, C., HAASTERT, K. & JUNGNICHEL, J. 2006. Physiological function and putative therapeutic impact of the FGF-2 system in peripheral nerve regeneration—lessons from in vivo studies in mice and rats. *Brain research reviews*, 51, 293-299.
- GUAN, H. & YANG, K. 2008. RNA isolation and real-time quantitative RT-PCR. *Methods in molecular biology (Clifton, N.J.)*, 456, 259-270.
- GYDIKOV, A., GERILOVSKY, L., KOSTOV, K. & GATEV, P. 1980. Influence of some features of the muscle structure on the potentials of motor units, recorded by means of different types of needle electrodes. *Electromyogr Clin Neurophysiol*, 20, 299-321.
- HAASTERT-TALINI, K. 2020. Appropriate Animal Models for Translational Nerve Research. In: PHILLIPS, J., HERCHER, D. & HAUSNER, T. (eds.) *Peripheral*

Nerve Tissue Engineering and Regeneration. Cham: Springer International Publishing.

- HALL, S. 2005. The response to injury in the peripheral nervous system. *The Journal of bone and joint surgery. British volume*, 87, 1309-1319.
- HALL, S. M. & GREGSON, N. 1977. The effects of mitomycin C on the process of regeneration in the mammalian peripheral nervous system. *Neuropathology and Applied Neurobiology*, 3, 65-78.
- HANSEN, L., SHAHEEN, A. & CRANDALL, M. 2014. Outpatient follow-up after traumatic injury: Challenges and opportunities. *Journal of emergencies, trauma, and shock*, 7, 256-260.
- HANSEN, S. & BALLANTYNE, J. P. 1978. A quantitative electrophysiological study of motor neurone disease. *Journal of neurology, neurosurgery, and psychiatry*, 41, 773-783.
- HANSSON, T. & BRISMAR, T. 2003. Loss of sensory discrimination after median nerve injury and activation in the primary somatosensory cortex on functional magnetic resonance imaging. *J Neurosurg*, 99, 100-5.
- HARBISON, M. A. & HAMMER, S. M. 1989. Inactivation of human immunodeficiency virus by Betadine products and chlorhexidine. *Journal of acquired immune deficiency syndromes*, 2, 16-20.
- HÄRDLE, W. & SCHIMEK, M. 2013. *Statistical Theory and Computational Aspects of Smoothing: Proceedings of the COMPSTAT'94 Satellite Meeting Held in Semmering, Austria, 27-28 August 1994*, Springer Science & Business Media.
- HATZIS, C., SUN, H., YAO, H., HUBBARD, R. E., MERIC-BERNSTAM, F., BABIERA, G. V., WU, Y., PUSZTAI, L. & SYMMANS, W. F. 2011. Effects of Tissue Handling on RNA Integrity and Microarray Measurements From

- Resected Breast Cancers. *JNCI Journal of the National Cancer Institute*, 103, 1871-1883.
- HE, B., ZHU, Z., ZHU, Q., ZHOU, X., ZHENG, C., LI, P., ZHU, S., LIU, X. & ZHU, J. 2014. Factors predicting sensory and motor recovery after the repair of upper limb peripheral nerve injuries. *Neural regeneration research*, 9, 661-672.
- HECKEL, A., WEILER, M., XIA, A., RUETTERS, M., PHAM, M., BENDSZUS, M., HEILAND, S. & BAEUMER, P. 2015. Peripheral Nerve Diffusion Tensor Imaging: Assessment of Axon and Myelin Sheath Integrity. *PLOS ONE*, 10, e0130833.
- HERMENS, H. J., PROGRAMME, C. O. T. E. C. B. & HEALTH, R. 1999. *European Recommendations for Surface Electromyography: Results of the SENIAM Project*, Roessingh Research and Development.
- HERRERA-PEREZ, M., OLLER-BOIX, A., PEREZ-LORENSU, P. J., DE BERGUADOMINGO, J., GONZALEZ-CASAMAYOR, S., MARQUEZ-MARFIL, F., DIAZ-FLORES, L. & PAIS-BRITO, J. L. 2015. Intraoperative neurophysiological monitoring in peripheral nerve surgery: Technical description and experience in a centre. *Revista española de cirugía ortopédica y traumatología*, 59, 266-274.
- HEWITT, S. M., LEWIS, F. A., CAO, Y., CONRAD, R. C., CRONIN, M., DANENBERG, K. D., GORALSKI, T. J., LANGMORE, J. P., RAJA, R. G., WILLIAMS, P. M., PALMA, J. F. & WARRINGTON, J. A. 2008. Tissue handling and specimen preparation in surgical pathology: issues concerning the recovery of nucleic acids from formalin-fixed, paraffin-embedded tissue. *Archives of pathology & laboratory medicine*, 132, 1929-1935.
- HILZ, M. J., AXELROD, F. B., HERMANN, K., HAERTL, U., DUETSCH, M. & NEUNDORFER, B. 1998. Normative values of vibratory perception in 530 children, juveniles and adults aged 3-79 years. *J Neurol Sci*, 159, 219-25.

- HIROTA, H., KIYAMA, H., KISHIMOTO, T. & TAGA, T. 1996. Accelerated Nerve Regeneration in Mice by upregulated expression of interleukin (IL) 6 and IL-6 receptor after trauma. *The Journal of experimental medicine*, 183, 2627-2634.
- HIRSCH, T., KOERBER, A., JACOBSEN, F., DISSEMOND, J., STEINAU, H.-U., GATERMANN, S., AL-BENNA, S., KESTING, M., SEIPP, H.-M. & STEINSTRÄESSER, L. 2010a. Evaluation of toxic side effects of clinically used skin antiseptics in vitro. *The Journal of surgical research*, 164, 344-350.
- HIRSCH, T., SEIPP, H.-M., JACOBSEN, F., GOERTZ, O., STEINAU, H.-U. & STEINSTRÄESSER, L. 2010b. Antiseptics in Surgery. *Eplasty*, 10, e39-e39.
- HOFFMAN, H. 1950. LOCAL RE-INNervation IN PARTIALLY DENERVATED MUSCLE: A HISTO-PHYSIOLOGICAL STUDY. *Australian Journal of Experimental Biology and Medical Science*, 28, 383-398.
- HOKE, A. 2006. Mechanisms of Disease: what factors limit the success of peripheral nerve regeneration in humans? *Nature clinical practice. Neurology*, 2, 448-454.
- HOKE, A. & BRUSHART, T. 2010. Introduction to special issue: Challenges and opportunities for regeneration in the peripheral nervous system.
- HOKE, A., GORDON, T., ZOCHODNE, D. W. & SULAIMAN, O. A. R. 2002. A decline in glial cell-line-derived neurotrophic factor expression is associated with impaired regeneration after long-term Schwann cell denervation. *Experimental neurology*, 173, 77-85.
- HOLZGREFFE, R. E., WAGNER, E. R., SINGER, A. D. & DALY, C. A. 2019. Imaging of the Peripheral Nerve: Concepts and Future Direction of Magnetic Resonance Neurography and Ultrasound. *The Journal of Hand Surgery*, 44, 1066-1079.
- HOWE, F. A., FILLER, A. G., BELL, B. A. & GRIFFITHS, J. R. 1992. Magnetic Resonance Neurography. *Magnetic Resonance in Medicine*, 28, 328-338.

- HSUEH, I. P., LEE, M. M. & HSIEH, C. L. 2002. The Action Research Arm Test: is it necessary for patients being tested to sit at a standardized table? *Clin Rehabil*, 16, 382-8.
- HUGHES, S. M., TAYLOR, J. M., TAPSCOTT, S. J., GURLEY, C. M., CARTER, W. J. & PETERSON, C. A. 1993. Selective accumulation of MyoD and myogenin mRNAs in fast and slow adult skeletal muscle is controlled by innervation and hormones. *Development*, 118, 1137-47.
- IKEDA, M. & OKA, Y. 2012. The relationship between nerve conduction velocity and fiber morphology during peripheral nerve regeneration. *Brain and behavior*, 2, 382-390.
- IMBEAUD, S., GRAUDENS, E., BOULANGER, V., BARLET, X., ZABORSKI, P., EVENO, E., MUELLER, O., SCHROEDER, A. & AUFRAY, C. 2005. Towards standardization of RNA quality assessment using user-independent classifiers of microcapillary electrophoresis traces. *Nucleic Acids Research*, 33, e56-e56.
- ISAACS, J. & COCHRAN, A. R. 2019. Nerve transfers for peripheral nerve injury in the upper limb. *The bone & joint journal*, 101-B, 124-131.
- ISLA, A. & POZUELOS, J. 2011. Anatomic study in cadaver of the motor branch of the musculocutaneous nerve. *Acta Neurochir Suppl*, 108, 227-32.
- JACOBS, J. M. & LOVE, S. 1985. Qualitative and quantitative morphology of human sural nerve at different ages. *Brain : a journal of neurology*, 108 (Pt 4, 897-924.
- JACOBSEN, A. B., BOSTOCK, H. & TANKISI, H. 2018. CMAP Scan MUNE (MScan) - A Novel Motor Unit Number Estimation (MUNE) Method. *JoVE*, e56805.
- JAGTAP, S. A., KURUVILLA, A., GOVIND, P., NAIR, M. D., SARADA, C. & VARMA, R. P. 2014. Multipoint incremental motor unit number estimation versus amyotrophic lateral sclerosis functional rating scale and the medical research

- council sum score as an outcome measure in amyotrophic lateral sclerosis. *Annals of Indian Academy of Neurology*, 17, 336-339.
- JANG, S.-W., SRINIVASAN, R., JONES, E. A., SUN, G., KELES, S., KRUEGER, C., CHANG, L.-W., NAGARAJAN, R. & SVAREN, J. 2010. Locus-wide identification of Egr2/Krox20 regulatory targets in myelin genes. *Journal of neurochemistry*, 115, 1409-1420.
- JANG, S. Y., SHIN, Y. K., PARK, S. Y., PARK, J. Y., LEE, H. J., YOO, Y. H., KIM, J. K. & PARK, H. T. 2016. Autophagic myelin destruction by Schwann cells during Wallerian degeneration and segmental demyelination. *Glia*, 64, 730-742.
- JAYAKUMAR, P., OVERBEEK, C. L., LAMB, S., WILLIAMS, M., FUNES, C., GWILYM, S., RING, D. & VRANCEANU, A. M. 2018. What Factors Are Associated With Disability After Upper Extremity Injuries? A Systematic Review. *Clin Orthop Relat Res*, 476, 2190-2215.
- JENKINS, T. M., ALIX, J. J. P., DAVID, C., PEARSON, E., RAO, D. G., HOGGARD, N., O'BRIEN, E., BASTER, K., BRADBURN, M., BIGLEY, J., MCDERMOTT, C. J., WILKINSON, I. D. & SHAW, P. J. 2018. Imaging muscle as a potential biomarker of denervation in motor neuron disease. *J Neurol Neurosurg Psychiatry*, 89, 248-255.
- JEON, T., FUNG, M. M., KOCH, K. M., TAN, E. T. & SNEAG, D. B. 2018. Peripheral nerve diffusion tensor imaging: Overview, pitfalls, and future directions. *J Magn Reson Imaging*, 47, 1171-1189.
- JEROSCH-HEROLD, C. 2005. Assessment of sensibility after nerve injury and repair: a systematic review of evidence for validity, reliability and responsiveness of tests. *J Hand Surg Br*, 30, 252-64.
- JESPERSEN, S. N. 2012. Equivalence of double and single wave vector diffusion contrast at low diffusion weighting. *NMR Biomed*, 25, 813-8.

- JESSEN, K. R. & ARTHUR-FARRAJ, P. 2019. Repair Schwann cell update: Adaptive reprogramming, EMT, and stemness in regenerating nerves. *Glia*, 67, 421-437.
- JESSEN, K. R. & MIRSKY, R. 2008. Negative regulation of myelination: relevance for development, injury, and demyelinating disease. *Glia*, 56, 1552-1565.
- JESSEN, K. R. & MIRSKY, R. 2016. The repair Schwann cell and its function in regenerating nerves. *The Journal of Physiology*, 594, 3521-3531.
- JESSEN, K. R. & MIRSKY, R. 2019. The Success and Failure of the Schwann Cell Response to Nerve Injury. *Frontiers in Cellular Neuroscience*, 13, 33-33.
- JESSEN, K. R., WAGSTAFF, L. J., GOMEZ-SANCHEZ, J. A. & MIRSKY, R. 2017. Manipulation of repair Schwann cells to correct regeneration failures due to chronic denervation and advancing age. *Glia*, 65, E56-E56.
- JIANG, N., LI, H., SUN, Y., YIN, D., ZHAO, Q., CUI, S. & YAO, D. 2014. Differential gene expression in proximal and distal nerve segments of rats with sciatic nerve injury during Wallerian degeneration. *Neural Regeneration Research*, 9, 1186-1194.
- JIANG, X., LI, H., XIE, J., ZHAO, P., GORE, J. C. & XU, J. 2016. Quantification of cell size using temporal diffusion spectroscopy. *Magn Reson Med*, 75, 1076-85.
- JOPLING, C., BOUE, S. & IZPISUA BELMONTE, J. C. 2011. Dedifferentiation, transdifferentiation and reprogramming: three routes to regeneration. *Nature reviews. Molecular cell biology*, 12, 79-89.
- JOYCE, N. C. & CARTER, G. T. 2013. Electrodiagnosis in persons with amyotrophic lateral sclerosis. *PM & R : the journal of injury, function, and rehabilitation*, 5, S89-S95.
- JUNG, Y., NG, J. H., KEATING, C. P., SENTHIL-KUMAR, P., ZHAO, J., RANDOLPH, M. A., WINOGRAD, J. M. & EVANS, C. L. 2014. Comprehensive evaluation of peripheral nerve regeneration in the acute healing phase using tissue

- clearing and optical microscopy in a rodent model. *PLoS one*, 9, e94054-e94054.
- KADRIE, H. A., YATES, S. K., MILNER-BROWN, H. S. & BROWN, W. F. 1976. Multiple point electrical stimulation of ulnar and median nerves. *J Neurol Neurosurg Psychiatry*, 39, 973-85.
- KAISER, R., WALDAUF, P., ULLAS, G. & KRAJCOVÁ, A. 2020. Epidemiology, etiology, and types of severe adult brachial plexus injuries requiring surgical repair: systematic review and meta-analysis. *Neurosurg Rev*, 43, 443-452.
- KAKKAR, L. S., BENNETT, O. F., SLOW, B., RICHARDSON, S., IANUS, A., QUICK, T., ATKINSON, D., PHILLIPS, J. B. & DROBNJAK, I. 2018. Low frequency oscillating gradient spin-echo sequences improve sensitivity to axon diameter: An experimental study in viable nerve tissue. *Neuroimage*, 182, 314-328.
- KAMATH, S., VENKATANARASIMHA, N., WALSH, M. & HUGHES, P. 2008. MRI appearance of muscle denervation. *Skeletal radiology*, 37, 397-404.
- KAMHOLZ, J., AWATRAMANI, R., MENICHELLA, D., JIANG, H., XU, W. & SHY, M. 1999. Regulation of myelin-specific gene expression. Relevance to CMT1. *Annals of the New York Academy of Sciences*, 883, 91-108.
- KAOUTZANIS, C., KAVANAGH, C. M., LEICHTLE, S. W., WELCH, K. B., TALSMA, A., VANDEWARKER, J. F., LAMPMAN, R. M. & CLEARY, R. K. 2015. Chlorhexidine with isopropyl alcohol versus iodine povacrylex with isopropyl alcohol and alcohol- versus nonalcohol-based skin preparations: the incidence of and readmissions for surgical site infections after colorectal operations. *Dis Colon Rectum*, 58, 588-96.
- KARAMCHANDANI, J. R., NIELSEN, T. O., VAN DE RIJN, M. & WEST, R. B. 2012. Sox10 and S100 in the diagnosis of soft-tissue neoplasms. *Applied immunohistochemistry & molecular morphology : AIMM / official publication of the Society for Applied Immunohistochemistry*, 20, 445-450.

- KASSELMAN, L. J., SHEFNER, J. M. & RUTKOVE, S. B. 2009. Motor unit number estimation in the rat tail using a modified multipoint stimulation technique. *Muscle & nerve*, 40, 115-121.
- KAYA, Y. & SARIKCIOGLU, L. 2015. Sir Herbert Seddon (1903-1977) and his classification scheme for peripheral nerve injury. *Childs Nerv Syst*, 31, 177-80.
- KIKUCHI, Y., NAKAMURA, T., TAKAYAMA, S., HORIUCHI, Y. & TOYAMA, Y. 2003. MR imaging in the diagnosis of denervated and reinnervated skeletal muscles: experimental study in rats. *Radiology*, 229, 861-7.
- KIM, H. A., POMEROY, S. L., WHORISKEY, W., PAWLITZKY, I., BENOWITZ, L. I., SICINSKI, P., STILES, C. D. & ROBERTS, T. M. 2000. A developmentally regulated switch directs regenerative growth of Schwann cells through cyclin D1. *Neuron*, 26, 405-416.
- KLINE, D. G. 2012. CHAPTER 16 - Operative neurophysiology of the brachial plexus intraoperative electrodiagnostic studies. In: CHUNG, K. C., YANG, L. J. S. & MCGILLICUDDY, J. E. (eds.) *Practical Management of Pediatric and Adult Brachial Plexus Palsies*. Philadelphia: W.B. Saunders.
- KLINE, D. G. & HAPPEL, L. T. 1993. Penfield Lecture. A quarter century's experience with intraoperative nerve action potential recording. *Can J Neurol Sci*, 20, 3-10.
- KOBAYASHI, J., MACKINNON, S. E., WATANABE, O., BALL, D. J., GU, X. M., HUNTER, D. A. & KUZON, W. M., JR. 1997. The effect of duration of muscle denervation on functional recovery in the rat model. *Muscle & nerve*, 20, 858-866.
- KOLTZENBURG, M. & BENDSZUS, M. 2004. Imaging of peripheral nerve lesions. *Curr Opin Neurol*, 17, 621-6.

- KOSTROMINOVA, T., DOW, D., DENNIS, R., MILLER, R. & A. FAULKNER, J. 2005. Comparison of gene expression of 2-mo denervated, 2-mo stimulated-denervated, and control rat skeletal muscles. *Physiological genomics*, 22, 227-43.
- KOU, Y., ZHANG, P., YIN, X., WEI, S. Y., WANG, Y., ZHANG, H. & JIANG, B. 2011. Influence of different distal nerve degeneration period on peripheral nerve collateral sprouts regeneration. *Artificial Cells, Blood Substitutes, and Biotechnology*, 39, 223-227.
- KOVACIC, U., ZELE, T., OSREDKAR, J., SKETELJ, J. & BAJROVIC, F. F. 2004. Sex-related differences in the regeneration of sensory axons and recovery of nociception after peripheral nerve crush in the rat. *Exp Neurol*, 189, 94-104.
- KRAFT, G. H. 1990. Fibrillation potential amplitude and muscle atrophy following peripheral nerve injury. *Muscle Nerve*, 13, 814-21.
- KRARUP, C., BOECKSTYNS, M., IBSEN, A., MOLDOVAN, M. & ARCHIBALD, S. 2016. Remodeling of motor units after nerve regeneration studied by quantitative electromyography. *Clin Neurophysiol*, 127, 1675-1682.
- KULLMER, K., SIEVERS, K. W., REIMERS, C. D., ROMPE, J. D., MULLER-FELBER, W., NAGELE, M. & HARLAND, U. 1998. Changes of sonographic, magnetic resonance tomographic, electromyographic, and histopathologic findings within a 2-month period of examinations after experimental muscle denervation. *Arch Orthop Trauma Surg*, 117, 228-34.
- KUMAR, P., SINHA, R., PATIL, N. & KUMAR, V. 2019. Relationship between mid-upper arm circumference and BMI for identifying maternal wasting and severe wasting: a cross-sectional assessment. *Public Health Nutrition*, 22, 2548-2552.
- KUNTZ, C. T., BLAKE, L., BRITZ, G., FILLER, A., HAYES, C. E., GOODKIN, R., TSURUDA, J., MARAVILLA, K. & KLIOT, M. 1996. Magnetic resonance

- neurography of peripheral nerve lesions in the lower extremity. *Neurosurgery*, 39, 750-6; discussion 756-7.
- LANCASHIRE, H. T., VANHOESTENBERGHE, A., PENDEGRASS, C. J., AJAM, Y. A., MAGEE, E., DONALDSON, N. & BLUNN, G. W. 2016. Microchannel neural interface manufacture by stacking silicone and metal foil laminae. *J Neural Eng*, 13, 034001.
- LAWSON, V. H., GORDON SMITH, A. & BROMBERG, M. B. 2003. Assessment of axonal loss in Charcot-Marie-Tooth neuropathies. *Exp Neurol*, 184, 753-7.
- LEE, M. B., DAVID, A. H., RAJIV, M., ERIN, W. & MARCO, V. 2004. Neurogenic motor evoked potentials: role in brachial plexus surgery. *Neurosurgical Focus FOC*, 16, 607-610.
- LEE, R. G., ASHBY, P., WHITE, D. & AGUAYO, A. 1975. Analysis of motor conduction velocity in the human median nerve by computer simulation of compound muscle action potentials. *Electroencephalography and clinical neurophysiology*, 39, 225-237.
- LEE, S. K. & WOLFE, S. W. 2000. Peripheral nerve injury and repair. *J Am Acad Orthop Surg*, 8, 243-52.
- LEECHAVENGVONGS, S., WITONCHART, K., UERPAIROJKIT, C., THUVASETHAKUL, P. & KETMALASIRI, W. 1998. Nerve transfer to biceps muscle using a part of the ulnar nerve in brachial plexus injury (upper arm type): a report of 32 cases. *The Journal of hand surgery*, 23, 711-716.
- LEECHAVENGVONGS, S., WITONCHART, K., UERPAIROJKIT, C., THUVASETHAKUL, P. & MALUNGPASHROPE, K. 2006. Combined nerve transfers for C5 and C6 brachial plexus avulsion injury. *The Journal of hand surgery*, 31, 183-189.
- LEUKHARDT, W. H., GOLOB, J. F., MCCOY, A. M., FADLALLA, A. M. A., MALANGONI, M. A. & CLARIDGE, J. A. 2010. Follow-up disparities after

- trauma: a real problem for outcomes research. *American journal of surgery*, 199, 348-52; discussion 353.
- LEWIS, R. A., LI, J., FUERST, D. R., SHY, M. E. & KRAJEWSKI, K. 2003. Motor unit number estimate of distal and proximal muscles in Charcot-Marie-Tooth disease. *Muscle & nerve*, 28, 161-167.
- LI, H., TERENCEHI, G. & HALL, S. M. 1997. Effects of delayed re-innervation on the expression of c-erbB receptors by chronically denervated rat Schwann cells in vivo. *Glia*, 20, 333-347.
- LI, X., CHEN, J., HONG, G., SUN, C., WU, X., PENG, M. J. & ZENG, G. 2013. In vivo DTI longitudinal measurements of acute sciatic nerve traction injury and the association with pathological and functional changes. *Eur J Radiol*, 82, e707-14.
- LIU, P., PENG, J., HAN, G.-H., DING, X., WEI, S., GAO, G., HUANG, K., CHANG, F. & WANG, Y. 2019. Role of macrophages in peripheral nerve injury and repair. *Neural regeneration research*, 14, 1335-1342.
- LIU, Y. & WANG, H. 2020. Peripheral nerve injury induced changes in the spinal cord and strategies to counteract/enhance the changes to promote nerve regeneration. *Neural Regeneration Research*, 15, 189-198.
- LIU, Z., JIN, Y.-Q., CHEN, L., WANG, Y., YANG, X., CHENG, J., WU, W., QI, Z. & SHEN, Z. 2015. Specific marker expression and cell state of Schwann cells during culture in vitro. *PloS one*, 10, e0123278-e0123278.
- LIVAK, K. J. & SCHMITTGEN, T. D. 2001. Analysis of relative gene expression data using real-time quantitative PCR and the 2^{(-Delta Delta C(T))} Method. *Methods (San Diego, Calif.)*, 25, 402-408.
- LUBINSKA, L. 1982. Patterns of Wallerian degeneration of myelinated fibres in short and long peripheral stumps and in isolated segments of rat phrenic nerve.

- Interpretation of the role of axoplasmic flow of the trophic factor. *Brain Res*, 233, 227-40.
- LUTZ, A. B., CHUNG, W.-S., SLOAN, S. A., CARSON, G. A., ZHOU, L., LOVELETT, E., POSADA, S., ZUCHERO, J. B. & BARRES, B. A. 2017. Schwann cells use TAM receptor-mediated phagocytosis in addition to autophagy to clear myelin in a mouse model of nerve injury. *Proceedings of the National Academy of Sciences*, 114, E8072-E8080.
- MA, J., SHEN, J., GARRETT, J. P., LEE, C. A., LI, Z., ELSAIDI, G. A., RITTING, A., HICK, J., TAN, K. H., SMITH, T. L., SMITH, B. P. & KOMAN, L. A. 2007. Gene expression of myogenic regulatory factors, nicotinic acetylcholine receptor subunits, and GAP-43 in skeletal muscle following denervation in a rat model. *Journal of orthopaedic research : official publication of the Orthopaedic Research Society*, 25, 1498-1505.
- MA, J., SHEN, J., LEE, C. A., ELSAIDI, G. A., SMITH, T. L., WALKER, F. O., RUSHING, J. T., TAN, K. H., KOMAN, L. A. & SMITH, B. P. 2005. Gene expression of nAChR, SNAP-25 and GAP-43 in skeletal muscles following botulinum toxin A injection: a study in rats. *J Orthop Res*, 23, 302-9.
- MAATHUIS, E. M., DRENTHE, J., VAN DOORN, P. A., VISSER, G. H. & BLOK, J. H. 2013. The CMAP scan as a tool to monitor disease progression in ALS and PMA. *Amyotroph Lateral Scler Frontotemporal Degener*, 14, 217-23.
- MACAVOY, M. C. & GREEN, D. P. 2007. Critical reappraisal of Medical Research Council muscle testing for elbow flexion. *The Journal of hand surgery*, 32, 149-153.
- MACDONALD, W. M. 1918. TINEL'S SIGN IN PERIPHERAL NERVE LESIONS. *British medical journal*, 2, 6-8.
- MACKINNON, S. E. & DELLON, A. L. 1988. *Surgery of the peripheral nerve*, New York; Stuttgart; New York, Thieme Medical Publishers ; G. Thieme Verlag.

- MACKINNON, S. E., NOVAK, C. B., MYCKATYN, T. M. & TUNG, T. H. 2005. Results of reinnervation of the biceps and brachialis muscles with a double fascicular transfer for elbow flexion. *The Journal of hand surgery*, 30, 978-985.
- MAGILL, C. K., TONG, A., KAWAMURA, D., HAYASHI, A., HUNTER, D. A., PARSADANIAN, A., MACKINNON, S. E. & MYCKATYN, T. M. 2007. Reinnervation of the tibialis anterior following sciatic nerve crush injury: a confocal microscopic study in transgenic mice. *Exp Neurol*, 207, 64-74.
- MAGLIONI, S., GIRALDO, D. L., DUARTE, J., VELASCO, N. & ROMERO, E. 2018. *Description of brain volumetric changes in Alzheimer disease using region-based morphometry*, SPIE.
- MALLIK, A. & WEIR, A. I. 2005. Nerve conduction studies: essentials and pitfalls in practice. *Journal of Neurology, Neurosurgery & Psychiatry*, 76, ii23.
- MANN, P. T., FURNESS, J. B., POMPOLO, S. & MÄDER, M. J. J. O. T. A. N. S. 1995. Chemical coding of neurons that project from different regions of intestine to the coeliac ganglion of the guinea pig. 56, 15-25.
- MAR, F. M., BONNI, A. & SOUSA, M. M. 2014. Cell intrinsic control of axon regeneration. *EMBO reports*, 15, 254-263.
- MARAVILLA, K. R. & BOWEN, B. C. 1998. Imaging of the peripheral nervous system: evaluation of peripheral neuropathy and plexopathy. *AJNR Am J Neuroradiol*, 19, 1011-23.
- MARTINI, R., FISCHER, S., LÓPEZ-VALES, R. & DAVID, S. 2008. Interactions between Schwann cells and macrophages in injury and inherited demyelinating disease. *Glia*, 56, 1566-1577.
- MCALLISTER, R. M. R., GILBERT, S. E. A., CALDER, J. S. & SMITH, P. J. 1996. The epidemiology and management of upper limb peripheral nerve injuries in modern practice. *The Journal of Hand Surgery: British & European Volume*, 21, 4-13.

- MCCOMAS, A. J., FAWCETT, P. R., CAMPBELL, M. J. & SICA, R. E. 1971a. Electrophysiological estimation of the number of motor units within a human muscle. *Journal of neurology, neurosurgery, and psychiatry*, 34, 121-131.
- MCCOMAS, A. J., FAWCETT, P. R. W., CAMPBELL, M. J. & SICA, R. E. P. 1971b. Electrophysiological estimation of the number of motor units within a human muscle. *Journal of Neurology, Neurosurgery & Psychiatry*, 34, 121.
- MCDONNELL, M. 2008. Action research arm test. *Aust J Physiother*, 54, 220.
- MEE, B. C., CARROLL, P., DONATELLO, S., CONNOLLY, E., GRIFFIN, M., DUNNE, B., BURKE, L., FLAVIN, R., RIZKALLA, H., RYAN, C., HAYES, B., D'ADHEMAR, C., BANVILLE, N., FAHEEM, N., MULDOON, C. & GAFFNEY, E. F. 2011. Maintaining Breast Cancer Specimen Integrity and Individual or Simultaneous Extraction of Quality DNA, RNA, and Proteins from Allprotect-Stabilized and Nonstabilized Tissue Samples. *Biopreservation and Biobanking*, 9, 389-398.
- MENDLER, L., PINTÉR, S., KIRICSI, M., BAKA, Z. & DUX, L. 2007. Regeneration of Reinnervated Rat Soleus Muscle Is Accompanied by Fiber Transition Toward a Faster Phenotype. *Journal of Histochemistry & Cytochemistry*, 56, 111-123.
- MENORCA, R. M. G., FUSSELL, T. S. & ELFAR, J. C. 2013. Nerve physiology: mechanisms of injury and recovery. *Hand clinics*, 29, 317-330.
- MERCREDI, M., VINCENT, T. J., BIDINOSTI, C. P. & MARTIN, M. 2017. Assessing the accuracy of using oscillating gradient spin echo sequences with AxCaliber to infer micron-sized axon diameters. *Magma*, 30, 1-14.
- MIDHA, R. 1997. Epidemiology of brachial plexus injuries in a multitrauma population. *Neurosurgery*, 40, 1182-8; discussion 1188-9.
- MIETTINEN, M., MCCUE, P. A., SARLOMO-RIKALA, M., BIERNAT, W., CZAPIEWSKI, P., KOPCZYNSKI, J., THOMPSON, L. D., LASOTA, J., WANG, Z. & FETSCH, J. F. 2015. Sox10 – A marker for not only Schwannian

- and melanocytic neoplasms but also myoepithelial cell tumors of soft tissue. A systematic analysis of 5134 tumors. *The American journal of surgical pathology*, 39, 826-835.
- MILEDI, R. & SLATER, C. R. 1970. On the degeneration of rat neuromuscular junctions after nerve section. *The Journal of Physiology*, 207, 507-528.
- MILLES, H. 1985. Peripheral nerve repair: terminology, questions, and facts. *J Reconstr Microsurg*, 2, 21-31.
- MINTZ, E. L., PASSIPIERI, J. A., LOVELL, D. Y. & CHRIST, G. J. 2016. Applications of In Vivo Functional Testing of the Rat Tibialis Anterior for Evaluating Tissue Engineered Skeletal Muscle Repair. *Journal of visualized experiments : JoVE*, 54487.
- MIRSKY, R., WOODHOO, A., PARKINSON, D. B., ARTHUR-FARRAJ, P., BHASKARAN, A. & JESSEN, K. R. 2008. Novel signals controlling embryonic Schwann cell development, myelination and dedifferentiation. *Journal of the peripheral nervous system : JPNS*, 13, 122-135.
- MITOLO, M., STANZANI-MASERATI, M., CAPELLARI, S., TESTA, C., RUCCI, P., PODA, R., OPPI, F., GALLASSI, R., SAMBATI, L., RIZZO, G., PARCHI, P., EVANGELISTI, S., TALOZZI, L., TONON, C., LODI, R. & LIGUORI, R. 2019. Predicting conversion from mild cognitive impairment to Alzheimer's disease using brain (1)H-MRS and volumetric changes: A two- year retrospective follow-up study. *Neuroimage Clin*, 23, 101843.
- MOHTADI, N. G. 2016. Outcome Measure Development. *Instr Course Lect*, 65, 577-82.
- MORISAKI, S., KAWAI, Y., UMEDA, M., NISHI, M., ODA, R., FUJIWARA, H., YAMADA, K., HIGUCHI, T., TANAKA, C., KAWATA, M. & KUBO, T. 2011. In vivo assessment of peripheral nerve regeneration by diffusion tensor imaging. *J Magn Reson Imaging*, 33, 535-42.

- MORROW, J. M., SINCLAIR, C. D., FISCHMANN, A., MACHADO, P. M., REILLY, M. M., YOUSRY, T. A., THORNTON, J. S. & HANNA, M. G. 2016. MRI biomarker assessment of neuromuscular disease progression: a prospective observational cohort study. *Lancet Neurol*, 15, 65-77.
- MOSER, T., KREMER, S. & HOLL, N. 2009. Imagerie du nerf peripherique : anatomie, techniques d'exploration et principales pathologies. *Journal de Radiologie*, 90, 1448.
- MUELLER O, L. S. S. A. 2004. RNA Integrity Number (RIN)—standardization of RNA quality control. *Agilent Application Note, Publication Number-5989-1165EN*, 1-8.
- MÜLLER, M., DOHRN, M. F., ROMANZETTI, S., GADERMAYR, M., REETZ, K., KRÄMER, N. A., KUHL, C., SCHULZ, J. B. & GESS, B. 2020. Semi-automated volumetry of MRI serves as a biomarker in neuromuscular patients. *Muscle & Nerve*, 61, 600-607.
- MURPHY, P. & KOH, D. M. 2010. Imaging in clinical trials. *Cancer imaging : the official publication of the International Cancer Imaging Society*, 10 Spec no A, S74-S82.
- MYDLARZ, W. K. & BOAHENE, K. O. 2013. Sunderland Classification of Nerve Injury. In: KOUNTAKIS, S. E. (ed.) *Encyclopedia of Otolaryngology, Head and Neck Surgery*. Berlin, Heidelberg: Springer Berlin Heidelberg.
- NANDEDKAR, S. D. & BARKHAUS, P. E. 2007. Contribution of reference electrode to the compound muscle action potential. *Muscle Nerve*, 36, 87-92.
- NANDEDKAR, S. D., NANDEDKAR, D. S., BARKHAUS, P. E. & STALBERG, E. V. 2004. Motor unit number index (MUNIX). *IEEE Trans Biomed Eng*, 51, 2209-11.

- NAVARRO, X. 2016. Functional evaluation of peripheral nerve regeneration and target reinnervation in animal models: a critical overview. *The European journal of neuroscience*, 43, 271-286.
- NOAMAN, H. H., SHIHA, A. E. & BAHM, J. 2004. Oberlin's ulnar nerve transfer to the biceps motor nerve in obstetric brachial plexus palsy: indications, and good and bad results. *Microsurgery*, 24, 182-187.
- NONAKA, D., CHIRIBOGA, L. & RUBIN, B. P. 2008. Sox10: a pan-schwannian and melanocytic marker. *The American journal of surgical pathology*, 32, 1291-1298.
- NOVAK, J. & SALAFSKY, B. 1967. Early electrophysiological changes after denervation of slow skeletal muscle. *Experimental Neurology*, 19, 388-400.
- O'BRIEN, T. D., REEVES, N. D., BALZOPoulos, V., JONES, D. A. & MAGANARIS, C. N. 2009. Strong relationships exist between muscle volume, joint power and whole-body external mechanical power in adults and children. *Exp Physiol*, 94, 731-8.
- OBERLIN, C., BEAL, D., LEECHAVENGVONGS, S., SALON, A., DAUGE, M. C. & SARCY, J. J. 1994. Nerve transfer to biceps muscle using a part of ulnar nerve for C5-C6 avulsion of the brachial plexus: anatomical study and report of four cases. *The Journal of hand surgery*, 19, 232-237.
- OCHOA, J. & MAIR, W. G. 1969. The normal sural nerve in man. II. Changes in the axons and Schwann cells due to ageing. *Acta neuropathologica*, 13, 217-239.
- OHANA, M., MOSER, T., MOUSSAOÛI, A., KREMER, S., CARLIER, R. Y., LIVERNEAUX, P. & DIETEMANN, J. L. 2014. Current and future imaging of the peripheral nervous system. *Diagnostic and Interventional Imaging*, 95, 17-26.

- OLNEY, R. K., BUDINGEN, H. J. & MILLER, R. G. 1987. The effect of temporal dispersion on compound action potential area in human peripheral nerve. *Muscle Nerve*, 10, 728-33.
- PAINTER, M. W. 2017. Aging Schwann cells: mechanisms, implications, future directions. *Current opinion in neurobiology*, 47, 203-208.
- PANEGYRES, P. K., MOORE, N., GIBSON, R., RUSHWORTH, G. & DONAGHY, M. 1993. Thoracic outlet syndromes and magnetic resonance imaging. *Brain*, 116, 823-841.
- PARKINSON, D. B., BHASKARAN, A., ARTHUR-FARRAJ, P., NOON, L. A., WOODHOO, A., LLOYD, A. C., FELTRI, M. L., WRABETZ, L., BEHRENS, A., MIRSKY, R. & JESSEN, K. R. 2008. c-Jun is a negative regulator of myelination. *Journal of Cell Biology*, 181, 625-637.
- PARKINSON, D. B., BHASKARAN, A., DROGGITI, A., DICKINSON, S., D'ANTONIO, M., MIRSKY, R. & JESSEN, K. R. 2004. Krox-20 inhibits Jun-NH2-terminal kinase/c-Jun to control Schwann cell proliferation and death. *The Journal of cell biology*, 164, 385-394.
- PARRINELLO, S., NAPOLI, I., RIBEIRO, S., DIGBY, P. W., FEDOROVA, M., PARKINSON, D. B., DODDRELL, R. D., NAKAYAMA, M., ADAMS, R. H. & LLOYD, A. C. 2010. EphB signaling directs peripheral nerve regeneration through Sox2-dependent Schwann cell sorting. *Cell*, 143, 145-155.
- PARSONS, E. C., JR., DOES, M. D. & GORE, J. C. 2006. Temporal diffusion spectroscopy: theory and implementation in restricted systems using oscillating gradients. *Magn Reson Med*, 55, 75-84.
- PATEL, P. G., SELVARAJAH, S., GUÉRARD, K.-P., BARTLETT, J. M. S., LAPOINTE, J., BERMAN, D. M., OKELLO, J. B. A. & PARK, P. C. 2017. Reliability and performance of commercial RNA and DNA extraction kits for FFPE tissue cores. *PLoS ONE*, 12, e0179732-e0179732.

- PAVLOV, S., GROSHEVA, M., STREPPPEL, M., GUNTINAS-LICHIUS, O., IRINTCHEV, A., SKOURAS, E., ANGELOVA, S., KUERTEN, S., SINIS, N., DUNLOP, S. & ANGELOV, D. 2008. Manually-stimulated recovery of motor function after facial nerve injury requires intact sensory input. *Experimental neurology*, 211, 292-300.
- PEETERS, M., HUANG, C. L., VONK, L. A., LU, Z. F., BANK, R. A., HELDER, M. N. & DOULABI, B. Z. 2016. Optimisation of high-quality total ribonucleic acid isolation from cartilaginous tissues for real-time polymerase chain reaction analysis. *Bone & Joint Research*, 5, 560-568.
- PEKER, T., GÜLEKON, N., COŞKUN, Z. K. & OMERÖĞLU, S. 2013. Investigation of the nerve distribution pattern of leg muscles in rat. *Anat Sci Int*, 88, 83-90.
- PETRONE, P. M., CASAMITJANA, A., FALCON, C., ARTIGUES, M., OPERTO, G., SKOURAS, S., CACCIAGLIA, R., MOLINUEVO, J. L., VILAPLANA, V., GISPERT, J. D. & SALVADÓ, G. 2018. CHARACTERISTIC BRAIN VOLUMETRIC CHANGES IN THE AD PRECLINICAL SIGNATURE. *Alzheimer's & Dementia: The Journal of the Alzheimer's Association*, 14, P1235.
- PETTE, D. & VRBOVA, G. 1985. Neural control of phenotypic expression in mammalian muscle fibers. *Muscle Nerve*, 8, 676-89.
- PEYRONNARD, J. M. & LAMARRE, Y. 1977. Electrophysiological and anatomical estimation of the number of motor units in the monkey extensor digitorum brevis muscle. *Journal of neurology, neurosurgery, and psychiatry*, 40, 756-764.
- PIASECKI, M., IRELAND, A., PIASECKI, J., STASHUK, D. W., MCPHEE, J. S. & JONES, D. A. 2018. The reliability of methods to estimate the number and size of human motor units and their use with large limb muscles. *European journal of applied physiology*, 118, 767-775.

- POLAK, J. F., JOLESZ, F. A. & ADAMS, D. F. 1988. Magnetic resonance imaging of skeletal muscle. Prolongation of T1 and T2 subsequent to denervation. *Invest Radiol*, 23, 365-9.
- POPOVA, T., MENNERICH, D., WEITH, A. & QUAST, K. 2008. Effect of RNA quality on transcript intensity levels in microarray analysis of human post-mortem brain tissues. *BMC genomics*, 9, 91-91.
- POWER, G. A., DALTON, B. H., BEHM, D. G., DOHERTY, T. J., VANDERVOORT, A. A. & RICE, C. L. 2012. Motor unit survival in lifelong runners is muscle dependent. *Med Sci Sports Exerc*, 44, 1235-42.
- QUICK, T. J., SINGH, A. K., FOX, M., SINISI, M. & MACQUILLAN, A. 2016. A quantitative assessment of the functional recovery of flexion of the elbow after nerve transfer in patients with a brachial plexus injury. *The bone & joint journal*, 98-B, 1517-1520.
- RAINEY, E. E., PETREY, L. B., REYNOLDS, M., AGTARAP, S. & WARREN, A. M. 2014. Psychological factors predicting outcome after traumatic injury: the role of resilience. *Am J Surg*, 208, 517-23.
- RAY, W. Z. & MACKINNON, S. E. 2010. Management of nerve gaps: autografts, allografts, nerve transfers, and end-to-side neuroorrhaphy. *Experimental neurology*, 223, 77-85.
- RAYNER, M. L. D., BROWN, H. L., WILCOX, M., PHILLIPS, J. B. & QUICK, T. J. 2019. Quantifying regeneration in patients following peripheral nerve injury. *Journal of Plastic, Reconstructive & Aesthetic Surgery*.
- REAUME, A. G., ELLIOTT, J. L., HOFFMAN, E. K., KOWALL, N. W., FERRANTE, R. J., SIWEK, D. F., WILCOX, H. M., FLOOD, D. G., BEAL, M. F., BROWN, R. H., JR., SCOTT, R. W. & SNIDER, W. D. 1996. Motor neurons in Cu/Zn superoxide dismutase-deficient mice develop normally but exhibit enhanced cell death after axonal injury. *Nat Genet*, 13, 43-7.

- REICHARDT, L. F. 2006. Neurotrophin-regulated signalling pathways. *Philos Trans R Soc Lond B Biol Sci*, 361, 1545-64.
- REICHMAN, D. E. & GREENBERG, J. A. 2009. Reducing surgical site infections: a review. *Reviews in obstetrics & gynecology*, 2, 212-221.
- ROBERT, M. B., PEGGY, M., JEAN, M. M. & FRANK, P. H. 1995. Continuous intraoperative electromyographic recording during spinal surgery. *Journal of Neurosurgery*, 82, 401-405.
- ROGERS-BROADWAY, K.-R. & KARTERIS, E. 2015. Amplification efficiency and thermal stability of qPCR instrumentation: Current landscape and future perspectives. *Experimental and Therapeutic Medicine*, 10, 1261-1264.
- RONCHI, G., MORANO, M., FREGNAN, F., PUGLIESE, P., CROSIO, A., TOS, P., GEUNA, S., HAASSTERT-TALINI, K. & GAMBAROTTA, G. 2019. The Median Nerve Injury Model in Pre-clinical Research – A Critical Review on Benefits and Limitations. *Frontiers in Cellular Neuroscience*, 13.
- RONCHI, G. & RAIMONDO, S. 2017. Chronically denervated distal nerve stump inhibits peripheral nerve regeneration. *Neural regeneration research*, 12, 739-740.
- ROSE, D., KURTIS, I. A., CYNTHIA, T. C., JOHN, W. E. & PHILIP, R. W. 2010. Magnetic resonance neurography for the evaluation of peripheral nerve, brachial plexus, and nerve root disorders. *Journal of Neurosurgery JNS*, 112, 362-371.
- ROSEN, B. & LUNDBORG, G. 2003. A new model instrument for outcome after nerve repair. *Hand Clin*, 19, 463-70.
- ROSSOR, A. M., SHY, M. E. & REILLY, M. M. 2020. Are we prepared for clinical trials in Charcot-Marie-Tooth disease? *Brain Res*, 1729, 146625.
- ROTSHENKER, S. 2011. Wallerian degeneration: the innate-immune response to traumatic nerve injury. *Journal of Neuroinflammation*, 8, 109-109.

- RUEDEN, C. T., SCHINDELIN, J., HINER, M. C., DEZONIA, B. E., WALTER, A. E., ARENA, E. T. & ELICEIRI, K. W. 2017. ImageJ2: ImageJ for the next generation of scientific image data. *BMC bioinformatics*, 18, 529-529.
- RUETTGER, A., NEUMANN, S., WIEDERANDERS, B. & HUBER, R. 2010. Comparison of different methods for preparation and characterization of total RNA from cartilage samples to uncover osteoarthritis in vivo. *BMC Research Notes*, 3, 7-7.
- SAITO, H. & DAHLIN, L. B. 2008. Expression of ATF3 and axonal outgrowth are impaired after delayed nerve repair. *BMC neuroscience*, 9, 88-88.
- SAMADANI, A. A., NIKBAKHSH, N., FATTAHI, S., POURBAGHER, R., AGHAJANPOUR MIR, S. M., MOUSAVI KANI, N., ABEDIAN, Z. & AKHAVANNIAKI, H. 2015. RNA Extraction from Animal and Human's Cancerous Tissues: Does Tissue Matter? *International Journal of Molecular and Cellular Medicine*, 4, 54-59.
- SANCHIS-MOYSI, J., IDOATE, F., SERRANO-SANCHEZ, J. A., DORADO, C. & CALBET, J. A. L. 2012. Muscle hypertrophy in prepubescent tennis players: a segmentation MRI study. *PloS one*, 7, e33622-e33622.
- SANDER, H. W. & OH, S. J. 2006. Temporal Dispersion Terminology: Multiphasic and Multiturn CMAPs. *Journal of Clinical Neuromuscular Disease*, 7, 173-174.
- SCHEIB, J. & HOKE, A. 2013. Advances in peripheral nerve regeneration. *Nature reviews. Neurology*, 9, 668-676.
- SCHEIB, J. & HÖKE, A. 2016. Impaired regeneration in aged nerves: Clearing out the old to make way for the new. *Experimental neurology*.
- SCHEMANN, M., SANN, H., SCHAAF, C., MADER, M. J. A. J. O. P.-G. & PHYSIOLOGY, L. 1993. Identification of cholinergic neurons in enteric nervous system by antibodies against choline acetyltransferase. 265, G1005-G1009.

- SCHEMANN, M., SCHAAF, C. & MÄDER, M. J. J. O. C. N. 1995. Neurochemical coding of enteric neurons in the guinea pig stomach. 353, 161-178.
- SCHROEDER, A., MUELLER, O., STOCKER, S., SALOWSKY, R., LEIBER, M., GASSMANN, M., LIGHTFOOT, S., MENZEL, W., GRANZOW, M. & RAGG, T. 2006. The RIN: an RNA integrity number for assigning integrity values to RNA measurements. *BMC Molecular Biology*, 7, 3-3.
- SEBBEN, J. E. 1983. Surgical antiseptics. *J Am Acad Dermatol*, 9, 759-65.
- SEDDON, H. J., MEDAWAR, P. B. & SMITH, H. 1943. Rate of regeneration of peripheral nerves in man. *J Physiol*, 102, 191-215.
- SEDDON, H. J. B. 1943. Three types of nerve injury. 66, 237-288.
- SEDGWICK, P. 2015. Clinical trials: outcome measures. *BMJ : British Medical Journal*, 350, h121.
- SEITZ, M., GROSHEVA, M., SKOURAS, E., ANGELOVA, S. K., ANKERNE, J., JUNGNICHEL, J., GROTHE, C., KLIMASCHEWSKI, L., HÜBBERS, C., DUNLOP, S. & ANGELOV, D. 2011. Poor functional recovery and muscle polyinnervation after facial nerve injury in fibroblast growth factor-2-/- mice can be improved by manual stimulation of denervated vibrissal muscles. *Neuroscience*, 182, 241-7.
- SEROR, P. 2017. Neuralgic amyotrophy. An update. *Joint Bone Spine*, 84, 153-158.
- SEVERINSEN, K. & JAKOBSEN, J. 2009. Chromatolysis. In: BINDER, M. D., HIROKAWA, N. & WINDHORST, U. (eds.) *Encyclopedia of Neuroscience*. Berlin, Heidelberg: Springer Berlin Heidelberg.
- SHEFNER, J. M. 2001. Motor unit number estimation in human neurological diseases and animal models. *Clinical neurophysiology : official journal of the International Federation of Clinical Neurophysiology*, 112, 955-964.
- SHEFNER, J. M., BROWN, R. H., COLE, D., CHATURVEDI, P., SCHOENFELD, D., PASTUSZAK, K., MATTHEWS, R., UPTON-RICE, M. & CUDKOWICZ, M. E.

2001. Effect of neurophilin ligands on motor units in mice with SOD1 ALS mutations. *57*, 1857-1861.
- SHEFNER, J. M., CUDKOWICZ, M. & BROWN, R. H., JR. 2006. Motor unit number estimation predicts disease onset and survival in a transgenic mouse model of amyotrophic lateral sclerosis. *Muscle Nerve*, *34*, 603-7.
- SHEFNER, J. M., REAUME, A. G., FLOOD, D. G., SCOTT, R. W., KOWALL, N. W., FERRANTE, R. J., SIWEK, D. F., UPTON-RICE, M. & BROWN, R. H. 1999. Mice lacking cytosolic copper/zinc superoxide dismutase display a distinctive motor axonopathy. *53*, 1239-1239.
- SHEMESH, N., ALVAREZ, G. A. & FRYDMAN, L. 2015. Size Distribution Imaging by Non-Uniform Oscillating-Gradient Spin Echo (NOGSE) MRI. *PLoS One*, *10*, e0133201.
- SHEN, Q., LOEWENSTEIN, D. A., POTTER, E., ZHAO, W., APPEL, J., GREIG, M. T., RAJ, A., ACEVEDO, A., SCHOFIELD, E., BARKER, W., WU, Y., POTTER, H. & DUARA, R. 2011. Volumetric and visual rating of magnetic resonance imaging scans in the diagnosis of amnesic mild cognitive impairment and Alzheimer's disease. *Alzheimer's & dementia : the journal of the Alzheimer's Association*, *7*, e101-e108.
- SHY, M., SHI, Y.-J., WRABETZ, L., KAMHOLZ, J. & SCHERER, S. 1996. Axon-Schwann cell interactions regulate the expression of c-jun in Schwann cells. *Journal of neuroscience research*, *43*, 511-525.
- SIMON, N. G., TALBOTT, J., CHIN, C. T. & KLIOT, M. 2016a. Chapter 40 - Peripheral nerve imaging. *In: MASDEU, J. C. & GONZÁLEZ, R. G. (eds.) Handbook of Clinical Neurology*. Elsevier.
- SIMON, N. G., TALBOTT, J., CHIN, C. T. & KLIOT, M. 2016b. Peripheral nerve imaging. *Handb Clin Neurol*, *136*, 811-26.

- SINIS, N., MANOLI, T., SCHIEFER, J. L., WERDIN, F., JAMINET, P., KRAUS, A., FORNARO, M., RAIMONDO, S., GEUNA, S. & SCHALLER, H.-E. 2011. Application of 2 different hemostatic procedures during microsurgical median nerve reconstruction in the rat does not hinder axonal regeneration. *Neurosurgery*, 68, 1399-1404.
- SLED, J. G., ZIJDENBOS, A. P. & EVANS, A. C. 1998. A nonparametric method for automatic correction of intensity nonuniformity in MRI data. *IEEE Trans Med Imaging*, 17, 87-97.
- SLIMP, J. C. 2000. Intraoperative monitoring of nerve repairs. *Hand clinics*, 16, 25-36.
- SMITH, J. W. & THESLEFF, S. 1976. Spontaneous activity in denervated mouse diaphragm muscle. *The Journal of Physiology*, 257, 171-186.
- SMITH, S. & KNIGHT, R. 2011. Clinical Neurophysiology in Peripheral Nerve Injuries BT - Surgical Disorders of the Peripheral Nerves. *In: BIRCH, R. (ed.)*. London: Springer London.
- SOLLERMAN, C. & EJESKAR, A. 1995. Sollerman hand function test. A standardised method and its use in tetraplegic patients. *Scand J Plast Reconstr Surg Hand Surg*, 29, 167-76.
- SPANDIDOS, A., WANG, X., WANG, H., DRAGNEV, S., THURBER, T. & SEED, B. 2008. A comprehensive collection of experimentally validated primers for Polymerase Chain Reaction quantitation of murine transcript abundance. *BMC genomics*, 9, 633-633.
- STALBERG, E. & FALCK, B. 1997. The role of electromyography in neurology. *Electroencephalogr Clin Neurophysiol*, 103, 579-98.
- STANISZ, G. J., MIDHA, R., MUNRO, C. A. & HENKELMAN, R. M. 2001. MR properties of rat sciatic nerve following trauma. *Magn Reson Med*, 45, 415-20.

- STASSART, R. M., MÖBIUS, W., NAVE, K.-A. & EDGAR, J. M. 2018. The Axon-Myelin Unit in Development and Degenerative Disease. 12.
- STEIN, R. B. & YANG, J. F. 1990. Methods for estimating the number of motor units in human muscles. 28, 487-495.
- STENBERG, L. & DAHLIN, L. B. 2014. Gender differences in nerve regeneration after sciatic nerve injury and repair in healthy and in type 2 diabetic Goto-Kakizaki rats. *BMC neuroscience*, 15, 107-107.
- STRONG, M. J., BROWN, W. F., HUDSON, A. J. & SNOW, R. 1988. Motor unit estimates in the biceps-brachialis in amyotrophic lateral sclerosis. *Muscle Nerve*, 11, 415-22.
- STURMA, A., HRUBY, L. A., PRAHM, C., MAYER, J. A. & ASZMANN, O. C. 2018. Rehabilitation of Upper Extremity Nerve Injuries Using Surface EMG Biofeedback: Protocols for Clinical Application. *Frontiers in neuroscience*, 12, 906-906.
- SULAIMAN, O. A. & GORDON, T. 2000. Effects of short- and long-term Schwann cell denervation on peripheral nerve regeneration, myelination, and size. *Glia*, 32, 234-246.
- SULAIMAN, O. A. R., MIDHA, R., MUNRO, C. A., MATSUYAMA, T., AL-MAJED, A. & GORDON, T. 2002. Chronic Schwann cell denervation and the presence of a sensory nerve reduce motor axonal regeneration. *Experimental neurology*, 176, 342-354.
- SULAIMAN, W. & GORDON, T. 2013. Neurobiology of peripheral nerve injury, regeneration, and functional recovery: from bench top research to bedside application. *The Ochsner journal*, 13, 100-108.
- SUNDERLAND, S. 1947. RATE OF REGENERATION IN HUMAN PERIPHERAL NERVES: Analysis of the Interval Between Injury and Onset of Recovery. *Archives of Neurology & Psychiatry*, 58, 251-295.

- SUNDERLAND, S. 1951. A classification of peripheral nerve injuries producing loss of function. *Brain*, 74, 491-516.
- SUTTER, M., EGGSPUEHLER, A., MULLER, A. & DVORAK, J. 2007. Multimodal intraoperative monitoring: an overview and proposal of methodology based on 1,017 cases. *European spine journal : official publication of the European Spine Society, the European Spinal Deformity Society, and the European Section of the Cervical Spine Research Society*, 16 Suppl 2, S153-S161.
- SUZUKI, K., LOVERA, M., SCHMACHTENBERG, O. & COUVE, E. 2015. Axonal degeneration in dental pulp precedes human primary teeth exfoliation. *Journal of dental research*, 94, 1446-1453.
- TABOROWSKA, M., BUKOWSKA, D., DRZYMAŁA-CELICHOWSKA, H., MIERZEJEWSKA-KRZYŻOWSKA, B. & CELICHOWSKI, J. 2016. Morphometric properties and innervation of muscle compartments in rat medial gastrocnemius. *Somatosens Mot Res*, 33, 200-208.
- TAGLIAFICO, A., TAGLIAFICO, G. & MARTINOLI, C. 2010. Nerve Density: A New Parameter to Evaluate Peripheral Nerve Pathology on Ultrasound. Preliminary Study. *Ultrasound in Medicine & Biology*, 36, 1588-1593.
- TAKEHARA, I., CHU, J., SCHWARTZ, I. & AYE, H. H. 2004. Motor unit action potential (MUAP) parameters affected by editing duration cursors. *Electromyogr Clin Neurophysiol*, 44, 265-9.
- TERENGI, G., CALDER, J. S., BIRCH, R. & HALL, S. M. 1998. A morphological study of Schwann cells and axonal regeneration in chronically transected human peripheral nerves. *Journal of hand surgery (Edinburgh, Scotland)*, 23, 583-587.
- THOMAS, P. K. 1963. The connective tissue of peripheral nerve: An electron microscope study. *Journal of Anatomy*, 97, 35-44.4.

- TIMOTHY, H. 2014. Nerve injury: Classification, clinical assessment, investigation, and management. *Handchirurgie Weltweit e.V., editor. Living Textbook of Hand Surgery*. Cologne: gms.
- TITELBAUM, D. S., FRAZIER, J. L., GROSSMAN, R. I., JOSEPH, P. M., YU, L. T., KASSAB, E. A., HICKEY, W. F., LAROSSA, D. & BROWN, M. J. 1989. Wallerian degeneration and inflammation in rat peripheral nerve detected by in vivo MR imaging. *AJNR Am J Neuroradiol*, 10, 741-6.
- TOMITA, K., KUBO, T., MATSUDA, K., FUJIWARA, T., YANO, K., WINOGRAD, J. M., TOHYAMA, M. & HOSOKAWA, K. 2007. The neurotrophin receptor p75NTR in Schwann cells is implicated in remyelination and motor recovery after peripheral nerve injury. *Glia*, 55, 1199-1208.
- TUNG, T. H. & MACKINNON, S. E. 2010. Nerve transfers: indications, techniques, and outcomes. *The Journal of hand surgery*, 35, 332-341.
- VALERO-CABRÉ, A. & NAVARRO, X. 2001. H reflex restitution and facilitation after different types of peripheral nerve injury and repair. *Brain Research*, 919, 302-312.
- VAN ROSMALEN, M., LIEBA-SAMAL, D., PILLEN, S. & VAN ALFEN, N. 2019. Ultrasound of peripheral nerves in neuralgic amyotrophy. *Muscle Nerve*, 59, 55-59.
- VANNUCCI, B., SANTOSA, K. B., KEANE, A. M., JABLONKA-SHARIFF, A., LU, C. Y., YAN, Y., MACEWAN, M. & SNYDER-WARWICK, A. K. 2019. What is Normal? Neuromuscular junction reinnervation after nerve injury. *Muscle Nerve*, 60, 604-612.
- VIDDELEER, A. R., SIJENS, P. E., VAN OOIJEN, P. M. A., KUYPERS, P. D. L., HOVIUS, S. E. R., DE DEYN, P. P. & OUDKERK, M. 2016. Quantitative STIR of muscle for monitoring nerve regeneration. *Journal of magnetic resonance imaging : JMRI*, 44, 401-410.

- VIDDELEER, A. R., SIJENS, P. E., VAN Ooyen, P. M. A., KUYPERS, P. D. L., HOVIUS, S. E. R. & OUDKERK, M. 2012. Sequential MR imaging of denervated and reinnervated skeletal muscle as correlated to functional outcome. *Radiology*, 264, 522-530.
- VIDT, M. E., DALY, M., MILLER, M. E., DAVIS, C. C., MARSH, A. P. & SAUL, K. R. 2012. Characterizing upper limb muscle volume and strength in older adults: A comparison with young adults. *Journal of Biomechanics*, 45, 334-341.
- VISSER, L. H. 2006. High-resolution sonography of the common peroneal nerve: Detection of intraneural ganglia. *Neurology*, 67, 1473.
- VOLK, G. F., KARAMYAN, I., KLINGNER, C. M., REICHENBACH, J. R. & GUNTINAS-LICHIUS, O. 2014. Quantitative magnetic resonance imaging volumetry of facial muscles in healthy patients with facial palsy. *Plastic and reconstructive surgery. Global open*, 2, e173-e173.
- VOYTIK, S. L., PRZYBORSKI, M., BADYLAK, S. F. & KONIECZNY, S. F. 1993. Differential expression of muscle regulatory factor genes in normal and denervated adult rat hindlimb muscles. *Dev Dyn*, 198, 214-24.
- WALI, A. R., SANTIAGO-DIEPPA, D. R., BROWN, J. M. & MANDEVILLE, R. 2017. Nerve transfer versus muscle transfer to restore elbow flexion after pan-brachial plexus injury: a cost-effectiveness analysis. *Neurosurg Focus*, 43, E4.
- WALKER, D. G., WHETZEL, A. M., SERRANO, G., SUE, L. I., LUE, L.-F. & BEACH, T. G. 2016. Characterization of RNA isolated from eighteen different human tissues: results from a rapid human autopsy program. *Cell and tissue banking*, 17, 361-375.
- WALLER AUGUSTUS, V. & OWEN, R. 1851. Experiments on the section of the glossopharyngeal and hypoglossal nerves of the frog, and observations of the alterations produced thereby in the structure of their primitive fibres. *Abstracts of the Papers Communicated to the Royal Society of London*, 5, 924-925.

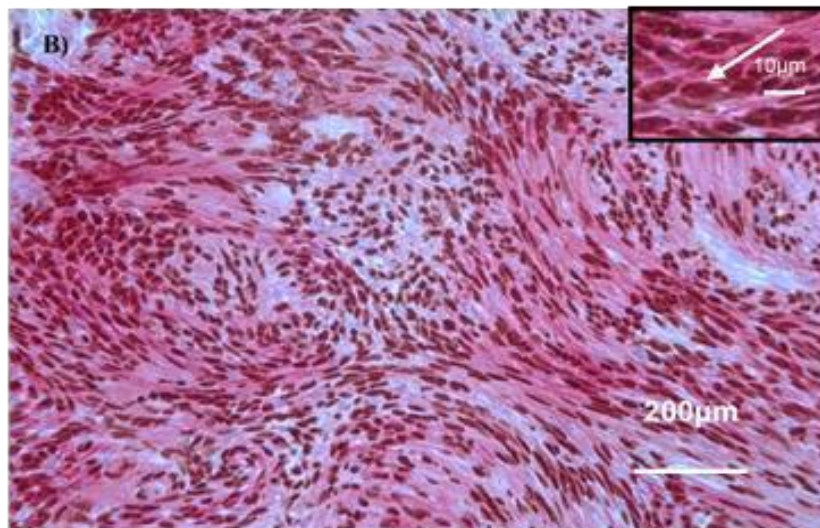
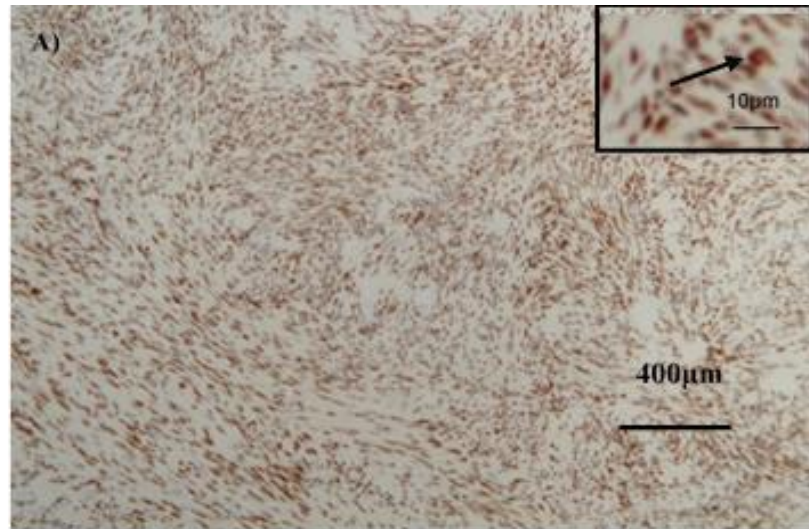
- WANG, F. C. & DELWAIDE, P. J. 1995. Number and relative size of thenar motor units estimated by an adapted multiple point stimulation method. *Muscle Nerve*, 18, 969-79.
- WANG, X. & SEED, B. 2003. A PCR primer bank for quantitative gene expression analysis. *Nucleic acids research*, 31, e154-e154.
- WEINSTEIN, S. 1993. Fifty years of somatosensory research: from the Semmes-Weinstein monofilaments to the Weinstein Enhanced Sensory Test. *J Hand Ther*, 6, 11-22; discussion 50.
- WEIS, J., KAUSSEN, M., CALVO, S. & BUONANNO, A. 2000. Denervation induces a rapid nuclear accumulation of MRF4 in mature myofibers. *Dev Dyn*, 218, 438-51.
- WENG, J., ZHANG, P., YIN, X. & JIANG, B. 2018. The Whole Transcriptome Involved in Denervated Muscle Atrophy Following Peripheral Nerve Injury.
- WENG, L. Y., HSIEH, C. L., TUNG, K. Y., WANG, T. J., OU, Y. C., CHEN, L. R., BAN, S. L., CHEN, W. W. & LIU, C. F. 2010. Excellent reliability of the Sollerman hand function test for patients with burned hands. *J Burn Care Res*, 31, 904-10.
- WESSIG, C., KOLTZENBURG, M., REINERS, K., SOLYMOSI, L. & BENDSZUS, M. 2004. Muscle magnetic resonance imaging of denervation and reinnervation: correlation with electrophysiology and histology. *Experimental neurology*, 185, 254-261.
- WEST, G. A., HAYNOR, D. R., GOODKIN, R., TSURUDA, J. S., BRONSTEIN, A. D., KRAFT, G., WINTER, T. & KLIOT, M. 1994. Magnetic Resonance Imaging Signal Changes in Denervated Muscles after Peripheral Nerve Injury. *Neurosurgery*, 35, 1077-1086.

- WILCOX, M., BROWN, H., JOHNSON, K., SINISI, M. & QUICK, T. 2019a. An assessment of fatigability following nerve transfer to reinnervate elbow flexor muscles. *The Bone & Joint Journal*, 101-B, 867-871.
- WILCOX, M., GREGORY, H., POWELL, R., QUICK, T. J. & PHILLIPS, J. B. 2020a. Strategies for Peripheral Nerve Repair. *Current Tissue Microenvironment Reports*.
- WILCOX, M., GREGORY, H., POWELL, R., QUICK, T. J. & PHILLIPS, J. B. 2020b. Strategies for Peripheral Nerve Repair. *Current Tissue Microenvironment Reports*, 1, 49-59.
- WILCOX, M., QUICK, T. J. & PHILLIPS, J. B. 2019b. The Effects of Surgical Antiseptics and Time Delays on RNA Isolated From Human and Rodent Peripheral Nerves. *Frontiers in Cellular Neuroscience*, 13, 189-189.
- WILCOX, M. B., LARANJEIRA, S. G., ERIKSSON, T. M., JESSEN, K. R., MIRSKY, R., QUICK, T. J. & PHILLIPS, J. B. 2020c. Characterising cellular and molecular features of human peripheral nerve degeneration. *Acta Neuropathologica Communications*, 8, 51.
- WILKES, T. M., DEVONSHIRE, A. S., ELLISON, S. L. R. & FOY, C. A. 2010. Evaluation of a novel approach for the measurement of RNA quality. *BMC Research Notes*, 3, 89-89.
- WINDISCH, A., GUNDERSEN, K., SZABOLCS, M. J., GRUBER, H. & LØMO, T. 1998. Fast to slow transformation of denervated and electrically stimulated rat muscle. 510, 623-632.
- WOOD, M. D., KEMP, S. W., WEBER, C., BORSCHHEL, G. H. & GORDON, T. 2011a. Outcome measures of peripheral nerve regeneration. *Ann Anat*, 193, 321-33.
- WOOD, M. D., KEMP, S. W. P., WEBER, C., BORSCHHEL, G. H. & GORDON, T. 2011b. Outcome measures of peripheral nerve regeneration. *Annals of Anatomy - Anatomischer Anzeiger*, 193, 321-333.

- WU, G., XU, S., CHEN, B. & WU, P. 2017. Relationship between changes in muscle fibers and CMAP in skeletal muscle with different stages of aging. *Int J Clin Exp Pathol*, 10, 11888-11895.
- WU, P., CHAWLA, A., SPINNER, R. J., YU, C., YASZEMSKI, M. J., WINDEBANK, A. J. & WANG, H. 2014. Key changes in denervated muscles and their impact on regeneration and reinnervation. *Neural regeneration research*, 9, 1796-1809.
- YAMAMOTO, T., NAKASHIMA, K., MARUTA, Y., KIRIYAMA, T., SASAKI, M., SUGIYAMA, S., SUZUKI, K., FUJISAKI, H., SASAKI, J., KAKU-USHIKI, Y., TANIDA, M., IRIE, S. & HATTORI, S. 2012. Improved RNA extraction method using the BioMasher and BioMasher power-plus. *The Journal of veterinary medical science*, 74, 1561-1567.
- YANG, D. P., ZHANG, D. P., MAK, K. S., BONDER, D. E., POMEROY, S. L. & KIM, H. A. 2008. Schwann cell proliferation during Wallerian degeneration is not necessary for regeneration and remyelination of the peripheral nerves: axon-dependent removal of newly generated Schwann cells by apoptosis. *Molecular and cellular neurosciences*, 38, 80-88.
- YARNITSKY, D. & SPRECHER, E. 1994. Thermal testing: normative data and repeatability for various test algorithms. *J Neurol Sci*, 125, 39-45.
- YI, S., TANG, X., YU, J., LIU, J., DING, F. & GU, X. 2017. Microarray and qPCR Analyses of Wallerian Degeneration in Rat Sciatic Nerves. *Frontiers in cellular neuroscience*, 11, 22-22.
- YOCKTENG, R., ALMEIDA, A. M. R., YEE, S., ANDRE, T., HILL, C. & SPECHT, C. D. 2013. A method for extracting high-quality RNA from diverse plants for next-generation sequencing and gene expression analyses. *Applications in Plant Sciences*, 1, apps.1300070-apps.1300070.

ZIVADINOV, R., KHAN, N., MEDIN, J., CHRISTOFFERSEN, P., PRICE, J., KORN, J. R., BONZANI, I., DWYER, M. G., BERGSLAND, N., CARL, E., SILVA, D. & WEINSTOCK-GUTTMAN, B. 2017. An Observational Study to Assess Brain MRI Change and Disease Progression in Multiple Sclerosis Clinical Practice-The MS-MRIUS Study. *Journal of neuroimaging : official journal of the American Society of Neuroimaging*, 27, 339-347.

Appendix 1



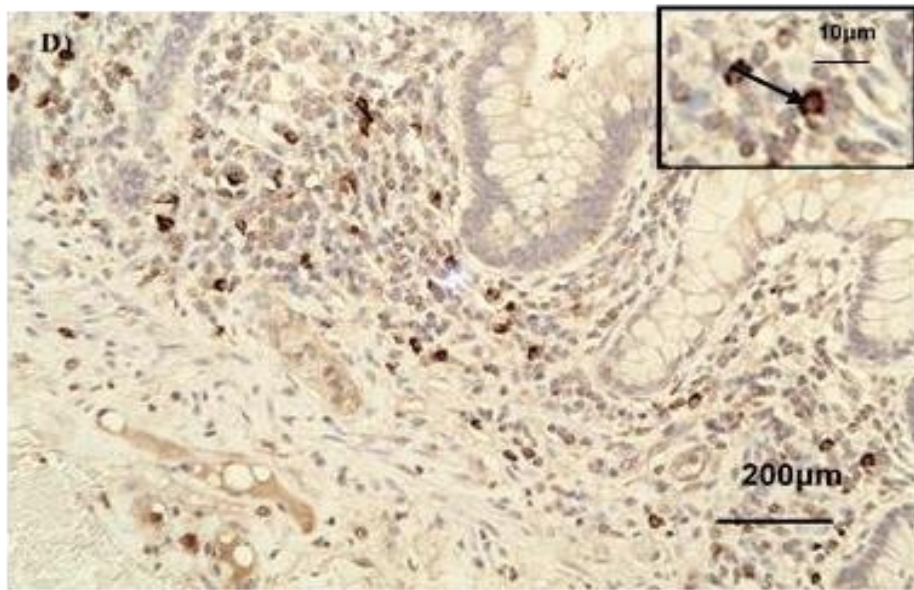
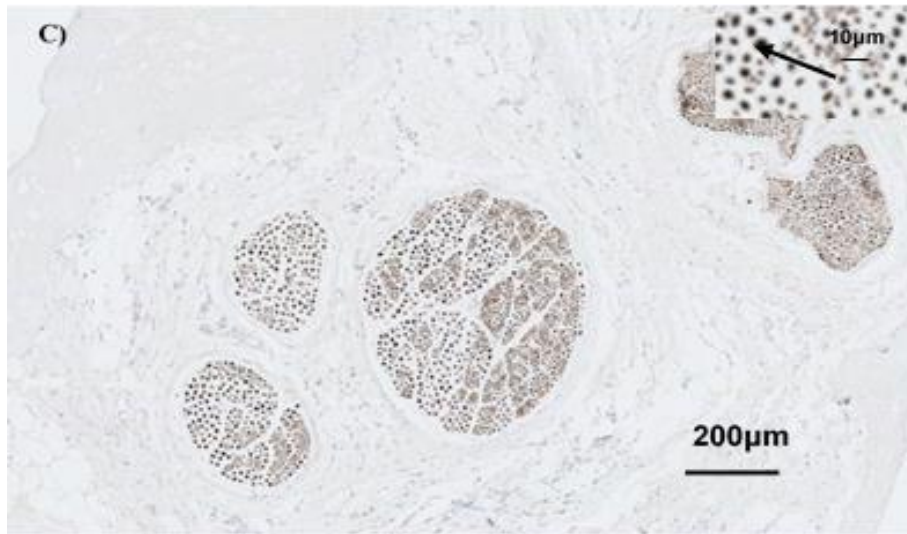


Figure 9.1 – Positive controls for immunohistochemistry. The black arrows in the micrographs indicate positive staining. **a)** Staining of Schwannoma for c-Jun (brown), **b)** co-staining of Schwannoma tissue for SOX10 (brown) and P75NTR (red), **c)** neurofilament (brown) staining of uninjured sural nerve, **d)** human colon stained for Krox-20 (brown). The black arrows indicate cells that are positive for the marker of interest.

Appendix 2

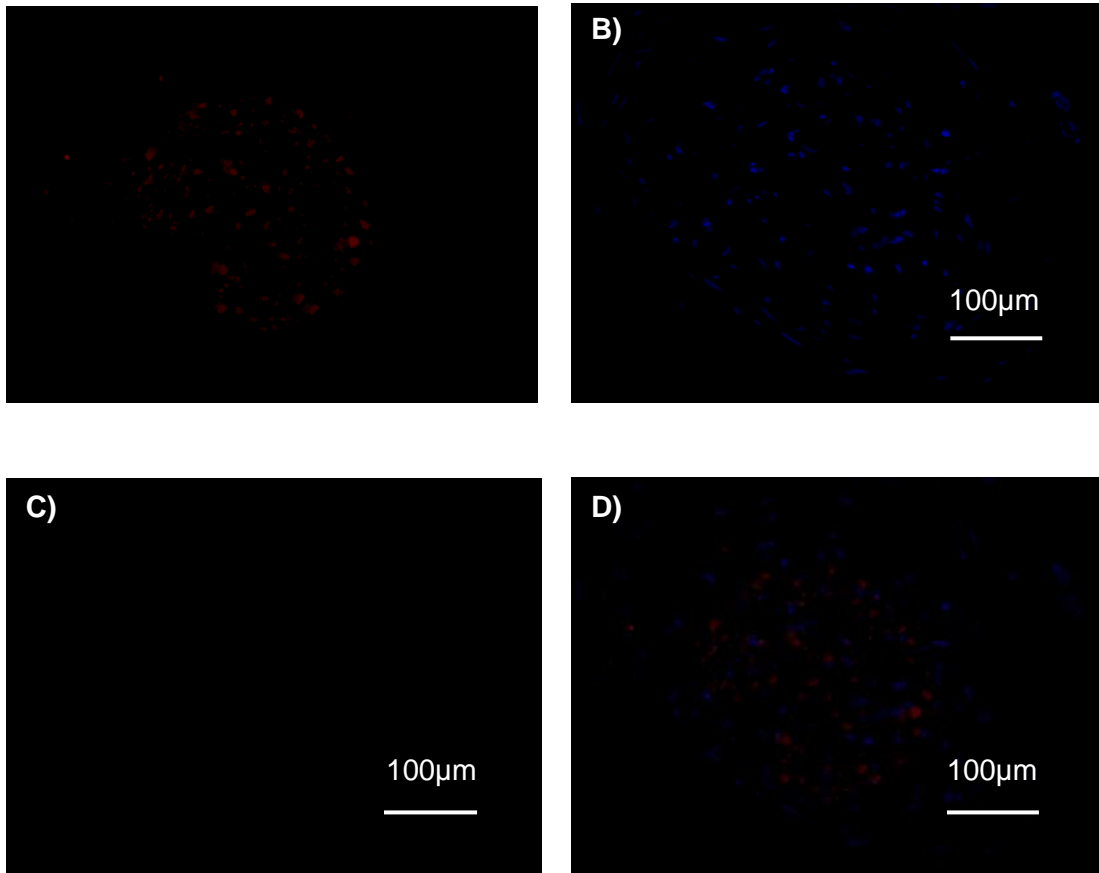


Figure 10.1 - ChAT staining of sural nerve section (negative control). **A)** Neurofilament **B)** DAPI **C)** ChAT **D)** Merged.

Appendix 3

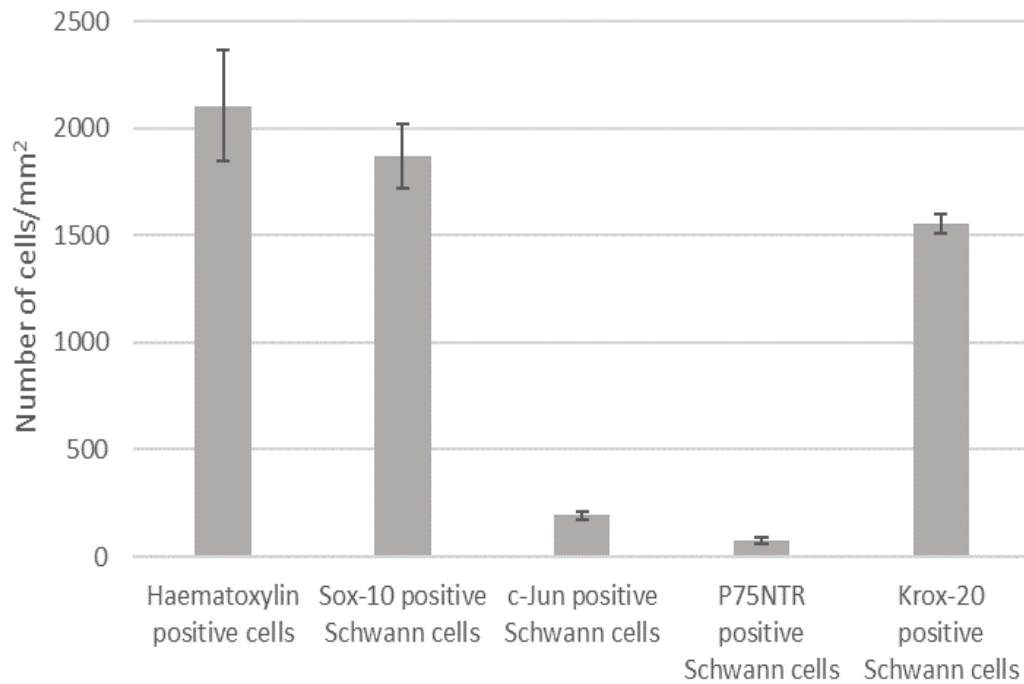


Figure 11.1 - Quantitative immunohistochemistry analysis of healthy nerves. Bar charts to represent quantification of immunohistochemically stained healthy nerve samples (case number 4 (sural) and case number 8 (intercostal) as reported in **Table 2.1**) for the markers SOX10, c-Jun, P75NTR and Krox-20.

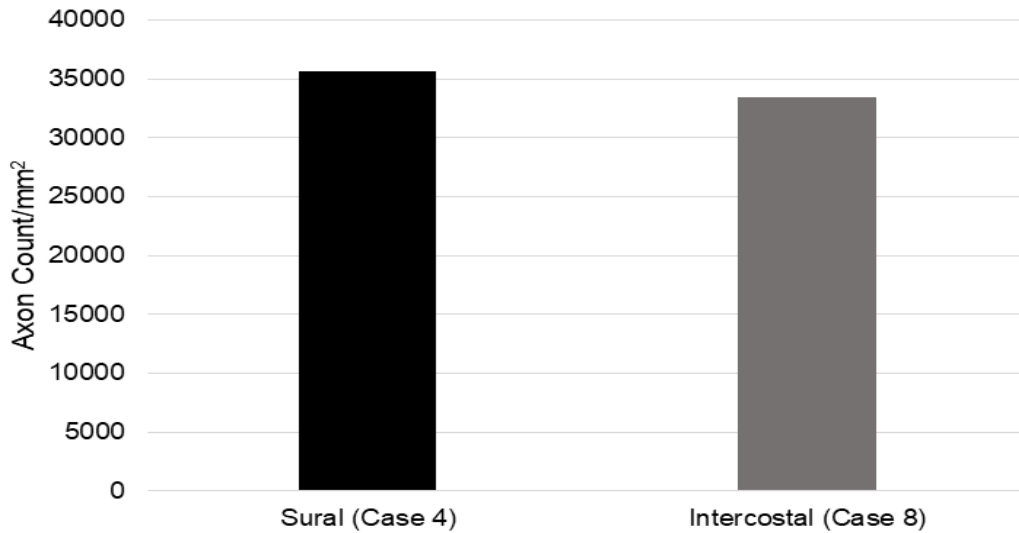


Figure 11.2 - Axon counts in healthy nerves. A bar chart to represent axons/mm² in the healthy sural (Case Number 4) and intercostal nerve samples (case number 8) as reported in **Table 2.1**.

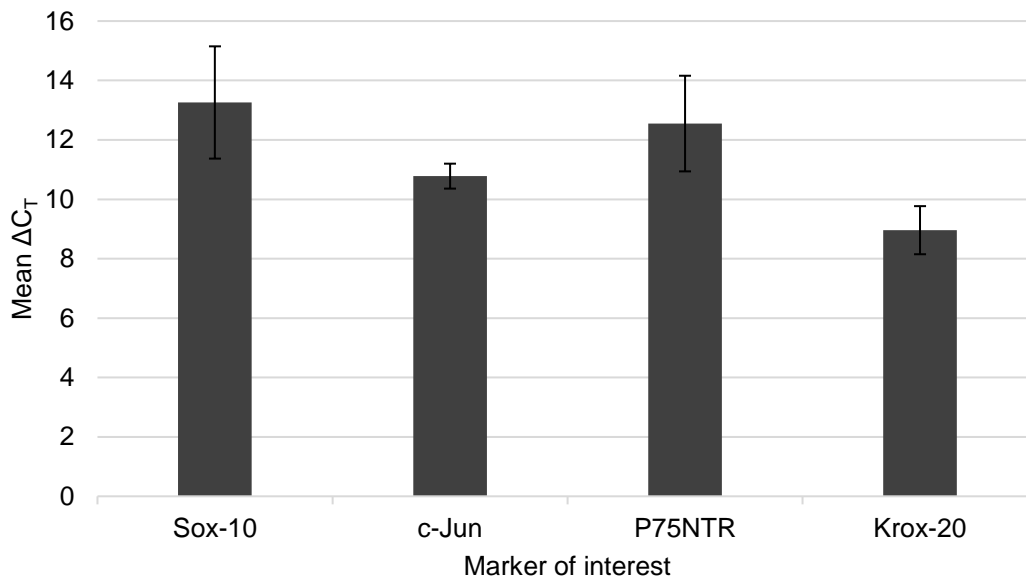


Figure 11.3 - RT-qPCR data for healthy nerve group. Bar chart to represent the mean $\Delta C_T \pm 1$ Standard Deviation (SD) of the genes SOX10, c-Jun, P75NTR and Krox-20 across the healthy nerve population (from case numbers 4 (sural nerve), 8 (intercostal nerve) and 24 (intercostal nerve) as reported in **Table 2.1**).